Photosensitiser functionalised nanofiber fabric for efficient light driven water disinfection

Hussaini Mohammed Majiya

Submitted in accordance with the requirements for the degree of

Doctor of Philosophy

The University of Leeds

School of Biomedical Sciences

Faculty of Biological Sciences

November, 2017

Declaration

The candidate confirms that the work submitted is his own, except where work which has formed part of jointly-authored publications has been included. The contribution of the candidate and the other authors to this work has been explicitly indicated below. The candidate confirms that appropriate credit has been given within the thesis where reference has been made to the work of others.

Jointly authored publications:

(1) Some parts of Chapter One, Chapter Four and Chapter Five have been published in TMPyP functionalised chitosan membrane for efficient sunlight driven water disinfection, 2017, **Majiya H,** Chowdhury KF, Stonehouse NJ, Millner P.; Journal of Water Process Engineering.

Hussaini Majiya contributed all of the research work and writing in this research paper. Kaniz F Chowdhury, Prof. Nicola J Stonehouse and Prof. Paul A Millner helped with research planning, provided critical feedback and editorial support. Copyright © 2017, Elsevier, Journal of Water Process Engineering.

(2) Some parts of Chapter One, Chapter Three and Chapter Four have been published in Photodynamic inactivation of bacteriophage MS2: the A- protein is the target of virus inactivation, 2018, **Majiya H,** Adeyemi O, Stonehouse NJ, Millner P.; Journal of Photochemistry & Photobiology, B: Biology.

Hussaini Majiya did all of the research work and most of the writing in this research paper. Dr Oluwapelumi Adeyemi in addition to editorial support, provided PyMOL structures of MS2 capsid and A-protein. Prof. Nicola J Stonehouse and Prof. Paul A Millner helped with research planning, provided critical feedback and editorial

“Valid criticism does you a favour”

- Carl Sagan

Acknowledgements

I appreciate and thankful to Petroleum Technology Development Fund (PTDF), Nigeria for sponsoring my PhD research. I also appreciate my employer- Ibrahim Badamasi Babangida University, Lapai, Nigeria, for giving me a study-leave to pursue my PhD degree.

I am grateful to my supervisor, Prof. Paul Millner for his support and educative suggestions throughout my PhD research. My research under supervision of Paul was awesome and I learnt several good things including good supervisor-student relationship. He was always encouraging, ever ready to listen and humour. He never for once talked down my write-ups, suggestions and experiments. These gave me confidence and ability to be a driver of my research and also improved my independent and critical thinking ability. His style of supervision has inspired me to become an academic like him in my future career.

I appreciate the efforts of my co-supervisor, Prof. Nicola Stonehouse. She was always there for me especially in virology. I learnt several skills under her supervision. She made me a better scientist and will forever be grateful. I am also grateful to my assessor Dr Alexander O'Neill. His patience, comments and feedback has tremendously improved my work.

Thanks to Mr Martin Fuller for his kindness, enthusiasm and expertise in teaching me TEM and doing TEM of most of my samples. Special thanks to all of the previous and present Millner group members I have met during my PhD especially Dr Carolyn Jackson, Dr Asif Ahmed, Dr Jack Goode and Dr Tim Gibson. All of you have made my journey smooth some way or other. I am thankful to Nicola Stonehouse group especially Dr Oluwapelumi Adeyemi and Dr Morgan Herod for their patience and kindness in

teaching me many skills in virology. Thanks to Prof. Peter Stockley and group especially Mrs Amy Barker for providing me with the stock samples of bacteriophages MS2 and Qβ and their *E. coli* host. Thanks to Dr A. M. Afifi for her kind gift of chitosan/polyethylene oxide electrospun nanofiber mats we used in this work.

I will forever be grateful to my family members especially my parents for their supports, blessings and prayers. My brothers and sisters especially Hassan were encouraging and supportive. My beloved wife Hauwa Abubakar and loving daughters Ummulkhairri and Fatima have made my every stressful day easier with their love, affection and presence. Finally, to all my friends and well-wishers, you all mean a lot to me, I thank you all.

Abstract

Sunlight-driven water disinfection system could help provide clean water to some of the world's poorest regions where contaminated surface water is a major public health problem and bright solar irradiation is available for free. In this work, photosensitiser - 5, 10, 15, 20-tetrakis (1-methyl-4-pyridinio) porphyrin tetra *p*-toluene sulfonate (TMPyP) was chosen and immobilised onto chitosan nanofiber mats and chitosan membranes for photodynamic disinfection of water since preliminary studies with TMPyP in solution showed it caused a high rate of photodynamic inactivation (PDI) of model viral organisms (bacteriophages MS2 and Qβ, murine norovirus and bovine enterovirus 2). Native gel electrophoresis, SDS-PAGE and western blotting, TEM and DLS were used to analyse pre- and post-PDI samples of the model viruses. The rate of PDI in model viruses was in the order MS2 > phage Qβ > murine norovirus > bovine enterovirus 2. Our data showed that PDI caused aggregation of MS2 particles and crosslinking of MS2 coat protein. However, the aggregation and crosslinking did not correlate to the rate of PDI we observed in MS2. Using sequence specific antibodies raised against MS2 A-protein (host attachment protein), our results suggest that the rate of PDI is relative to loss of antigenicity of sites on the A-protein. The differences in the rate of PDI were compared to amino acid compositions and surface accessibility of host attachment proteins/sites of the model viruses. Possible modes of action are discussed as a means to gaining insight to the targets and mechanisms of PDI of viruses. Chitosan electrospun nanofibers and chitosan membranes were modified by pyromellitic dianhydride in order to introduce carboxyl groups and facilitate adsorption of the cationic TMPyP. The physico-chemical properties of these modified nanofibers and membranes were investigated by microscopy, absorption spectroscopy, Fourier-transform infrared spectroscopy and Midland surface blotting approaches.The chitosan

nanofiber/membrane-TMPyP composite showed photodynamic inactivation of MS2 and *E. coli* BL21.

Abbreviations

^{0}PS	photosensitizer (ground state)
^{1}PS	photosensitizer (singlet excited state)
^{3}PS	photosensitizer (triple excited state)
BEV 2	Bovine enterovirus 2
Biotin-NHS	Biotin-tagged N-Hydroxysuccinimde
CM	Chitosan membrane
CM-T	TMPyP functionalised chitosan membrane
CPN	Chitosan/polyethylene oxide electrospun nanofiber
CPN-T	TMPyP functionalised Chitosan/polyethylene oxide electrospun nanofiber
DBPs	Disinfection by-products
DMEM	Dulbecco's Modified Eagle's Medium
ECL	Enhanced chemiluminescence
EDC	1-Ethyl-3-(3-dymethylaminopropyl) carbodiimide
FBS	Foetal bovine serum
FDA	fluorescein diacetate
HAAs	Haloacetic acids
MB	Methylene blue
MEM	Minimum Essential Medium
MF	Microfiltration
MNV	Murine norovirus
NF	Nanofiltration
NHS	N-Hydroxysuccinimde ester
P/S	penicillin – streptomycin
PDI	Photodynamic inactivation
PDT	Photodynamic therapy
PEO	polyethylene oxide
PI	Propidium iodide
PMA	Pyromelitic dianhydride
PS	Photosensitiser
Q	Net charge
RB	Rose Bengal
RO	Reverse osmosis
ROS	Reactive oxygen species
$TCID_{50}$	50 % tissue culture infective dose
THMs	Trihalomenthanes
TMPyP	5, 10, 15, 20-tetrakis (1-methyl-4-pyridinio) porphyrin tetra (p-toluenesulfonate)
TSA	Tryptic soy agar
TSB	Tryptic Soy Broth

UF	Ultrafiltration

Table of Contents

Lists of Tables

Lists of Figures

Chapter One: Introduction

Chapter 1: Introduction

1.1 Overview

Conventional methods of wastewater disinfection are costly and complex because of intensive use of chemical, manpower and energy, as well as the centralised nature of their infrastructures and operations. As such, they are not affordable in most instances in rural areas of developing countries. Also, the rural areas of developing countries especially in the Sub-Saharan Africa and South-East Asia lack energy infrastructures that will power centralised wastewater disinfection systems. The consequence is the high number of deaths which are recorded daily due to unsafe water especially in children in these regions of the world (Loeb et al., 2016, UNICEF, 2016, WHO, 2015). New methods of water disinfection that are cheap, simple, efficient and environmentally friendly are needed to inactivate and or remove dangerous waterborne pathogens including those resistant to chlorination such as enteric viruses, *Cryptosporidium parvum*, cysts of *Entamoeba hystolytica* and *Giardia lamblia* (Shannon et al., 2008).

Photosensitisers, when irradiated with visible light and in the presence of oxygen can generate reactive oxygen species (ROS) in aqueous solution which may efficiently inactivate waterborne pathogens including those resistant to chlorine. The ability and effectiveness of ROS to oxidise biomolecules has been studied and exploited with some success in the treatment of cancer, dental and dermatological diseases, as well as for synthetic chemistry and environmental remediation (DeRosa and Crutchley, 2002, Costa et al., 2013, Dolmans et al., 2003, Dwivedi and Pande, 2012, Lucena et al., 2015, Usuda et al., 2006). However, the environmental applications are still in their infancy.

For water disinfection, there is a consensus for the need to attach the photosensitiser onto a solid support such as nanofibers, glass fibres, chitosan polymeric membrane and so on. So that after phototreatment of water the supported photosensitiser is not

released into the water (Bonnett et al., 2006). This will allow re-utilisation of the photosensitiser functionalised solid support, thereby reducing the overall cost and increasing the advantage of using an environmental-friendly technology. Also, the prospect of using sunlight as the source of visible light for a photosensitiser functionalised solid support disinfection system is attractive as it could be used to clean water even in those places where there is no man-made energy infrastructure.

In this study, photosensitiser - 5, 10, 15, 20-tetrakis (1-methyl-4-pyridinio) porphyrin tetra p-toluene sulfonate (TMPyP) was chosen for immobilisation onto chitosan nanofiber/ polymeric membrane for light driven water disinfection. This was because our preliminary investigation with TMPyP in solution showed it causes a rapid and high rate of photodynamic inactivation (PDI) of our model viral organisms (bacteriophages MS2 and Qβ, murine Norovirus and bovine enterovirus). Chitosan nanofiber and polymeric membranes were used as solid supports for attaching TMPyP because of chitosan's properties such as easy fabrication, presence of numerous reactive groups, rigid D-glucosamine structure, and lack of toxic reactions. Chitosan is also biodegradable, cheap and readily available. In the Introduction chapter (Chapter 1), brief overviews of waterborne pathogens/diseases, conventional water disinfection, photodynamic effect, photodynamic inactivation and photosensitised reaction, biological targets of singlet oxygen, photodynamic inactivation of viruses, solid supports and coupling chemistry for attaching photosensitisers, types and characteristics of photosensitisers, TMPyP, bacteriophage MS2, bacteriophage Qβ, bovine enterovirus and murine norovirus and project aims are presented. Then general methods are presented in Chapter 2 followed by research data presented in the subsequent chapters. An overall General Discussion is presented in Chapter 6 at the end with focus

on future work. Overall, the information and primary findings presented here will aid in the development of simple sunlight driven water disinfection devices that could be used with the UK to save energy or in developing countries as a zero-man-made energy input system to produce clean and safe drinking water. Additionally, it could lead the way to understanding from a biological perspective the targets and mechanisms of photodynamic inactivation in viruses; whilst waterborne pathogens can be eukaryotic, bacterial and viral, the work in this thesis concentrated on viral inactivation.

1.2 water availability and public health importance

Water is one of the most basic essential needs of man and other life forms. It is the medium of support for life processes. The average recommended intake of water for adult human being is about 3 litres per day, via food and drink consumption (WHO, 2012). Water covers about two-third (70.9%) of earth surface (Figure 1.1). About 96.5% of earth's water is found in oceans (salt water) and only 2.5% of the earth's water that is fresh water (Figure 1.1). However, the amount of fresh water on earth is limited, only very small portion of it (about 1.2% of all fresh water) is available for immediate and essential needs of man (Figure 1.1). The remaining fresh water (about 98.8%) is held in glacier and ground water (Figure 1.1) (Gleick and Howe, 1995).

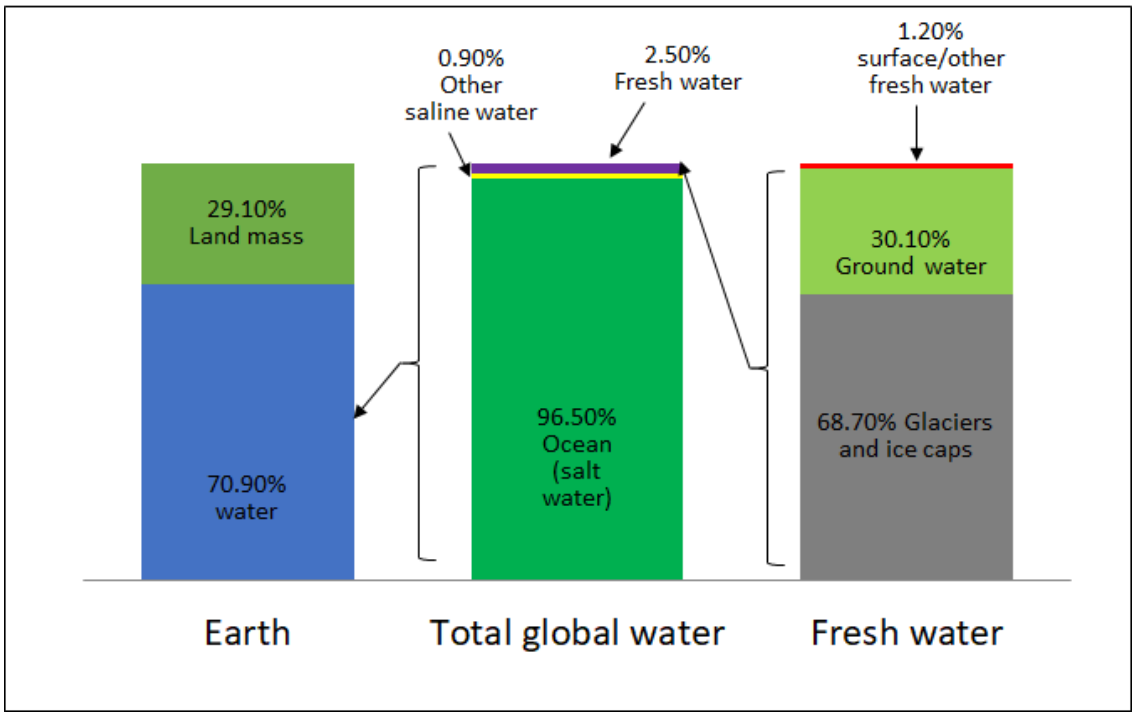

Figure 1. 1: Earth's water availability and distribution. Only 1.2% of all fresh water, which is also 2.5% of earth's water, is available for immediate and essential needs of man (Gleick and Howe, 1995).

The quality of the available fresh water is under constant pressure due to human activities and industrialisation which have produced dangerous pathogens and toxic pollutants into our environment including water (WHO, 2015). Open defecation, indiscriminate discharge of untreated sewage and runoff of animal farm wastes in to surface waters (rivers, ponds, streams, lakes), drainage of pit latrines into wells that are in close proximity, etc. are some of the ways sources of water are continuously contaminated with waterborne pathogens in Sub-Saharan Africa and South East Asia (WHO, 2016, UNICEF, 2016). However, despite continuous pollution of water in these regions of the world, in most cases, they lack or have least developed and efficient systems of wastewater treatment and disinfection especially in the rural areas. The lack of efficient water clean-up systems to produce safe drinking water is attributable to the cost of conventional methods of wastewater treatment and disinfection and also, the

lack of energy infrastructures in these parts of the world (Loeb et al., 2016). From a public health perspective, it is important to ensure the microbiological quality of drinking water through adequate and efficient treatment and disinfection of wastewater (WHO, 2016). This is to prevent transmission of waterborne pathogens that can cause diseases and deaths especially in children (UNICEF, 2016). Epidemics of historic diseases like cholera and many other waterborne diseases are still reoccurring in developing countries in the sub-Saharan Africa and South East Asia including IDPs and refugee camps, war torn areas and places afflicted with natural disasters such as flooding and earth quake (UNICEF, 2016, WHO, 2016).

1.3 Waterborne diseases and the need for alternative water disinfection methods

Lack or inadequate access to clean water is a serious global problem. It was estimated more than 700 million people still lack access to improved sources of drinking water and nearly half are in sub Saharan Africa (UNICEF, 2014, WHO, 2015). More than 660 million people lack access to safe drinking water with 530 million of them living in rural areas especially in the sub-Saharan Africa and south East Asia (Loeb et al., 2016). About 2.5 billion people - one third of the world population have little or no sanitation (UNICEF, 2014, WHO, 2015, WHO, 2011b). The consequence of lack or inadequate access to safe water is high mortality rate in the sub-Saharan Africa and south East Asia (Figure 1.2).

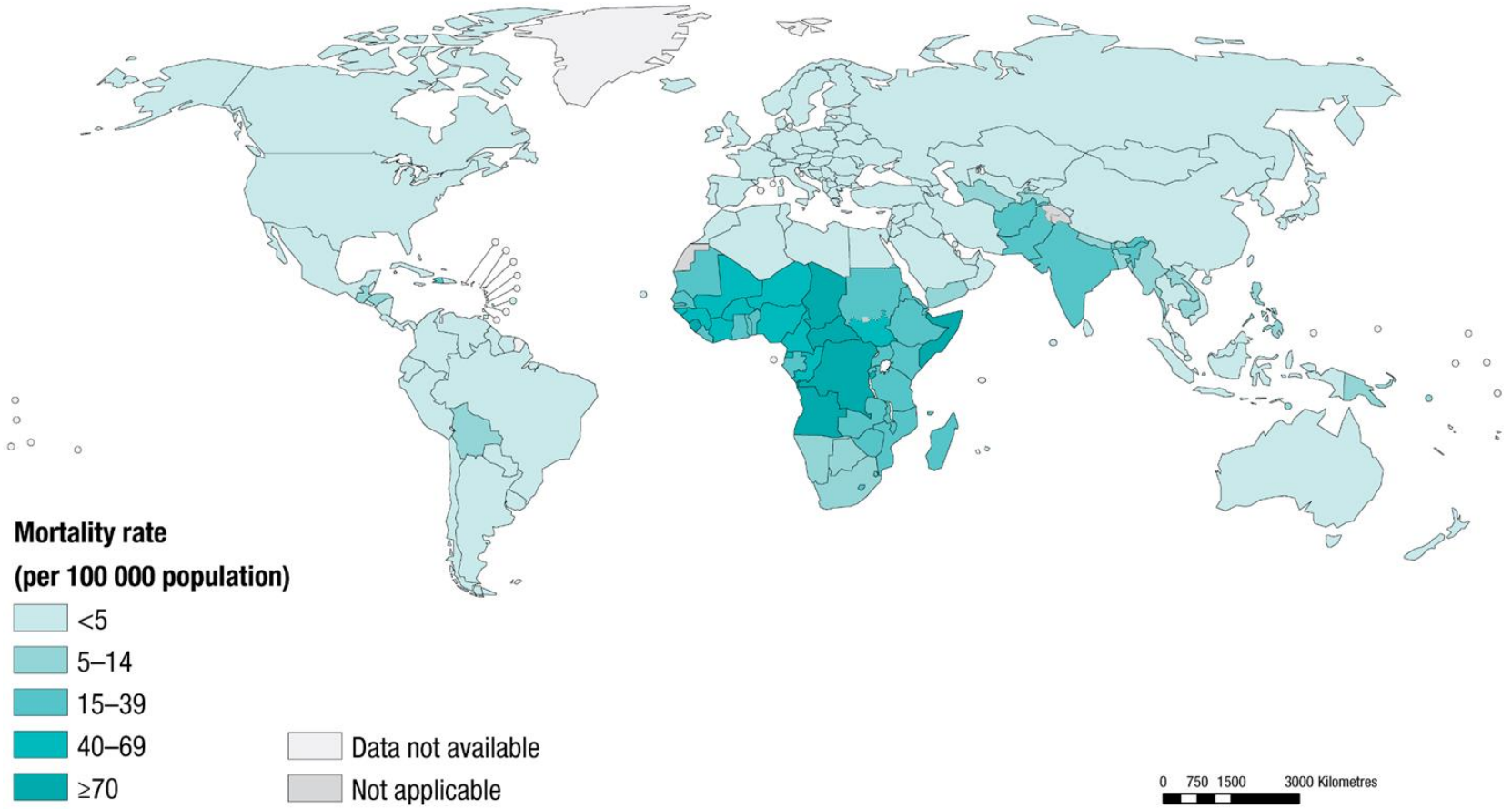

Figure 1. 2 Global mortality rate attributed to unsafe water, sanitation and hygiene (WASH) services 2012. There is usually high mortality rate (≤70 deaths per 100,000 population) in the sub-Saharan Africa and south East Asia (WHO, 2015).

Millions of people die annually from diseases (Table 1.1) transmitted through unsafe water and many more are made ill (Shannon et al., 2008). Gastroenteritis and diarrheal disease caused by waterborne pathogens (Table 1.1) have become a leading cause of malnutrition owing to poor digestion of the food eaten by people made ill by water borne pathogens (Shannon et al., 2008).

Table 1. 1: Common water borne diseases and their primary sources of transmission and infection

Pathogen	Diseases	Primary sources
Bacteria		
Salmonella typhi	Typhoid fever	Human faeces
Salmonella paratyphi	Paratyphoid fever	Human faeces
Other *Salmonella*	Salmonellosis	Human and animal faeces
Shigella spp.	Bacillary dysentery	Human faeces
Vibrio cholerae	Cholera	Human faeces and zooplankton
Enteropathogenic *E. coli*	Gastroenteritis	Human faeces
*Yersinia enterocolitica**	Gastroenteritis	Human and animal faeces
Campylobacter jejuni	Gastroenteritis	Human and animal faeces
*Legionella pneumophila**	legionellosis	Thermally enriched water
Leptospira spp.	Leptospirosis	Animal and human urine
Various mycobacteria	Pulmonary illness	Soil and water
Opportunistic bacteria	Variable	Natural waters
*Pseudomonas aeruginosa**	Necrotising enterocolitis	Soil, water, human skin flora
*Atypical mycobacteria**	Case of fish tank granuloma	Soil, water
*Aeromonas hydrophila**	Gastroenteritis	Water
*Acinetobacteria**	Urinary tract infection	Soil
Enteric viruses		
Poliovirus	Poliomyelitis	Human faeces
Coxsackie virus A	Aseptic meningitis	Human faeces
Coxsackie virus B	Aseptic meningitis	Human faeces
Echo viruses	Aseptic meningitis	Human faeces

Table 1.1 continued

Other enteroviruses	Encephalitis	Human faeces
Rotaviruses	Gastroenteritis	Human faeces
Adenoviruses	Upper respiratory and gastrointestinal illness	Human faeces
Hepatitis A virus	Infectious hepatitis	Human faeces
Hepatitis E virus	Infectious hepatitis miscarriage and death	Human faeces
Norovirus	Gastroenteritis	Fomites and water
Protozoa		
*Acanthamoeba castellani**	Amoebic meningoencephalitis	Human faeces
Balantidium coli	Balantidosis (dysentery)	Human and animal faeces
Cryptosporidium homonis	Cryptosporidiosis	Water, human and other
Cryptosporidium parvum	Cryptosporidiosis (gastroenteritis)	Mammal faeces
Entamoeba histolytica	Amoebic dysentery	Human and animal faeces
Giardia lamblia	Giardiasis (gastroenteritis)	Water and animal faeces

Table 1.1 continued

*Naegleria fowleri**	Primary amoebic meningoencephalitis	Warm water
Helminths		
Ascaris lumbricoides	Ascariosis	Animal and human faeces

List of common waterborne pathogens and diseases and their primary sources of transmission and infection. There are 4 major groups of water borne pathogens which are bacteria, enteric viruses, protozoa and helminths. (*), Pathogens which can proliferate in water distribution systems.

Unsafe water and inadequate sanitation is responsible for about 90% of diarrheal deaths worldwide (UNICEF, 2016, WHO, 2011b, WHO, 2016) and diarrhoea is the second leading cause of deaths in children under age of five (UNICEF, 2016, UNICEF, 2012). About 1, 400 children die daily due to diarrhoea mostly caused by rotaviruses especially in sub-Saharan Africa and south-east Asia (Figure 1.3) (UNICEF, 2016).

Waterborne pathogens such as *Cryptosporidium parvum*, cysts of *Entamoeba hystolytica*, *Giardia lamblia* and enteric viruses are resistant to chlorination which is the gold standard presently for water disinfection during wastewater treatment (Shannon et al., 2008). Generally, compared to faecal bacteria, viruses are more difficult to remove and inactivate during wastewater treatment. The small size and higher resistance of viruses to disinfectants has made it almost impossible to completely remove viruses from water by conventional treatment processes such as sedimentation and filtration (Silverman et al., 2013). There are several instances where infectious human viruses have been found in wastewater effluents treated by these conventional methods (Silverman et al., 2013). The resistance of these pathogens to chlorination allows them to transmit diseases and cause outbreaks even in developed nations. The annual cases of waterborne diseases such as cryptosporidiosis in developed nations have been reported (WHO, 2009). In the UK, unreported rate of disease from a single pathogen group, *Cryptosporidium* spp., has been estimated at 60,000 cases per year, and tap water is the most common risk factor in recorded cases of cryptosporidiosis (Chalmers and Giles, 2010, Gormley et al., 2011, Hill et al., 2011). Viral gastroenteritis is one of the most common causes of morbidity and mortality globally with more impact in developing countries and on children. An estimated 2.5-3.2 million children aged <5 years old die annually (Lodder

et al., 2010). Rotavirus causes about 2 million hospitalisations and up to 600,000 deaths annually in children under 5 years of age (Clark and McKendrick, 2004, Parashar et al., 2003). This mortality rate associated with rotavirus has been strongly linked to lack of, or inadequate, access to safe water and poor hygiene especially in the developing countries (Parashar et al., 2003, Clark and McKendrick, 2004). Noroviruses which account for over 90% of the cases of acute viral gastroenteritis causes the disease in patients of all age groups, in both developed and developing countries (Haramoto et al., 2004, Lodder and Husman, 2005). It causes annually several hundreds of millions of cases and hospitalisations worldwide (Haramoto et al., 2004).

However, fortunately, the regions of the world that cannot afford conventional water disinfection (especially sub-Saharan Africa and south-East Asia) have enough solar irradiation throughout the year (Figure 1.4) that could be harnessed and used for sunlight driven water disinfection (Figure 1.5) which would be a cheap, simple, efficient and environmentally friendly way to produce safe water for consumption.

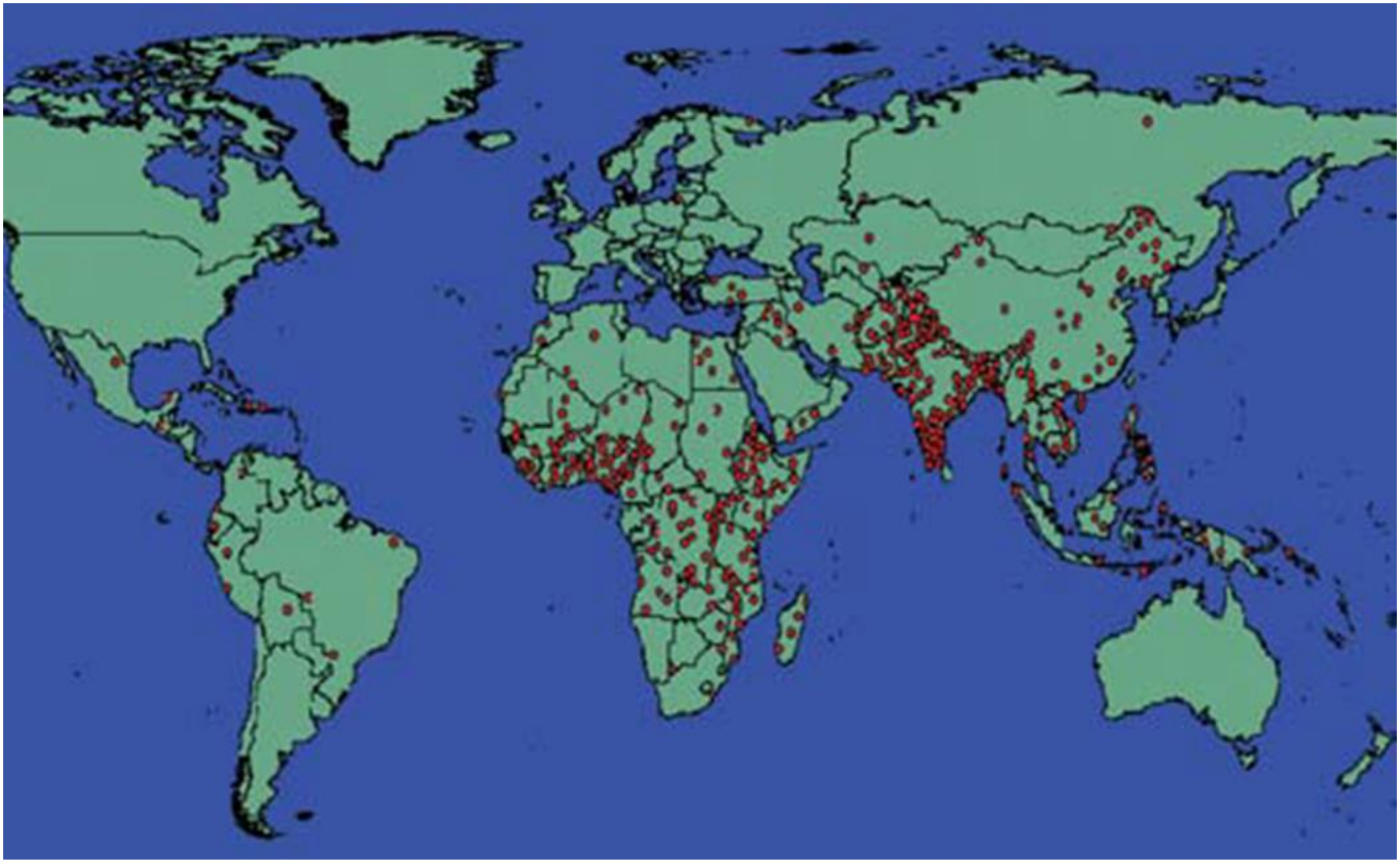

Figure 1. 3: Estimated global distribution of 440,000 annual deaths in children caused by rotavirus diarrhoea. One red dot = 1,000 deaths. There is usually more deaths in the sub-Saharan Africa and south East Asia (Parashar et al., 2003).

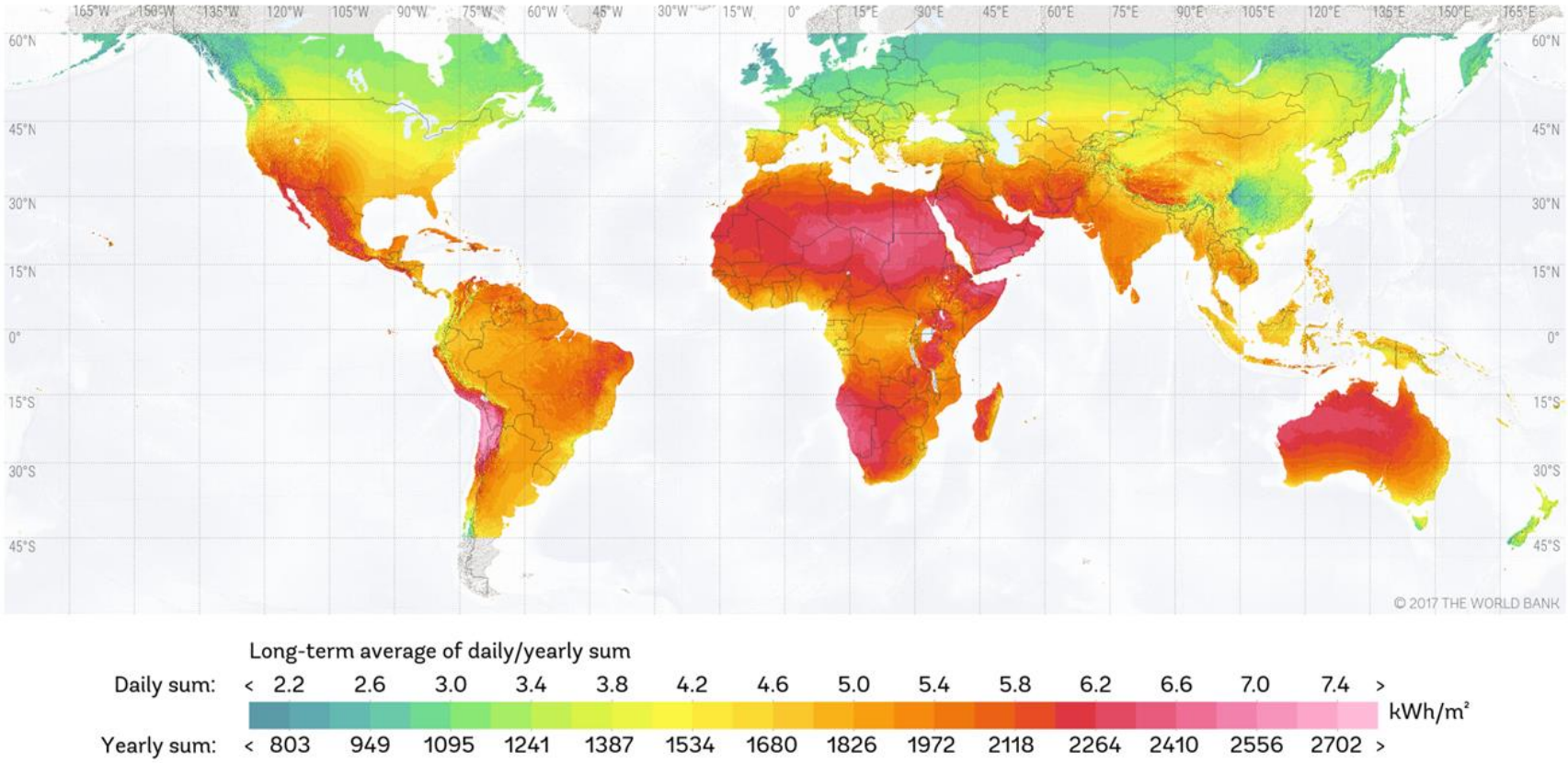

Figure 1. 4: World map of horizontal irradiation by GeoModel Solar. Sub-Saharan Africa and south-East Asia have daily sunlight that could be harnessed for water disinfection.

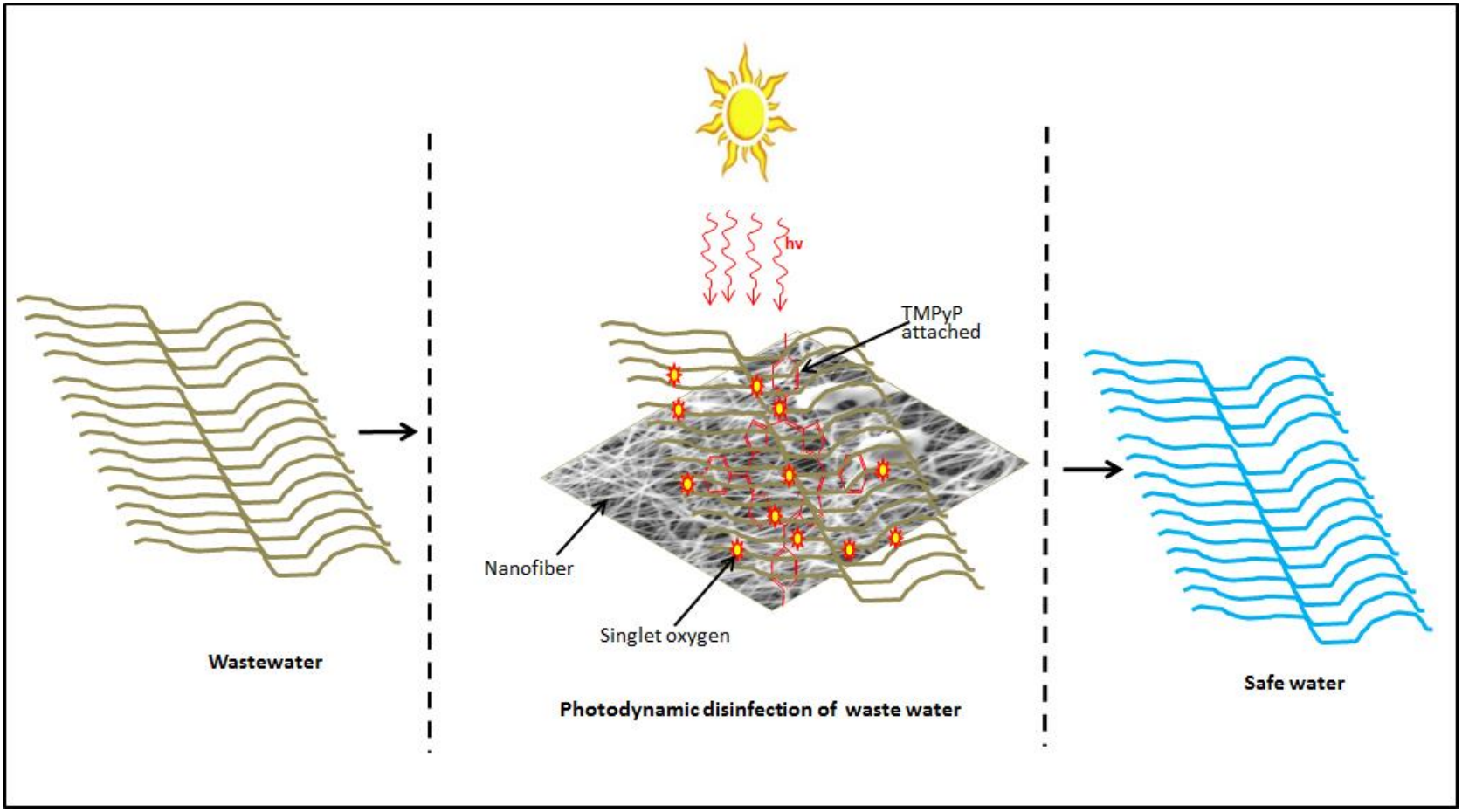

Figure 1. 5: A scheme showing the potential for harnessing solar irradiation for water disinfection. Photosensitisers such as TMPyP are attached onto a solid support which can then be used for water disinfection. The TMPyP functionalised nanofiber in the presence of sunlight & the molecular oxygen generates singlet oxygen and other ROS that can inactivate/kill waterborne pathogens to make the water safe.

1.4 Wastewater treatment and disinfection

Measures to eliminate the risk of infectious diseases transmitted by water were used even before the discovery of their etiologic agents (Amin et al., 2013). These measures include boiling, filtration and storage of water in silver vessels. Contemporary knowledge shows that these measures can suppress pathogenic organisms in water, either partially or completely (Amin et al., 2013). However, they are most effective and can be applied only when dealing with smaller quantities of water.

The rapid increase of population as well as industrialisation and urbanisation of different cities and towns in the early 19th century led to sharp increase in water demand. Water distribution systems were built to cater for these industrial, business, domestic, agricultural and community needs but with little concern for water quality. As a consequence, cholera and typhoid fever outbreaks were on the increase and were a serious problem (Amin et al., 2013). The findings in the field of bacteriology in the second half of 19th century provided the clue and led to the development and adoption of an efficient and centralised wastewater treatment plants (Figure 1.6) in cities and towns (USEPA, 1999a). The centralised system of wastewater treatment which has since been in practice in the developed nations is the most effective way of managing the amount and quality of limited surface fresh waters on earth because of reuse and recycling of wastewaters (USEPA, 1999a). However, it is chemically, operationally and energy intensive.

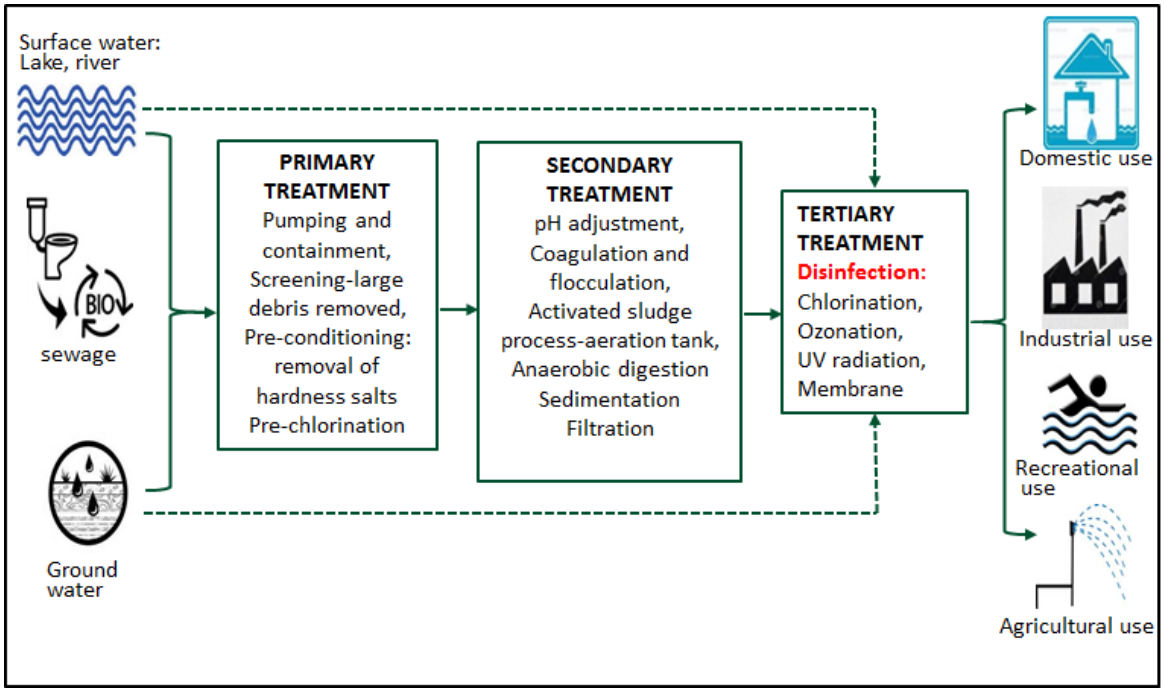

Figure 1. 6: Schematic showing sources of water for treatment, different stages of wastewater treatment and possible end users of water after treatment. Dotted arrows indicate that the first two stages of water treatment could be missed and avoided depending on the physico-chemical characteristics of the source of water (surface water; river, lake, and ground water) unlike sewage that will have to pass through all the three stages of water treatment. Irrespective of the sources of wastewater, it is necessary for it to pass through the last stage of water treatment (disinfection) before it is safe for domestic usage to avoid transmission and outbreak of waterborne disease.

1.4.1 Types of water disinfection

Disinfection is the last and most important stage of waste water treatment (Figure 1.6) from public health perspective (Amin et al., 2013). The choice of a disinfectant or disinfection process for wastewater treatment is dependent on criteria such as;

- Ability of the disinfectant/disinfection process to kill all or majority of pathogens under normal operating conditions.
- Safety and simplicity of the disinfectant/disinfection process: Safe and easy handling, storage and shipping.

- Absence of or minimal toxic residuals and mutagenic/carcinogenic compounds after disinfection in treated water.
- Affordable capital and operation and maintenance costs.

Generally, disinfectants/disinfection processes both conventional and alternatives presently in-use to clean water could be classified into three (3) main groups, namely;

- Chemical disinfection
- Radiations and
- Membrane systems.

1.4.1.1 Chemical disinfectants/disinfection

Chemical disinfection involves the use of chlorine, ozone or other chemical oxidants to kill or inactivate waterborne pathogens during wastewater treatment. However, in most cases chlorine is used to disinfect water (USEPA, 1999a).

1.4.1.1.1 Chlorination

The use of chlorine started from the late 19th century. However, most records showed that full adoption of chlorine as a disinfectant in water treatments was in the early 20th century (Snowden-Swan et al., 1998). This was a response to a rise in population across major cities of the world because of industrial revolution and simultaneous outbreaks of cholera and typhoid fever. Chlorination was fully adopted in Middelkerke (Oostende in Belgium) in 1902 and in Lincoln (England) in 1905. Baker and Whipple introduced chlorine disinfection of water in the USA in 1906. Since then, chlorine disinfection has been employed globally especially in developed nations and is at present taken as a decisive measure to eliminate water assisted transmission of pathogens (USEPA, 1999a).

Chlorine inactivates pathogens by oxidising their cellular materials (Schoenen, 2002, Shannon et al., 2008). Chlorine is available for use and can be supplied in many forms such as chlorine gas, hypochlorite solutions, chloramine and chlorine dioxide (Chen and Westerhoff, 2010). However, despite establishment of chlorine as water disinfectant globally, there are some drawback (Table 1.2). One of such setback is that chlorine react with compounds like nitrite in wastewater which can result in the formation of suspected mutagenic and carcinogenic disinfection by products (DBPs) such as trihalomethanes (THMs), and haloacetic acids (HAAs).

Table 1. 2: Advantages and disadvantages of chlorination (USEPA, 1999a).

Advantages	Disadvantages
chlorination is a well and most established method of waste water disinfection	Chlorine residual even at low concentrations is toxic to aquatic life and may require dechlorination
Presently, it is more cost-effective compared to UV or ozone disinfection (except when dechlorination is required after disinfection)	All forms of chlorine are highly corrosive and toxic. Thus, storage, shipping and handling pose a risk, requiring increased regulations
The chlorine residual that remains in the wastewater effluent can prolong disinfection even after initial treatment and can be measured to evaluate the effectiveness	Chlorine oxidizes certain types of organic matter in wastewater, creating more hazardous compounds such as THMs and HAAs
It is reliable and effective against a wide spectrum of pathogenic organisms	The total dissolved solids are increased in the treated effluent
It is effective in oxidising certain organic and inorganic compounds	The chloride content of the wastewater is increased
It has flexible dosing control	Chlorine residual is unstable in the presence of high concentrations of chlorine-demanding materials, thus requiring higher doses to effect adequate disinfection
It can eliminate certain noxious odours during disinfection	Some parasitic species have shown resistance to chlorine including oocysts of *Cryptosporidium parvum*, cysts of *Entamoeba hystolytica* and *Giardia lamblia* and eggs of parasitic worms, also enteric viruses
	Long-term effect of discharging dechlorinated compounds into the environment are unknown

1.4.1.1.2 Ozonation

Ozone was the disinfectant used from late 19th century to early 20th century and during this period water supply systems were equipped with ozone treatment unit especially in France and Germany. After 1920, ozone treatment lost most of its importance, but was reintroduced on a massive scale in 1960s and 1970s as an oxidant to remove undesirable organic substances from water. Starting in the 1990s, it has been used as a disinfectant for killing parasites (Amin et al., 2013).

Ozone is a relatively unstable molecule of oxygen which readily gives up one atom of oxygen providing a powerful oxidising agent which is toxic to most waterborne organisms (Amin et al., 2013). Conventional mechanical diffuser ozonation and dissolved ozone flotation (DOF) systems have been used to disinfect downstream municipal wastewater (Amin et al., 2013). Although fewer dangerous by-products are formed by ozonation, it has been shown that the use of ozone also produces a small amount of the suspected carcinogen (bromate). Some incentives in the use of ozone as disinfectant during wastewater treatment are summarised in Table 1.3.

Table 1. 3: Advantages and disadvantages of ozonation (USEPA, 1999a, Amin et al., 2013).

Advantages	Disadvantages
Ozonation is an effective method to kill harmful protozoans that form cyst	Relatively more expensive than chlorination
Production of relatively fewer harmful by products in comparison to chlorination	It leaves no disinfectant residual in the water, so the process of disinfection is not prolonged
Unlike chlorination, it does not produce taste and odour	Ozonation can result in the production of bromate-a suspected carcinogen

1.4.1.2 Disinfection by radiations

Wastewater can be disinfected by both ionising (e.g., gamma ray) and non-ionising (e.g., UV radiation, ultrasonic radiation) radiations. However, UV radiation is mostly employed in water disinfection during wastewater treatment (USEPA, 1999b).

1.4.1.2.1 UV light disinfection

UV light is well established for disinfection of drinking water during wastewater treatment (USEPA, 1999b). UV light in the UV-C region is germicidal. UV radiation generated by an electrical discharge through mercury vapour can be absorbed by genetic material (DNA) of microorganisms and retards their ability to replicate (USEPA, 1999b). The effectiveness of a UV light disinfection system depends on the characteristics of the wastewater, the intensity of UV radiation, the amount of time the microorganisms are exposed to the radiation and reactor configuration (Jackson et al., 1999). The main components of a UV disinfection system are mercury arc lamps, a rector and ballasts. The source of UV radiation is either low-pressure or medium-pressure mercury arc lamp with low or high intensities and the optimum wavelength to effectively inactivate microorganisms is in the range of 250nm to 270nm (Jackson et al., 1999). Effectiveness of the UV radiation against viruses, spores and cysts is one of the several advantages (Table 1.4) of using it as disinfectant during wastewater treatment.

Table 1. 4: Advantages and disadvantages of UV disinfection (USEPA, 1999b).

Advantages	Disadvantages
UV disinfection is effective at inactivating most viruses, spores and cysts	Low dose may not effectively inactivate some viruses, spores and cysts
UV disinfection is a physical process rather than a chemical disinfectant, which eliminates the need to generate, handle, transport or store toxic/hazardous or corrosive chemicals	Organisms can sometimes repair and reverse the destructive effects of UV through a repair mechanism known as photoreactivation or in the absence of light known as dark repair
There is no residual effect that can be harmful to humans or aquatic life	A preventive maintenance program is necessary to control fouling of tubes
It is user friendly for operators	Turbidity and total suspended solids (TSS) in the wastewater can render UV disinfection ineffective
UV disinfection has a shorter contact time when compared with other disinfectants (about 20-30 seconds with low-pressure lamps)	UV disinfection is not as cost-effective as chlorination but costs are competitive when dechlorination is required after chlorine disinfection
UV disinfection equipment requires less space than other methods	

1.4.1.3 Disinfection by membrane systems

Membrane filters are powerful tools for various applications including wastewater treatment and the removal of particulate contaminants from drinking water. However, membrane microfiltration does not generally remove soluble pollutants (Amin et al., 2013, Jackson et al., 1999). A range of pressure driven membrane processes are available for wastewater disinfection;

1. Microfiltration (MF) is a direct extension of conventional filtration capable of sieving out particles greater than 0.05 to 2 μm depending on the membrane and including bacteria and cysts.
2. Ultrafiltration (UF) is a molecular sieving process and will reject organic material to the membrane cut-off (~100 Da), viruses, bacteria and large pathogens.
3. Reverse osmosis (RO) is a high efficiency, high pressure membrane process capable of rejecting monovalent ions such as sodium and organics of molecular weight greater than 50 Da. It is typically used for desalination in arid countries, but is energy-expensive
4. Nanofiltration (NF) is a low-pressure membrane process combining low efficiency reverse osmosis and high efficiency ultrafiltration. NF is capable of rejecting multivalent ions and dissolved organic matter of molecular weight above 200 Da (Amin et al., 2013).

One of the main setback (Table 1.5) of membrane system is that in terms of whole life cost, it is not cost effective.

Table 1. 5: Advantages and disadvantages of membrane disinfection (Amin et al., 2013).

Advantages	Disadvantages
The use of membrane processes would avoid the formation of disinfection by-products and reduce the concentrations of other undesirable chemicals	The integrity of the membrane and efficiency of microorganism removal cannot be monitored.
Depending on the pore size, all pathogens could be removed from water by membrane system	In terms of whole life costs, membrane systems are more expensive than conventional method
	Membrane systems generate liquid waste which might require treatment to destroy toxic chemicals or kill microorganisms

1.4.2 Effects of wastewater characteristics on different disinfection methods and cost implications

The source and characteristics of wastewater can affect the efficiency and performance of disinfection process during wastewater treatment (Table 1.6). In terms of whole life costs, both UV radiation and membrane systems disinfection are generally more expensive than chlorination (Snowden-Swan et al., 1998). This is particularly so for larger plants because there are economies of scale with chlorination plants that are not realised with UV and membrane systems which are essentially modular. Chemical costs for membranes and UV treatment are lower than for chlorination processes but their energy consumption is greater(Snowden-Swan et al., 1998). The overall assessment of the different types of water disinfection against several criteria (Table 1.7) shows that synergistic effect of 2 or more disinfection methods and or pre-treatment is the best way to adequately and efficiently inactivate resistant waterborne pathogens. Also, the source of water and

its characteristics can determine the choice of best disinfection method, its efficiency, performance and cost implication.

Table 1. 6: Effects of some water characteristics on the performance and efficiency of disinfection processes (USEPA, 1999a).

Water characteristics	Chlorination	Ozonation	UV radiation	Membrane system
Ammonia	Forms chloramines when combined with chlorine	Minor effect, if any	Minor effect, if any	Minor effect, if any
Biochemical Oxygen Demand (BOD)	The degree of interference depends on their functional groups and chemical structures	The degree of interference depends on their functional groups and chemical structures	Minor effect, if any	Minor effect, if any
Hardness, iron	Minor effect, if any	Minor effect, if any	Affects solubility of metals that can absorb UV light. Can lead to the precipitation of carbonates on quartz tubes	Minor effect, if any
Nitrate	Minor effect, if any	Minor effect, if any	Minor effect, if any	Minor effect, if any
Nitrite	Reduces effectiveness of chlorine	Minor effect, if any	Minor effect, if any	Minor effect, if any
pH	Affects distribution between hypochlorous acid and hypochlorite ions and among the various chloramine species	Affects oxidising capacity of zone	Affects solubility of metals and carbonates	Minor effect, if any
Total suspended solids	Shielding of embedded bacteria	Shielding of embedded bacteria	Absorbs UV radiation and shields embedded bacteria	Might block the membrane pores
Humic materials	The degree of interference depends on their functional groups and chemical structures	The degree of interference depends on their functional groups and chemical structures	High absorbency of UV radiation	Minor effect, if any

Table 1. 7: An overall assessment of different types of water disinfection against several criteria (Jackson et al., 1999).

		Microbiological safety	Chemical safety	Customer aesthetic	Ease of monitoring	Ability to treat difficult water	Operating costs	Capital costs	Commercial development	Scale-up	Waste and energy use	Reliability
Ground water	Chlorine	-	-	-	+	+	+	+	+	+	+	+
	UF only	-	+	+	-	+	.	.	-	-	.	-
	UV only	+	+	+	.	+	+	.	+	+	.	.
Surface water and sewage	Chlorine only	-	-	-	+	-	+	+	+	+	+	-
	Pre-treat + chlorine	+	-	-	+	-	.	.	+	+	.	-
	UF only	-	-	.	-	-	.	.	-	-	.	-
	Pre-treat + UF	.	+	+	-	+	-	-	-	-	-	-
	Pre-treat + Ozone + UF	-	.	-	-	+	-	-	-	-	-	-
	MF + UV	.	+	-	.	-	+	.	-	-	.	+
	Pre-treat + UV	.	+	+	.	-	+	.	+	+	.	.
	Pre-treat + Ozone + UV	+	.	+	+	+	-	-	+	+	.	+

UF, ultrafiltration**; MF**, microfiltration**; UV,** ultraviolet; **Pre-treat** e.g. coagulation/sedimentation; **+**, better than average; **-,** worse than average; **.**, average.

1.5 Photodynamic effect, photodynamic inactivation and photosensitised reaction

The photodynamic effect is the result of generation of singlet oxygen and other ROS by interaction of photosensitizer, visible light and oxygen (Figure 1.7). Photodynamic inactivation is a process in which the generated singlet oxygen and other ROS oxidise and cause irreversible damage to proteins, lipids, nucleic acid and other cellular components of microorganisms and ultimately inactivate them (Costa et al., 2013, Komagoe et al., 2011, Tavares et al., 2011, Spannberger et al., 2012). The indirect photochemical reactions (also called photosensitised reactions) arise from the possibility that the energy of the excited photosensitizer molecule in its triplet state can be transferred to another molecule such as oxygen by a non-radiative mechanism (Figure 1.7) (Costa et al., 2013). The transfer can occur either by a charge transfer mechanism (type 1 photoreaction) or electronic energy transfer mechanism (type 2 photoreaction) (Figure 1.7) (DeRosa and Crutchley, 2002, Costa et al., 2013). These transfers inhibit emission of radiation by the excited photosensitizer molecule and this is called quenching. Quenchers, such as oxygen, become excited and can undergo various photophysical and photochemical processes according to their own characteristics. The energy transfer occurs before the excited photosensitizer molecule can radiate fluorescence and the acceptor molecule is thus excited indirectly, undergoing various photophysical and photochemical processes called photosensitisation or photosensitised reactions (Figure 1.7) (Costa et al., 2013, DeRosa and Crutchley, 2002).The characteristic feature of a photosensitised reaction is that the light absorbing species remains unchanged whilst the acceptor molecule undergoes chemical reactions.

The quenching efficiency of oxygen is due to its paramagnetic property, i.e. having two outer electrons with parallel spins. The absorption of visible light generally leads to electronic excitation of the photosensitizer molecules and since oxygen permeates most organic matter in solution it quenches their electronic excited state. This results in formation of singlet molecular oxygen which acts as an oxidising agent for the organic molecules present in the solution (DeRosa and Crutchley, 2002). This is the basis for photodynamic inactivation (PDI) of microorganisms and PDT of cancers, dental, skin and autoimmune diseases (Costa et al., 2013, Lucena et al., 2015, Dolmans et al., 2003, Usuda et al., 2006).

Molecular oxygen has two low lying singlet oxygen excited states $^1\Delta_g$ and $^1\sum_g^+$, 95 and 158 KJ mol^{-1} respectively above the triplet state (DeRosa and Crutchley, 2002). The electronic configurations of these states differ only by π-antibonding orbitals. The first singlet oxygen excited states $^1\Delta_g$ is different from the ground state $^3\sum_g^-$ because of its last two electrons which have antiparallel spins in one orbital. In the second excited state $^1\sum_g^+$, the electronic configuration is identical to that of the ground state except that the last two electrons have antiparallel spins. The transition from $^1\Delta_g$ state to the $^3\sum_g^-$ state is spin forbidden, thus the $^1\Delta_g O_2$ is relatively long-lived species. The second excited state of oxygen, on the other hand, is short-lived due to spin allowed transition to $^1\Delta_g$ state (DeRosa and Crutchley, 2002).

Once dioxygen is in its singlet excited state, it can be deactivated by other species to return to its ground state. Singlet oxygen is more electrophilic than oxygen, thereby reacting rapidly with unsaturated carbon-carbon bonds, nucleophiles such as sulphides and amines, and anions (DeRosa and Crutchley, 2002).

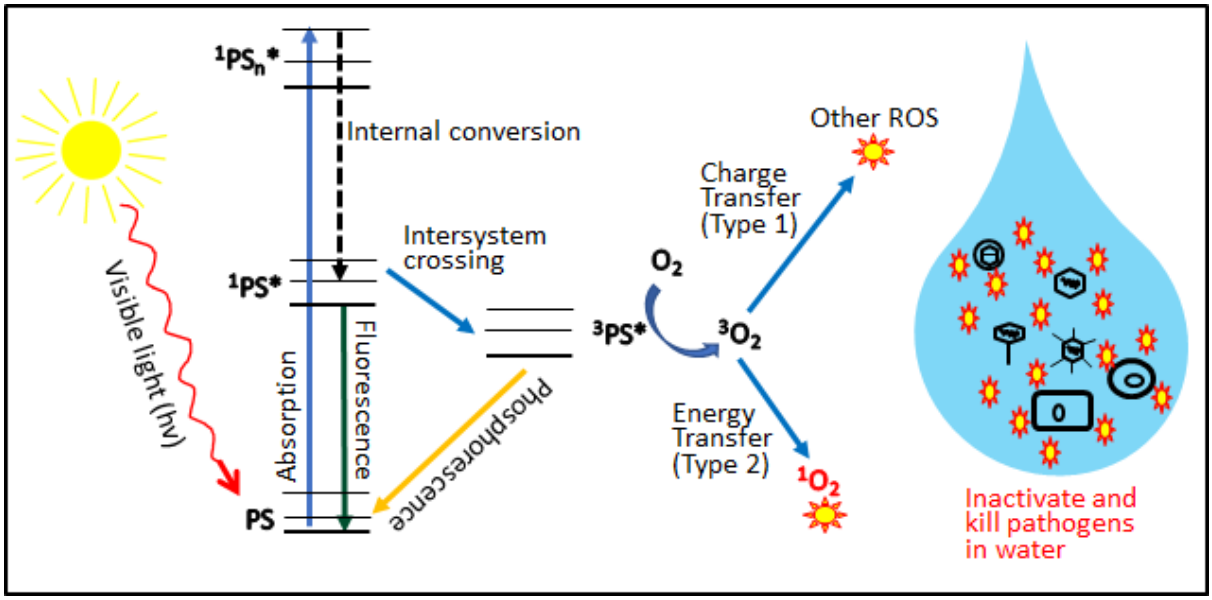

Figure 1. 7: Jablonski diagram showing photosensitisation. PS, photosensitiser at ground state; ^{1}PS*, photosensitiser at singlet excited state; ^{3}PS*, photosensitiser at triplet excited state; O_2, molecular oxygen in aqueous solution; $^3O_2$, triple oxygen; $^1O_2$*, singlet oxygen; other ROS: $O_2^{\cdot}$, superoxide anion; $O_2^{\cdot -2}$, peroxide; .OH, hydroxyl radical; OH-, hydroxyl ion; The singlet oxygen and other ROS oxidise and cause irreversible damage to proteins, lipids, nucleic acid and other cellular components of microorganisms including viruses and ultimately inactivates them (Costa et al., 2013, DeRosa and Crutchley, 2002).

1.6 Photosensitisers used for photodynamic inactivation of microorganisms

Photosensitisers are molecules capable of absorbing light and become excited to form a long lived excited triplet state. Several photosensitisers including methylene blue, Rose Bengal, porphyrines and phthalocyanines have been identified and used for PDT and PDI (Table 1.8) (DeRosa and Crutchley, 2002). After earlier studies with photosensitisers in solution, it has become clear that the desired properties of a good photosensitiser should include good solubility in water, intense absorption in the visible region (preferably extending to the near infra-red), good stability upon prolonged storage in aqueous solution, with few or no side photoreactions, high triplet yield and efficient production of separate ion products upon irradiation in the

presence of electron donor or acceptor (DeRosa and Crutchley, 2002). Organic dyes and aromatic hydrocarbons such as Rose Bengal, eosin and methylene are very good photosensitisers because they possess triplet states of appropriate energies for oxygen sensitisation. These dyes exhibit intense absorption within the visible spectrum and show high singlet oxygen yields (DeRosa and Crutchley, 2002). Many porphyrins and phthalocyanines (either in solution or attached onto solid supports) have been used and reported in photodynamic inactivation experiments (Table 1.8) because they have most, if not all of desired properties of a good photosensitiser. Additionally, because of their presence in natural systems, it is believed that porphyrins and phthalocyanines might generally lack cytotoxicity in the dark. This is good in some applications where only photosensitisation is required (DeRosa and Crutchley, 2002). Some experts have shown and argued that since most microorganisms have net negative charge, cationic photosensitisers (Table 1.3) should be more efficient in PDI of bacteria and viruses. This is due to positive charge favouring binding of photosensitiser molecule at critical cellular sites, that once damaged by exposure to light, cause loss of cell viability. Also, because the negatively charged microorganisms can bind to the positively charged photosensitiser, this increases the proximity of microorganisms to the singlet oxygen generated. Thus, rate and extent of PDI is faster and higher as compared to anionic and neutral photosensitisers (Alves et al., 2009, Costa et al., 2012a, Eichner et al., 2012). Furthermore, many PDI studies have revealed that just like other antimicrobial agents, there are factors that proportionally affect it. Several reports (Table 1.8) have shown that the rate and extent of PDI of microorganisms is dependent on the concentration/dose of photosensitiser and time/duration of PDI. However, there are

very few investigations of how other factors such as source of light, light intensity, co-pollutant and type of microorganisms could affect PDI of microorganisms. In most of the PDI studies (Table 1.8), much of the work has been focused on the physical and quantitative aspects of the inactivation with no or little emphasis on the molecular targets of the PDI within the microorganisms or its mechanisms from a biological perspective. Although, there are studies that demonstrate the evolution of viruses to drugs and common water disinfectants (Zhong et al., 2016), there are none that show whether viruses could be resistant to PDI.

Table 1. 8: Summary of some photodynamic inactivation studies with photosensitisers in solution

PS	Q	C (μM)	Light source	Light intensity ($mW\ cm^{-2}$)	Illumination time (min)	Model organism	PDI reductions of log PFU/ml or CFU/ml	Reference
TPF	+3	50	WL[1]	4	270	*V. fischeri*	≈7	(Alves et al., 2011)
TPM	+4	5	"	"	"	*E. coli*	6.2	(Tavares et al., 2011)
TSF	+3	0.5	"	"	"	"	6.1	"
TPP	+4	50	WL[2]	200	20	*P. chrysogenum*	3.4	(Gomes et al., 2011)
TPM	"	5	"	169	45	T4-like	>7	(Costa et al., 2010)
TPF	+3	"	"	"	25	"	>7	"
TPM	+4	1	"	"	30	"	1.3	"
TPF	+3	"	"	"	"	"	2.2	"
TPM	+4	5	Sun	60	180	"	7.0	"
TPF	+3	"	"	"	90	"	7.2	"
TPM	+4	0.5	"	"	"	"	0.1	"
TPF	+3	"	"	"	"	"	1.5	"
TPM	+4	5	WL[1]	4	270	"	7.2	"
TPF	+3	"	"	"	180	"	7.0	"
TPM	+4	1	"	"	270	"	1.5	"
TPF	+3	"	"	"	"	"	3.6	"
TPM	+4	5	"	"	"	*E. coli*	6.2	(Alves et al., 2013)
TPF	+3	"	"	"	"	"	7.7	"
TPM	+4	0.5	"	"	40	*S. warneri*	0.4	"
TPF	+3	"	"	"	"	"	4.8	"
TPM	+4	"	"	40	270	T4-like	<2	(Costa et al., 2008)
"	"	1	"	"	"	"	<2	"
"	"	5	"	"	"	"	>7	"
TPF	+3	0.5	"	"	"	"	≈2	"
"	"	1	"	"	"	"	≈4	"

Table 1.8 continued

TPF	+3	5	WL[1]	40	180	T4-like	>7	(Costa et al., 2008)
TPMM	"	0.5	"	"	270	"	≈1	"
"	"	1	"	"	"	"	≈2	"
"	"	5	"	"	"	"	>7	"
TPMC	"	0.5	"	"	"	"	<1	"
TPMC	"	1	"	"	"	"	<1	"
TPMC	"	5	"	"	"	"	3.9	"
DiPa	+2	0.5	"	"	"	"	<0.2	"
"	"	1	"	"	"	"	<0.2	"
"	"	5	"	"	"	"	>1	"
DiPo	"	0.5	"	"	"	"	<0.2	"
"	"	1	"	"	"	"	<0.2	"
"	"	5	"	"	"	"	<1	"
MB	+1	≈0.1	WL[3]	9	10	*H. pylori*	≈1	(Choi et al., 2010)
"	"	≈0.15	"	"	"	"	≈4	"
"	"	≈1	"	"	"	"	≈8	"
TMPyP	+4	1000	UV	2.2	1	MS2	>4.1	(Casteel et al., 2004)
TMPyP	"	10	"	"	"	"	>4.1	"
TPPS	"	1000	"	"	30	"	>3.8	"
TPPS	"	10	"	"	"	"	>3.6	"
TMPyP	"	"	"	"	10	HAV	>3.7	"
TPPS	"	10	UV	2.2	90	HAV	3.6	"
TBuPyP	"	"	"	"	30	"	>3.8	"
TOcPyP	"	"	"	"	1	"	>3.9	"
TPF	+3	5	WL[1]	4	90	*P. damselae*	≈8	(Arrojado et al., 2011)
"	"	"	"	"	180	*P. piscicida*	≈8	"
"	"	"	"	"	"	*V. parahaemolyticus*	≈8	"
"	"	"	"	"	270	*V. anguillarum*	≈8	"

Table 1.8 continued

"	"	"	"	"	"	*Pseudomonas* sp.	≈8	"
TPF	+3	"	"	"	180	*E. coli*	≈8	(Arrojado et al., 2011)
"	"	"	"	"	270	*A. salmonicida*	>6	"
"	"	"	"	"	90	*E. faecalis*	≈8	"
"	"	"	"	"	60	*S. aureus*	≈8	"

The photosensitisers used were: TPF, 5, 10, 15-tris (1-methylpyridinium-4-yl)-20-(pentafluorophenyl) porphyrin tri-iodide; TPM, 5,10,15,20-tetrakis (1-methylpyridinium-4-yl) porphyrin tetra-iodide; TSF, 5-(pentafluorophenyl)-10,15,20-tris [2,3,5,6-tetrafluoro-4-(1-methylpyridinium-4-ylsulfanyl) phenyl] porphyrin tri-iodide; TPP, 5,10,15,20-tetrakis (N-pentylpyridinium-4-yl) porphyrin tetra-iodide; TPMM, 5-(4-methoxy carbonylphenly)-10,15,20-tris (*N*-methylpyridium-4-yl) porphyrin tri-iodide; TPMC, 5-(4- carboxyphenly)-10,15,20-tris (N-methylpyridium-4-yl) porphyrin tri-iodide; DiPa, 5, 10-bis (4- carboxyphenly)-15,20-bis (N-methylpyridium-4-yl) porphyrin di-iodide; DiPo, 5, 15-bis (4- carboxyphenly)-10,20-bis (N-methylpyridium-4-yl) porphyrin di-iodide; TMPyP, Meso-tetrakis (N-methyl-4-pyridiniumyl) porphyrin tetratosylate; TPPS, Tetrakis (4-sulfonatophenyl) porphyrin; TBuPyP, Tetrakis (N-[n-butyl] -4-pyridiniumyl) porphyrin; TOcPyP, Tetrakis (N-[n-octyl] -4-pyridiniumyl) porphyrin. PS, photosensitiser; Q, net charge of photosensitiser in solution; C, concentration of photosensitiser used for the PDI; WL^1, white light (PAR radiation, 380-700 nm, 13 OSRAM 21 lamps of 18 W each; WL^2, white light from a compatible fiber optic probe (400-800 nm) attached to a 250 W quartz/halogen lamp; WL^3, fujinon endoscopy system EPX-4400, EG-590WR. *V. fischeri, Vibrio fischeri*; *E. coli*, *Escherichia coli*; *P. chrysogenum*, *Penicillium chrysogenum*; T4-like, bacteriophage T4-like; *S. warneri, Staphylococcus warneri*; *H. pylori, Helicobacter pylori*; MS2, bacteriophage MS2; HAV, Hepatitis A virus; *P. damselae, Photobacterium damselae; P. piscicida, Photobacterium piscicida; V. parahaemolyticus; Vibrio parahaemolyticus; V. anguillarum, Vibrio anguillarum; A. salmonicida, Aeromonas salmonicida; E. faecalis, Enterococcus faecalis; S. aureus, Staphylococcus aureus.*

1.7 Biological targets of singlet oxygen

Singlet oxygen is the most common ROS implicated in the PDI of bacteria and viruses (Costa et al., 2013). Singlet oxygen can react with a range of biomolecules such as proteins, DNA, RNA and lipids. Singlet oxygen readily and rapidly reacts with proteins with a bimolecular rate constant ranging from 10^5 to 10^9 M^{-1} S^{-1}. This is much higher than with other biomolecules including RNA, where the rate constant ranges from 10^4 to 10^6 M^{-1} S^{-1} (Cho et al., 2010, Davies, 2003). The interaction of singlet oxygen with potential targets can either be by physical quenching, which is only observed in tryptophan, or chemical modification which is observed in almost all amino acids. Chemical modification usually results in irreversible changes in amino acids (Davies, 2003). The bimolecular rate constant and oxidation effects and products vary among different amino acids (Table 1.9). Amino acids tryptophan, histidine, methionine, cysteine and tyrosine are the most susceptible to singlet oxygen mediated oxidation (Table 1.9). Side chains of some α-amino acids, principally the aromatic and sulphur containing amino acid residues, unsaturated lipids and nucleic acids are most likely the targets of PDI in microorganisms. These constituents are associated mainly with cellular and subcellular membranes such as plasma, mitochondrial, lysosomal and nuclear membranes in bacterial and eukaryotic cells, as well as the viral envelope glycoproteins, coat proteins, host receptor recognition and binding proteins. However, little is known about the exact mechanism of PDI, especially in viruses because of diversity of the viral components (Costa et al., 2013). Gram positive bacteria are easily inactivated by singlet oxygen oxidation as compared to gram negative bacteria due to differences in the structure of their cell membrane (Alves et al., 2013, Bourre et al., 2010, Carvalho et al., 2007, Costa et al., 2012a, Komagoe et

al., 2011, Maisch et al., 2012a). Gram negative bacteria have an additional outer membrane apart from the cytoplasmic (inner) membrane (Figure 1.8), giving them extra protection against antimicrobial agents including singlet oxygen and other ROS produced during photosensitisation. For viruses, although protein photo-oxidation by singlet oxygen has been extensively studied and the most sensitive viral components are protein in nature, it is an over-generalisation to assume a particular mechanism of protein photo-oxidation for viral PDI. This is because apart from diversity of PDI targets within viruses, the reaction of singlet oxygen with proteins can produce a range of effects such as oxidation of side chains, peptide backbone fragmentation, dimerisation/aggregation, unfolding or conformal changes, enzymatic inactivation and alterations in cellular handling and turnover (Gracanin et al., 2009, Gracanin et al., 2007).

Table 1. 9 : The most susceptible amino acids to singlet oxygen mediated oxidation

Amino acid	***k*** **(M^{-1} S^{-1})**	**Oxidation products**	**Effects of $^1O_2$* mediated oxidation on protein**
Trp	3×10^7 $2\text{-}7 \times 10^7$	Dioxetane, hydroperoxide, *N*-formylkynurenine, kynurenine, aspartic acid, CO_2, NH_3	Protein peroxide formation, side chain product formation, enzyme inactivation
His	3.2×10^7	Endoperoxides, aspartic acid, asparagine derivatives and urea, His-His and His-Lys crosslinks	Protein peroxide formation, side chain product formation, formation of cross-links and aggregates, enzyme inactivation
Met	1.6×10^7	Sulphoxide, H_2O_2	Protein peroxide formation, enzyme inactivation
Cys	8.9×10^6	Disulphide, cysteic acid	Formation of cross-links and aggregates
Tyr	0.8×10^7	3a-hydroxy-6-oxo-2,3,3a,6,7,7a-hexahydro-1H-indole-2-carboxylic acid (HOHICA)	Protein peroxide formation, side chain product formation, back bone fragmentation, enzyme inactivation

List of the most susceptible amino acids to singlet oxygen mediated oxidation as well as their oxidation products and effects on proteins. Trp (Tryptophan), His (Histidine), Met (Methionine), Cys (Cysteine) and Tyr (Tyrosine) (Davies, 2003).

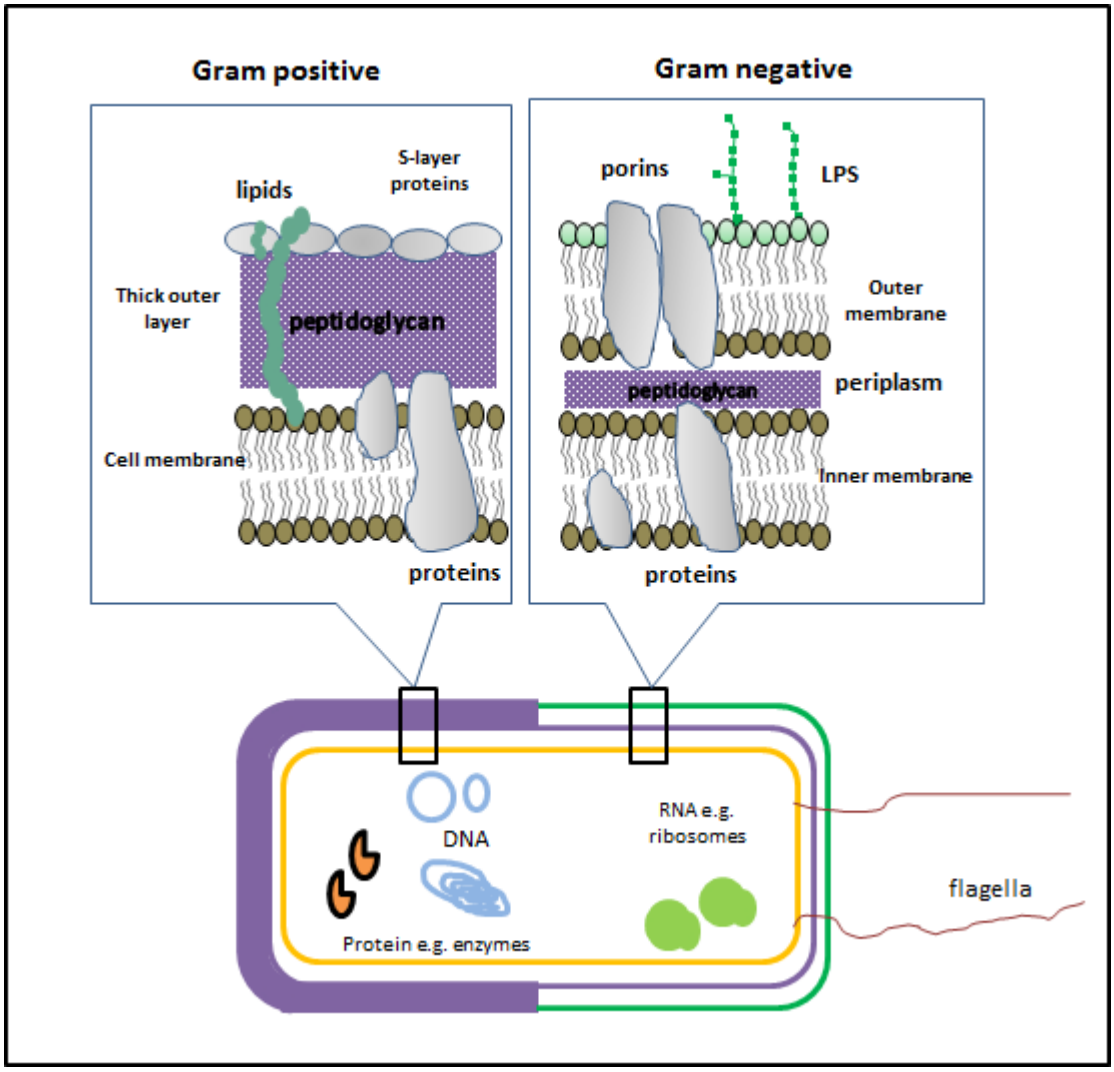

Figure 1. 8: Schematic of a bacterial cell showing the differences in the structure and morphology of membrane of Gram positive and Gram negative bacteria. Gram positive bacteria have one cytoplasmic membrane while gram negative bacteria have additional outer membrane apart from the cytoplasmic (inner) membrane, giving them an extra protection against antimicrobial agents including singlet oxygen and other ROS produced during photosensitisation process (Ahmed et al., 2014a).

1.8 Photodynamic inactivation of viruses

Photodynamic inactivation (PDI) of viruses has been shown to be an efficient alternative to antiviral agents in the control of resistant and emerging viruses (Costa et al., 2012b, Casteel et al., 2004, Costa et al., 2008, Costa et al., 2010, Costa et al., 2009, Wainwright, 2004). When irradiated with visible light and in the presence of molecular oxygen in aqueous solution, photosensitisers such as 5,10,15,20-tetrakis

(1-methyl-4-pyridinio)porphyrin tetra *p*-toluenesulfonate (TMPyP) can generate singlet oxygen by a type 2 reaction and other ROS by type 1 reaction (Costa et al., 2013, Costa et al., 2014, DeRosa and Crutchley, 2002). Singlet oxygen and other ROS can react rapidly and cause irreversible damage to biomolecules thereby leading to the inactivation of viruses and other microorganisms (Costa et al., 2013, Baumler and Maisch, 2012, Maisch et al., 2012b, Spannberger et al., 2012, Alves et al., 2013, Carvalho et al., 2007, Komagoe et al., 2011). Singlet oxygen is the most likely ROS involved in the viral PDI (Costa et al., 2013, Silverman et al., 2013). All ROS have a short-life and high reactivity, thereby causing damage only to the surrounding molecules close to the point of ROS generation (Costa et al., 2013). Capsid proteins including host recognition proteins are immediate targets of singlet oxygen mediated oxidation in non-enveloped viruses, while envelope glycoproteins, including host-recognition proteins are potential targets of singlet oxygen oxidation in enveloped viruses. (Figure 1.9). Prolonged exposure to singlet oxygen may also result in oxidative damage to viral nucleic acid (Davies, 2003, Gracanin et al., 2009, Hotze et al., 2009, Cho et al., 2010).

Although virus capsids serve to protect the genome, they may contain small pores. Furthermore, under physiological conditions, the capsids of non-enveloped viruses can undergo constant motion that suggests a dynamic state otherwise referred to as “capsid breathing” e.g. picornaviruses (Lewis et al., 1998, Jimenez-Clavero et al., 2000, Pulli et al., 1998), nodaviruses (Bothner et al., 2005), tombusviruses (Jaegle et al., 1988), sobemoviruses (Witz and Brown, 2001) and others. By means of a thermofluor assay that incorporates a pair of dyes to bind the nucleic acid and hydrophobic capsid residues respectively, capsid permeability of picornaviruses has

been shown to increase with temperature (Wang et al., 2015, Adeyemi et al., 2017, Walter et al., 2012). Although the permeability of viral capsids to singlet oxygen molecules has not been shown, it has been suggested that access to the viral genome could result to oxidation-induced damages to the viral genome as well or the capsid.

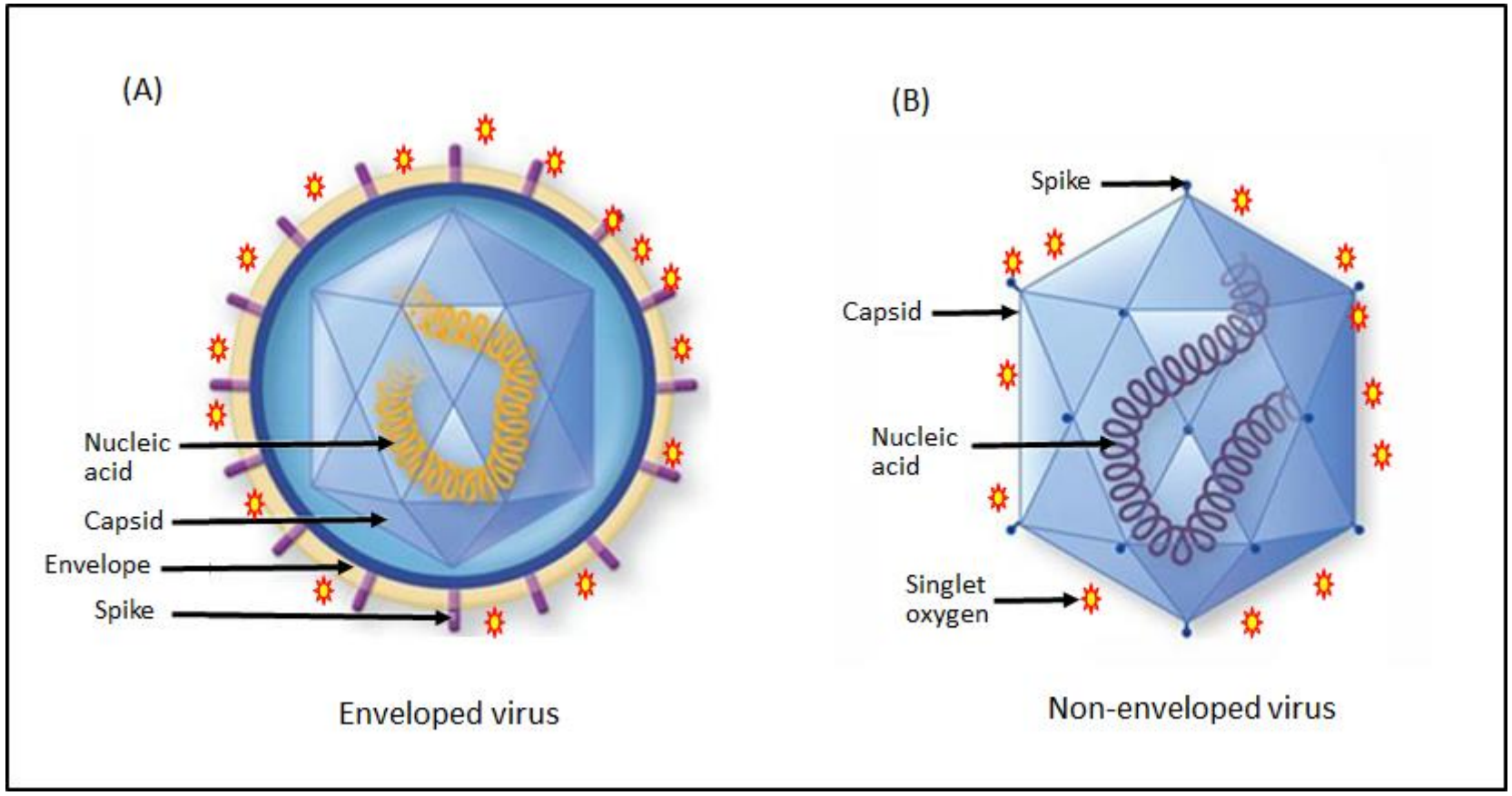

Figure 1. 9: Schematic of (A) enveloped and (B) non-enveloped viral particles showing first targets of singlet oxygen mediated oxidation. Envelope including host recognition glycoproteins/spikes are the first targets of the oxidation in enveloped viruses while in non-enveloped viruses, capsid proteins including host recognition proteins and spikes are the immediate targets of the oxidation.

1.9 Solid supports for attaching photosensitisers

The possibility of removing supported porphyrins and other photosensitiser from environmental or drinking water after phototreatment is attractive as it can allow re-use of sensitiser functionalised solid supports thereby reducing the cost. Also, because the sensitisers will not be let into the water during and after treatment, it would be an environmental-friendly technology. However, all these features could be achieved by finding the right solid supports and coupling chemistry for attaching the desired sensitisers.

Studies are on-going for the development of novel hybrid materials (e.g. polymers, silica, glass) for attachment of photosensitisers which could be used to efficiently inactivate bacteria and viruses in water. The focus of the studies has been on producing a solid phase support with the desired physical, chemical and mechanical characteristics (Table 1.10).

Table 1. 10: Desired characteristics of a solid phase support for attachment of photosensitisers

Physical characteristics	Chemical characteristics	Mechanical characteristics
• a large surface to volume ratio	• easy and reproducible immobilization	• good mechanical strength
• good porosity and compatibility with the photosensitiser	• avoids photosensitiser leaching to the water	• stability towards sunlight
• high biocompatibility to maximize the interaction between the immobilized sensitizer and the microorganism	• good oxygen permeability for efficient singlet oxygen quenching	
• commercial availability and low cost		
• insolubility in water		

List of desired characteristics of a solid phase support for attaching photosensitisers for water disinfection application (Li et al., 2008, Narband et al., 2009, Ma et al., 2005, Bechet et al., 2008)

Solid supports such as chitosan electrospun nanofibers and polymeric membranes fulfil most of the desired qualities required for the attachment of photosensitisers for photodynamic disinfection of water (Suchanek et al., 2014, Crini and Badot, 2008). Nanofiber cloths are made-up of fibres with diameters ranging from tens of nm to a few µm and are often produced by the process of electrospinning. Several electrospun nanofibers have been successfully produced from different polymers (Table 1.11). A nanofiber could either be produced from one polymer or a blend of 2 or more polymers (Table 1.11). Depending on the coupling chemistry needed, their

surfaces can be modified with functional groups possessing a diverse array of chemical properties. Electrospun nanofibers have found applications in tissue engineering, drug delivery systems, wound dressing, antibacterial fabrics, water desalination and filtration, protective clothing and biosensors (Haider et al., 2015). The polymeric architecture and nature of electrospun nanofibers provides a functional nano-environment and can alter the photophysical behaviour of photosensitisers and affect the photoreaction activity and selectivity (Suchanek et al., 2014). Hypothetically, the small diameter and porosity of nanofiber should allow diffusion of the singlet oxygen (and other ROS) outside of the fibres where biological and organic chemical targets can be oxidised. Retention and maintenance of a porous structure by electrospun nanofibers even after attachment of photosensitisers and immersion in several solutions of varying pH and temperature is of importance if they are to be used continuously to generate ROS for water disinfection.

Table 1. 11: Types of electrospun nanofibers

Polymer	Reference	Polymer	Reference
PAN	(Mei et al., 2012)	Whey protein*	(Sullivan et al., 2014)
PAA	(Haider et al., 2015)	Elastin*	(Huang et al., 2000)
PVA	(Hang et al., 2010)	Soy protein*	(Gerstenhaber et al., 2014)
PCL	(Ramesh Kumar et al., 2012)	Wheat protein*	(Woerdeman et al., 2005)
HA*	(Ji et al., 2006)	PCL-EEP	(Haider et al., 2015)
Chitosan*	(Schiffman and Schauer, 2007)	PGA	"
CA*	(Deng et al., 2013)	PLA	(Thakur et al., 2008)
PVP	(Ramesh Kumar et al., 2012)	PLA/PCL	(Del Valle et al., 2011)
PLGA	(Katti et al., 2004)	PLA/PEVA	(Hong et al., 2008)
PEVA	(Ramesh Kumar et al., 2012)	Collagen*	(Rho et al., 2006)
PVDF	"	PLA/PEG/PU	(Haider et al., 2015)
PES	"	PLA/Collagen	(Torres-Giner et al., 2012)
PET	"	PAN/PLA	(Haider et al., 2015)
PEO	"	PLA/PEG	"
Chitosan/PEO	(Spasova et al., 2004)	CA/PEU	(Liu et al., 2012)
PU	(Haider et al., 2015)	PDLA/PEO	(Heunis et al., 2011)
PCL/PEG	(Zhang et al., 2005)	PLA/PCL/PAN/PVA/ PEO	(Au et al., 2012)
PCL/Collagen	"	PLA/ Chitosan	"
Gelatin*	(Huang et al., 2004)	PVA/ Chitosan	(Hang et al., 2010)
PGA/Chitin	(Haider et al., 2015)	PU/PVA/Silk fibroin	(Lee and Lee, 2012)
Fibrinogen*	(Wnek et al., 2003)	Nylon 6	(Haider et al., 2015)
Chitin*	(Holzwarth and Ma, 2011)	PET/PCL/PEO	(Cooper et al., 2013)
Silk fibroin*	(Hang et al., 2012)		

List of electrospun nanofibers from different polymers. PAN, Polyacrylonitrile; PAA, Polyacrylic acid; PVA, Polyvinyl alcohol; PCL, Polycaprolactone; HA, Hyaluronic acid; CA, Cellulose acetate; PVP, Poly (vinylpyrrolidone); PLGA, Poly (lactic acid-co-glycolic acid); PEVA, Poly (ethylene-co-vinyl acetate); PVDF, Polyvinylidene fluoride; PES, polyether sulfone; PET, Polyethylene terephthalate; PEO, Polyethylene oxide; PU, Polyurethane; PGA, Polyglycolic acid; PLA, Polylactic acid; PCL-EEP, Poly (caprolactone-co-ethyl ethylene phosphate); PEG, Polyethylene glycol; PDLA, Poly (D, L-Lactic acid). (*), Biopolymers.

1.10 Chitosan

Chitosan (Figure 1.10) is a partially deacetylated form of chitin which is the most abundant aminopolysaccharide in nature. It can be found in the exoskeleton of crustaceans, the cuticles of insects, and the cell walls of fungi (Crini and Badot, 2008). Chitin is usually extracted from waste materials of the sea food-processing industries, such as crab shells, shrimp, prawn and krill (Crini and Badot, 2008). Thus, chitin is a high abundant waste material and this makes chitosan a low cost material. In addition, chitosan is non-toxic, biocompatible, biodegradable, rigid, insoluble in water, adsorbable and has many reactive amine groups for chemical activation and crosslinking. This makes it one of the most used support biomaterial in many fields including agriculture, biomedical engineering, biotechnology, chemical industry, cosmetics and toiletries, food production, pharmaceutics, textiles and dentistry (Crini and Badot, 2008, Tangpasuthadol et al., 2003, Hoven et al., 2007, Amornchai et al., 2004).

Chemically, chitosan is a linear homopolymer which is composed of β (1-4)-linked N-acetyl glucosamine. It is structurally similar to cellulose, but it is an aminopolymer and has acetamide groups at the C-2 positions instead of hydroxyl groups. The repeating units of β (1-4)-linked N-acetyl glucosamines have large number of hydroxyl and amino groups which offer several possibilities for functionalisation and immobilisation of biological and photo-active molecules. Several studies showed that because chitosan has intrinsic characteristics such as its low cost and outstanding chelating behaviour, it is a good biosorbent material for waste water remediation of dyestuff and heavy metals (Crini and Badot, 2008, Crini et al., 2008, Hoven et al., 2007, Krajewska et al., 1990, Martel et al., 2001).

In this work we chose chitosan electrospun nanofibers and membranes as solid supports for attaching the photosensitiser TMPyP for development of sunlight driven water disinfection system that is cheap, simple, efficient and environmental friendly.

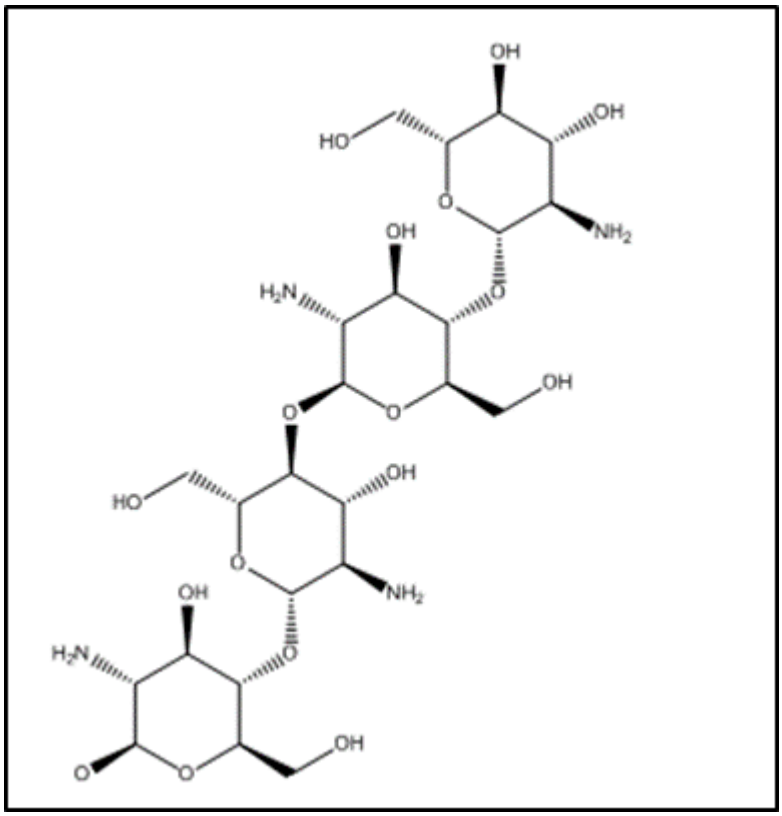

Figure 1. 10**:** Chemical structure of chitosan. The amine side chains are useful reactive groups for coupling of photosensitisers and other modifications; they are shown as neutral but at pH 7.0 would be protonated. The chitosan structure was from ChemACX.com, ChemDraw Pro 13.0.

1.11 Coupling chemistry

Irreversible covalent bonding of a photosensitiser onto a solid support is possible when functional groups are available and chemically compatible. Reactive groups that are able to couple with amine containing materials are by far the commonest (Hermanson, 2013). The main coupling reaction for modification of amines occurs by nucleophilic attack e.g. acylation (Figure 1.11) (Hermanson, 2013). Most of these reactions are rapid and give a stable amide bond (Figure 1.11). However, in some

cases, and to increase the coupling efficiency, N-hydroxy succinamide (NHS) ester, which is the most common activation chemistry for creating acylation agents, is often used (Hermanson, 2013)(Figure 1.11 B). Carbodiimides such as 1-ethyl-3-(3-dimethylaminopropyl) carbodiimide (EDC) are zero-length crosslinking agents often used to mediate the formation of an amide bond between a carboxylate group and an amine (Figure 1.11 Ci and Cii)(Hermanson, 2013). Acid anhydrides are also very reactive toward nucleophiles and can acylate many important functional groups including amino group. Upon nucleophilic attack, the anhydrides yield one carboxylic acid for every acylated product. If the acid anhydride is dicarboxylic such as succinic acid anhydride (SA), upon reaction with a nucleophile, the ring structure of the anhydride opens, forming the acylated product modified to contain a newly formed carboxylate group (Figure 1.11 D) (Hermanson, 2013). Amine reaction involving dianhydrides such as pyromelitic dianhydride will typically generates three free carboxyl groups since the second anhydride ring is prone to attack by H_2O, i.e. it is easily hydrolysed. This was the chemistry we used in this work (Section 5.2.2) to modify chitosan electrospun nanofiber and polymeric membrane. Direct covalent coupling of TMPyP onto chitosan was not possible, so, the nanofibers/membranes were first modified by pyromellitic dianhydride in order to introduce carboxyl groups and facilitate electrostatic adsorption of the highly basic TMPyP.

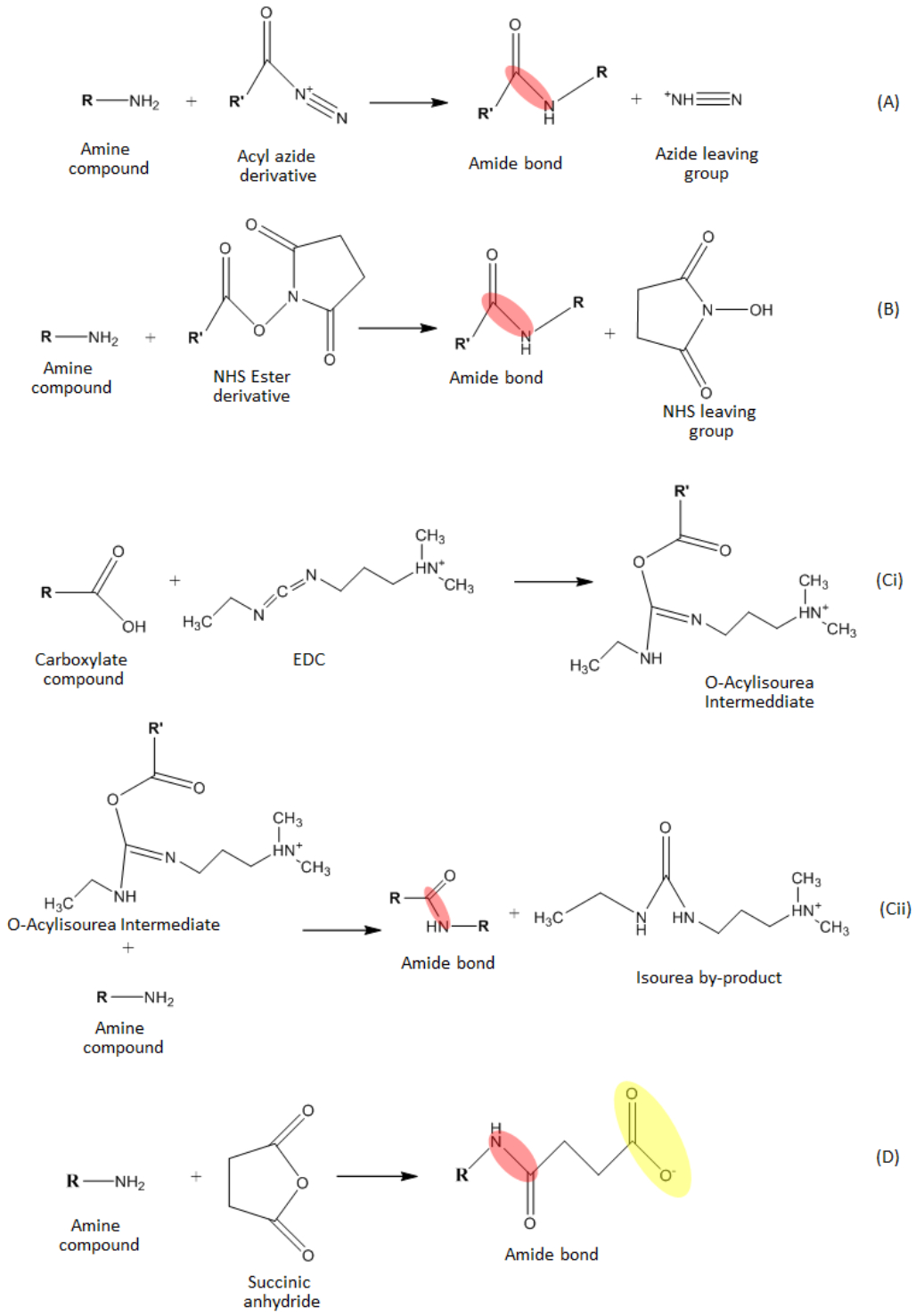

Figure 1. 11: Amine coupling reaction schemes. These are some examples of amine coupling reactions that proceed by acylation to form amide bond (highlighted in red). (NHS), N-hydroxy succinamide ester, is the most common activation chemistry for creating acylation agents. (EDC), 1-ethyl-3-(3-dimethylaminopropyl) carbodiimide, is a zero-length crosslinking agent often used to mediate the formation of an amide bond between a carboxylate group and an amine. Reaction scheme (D) was used in this work to modify chitosan electrospun nanofibers and polymeric membranes to generate carboxylate groups (highlighted in yellow). The schemes were prepared by ChemDraw Pro 13.0 (Hermanson, 2013).

Reactive groups able to couple with sulfhydryl containing materials are the second commonest after amino reactive reagents (Hermanson, 2013). The main coupling reactions for modification of sulfhydryls occur by either alkylation or disulfide interchange to form a thioether or disulfide bond (Figure 1.12)(Hermanson, 2013). Compounds that have disulfide groups can participate in disulphide exchange reactions with another thiol (Figure 1.12 C). The disulfide exchange involves attack of the thiol at the disulfide, thereby breaking –S-S- bond, with subsequent formation of a new mixed disulfide comprising a portion of the original disulfide compound (Figure 1.12 C) (Hermanson, 2013). A vinylsufone group can be used to couple with nucleophiles especially thiol groups in aqueous solution and under mild conditions (Figure 1.12 D). The vinylsufone group can also react with amines and hydroxyls under higher pH (Hermanson, 2013). Metal ions can interact with thiol containing molecules to form thioether bonds commonly called dative or coordinate bonds (Figure 1.12 E). The dative bond differ from normal covalent bonds because they are formed by two electrons from a single atom, instead of two atoms each sharing one electron (Hermanson, 2013).

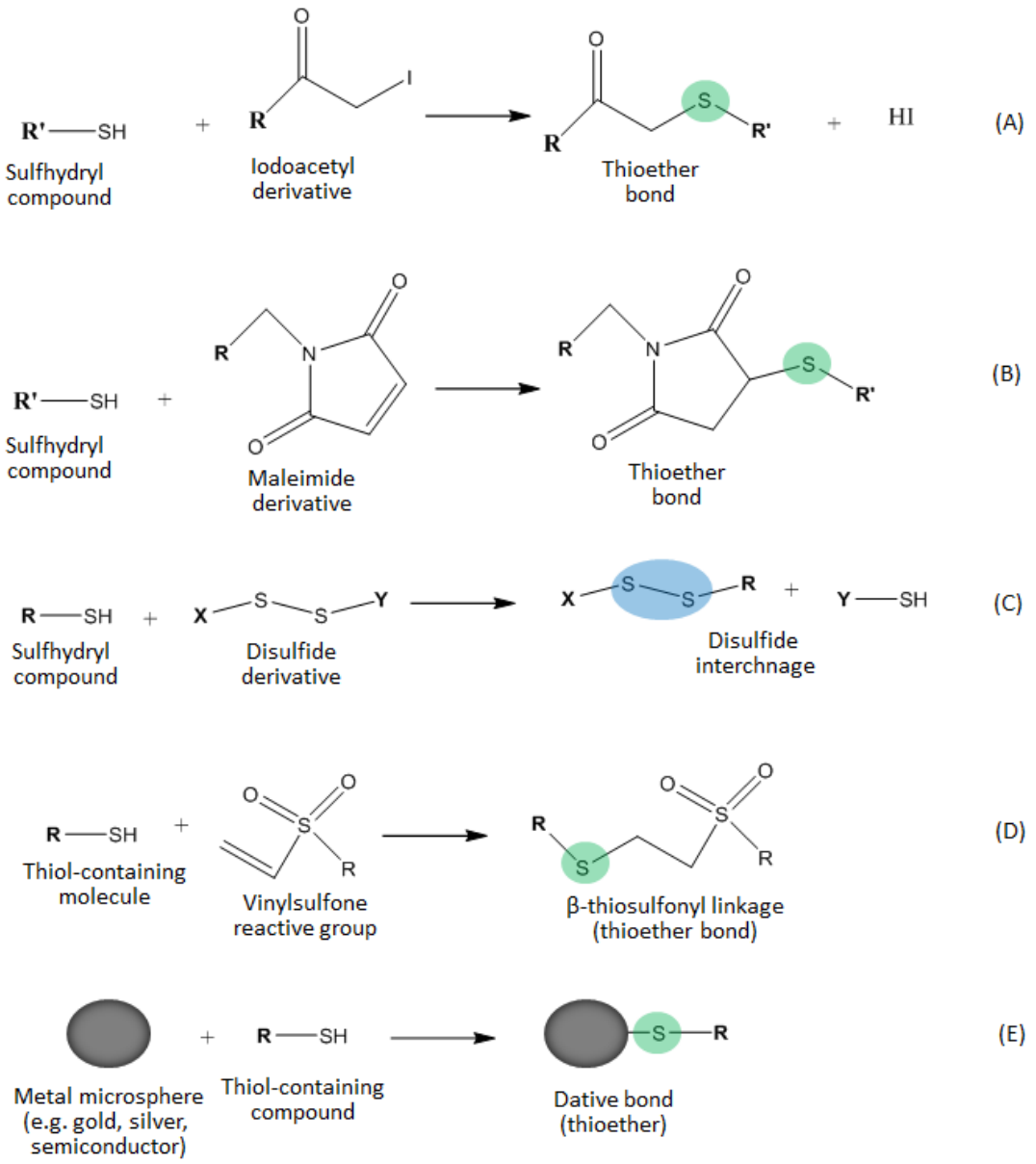

Figure 1. 12: Thiol coupling reaction schemes. These are some examples of thiol coupling reactions that proceed by alkylation to form thioether bond (highlighted in green). Reaction scheme (C) is an example of disulfide inter change to form another disulfide linkage (highlighted in blue). The schemes were prepared by ChemDraw Pro 13.0 (Hermanson, 2013).

Photosensitisers can be bound to solid supports externally or incorporated within the supports for water purification applications (Table 1.12). The sensitisers can be attached at the point of making the solid supports, or for externally bound sensitisers, they can be attached after the production of the supports using suitable

coupling chemistry. Fewer chemicals are involved for internally bound sensitisers and hypothetically, such composite fibres should be safer for water purification. However, internally bound sensitisers have the limitation that the diffusion length of singlet oxygen is only tens to hundreds of nm and this limits photodynamic inactivation of microorganisms to areas in close proximity to the fibre surface (Henke et al., 2013). There are several studies that showed that immobilisation of photosensitisers onto the surface of inert solid supports does not impair their photobiological activities (Table 1.12). Many experts have shown successful immobilisation of photosensitisers onto solid supports such as chitosan polymeric membrane, electrospun nanofiber, silicate matrix, nanoparticles and nanomagnetic particles, glass fibres etc. could be used for photodynamic disinfection of microbial polluted water (Table 1.12).

Table 1. 12: Some studies that showed photodynamic inactivation of microorganisms with photosensitisers attached onto solid supports

Solid support	PS	Coupling chemistry	Photosensitiser bound externally or internally to support	Illumination time (min)	Model organisms	Antimicrobial effect	References
Electrospun nanafiber	TMPyP	Adsorption by ion-exchange	external	2	*E. coli*	**	(Henke et al., 2013)
"	TPP	Nano-spider electrospinning	internal	20	"	*	(Suchanek et al., 2014)
"	TMPyP	Adsorption by ion-exchange	external	"	"	**	"
Chitosan membrane	p-THPP	Adsorption from aqueous alkaline solution	"	90	"	**	(Bonnett et al., 2006)
"	p-TAPP	Dissolution and casting	Internal	"	"	**	"
"	ZnPcS	Covalent bonding	External	160	"	***	"
"	TMPyP	Dissolution and casting	Internal	180	"	**	(Camargo et al., 2014)
"	p-TAPP	"	Internal	"	"	**	"
Nano-magnetic particles	TMF	Covalent grafting	External	270	*E. coli, E. faecalis,* T4-like	***	(Carvalho et al., 2010)
"	TPF	Covalent grafting	External	270	"	***	"
"	TTPF	Covalent grafting	External	270	"	*	"

The photosensitisers used were: TMPyP, 5, 10, 15, 20-tetrakis (1-methyl-4- pyridinio) porphyrin tetra (p-toluenesulfonate); TPP, 5,10,15,20-tetraphenylporphyrin; p-THPP, 5,10,15,20-Tetrakis(p-hydroxyphenyl) porphyrin; p-TAPP, 5,10,15,20-Tetrakis (p-aminophenyl)porphyrin; ZnPcS, Zinc (II) phthalocyanine tetrasulfonic acid tetrasodium salt; TMF, 5,10,15-tris (1-methylpyridinium-4-yl)-20-(pentafluorophenyl) porphyrin tri-iodide; TPF, 5-(pentafluorophenyl)-10,15,20-tris (4-pyridyl) prophyrin; TTPF, 5-(pentafluorophenyl)-10,15,20-triphenyl prophyrin. *E. coli*, *Escherichia coli*; T4-like, bacteriophage T4-like; *E. faecalis, Enterococcus faecalis.* (***), strong antimicrobial effect; (**), moderate antimicrobial effect; (*), low antimicrobial effect. PS, photosensitiser.

1.12 Photosensitisers: Types and characteristics

There are several group of photosensitisers that have shown singlet oxygen generating ability. The singlet oxygen generating ability of a photosensitiser is measured by its quantum yield (Table 1.13). Singlet oxygen quantum yield (Φ_{Δ}) of a photosensitiser is the number of times a singlet oxygen is produced from an excited triplet state photosensitiser molecule per photon of light absorbed.

The methods used to measure the quantum yield of singlet oxygen generation ranges from;

- Direct detection of the luminescence produced (at 1270 nm) upon relaxation of singlet oxygen (time resolved or steady-state infrared luminescence).
- Calorimetric techniques (photoacoustic calorimetry and time resolved thermal lensing) and
- Quantitative analysis of photooxidation reactions (loss of absorbance, or fluorescence of a probe molecule or oxygen uptake)(DeRosa and Crutchley, 2002). The loss of absorbance caused by singlet oxygen mediated oxidation of 2-amino-3-hydroxypyridine was used in this work for quantitative analysis and indication of singlet oxygen generation by the photosensitisers TMPyP, Rose Bengal and methylene blue.

Table 1. 13: Some photosensitisers and their singlet oxygen quantum yield.

Photosensitiser	**Singlet oxygen quantum yield (Φ_Δ)**			**Reference**
	Φ_Δ (A)	**Φ_Δ (B)**	**Φ_Δ (C)**	
Rose Bengal	0.75	0.68	0.76	(Redmond and Gamlin, 1999)
Eosin blue	0.52	0.37		"
Methylene blue		0.52		"
MBQ	0.11			(Alegría et al., 1999)
SAS	0.44			"
H_2TPP		0.63		(Redmond and Gamlin, 1999)
MgTPP		0.62		"
ZnTPP		0.83		"
PdTPP		0.88		"
ZnPcTS	0.45			(Darwent et al., 1982)
Pc			0.16	"
PcTS			0.17	"
Haematoporphyrin	0.65			(Spiller et al., 1996)
Photofrin II	0.2			(Bonnett, 1995)
Bacteriochlorin	0.32			"
Benzoporphyrin	0.6			"
TMPyP	0.74			(Lei et al., 2010)

List of some photosensitisers and their singlet oxygen quantum yield in solution. MBQ, 2-methyl-1, 4-benzoquinone; SAS, sodium 9, 10-anthraquinone-2-sulfonate; TPP, tetraphynyl porphyrine; Pc, phthalocyanine; PcTS, phthalocyanine tetrasulfonate; TMPyP, 5, 10, 15, 20-tetrakis (1-methyl-4-pyridinio) porphyrin tetra (*p*-toluene sulfonate). (A), water; (B), ethanol; (C), methanol. These are the solvents in which singlet oxygen quantum yields of the photosensitisers were determined.

Organic dyes such as Rose Bengal, eosin and methylene blue (Figure 1.13) have good quantum yield of singlet oxygen (Table 1.13). Methylene blue is a phenothiazinium dye with a strong absorbance in the range 550-700 nm (DeRosa and Crutchley, 2002). Xanthene dyes such as Rose Bengal and eosin exhibit intense absorption in the range 480- 550 nm (DeRosa and Crutchley, 2002). Aromatic hydrocarbons such as napthalenes, anthracenes and biphenyls have also be shown to possess photosensitising ability (DeRosa and Crutchley, 2002, Redmond and Gamlin, 1999). Quinones and anthraquinone derivatives (Figure 1.13) have been reported to be an

excellent sensitisers for singlet oxygen generation in aprotic solvents (Alegría et al., 1999, DeRosa and Crutchley, 2002). Porphyrins and phthalocyanines (Figure 1.13) are another group of photosensitisers that has been shown to have high quantum yields of singlet oxygen in solution (Table 1.13). Porphyrins and their derivatives can absorb several wavelenths in the UV-vis range. The Soret band in the blue and the Q-band in the red are major bands which represent important components of sunlight (DeRosa and Crutchley, 2002). Porphyrins are a large class of deeply coloured red or purple, fluorescent crystalline pigments, with natural or synthetic origin, having in common a susbstituted aromatic macrocyclic ring joined by four methane bridging groups (Figure 1.13). The large planar core aromatic ring system (Figure 1.13) is believed to be an important feature because it is common to all of the tetrapyrrole inhibitors, whereas the peripheral substituents and metal ions (or lack thereof) can vary widely. The cyclic tetradentate (Figure 1.13) framework of the four central nitrogen atoms makes porphyrins a unique chelating agents; almost every metal on the periodic table is capable of forming a metalloporphyrin complex (Banfi et al., 2006, Oliveira et al., 2009). Porphyrins belong to compounds that form vital constituents of several important and diverse biological functions, and as such, all life form depends on the ability of porphyrins to undergo oxidation-reduction and electron transfer reactions. The porphyrin-type nucleuses along with metal ions are found in cytochromes, peroxidases and catalases, haemoglobin and myoglobin (Fe-porphyrin), chlorophyll (Mg-porphyrin), vitamin B12 (co-porphyrin) (Oliveira et al., 2009, Banfi et al., 2006). Phthalocyanines are derivatives of the porphyrin skeleton and in addition have nitrogen atoms linked to the individual pyrrole units (Figure

1.12). Extended conjugation by the peripheral benzene ring gives phthalocyanines the ability to absorb at longer wavelengths (DeRosa and Crutchley, 2002).

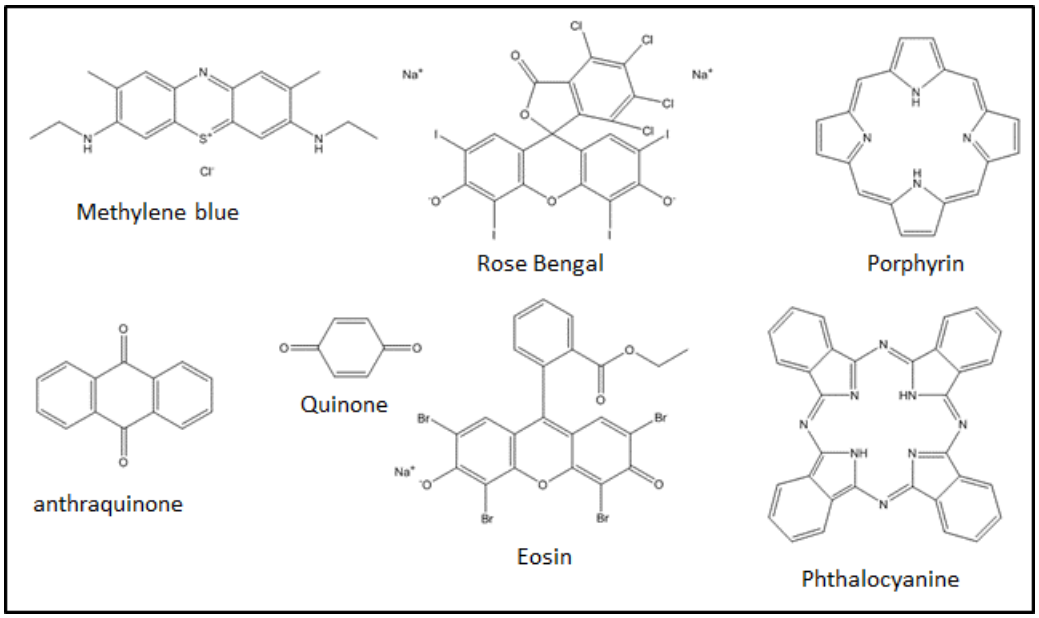

Figure 1. 13: Chemical structures of some groups of photosensitisers. Prepared by using ChemDraw Pro 13.0.

1.13 TMPyP

Photosensitiser - 5, 10, 15, 20-tetrakis (1-methyl-4-pyridinio) porphyrin tetra (*p*-toluene sulfonate) (TMPyP) is our photosensitiser of choice (Figure 1.14). It is a planar tetra cationic porphyrin and is available commercially. TMPyP is soluble in water and has an absorption peak at 420 nm (Ceklovsky et al., 2008, Ye et al., 2012). This peak is within the visible region of the natural light spectrum and that makes it an ideal photosensitiser for the development of sunlight driven water disinfection. The singlet oxygen quantum yield of TMPYP is 0.74 (74%) in PBS (Lei et al., 2010). TMPyP in solution or attached onto a solid support in solution can absorb sunlight and ultimately become excited to its triple state which can interact with molecular oxygen in solution by type 2 reaction mechanism to generate singlet oxygen and by type 1

reaction mechanisms to generate other ROS. These ROS can then inactivate waterborne microorganisms including viruses. TMPyP has been extensively studied and because of its photo-physical and electrochemical properties, it has been used as useful probe of nucleic acid structure and dynamics (Lubitz et al., 2007, Jin et al., 2008), construction of devices for optical sensors (Zhao et al., 2016, Jang et al., 2011) and as an efficient photosensitiser for PDT of cancers and microorganisms (Hanakova et al., 2014, Eichner et al., 2013). Several reports showed that when an intense pulsed light source is used, TMPyP is a potent photosensitiser for the PDI of microorganisms including antibiotic resistant bacteria (Eichner et al., 2013, Maisch et al., 2012b, Baumler and Maisch, 2012).

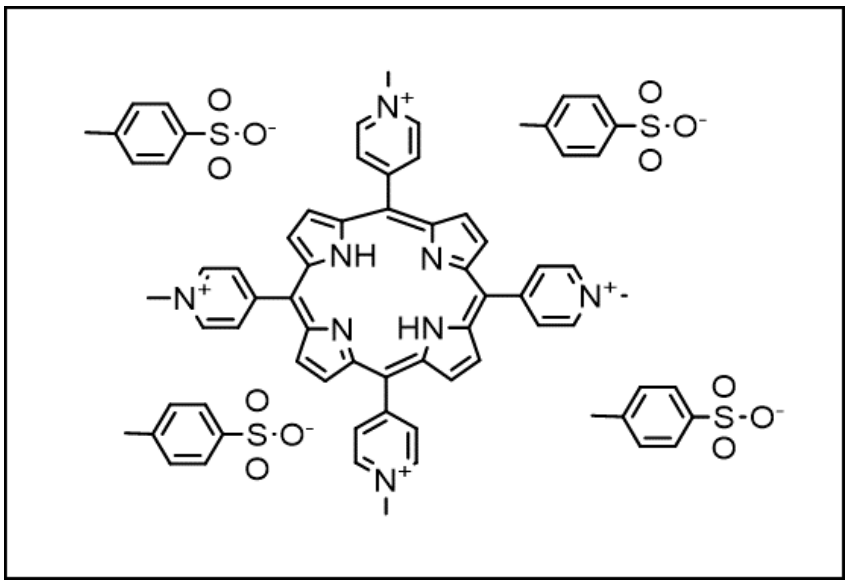

Figure 1. 14**:** Chemical structure of TMPyP shown with benzene sulphonate counter ions. The TMPyP structure was from ChemACX.com, ChemDraw Pro 13.0.

1.14 Photodynamic inactivation experimental model

Getting it right in the experimental setup of photodynamic inactivation studies is the first step towards successful development of a photodynamic disinfection device. Irrespective of materials and methods used, a good setup for photodynamic

inactivation experiment should be one that excludes factors (other than the photodynamic effect) which can inactivate model organisms. In many photodynamic experimental rigs, efforts have been made to exclude UV light by using cut-off filters or by using light sources that only generate visible light. UV-C (100-280 nm) is antimicrobial and can degrades range of biomolecules particular those with aromatic character. In this study, we avoided using a UV light source and used cold visible light source instead. In addition, the majority of our experiments were carried at room temperature 20-22 ^{o}C. However, a range of temperature should be studied so as to mimic waste water treatment plants in locations with moderate to high temperatures such as tropical countries. The amount and availability of molecular oxygen is a vital factor in the photosensitisation process and as such photodynamic reactors should be built to allow easy diffusion of molecular oxygen and to create the desired aerobic environment. Presently, the majority of photoinactivation and photodegradation experimental set-ups are stationary based models which do not actually mimic waste water treatment plants or reactors and there is need to simulate a flowing system to see if the photosensitizing devices could achieve the same level of photodynamic inactivation performance. In this study, both stationary and flowing water experimental models were used.

1.15 Model viruses used for PDI

In most studies aimed at photodynamic inactivation of human viruses, enteric and non-enteric, pathogenic and non-pathogenic, bacteriophage MS2 has been used as a model organism because of its similarity in size and morphology to some human viruses. However, there are views that to use phage as a model organism in photoinactivation experiments may not accurately model inactivation of human

viruses under all experimental conditions (Silverman et al., 2013). It was argued that to fully understand photodynamic inactivation of human viruses, including poliovirus, adenovirus, and hepatitis A virus, the only approach is to study them directly. This was one of the reasons for using bovine enterovirus and murine norovirus in addition to bacteriophages MS2 and Qβ as model organisms in our study.

1.15.1 MS2

MS2 is a small (~ 27 nm), positive sense, single stranded RNA bacteriophage belonging to the genus *Levivirus* in the family *Leviviridae*. MS2 has been used as a viral model organism in several studies aimed at photoinactivation and chemical disinfection of human viruses because of its similarity in size and morphology to some human viruses such as noroviruses and picornaviruses (Kohn and Nelson, 2007, Zhong et al., 2016). Also, because it is non-pathogenic to human, so poses no health risk and easy to propagate. The MS2 virion consists of an RNA genome (3,569 nt) enclosed in a non-enveloped icosahedral capsid with T = 3 quasi-symmetry that is composed of 178 copies of coat protein (13.7 KDa) and one copy of maturation protein also called A-protein (44 KDa) (Figure 1.6) (Koning et al., 2016, Dai et al., 2017). The assembled MS2 capsid has 32 pores, each of which is about 2 nm in diameter. This allows small molecules to diffuse more readily into and out of the capsid (Dedeo et al., 2010, Valegård et al., 1990). The genome encodes 4 proteins comprising of A-protein, coat protein, lysis protein and replicase. The A-protein is attached to viral RNA from inside the capsid and during infection, it recognises and binds to the host bacteria pilus during infection (Figure 1.15).

(Placeholder1p. This image has been removed by the author of this thesis for copyright reasons)

Figure 1. 15: MS2 capsid showing the coat protein 13.7 KDa (178 copies) labelled blue and the A-protein 44 KDa (one copy) labelled red. The A- protein is shown slightly tilted from the surface of the coat protein and (as inset) projecting into the capsid lumen. The α-helix domain of the A-protein is attached to the RNA inside the capsid, while the β-sheet domain is surface-exposed and is believed to recognise and bind to the host bacteria pilus during infection. The model was created by docking the MS2 A-protein [PDB-5tc1] onto the MS2 capsid [PDB-2MS2] using PyMOL version 1.7rc1.

1.15.2 Phage Qβ

Phage Qβ is a small (~ 27 nm), positive sense, single stranded RNA bacteriophage belonging to the genus *Allolevivirus* in the family *Leviviridae.* The RNA genome (4,220 nt) of phage Qβ encodes 4 proteins comprising of A1 (38 KDa), A2, coat protein (13.7 KDa) and Qβ replicase (61-65 KDa) (Golmohammadi et al., 1996). It has a non-enveloped icosahedral capsid (Figure 1.16) with T = 3 quasi-symmetry consisting of 178 copies of coat protein and one copy of A2 maturation protein (corresponding to the 44 KDa A-protein in MS2) which participate in host the bacterial cell recognition and attachment to bacteria pilus during replication (Gorzelnik et al., 2016). However, unlike MS2, It has been shown that coat protein subunits of Qβ are linked together by disulphide bonds in covalent pentamers and hexamers with a stoichiometric ratio 12:20 that is consistent with icosahedral symmetry (Takamatsu and Iso, 1982).

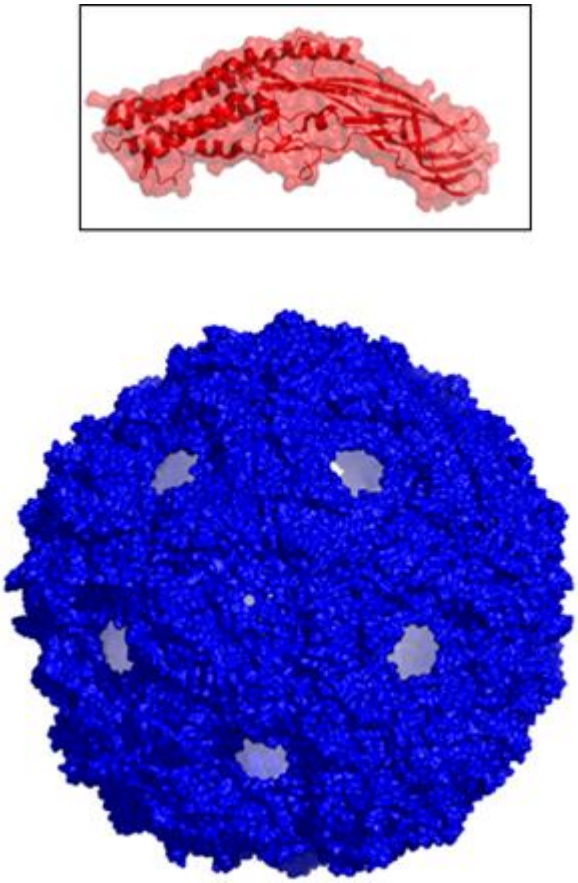

Figure 1. 16: Phage Qβ capsid showing the coat protein 13.7 KDa (178 copies) labelled blue. The A2-protein 44 KDa (one copy) labelled red is also part of the capsid and its α-helix domain is attached to the RNA inside the capsid, while the β-sheet domain is surface-exposed and is believed to recognise and bind to the host bacteria pilus during infection. The images were created from the phage Qβ capsid [PDB-1QBE] and maturation protein (A2-protein) [PDI-5MNT] using PyMOL version 1.7rc1.

1.15.3 Bovine enterovirus 2

Bovine enterovirus 2 (BEV 2) also called enterovirus F, is a positive sense, single stranded RNA virus belonging to the genus *Enterovirus* in the family *Picornaviridae.* BEV 2 shows similarities with other viruses belonging to the same family of *Picornarviridae*. These include poliovirus, foot and mouth disease virus, human rhinovirus, and encephalomyocarditis virus (Goens et al., 2004, Smyth et al., 1993, Smyth et al., 1995). BEV 2 is about 27-30 nm in diameter and is usually part of the cattle gut normal flora. However, following infection of the reproductive tract, BEV can cause abortion, stillbirth, infertility, and neonatal mortality in cattle. It can also

cause enteric and respiratory diseases in cattle. Enteric symptoms include diarrhoea and weight loss (Goens et al., 2004). The BEV 2 virion consist of an RNA genome (~7500 nt) enclosed in a non-enveloped icosahedral capsid (Figure 1.17) that is composed of 60 copies each of VP1 (34 KDa), VP2 (29 KDa), VP3 (27 KDa) and VP4 (7 KDa). Proteins VP1, VP2 and VP3 are exposed on the surface of the capsid while VP4 is internal and is myristylated at its N-terminal residue during replication and assembly. The host attachment sites occur on the surface ridge and they are analogous to canyon in polio and rhinoviruses (Figure 1.17).

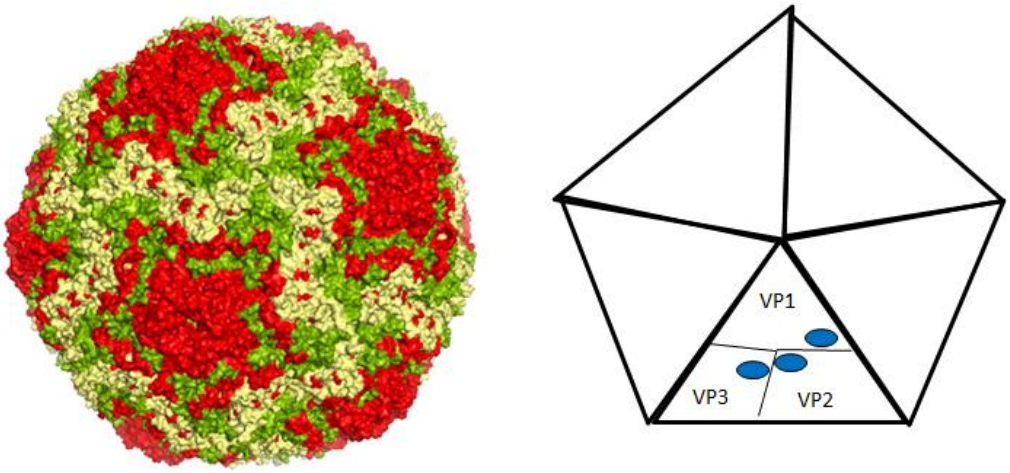

Figure 1. 17: BEV 2 capsid showing the 3 capsid proteins exposed on the surface of the capsid. The capsid is composed of 60 copies each of VP1 (34 KDa) labelled pale yellow, VP2 (29 KDa) labelled red and VP3 (27 KDa) labelled green, exposed on the surface of the capsid while VP4 (7 KDa) is internal. The host attachment sites (labelled blue) occur on the surface ridge across the 3 surface capsid proteins (Smyth et al., 1995). The image was created from the capsid of bovine enterovirus VG-5-27 [PDB-1BEV] using PyMOL version 1.7rc1.

1.15.4 Murine norovirus

Murine norovirus (MNV) is a positive sense, and single stranded RNA virus belonging to the genus *Norovirus* in the family *Calciviridae.* Human norovirus (HNV) belongs to the same genus of *norovirus* as MNV and because of a lack of good replication of HNV in animal models, MNV is currently used as a model to study biology of norovirus

(Katpally et al., 2010, Taube et al., 2010, Orchard et al., 2016). Human norovirus is the most common cause of viral gastroenteristis in humans. It affects people of all ages worldwide. The virus is fecal-orally transmitted through contaminated food, water, person-to-person contact, and via aerosolisation of vomited virus and subsequent contamination of surfaces (Patel et al., 2008). Annually, norovirus is associated with about 1 million outpatient visits and about 65,000 in patient hospitalisations in developed countries. In developing countries, it is associated with about 1.1 million hospitalisations with an estimated 218,000 deaths (Ahmed et al., 2014b). Clinical symptoms of norovirus infection in human include nausea, vomiting, watery diarrhoea and abdominal pain (Patel et al., 2008). MNV is the most prevalent virus in laboratory mice. It can only cause clinical signs in immunodeficient mice (Karst et al., 2003). MNV infection can cause wasting, diarrhoea and death in mice with severe deficiencies in innate immunity, specifically the interferon signalling pathways or multiple interferon receptors. Microscopically, hepatitis, peritonitis, and interstitial pneumonia can be seen in infected immunodeficient mice (Karst et al., 2003, Mumphrey et al., 2007). The norovirus genome is composed of 3 major open reading frames (ORFs). ORF1 encode the non-structural poly protein (200 KDa), ORF2 encode the major capsid protein VP1 (58 KDa) and ORF3 encode the minor capsid protein VP2 (20 KDa). ORF4 has been identified but its product and function have not been established (Taube et al., 2010). Norovirus capsids are formed from 180 copies of VP1 organised in a T = 3 quasi equivalent icosahedral symmetry. Each capsid protein is divided into an N-terminal arm (N), a shell (S), and C-terminal protruding (P) domain. The S and P domains are connected by a short hinge. The P domains form dimers appearing as an arch structure on the capsid surface (Figure 1.18). The P

domain is subdivided into P1 (stem of the arch) and P2 (top of the arch) domains (Figure 1.18). The P domain, specifically P2 domain contains the sites for antigenicity and host cell binding during infection (Taube et al., 2010).

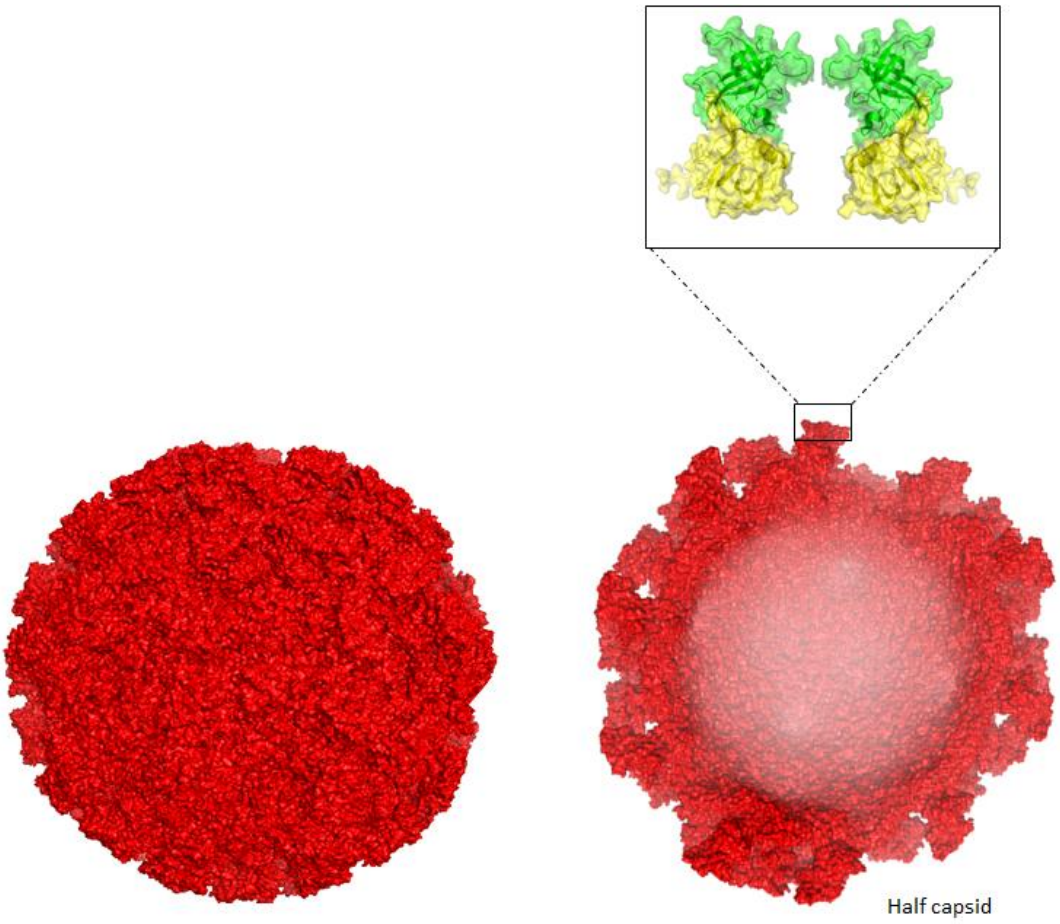

Figure 1. 18: Murine norovirus capsid showing the major capsid protein VP1 (58 KDa) (180 copies) labelled red. Each VP1 is divided into an N-terminal arm (N), a shell (S), and C-terminal protruding (P) domain. The P domain has two parts (inset); P1 domain labelled yellow and P2 domain labelled green. The P domains form dimer to look like an arch structure on the capsid surface and it is believed that host binding occurs at P2 domain. The images were created from the full and half capsid of Norwalk virus [PDB-1HIM] and murine norovirus P domain [PDB-3LQ6] using PyMOL version 1.7rc1.

1.16 Project aim

The overall goal of this project was to develop a sunlight-driven water disinfection system which is simple, cheap, re-usable and environmentally friendly. These features would allow use in rural areas of developing countries where water treatment infrastructure is either absent or poorly developed. However, the low energy input is also an attractive feature for water companies in developed nations. Here, disinfection of “grey water” might allow this to be excluded from full water processing and returned to the environment. This would reduce overall energy usage.

The specific objectives include;

To examine the PDI of model viruses with photosensitisers in solution. The rate and extent of PDI among model viruses will be compared and analysed. Effects of factors such as light intensity, time of illumination, types of photosensitiser, concentration of photosensitiser and co-pollutants on the PDI of viruses will be examined. This should reveal information on all factors that should be considered when establishing an optimal PDI conditions for the control of viruses.

A further objective is to examine mechanisms and targets of PDI in viruses from a biological perspective. Even though PDI of viruses in solution by photosensitisers has been reported previously, the molecular effect of PDI on virus particles has been poorly described.

Another objective is to attach the most efficient photosensitiser onto a solid support and then use photosensitiser-functionalised solid support for PDI of model viruses.

Irreversible coupling of the photosensitiser onto solid support will make it suitable for all water disinfection application or the attached photosensitiser will not be leached into the water during treatment there by making it safe and environmentally friendly. Both stationary and flowing water models will be employed during PDI experiments.

The proposed work will lead the way in the development of simple sunlight driven water disinfection devices that could be used within the UK to save energy, or in developing countries as a zero-man-made energy input system to produce clean and safe drinking water.

Chapter Two: Materials and method

Chapter 2: Materials and methods

2.1 Materials

2.1.1 Chemicals

Inorganic chemicals were purchased from Sigma-Aldrich (UK) unless otherwise stated. Organic chemicals are listed beside the company where they were purchased (Table 2.1).

Table 2. 1: Organic chemicals used in this work are listed beside the company where they were purchased.

Sigma-Aldrich (UK)	ethanol, formaldehyde (36.5 – 38% v/v in H_2O), propidium iodide, sucrose, bromophenol blue, Tween-20, acetic acid, uranyl acetate, carbenicillin, agarose, chitosan, pyromelitic dianhydride, succinic anhydride, anti-Rabbit IgG, Hepes, skimmed milk, TMPyP, methylene blue hydrate, Rose Bengal, biotin-N-hydroxysuccinimide (biotin-NHS) and dimethyl sulfoxide (DMSO)
BDH laboratory supplies (UK)	1-ethyl-3-(3-dimethylamiopropyl) carbodiimide (EDC)
Generon (UK)	Coomassie Blue
Oxoid Ltd, UK	Agar Technical
Alfa Aesar (UK)	Fluorescein diacetate (FDA)
Thermo Fisher Scientific (UK)	Tris Base, methanol, glycerol, Lipofectin reagent, Pierce ECL western blotting substrate, HRP-streptavidine and HRP-conjugate secondary antibodies and Spectra multicolour broad range protein ladder
Amersham - GE Healthcare Life Sciences (Germany)	Nitrocellulose blotting membrane
Bio-Rad Laboratories (Germany)	Mini Protean Tris-Glycine (TGX) precast gels and Mini Proteans Tris-Tricine precast gels
Expedeon (UK)	Instant Blue
Acros organics (UK)	2-amino-3-hydroxypyridine

2.1.2 Solvents and buffers

Solvents and buffers used in this study were shown in Table 2.2.

Table 2. 2: Buffers

Buffers	**Composition**
1 X Phosphate buffer saline (PBS), pH 7.4	10 mM Na_2HPO_4, 1.8 mM KH_2PO_4, 137 mM NaCl, and 2.7 mM KCl
Electron microscopy buffer, pH 8.0	10 mM Hepes, 100 mM NaCl, and 1.274 mM EDTA
Bio-Rad 1 X Tris/Glycine/SDS (TGS) running buffer, pH 8.3	25 mM Tris, 192 mM Glycine, and 0.1% (w/v) SDS
Bio-Rad 1 X Tris/Tricine/SDS running buffer, pH 8.3	25 mM Tris, 192 mM Tricine, and 0.1% (w/v) SDS
1 X TAE Buffer, pH 8.6	40 mM Tris, 20 mM acetate and 1 mM EDTA
1 X Transfer buffer for western blotting	25 mM Tris, 192 mM glycine and 20% (v/v) methanol
1 X Tris buffer saline (TBS)	20 mM Tris and 150 mM NaCl
Tris buffer saline with Tween-20 (TBST)	0.1% (v/v) Tween-20 in TSB
2 X lammeli loading buffer (reducing), pH 6.8	4% SDS (w/v), 10% (v/v) mercaptoethanol, 20% (v/v) glycerol, 0.004% (w/v) bromophenol and 0.125 M Tris-HCl
2 X Loading buffer for native agarose gel	5% (v/v) glycerol and 0.004% (w/v) bromophenol

2.1.3 Antibodies

Rabbit anti MS2 virus protein polyclonal antibodies were sourced commercially from Genscript, USA. Four synthetic peptides corresponding to the amino acid sequences of antigenic determinant sites of MS2 A-protein (Figure 2.1) were commercially synthesised by Genescript, USA. Sequence specific antibodies against these peptides were raised in rabbits and the IgG fraction purified by protein A/G chromatography, then by peptide affinity chromatography.

Figure 2. 1: MS2 A-Protein, showing positions of four predicted antigenic sites. The RNA-binding domain of protein A, located within the capsid lumen, is shaded in darker grey, while the surface exposed domain is shaded in lighter grey. Antigenic sites 1, 2, 3 and 4 are shown in green, red, blue and purple underlined bold characters and spheres, respectively on the amino acid sequence and the model. The model was created from the MS2 A-protein [PDB-5tc1] using PyMOL version 1.7rc1. Predictions of antigenic binding sites were performed by Genscript using their proprietary software.

2.1.4 Bacterial and viral strains

The phage MS2 ATCC 15597-B1, phage Qβ and their *E. coli* host cell ATCC 15597 stocks were donated by Prof. Peter Stockley (School of Molecular and Cellular Biology, University of Leeds, UK). The bovine enterovirus 2 (BEV2) and murine norovirus (MNV) and their host cells (BHK-21 and RAW 264.7 cells respectively) were provided by Prof. Nicola Stonehouse (School of Molecular and Cellular Biology, University of Leeds, UK). BL21 *E. coli* was from standard laboratory stocks.

2.1.5 Growth media for bacteria

Tryptic Soy Broth was purchased from Sigma and used throughout this work. Tryptic Soy Broth (TSB) and Tryptic Soy Agar (TSA) were prepared according to manufacturer's instructions.

2.1.6 Growth media for BHK-21 and RAW 264.7 cells

The tissue culture media - Dulbecco's Modified Eagle's Medium (DMEM) and Minimum Essential Medium (MEM), penicillin – streptomycin (P/S), trypsin and L-glutamine were all purchased from Sigma-Aldrich (UK). Foetal bovine serum (FBS) and Horse serum (HS) were purchased from Biosera (UK). The media were prepared according to standard required compositions. The media for culturing of RAW 264.7 cells and propagation as well as $TCID_{50}$ assays of MNV was composed of DMEM, 10% (v/v) FBS and 1% (v/v) P/S. The media for propagation of BHK-21 cells and plaque assays was composed of DMEM, 10% (v/v) HS and 1% (v/v) P/S. The transfection media was composed of MEM, 10% (v/v) FBS and 1% (v/v) P/S. Serum-free media (SFM) were made of either DMEM, 1% (v/v) P/S or MEM, 1% (v/v) P/S.

2.1.7 Light source and conditions for PDI

The light source for PDI experiments was a Schott KL 2500 LCD (Schott Ltd., UK) which provides a cool visible light (Figure 2.2). Fluence rates of illumination during photoinactivation experiments were measured using a light meter (Clas Ohlson, UK).

Stationary and flow models were adopted for PDI using TMPyP-functionalised chitosan membrane (CM-T). Visible light was used and fluence rates (radiant exposure) were 32 mW cm^{-2} unless otherwise stated. This fluence rate is low, about 10% of typical UK summer mid-day sunshine, but allowed a graded response after PDI (rather than an “all or none” response) to be measured. The conversion factor is; 1 lux = 9.5 X 10^{-3} mW cm^{-2} = 1.8 X 10^{-3} µM m^{-2} s^{-1} of visible photons (400- 700 nm). The buffer used for PDI was 1 X PBS under aerobic conditions.

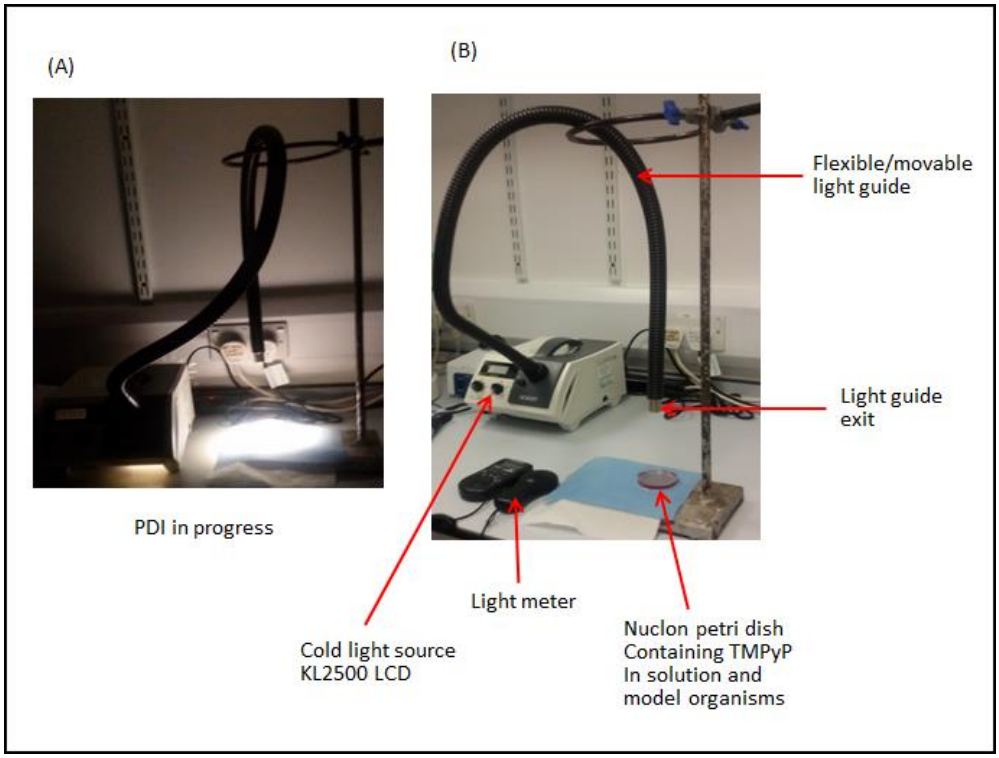

Figure 2. 2: Images of PDI experimental setup. (A), PDI experiment in progress; (B), labels of the components of the PDI experimental setup in solution.

2.1.8 Equipment

A Malvern Zetasizer (Malvern Instruments Ltd, Malvern, UK) was used for dynamic light scattering analysis (DLS) of pre-PDI and post PDI MS2 samples whilst a NanoDrop spectrophotometer (NanoDrop 2000_C, Thermo Scientific, USA) was used to determine the concentration and purity of purified virus (proteins) samples at 280 nm and extracted RNA from pre-PDI and post-PDI virus samples at 260 nm.

Spectral properties of PDI light source and photosensitisers-TMPyP, Rose Bengal and methylene blue used in this study were determined by a spectrometer (QE Pro, Ocean Optics, USA) whilst fluorescence of dyes during dead and enzyme activity assays of the *E. coli* host cell were measured by Cary eclipse fluorescence spectrophotometer (Varian Australia Pty Ltd, Mulgrave Victoria, Australia).

Bacterial assays were carried out in a lamina flow cabinet (BSB-48, Gelaire Ltd., Sydney, Australia). Incubation of bacteria broth culture, bacteria agar plates and double layer plaque assay agar plates of purified, pre-PDI and post-PDI samples of bacteriophages MS2 and Qβ were performed in an Innova TM 4000 incubator (New Brunswick Scientific co., Edison, USA) with or without shaking.

Mammalian cell culture works were carried out in UniMat-BS, Class II Microbiological Safety Cabinet (Envair Ltd., Lancashire, England). Incubation of cells (BHK and Raw cells) for propagation and titre determination of purified, pre-PDI and post-PDI samples of bovine enterovirus 2 (BEV 2) and murine norovirus (MNV 2) were performed in a NuAire DH Autoflow CO_2 air jacketed incubator (NuAire, Plymouth, USA).

A Philips CM10 electron microscope was used for the imaging of purified, pre-PDI and post-PDI virus samples. A Leica microscope (Leica Micro Systems LTD, Switzerland) was used to observe the growth and confluence of tissue cultures (BHK and Raw cells). A Hitachi tabletop scanning electron microscope TM3030 (Hitachi High-Tech, Tokyo, Japan) was used for the imaging of modified and unmodified chitosan electron spun nanofibers and polymeric membranes.

2.2 Standard methods

2.2.1 Growth curve of *Escherichia coli*

A growth curve was used to determine the growth, viability and colony forming unit per ml (CFU/ml) of *E. coli* strains used throughout the work. *E. coli* (ATCC 15597) is the host bacteria for bacteriophages MS2 and Qβ while E. *coli* BL21 is a carbenicillin resistant bacterium that was used as the bacteria model organism during PDI

experiments. TSB (100 ml) was inoculated with 1 ml of overnight culture of *E. coli* and was then placed on the shaking incubator set at 37 ^{o}C and 150 rpm. At 30 min intervals, the optical density (600 nm) of the culture was determined over a total of 4 h. Tenfold serial dilution from 10^2 to 10^6 were carried out at each time point and 0.1 ml of dilutions from 10^3 to 10^6 were plated out on TSA plates which were incubated at 37 ^{o}C for up to 24 h. After the incubation those plates that contained 30-300 colonies were counted. For those time sets that had more than one plate with 30-300 colonies, the average was taken and recorded for that particular time set.

2.2.2 Propagation, purification and enumeration of MS2 bacteriophage stock culture

2.2.2.1 Propagation and purification of bacteriophages MS2 and Qβ

The bacteriophages MS2 and Qβ were propagated according to the method described in (Lima et al., 2004) with slight modifications. One litre of exponential phase growth culture of *E. coli* (ATCC 15597) was infected with 300 µl of MS2 at 10^9 PFU/ml or phage Qβ 10^{10} PFU/ml respectively and was incubated at 37 ^{o}C with shaking at 150 rpm for 48 h until *E. coli* cells were completely lysed. The lysates were then centrifuged at 1,431 xg for 30 min to removed bacterial cell debris. The material was precipitated using 50% (v/v) saturated ammonium sulphate overnight at 4 ^{o}C. Samples were then centrifuged at 1,431 xg for 30 min. Supernatants were discarded and the pellets re-suspended in 10 ml PBS. The re-suspended pellets were clarified again by centrifuging at 1,431 xg for 30 min. Phage particles in the supernatants were pelleted through 30% (w/v) sucrose cushion by ultracentrifugation at 32,000 rpm for 3 h using a Beckmann SW 32 Ti rotor. Pellets were re-suspended in 800 µl PBS

overnight at 4 ^{o}C. Re-suspended pellets were each purified through 15% - 45% (w/v) sucrose gradient by ultracentrifugation at 50,000 rpm for 50 minutes using a Beckmann SW 55 Ti rotor. Gradient fractions were collected from top to bottom and analysed by SDS-PAGE to identify MS2 and phage Qβ protein peak fractions respectively.

2.2.2.2 Plaque assay of bacteriophages MS2 and Qβ

A double layer agar plaque assay was used to determine the infectivity and titre of bacteriophages MS2 and Qβ before and after PDI to determine the titre after purification and as well as the extent and rate of PDI. In order to prepare 100 ml of top agar, 0.6 g of agar was added to 100 ml of TSB was then autoclaved. After sterilisation, 3 ml each of the top agar was dispensed into 15 ml falcon tubes and were placed in a water bath set at 45 ^{o}C. Tenfold serial dilutions of MS2 and phage Qβ from 10^{2} to 10^{14} were carried out in TSB. Microcentrifuge tubes (1.5 ml) were set up and labelled with dilution factor for the initial incubation of the bacteriophages and their host *E. coli* cells. To each of these, 0.1 ml of the corresponding MS2 or phage Qβ dilution and 0.3 ml log phase *E. coli* (ATCC 15597) culture (0.5 OD at 600 nm) were added and incubated for 20 min at 37 ^{o}C. After the incubation, they were added to their corresponding top agars in water bath and were votex before plating them out on their respective corresponding agar plates. After the top agar has solidified, the plates were incubated at 37 ^{o}C for 24 h. After incubation, the plates with 30-300 plaques were counted.

2.2.3 Propagation, purification and enumeration of BEV

2.2.3.1 Propagation and purification of BEV

BHK-21cells were grown to 80-90% confluence in T175 flasks (10 flasks were used). Then the media (DMEM, 10% (v/v) HS, 1% (v/v) P/S) was removed and cells monolayer was washed with 10 ml PBS for each flask. To each flask, 10 ml of pre-warmed media (DMEM, 10% (v/v) HS, 1% (v/v) P/S) was added. Each flask was then infected with 600 µl of stock BEV 2. The flasks were then incubated at 37 ^{o}C, 5% CO_2 for 48 h until full lysis. The flasks were then frozen at -20 ^{o}C overnight. The flasks were then thawed and lysate transferred to Falcon tubes and were centrifuged at 1,431 xg for 30 min. The supernatant was then precipitated by 50% (v/v) saturated ammonium sulphate overnight at 4 ^{o}C. After precipitation, this was centrifuged at 1,431 xg for 30 min. The supernatant was discarded and the pellet re-suspended in 10 ml PBS at 37 ^{o}C. The re-suspended pellet was clarified again by centrifuging at 1,431 xg for 30 min. The supernatant was then concentrated using 30% (w/v) sucrose cushion which was centrifuged at 32,000 rpm for 3 h using a Beckmann SW 32 Ti rotor. The pellet was re-suspended in 900 µl PBS overnight. The sample was then subjected to a 15 - 45% (w/v) sucrose gradient at 30,000 rpm for 2 h using a Beckmann SW 40 Ti rotor. Gradient fractions were collected from top to bottom and analysed by SDS-PAGE to identify BEV 2 protein peak fractions.

2.2.3.2 Plaque assay of BEV

Plaque assay was used to determine the infectivity and titre of BEV before and after PDI experiments. BHK-21 cells were first split from a T175 ml flask into 6 well cell culture plates. Media (DMEM, 10% (v/v) HS, 1% (v/v) P/S) was removed and cells (80–90% confluence) monolayer washed with 10 ml PBS. Then 5 ml of 0.25% (v/v) trypsin

was added. It was incubated at 37 ^{o}C for 2-3 min, until the cells appeared rounded by microscopy. The side of the flask was gently tapped to detach cells. Then 5 ml media (DMEM, 10% (v/v) HS, 1% (v/v) P/S) was added to cells. It was then split in the ratio 1:10. Finally, 0.2 ml was placed into each well and 2 ml of media was added to each well and the plate Incubated at 37 ^{o}C, 5% CO2, usually for around 24 h of incubation. After incubation, 1 ml of media was pipetted off and discarded from each well leaving 1 ml of media on each cell monolayer. Then 10-fold dilutions of virus samples (10^{1}-10^{6}) were made and each well was labelled with the respective diluent. Each well was then infected with 100 µl of virus diluent. The plates were then incubated at 37 ^{o}C for 1 h and after internalisation of virus (i.e. 1 h post-infection), each well was overlaid with 2 ml of pre-warmed molten 1% (w/v) agarose in serum free media (DMEM, 1% P/S). After solidification of the agarose, the plates were incubated at 37 ^{o}C, 5% CO_2 for the duration of around 6-8 cycles of replication. Thus, infected cells were incubated for 48 h in order to see visible plaques. After full incubation for the completed number of cycles, infected cells were fixed for 1 h with 4% (v/v) formaldehyde. Supernatant serum-free media was removed. Solidified agar was carefully removed from each well without scratching the cell surface. Each cell monolayer was then stained with crystal violet and visible plaques counted.

2.2.4 Propagation, concentration and enumeration of MNV

2.2.4.1 Propagation and concentration of MNV

RAW 264.7 cells were grown to 70-80% confluence in T75 flask (10 flasks were used). Then 5 ml of media (DMEM, 10% (v/v) FBS, 1% (v/v) P/S) was removed from each flask so that only 7 ml of the media remained. Each flask was then infected with 1 ml of stock MNV and flasks were incubated at 37 ^{o}C, 5% CO_2 for 72 h until full cell lysis.

The flasks were then frozen at -20 ^{o}C and thawed intermittently 4 times. The lysate was then transferred to 50 ml Falcon tube (lysate from 5 flasks per tube). Then the lysate was clarified by centrifuging at 1,431 xg for 30 min and supernatant was taken and pellet discarded. This clarification step was repeated twice. The supernatant was then concentrated by ultracentrifugation at 32,000 rpm for 3 h using a Beckmann SW 32 Ti rotor. After ultracentrifugation, the supernatant was discarded and the pellet was re-suspended in 1 ml PBS overnight. The concentrated MNV was then used with no further purification.

2.2.4.2 $TCID_{50}$ assay of MNV

$TCID_{50}$ assay was used to determine the infectivity and titre of MNV before and after PDI experiments to determine its titre after propagation and as well as extent and rate of PDI. RAW 264.7 cells were first split from a T75 ml flask into 96 well cell culture plates. Media (DMEM, 10% (v/v) FBS, 1% (v/v) P/S) (12 ml) was removed from cells (70–80% confluence) in a T75 flask. Then 6 ml of fresh media was added to the cell monolayer and the cells were scrapped using cell scrapper. An additional 6 ml media was added to the flask to make 12 ml. it was then pipetted up and down to wash the flask as well as to break the clumps of cells. The cells were first counted and 100 µl of 5 x 10^5 cells/ml were seeded per well. The plates were rocked gently to mix and disperse cells evenly in each well and then incubated at 37 ^{o}C, 5% CO_2 overnight. After overnight incubation, 10-fold dilution of MNV samples (10^1- 10^6) were made. Each well (usually with 5 wells as replicates) was then infected with 100 µl of the respective MNV diluent. The plates were then incubated at 37 ^{o}C, 5% CO_2 for 72 h. After the incubation, the plates were exposed to UV light for 1 h in a laminar flow hood. The media was removed and the cell monolayers stained with crystal violet.

The number of wells that showed cell death per MNV diluent were counted and MNV infectivity and titre were determined using Reed-Muench $TCID_{50}$ formula (Reed and Muench, 1938).

2.2.5 SDS-PAGE

Pre- and post-PDI viral proteins were separated on a Bio-Rad mini Protean TGX Precast Gels 4-15% (w/v) bisacrylamide - acrylamide and Tris/glycine/SDS as running buffer or Bio-Rad mini Protean Tris-Tricine Precast Gels 10-20% (w/v) bisacrylamide - acrylamide and Tris/Tricine/SDS as running buffer for the separation of peptides and small proteins. Samples were first mixed in 2x Laemmli sample buffer to give 1 x sample buffer and then heated at 100 ^{o}C for at least 5 min. The samples were then loaded on the gel and separated at 110 V for 1.5 h. The gel was then stained using Coomassie blue stain for 1 h while on a 3D rocking platform set at 30 rpm. After staining, the gel was destained in dH_2O for 2 h placed on a 3D rocking platform. The gel was imaged using a G-box gel imager (Syngene, UK).

2.2.6 Western blotting

Pre- and post-PDI viral proteins were detected and analysed by western blotting using a nitrocellulose membrane. A nitrocellulose blotting membrane (Amersham, GE Healthcare Life Sciences, Germany) was pre-wet in 1 x transfer buffer. Meanwhile, after SDS-PAGE, the gel was removed, edges were trimmed and the gel was placed in 1 x transfer buffer to equilibrate for 10 min on a 3D rocking platform. Two each fibre pads and Bio-Rad blotting papers, cut to the size of the gel were also pre-soaked in 1 x transfer buffer. Blotting sandwich was made using the gel holder cassette placed in a container with 1 cm deep 1 x transfer buffer with the black side of the cassette immersed in the buffer while the white side was up and out of the buffer.

One of the pre-soaked fibre pads was laid on the black side of the cassette. Then one of the pre-soaked blotting paper was placed on the pad. Throughout the sandwich construction a roller was used to remove any air bubbles between the gel and the membrane or between other layers. The sandwich was then inserted into an electroblotting machine (Bio-Rad) and blotting buffer and ice unit were added accordingly. The blot was run at 20 V for 2 h. After the transfer, the sandwich was disassembled, the nitrocellulose membrane removed and immediately immersed in 25 ml 5% w/v skimmed milk for 30 min at room temperature for blocking. After blocking, the skimmed milk was poured off and the membrane was washed twice in TBST. Then the membrane was incubated in 10 ml of primary antibodies dilutions from 1:1000 to 1:100 dilution in TBST for at least 1 h at room temperature or overnight at 4 ^{o}C on a rocking platform at 60 rpm. After incubation, the primary antibody was poured off and the membrane rinsed quickly in 20 ml of wash buffer. Another 20 ml TBST was then added and the blot allowed to wash for about 5 min on 3D rocking platform at 30 rpm. The wash buffer was then replaced with 10 ml of secondary goat anti-rabbit HRP conjugate (1:1000 dilution in TSBT) for 30 min at room temperature on a 3D rocking platform at 60 rpm. After incubation, the secondary antibodies were poured off and the membrane again rinsed quickly in 20 ml of wash buffer and then 20 ml TBST was then added and to wash for about 5 min. finally, after removing wash buffer, 10 ml of ECL (Pierce ECL Western Blotting Substrate, Thermo Scientific, USA) was added to the membrane and incubated at room temperature for at least 1 min before the image was captured using a G-box gel imager (Syngene, UK).

2.2.7 Transmission electron microscopy of viruses

Samples of viruses (pre- and post-PDI) were dialysed into electron microscopy (EM) buffer (10 mM Hepes, 100 mM NaCl, 1.274 mM EDTA, pH 8.0). The virions were then adsorbed onto a freshly prepared carbon coated copper grids prepared by adding 5 µl of sample onto the copper grids, waiting for 30 sec then washing the grid twice in dH_2O. Excess liquid on the grid was then removed using blotting paper. The grid was then treated with 4% (w/v) uranyl acetate for 10 sec to negatively stain the virus coated surface. This was then washed twice in dH_2O and excess liquid on the grid removed using blotting paper. The grids were observed using a CM10 Transmission Electron Microscope (Philips). This work was done with assistance of Mr Martin Fuller in the Astbury Centre Electron Microscopy unit (FBS Leeds)

2.2.8 Assay of dead *E. coli* to determine MS2 viability

Since plate based viral assays were time consuming, we investigated quantification of either dead bacteria or live bacteria after PDI. Assaying dead bacterial host cells by propidium iodide (PI) was tested as an indirect test MS2 viability. The assay of *E. coli* was carried out by measuring the fluorescence of PI at λ_{ex} of 470 nm. The method is based on the ability of PI to selectively go into cells with a compromised membrane, intercalate with DNA and fluoresce. Membrane impairment could be by bacteriophage infection, heat treatment or photooxidation. Two hours log phase broth culture of bacteria in TSB was incubated for 30 min with different dilutions of MS2 at a ratio of 3:1 (bacteria to diluted MS2) in TSB. After incubation, the samples were washed once by centrifugation at 201 xg for 10 min, supernatant removed and re-suspended in equal volume of PBS. From each sample, 5 ml was taken into a separate tube and incubated with 50 µl of 3 mM PI in the dark for 15 min. Then,

fluorescence of each sample was measured in a Cary Eclipse fluorescence spectrophotometer at λ_{ex} of 470 nm.

2.2.9 Enzyme activity assay of *E. coli* to determine MS2 viability

This approach was investigated as a complementary approach to the previous dead cell assay. Enzyme (esterase) activity of *E. coli* was measured by observing fluorescence of fluorescein diacetate (FDA). This method is based on the hydrolytic cleavage of FDA (colourless) into fluorescein (fluorescent yellow-green) by esterases inside the cell. Cells that have impaired membrane by phage infection are unable to retain the charged fluorescein. Two hours log phase broth culture of bacteria in TSB was incubated for 30 min with different dilutions of MS2 at a ratio of 3:1 (bacteria to diluted MS2) in TSB. From each sample, 5 ml was taken into separate tube and then incubated with 8 µl of 12 mM FDA for 15 min. The remaining samples (5ml each) were also incubated with 8 µl of 12 mM FDA for 15 min, then centrifuged at 201 xg for 20 min. The supernatant from each sample was removed and labelled supernatant sample and the pellet of each sample re-suspended in 5ml of PBS. The fluorescence of each sample was measured in a Cary Eclipse fluorescence spectrophotometer at λ_{ex} of 470 nm.

2.2.10 Spectral properties of PDI light source and photosensitisers

Spectral and optical absorption properties of the PDI light source and photosensitisers-TMPyP, Rose Bengal and methylene blue were determined. A spectrometer (QE Pro, high sensitivity spectrometer, Ocean Optics, USA) was used to determine spectral properties of PDI light source at different light intensities and colour temperatures/ filters. The different light intensities and colour temperatures/ filters measured were 32 mW cm^{-2} (2650 K, A), 200 mW cm^{-2} (2950 K, A), 450 mW

cm^{-2} (3000 K, B) and 950 mW cm^{-2} (3000 K, C). Absorption spectra of the photosensitisers in PBS were determined using a NanoDrop spectrophotometer (NanoDrop 2000_C, Thermo Scientific, USA).

2.2.11 Detection of singlet oxygen generated by photosensitisers

Singlet oxygen generated by photo-irradiation in the presence of photosensitiser was measured by spectrophotometry. The method is based on the measurement of a decrease in the absorbance (318 nm) of 2-amino-3-hydroxypyridine when it reacts with singlet oxygen (Komagoe et al., 2011). An assay solution of 2-amino-3-hydroxypyridine (200 µM) and photosensitiser (1 µM) dissolved in PBS was put in a conventional quartz cell with a light path length of 1 cm, and illuminated at 76.63 Wm^{-2} for 1 - 5 minutes and changes in the A_{318} before and after photo-irradiation were measured.

2.2.12 Statistical and graphical software

Data from different experiments were imported to Microsoft Excel. All graphical output was plotted in Origin Pro 8. Images and schematics were drawn in Microsoft Powerpoint. Chemical structures were drawn using ChemDraw Pro v13.0. Image J was used to quantify the intensity of protein bands on SDS-PAGE and western blot images.

Chapter Three: Results I

Chapter 3: Results I

Standard protocols

3.1 Overview

This research on this project began by propagation and growth curve of *E. coli* (ATCC 15597) which is the host bacteria for bacteriophages MS2 and Qβ. Then followed the propagation and purification of bacteriophages MS2 and Qβ. The double layer plaque assay, which is the gold standard method for determining titre and infectivity of bacteriophage was used before and after PDI to determine the rate and extent of PDI in bacteriophages. However, the double layer plaque assay is labour intensive and time consuming. As an alternative, attempts were made to standardise assays of dead host *E. coli* or live cell enzyme activity to more rapidly determine titre and infectivity of the bacteriophage. The bovine enterovirus (BEV) was also propagated and purified and a plaque assay was used to determine the titre and infectivity of BEV before and after PDI. For MNV, it was propagated and concentrated before use because of the low titre usually associated with it. $TCID_{50}$ assays was used to determine its titre and infectivity before and after PDI. SDS-PAGE, western blotting and TEM were used to confirm the purity of the viruses as well as to analyse viral particles/protein before and after PDI. Spectral properties of our light source for PDI and the spectra of photosensitisers-TMPyP, Rose Bengal and methylene blue were determined. This was to confirm whether the light source only produced visible light which these photosensitisers absorb within the visible light range. Also, in addition to showing of singlet oxygen induced oxidative damage which consequently lead to the inactivation of the viruses in solution, generation of singlet oxygen by the photosensitisers was shown.

3.2 Growth curve of *Escherichia coli*

The growth, viability and colony forming unit per ml (CFU/ml) of *E. coli* strains (ATCC 15597 and BL21) used in this work were determined by growth curves and serial dilutions as described in Section 2.2.1. The optical density at 600 nm and CFU/ml of the *E. coli* strains at 30 min interval over a period of 4 h were recorded and the growth curves (Figure 3.1) showed that the ATCC 15597 typically entered the log phase growth after 2 h of incubation with shaking at 150 rpm while BL21 typically entered the log phase growth after 2.5 h of incubation under the same conditions.

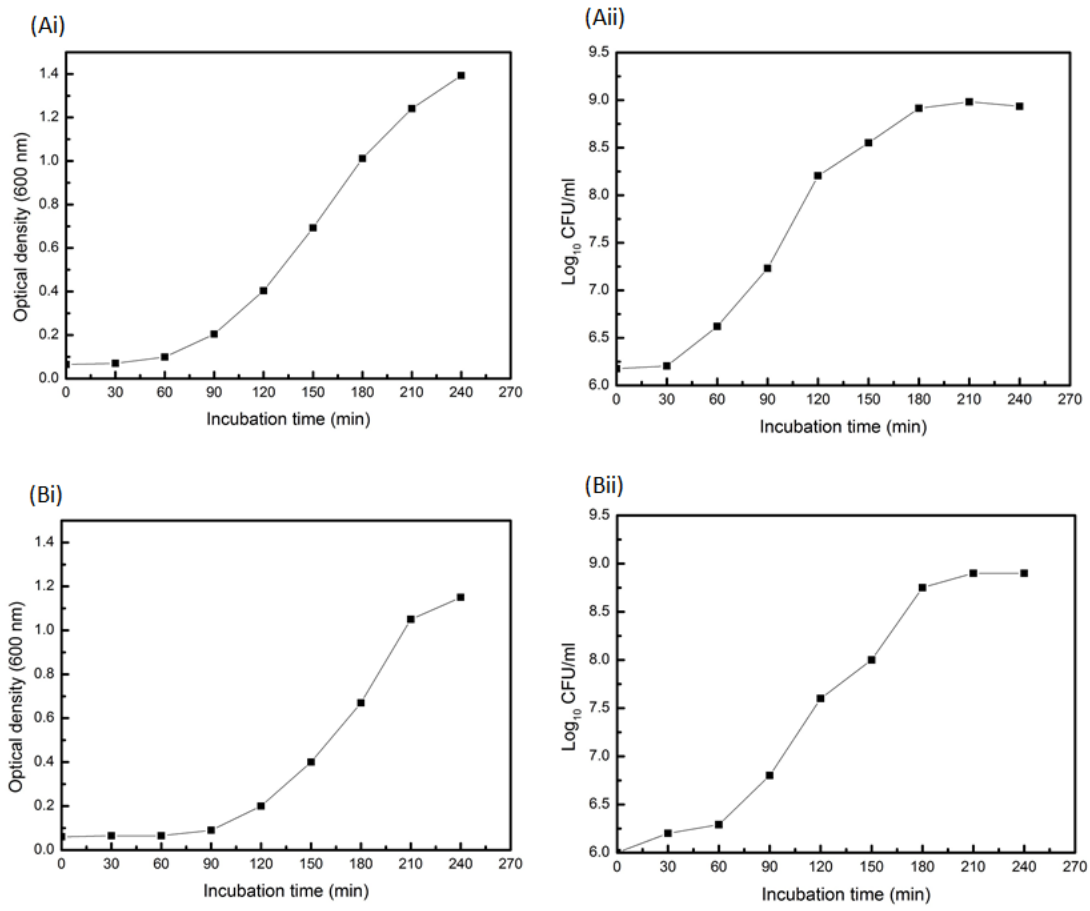

Figure 3. 1: Growth curves of *E. coli* strains used in this work. *E. coli* ATCC 15597 is the host bacteria for the bacteriophages MS2 and Qβ while *E. coli* BL21 is a carbenicillin resistant bacterium that was used as bacteria model organism during PDI experiment. (Ai) and (Bi), A_{600} of *E. coli* ATCC 15597 and BL21 respectively; (Aii) and (Bii), Log_{10} CFU/ml of *E. coli* ATCC 15597 and BL21 respectively. CFU/ml were determined by serial dilution and plating. Data are mean ± standard deviation (n = 3). Error bars are too small to be seen.

3.3 Infectivity and enumeration of model viruses

The double layer agar plaque assay as described in Section 2.2.2.2 was used to determine the infectivity and titre of bacteriophages MS2 and Qβ after purification and before and after PDI to know the rate and extent of PDI. MS2 and phage Qβ have the same host bacteria *E. coli* (ATCC 15597). The double layer plaque assay is a labour intensive and time consuming assay. Ideally, plaques are counted and titre determined in PFU/ml after 24 h of incubation of double layer agar plates. However,

we observed that when the host bacteria enter the log phase of growth after 2 h of incubation and was used immediately for double layer plaque assay protocol, phage plaques were form and could be counted after 3 h of incubation instead of the conventional 24 hr. The conventional double layer plaque assay protocol recommended that the 10-fold serial dilution of the phage should be done in media that has 1-10 mM $MgCl_2$ or $CaCl_2$. This is because some phages require divalent ions for bacterial host attachment (Kropinski et al., 2009). Lack of Mg^{2+} or Ca^{2+} in the diluent can drastically affects the infectivity and titre of the phages (Kropinski et al., 2009). However, we observed that for MS2 and Qβ infectivity and titre were not affected by the absence of Mg^{+2} or Ca^{+2} in the diluent and therefore in subsequent double layer plaque assays these were omitted. The virus plaques of double layer agar plates (Figure 3.2) were visible and could be counted without staining unlike animal viruses that require staining to make the plaques visible. The titres observed were 10^9 PFU/ml and 10^{10} PFU/ml for the purified MS2 and phage Qβ respectively.

Plaque assay as described in Section 2.2.3.2 was used to determine infectivity and titre of BEV 2 after purification and before and after PDI. For BEV 2, plaques were counted and titre determined after 48 h of incubation. The 6 well plates (Figure 3.3) were usually stained with crystal violet to make the plaques visible. We observed 10^8 PFU/ml for the purified BEV 2.

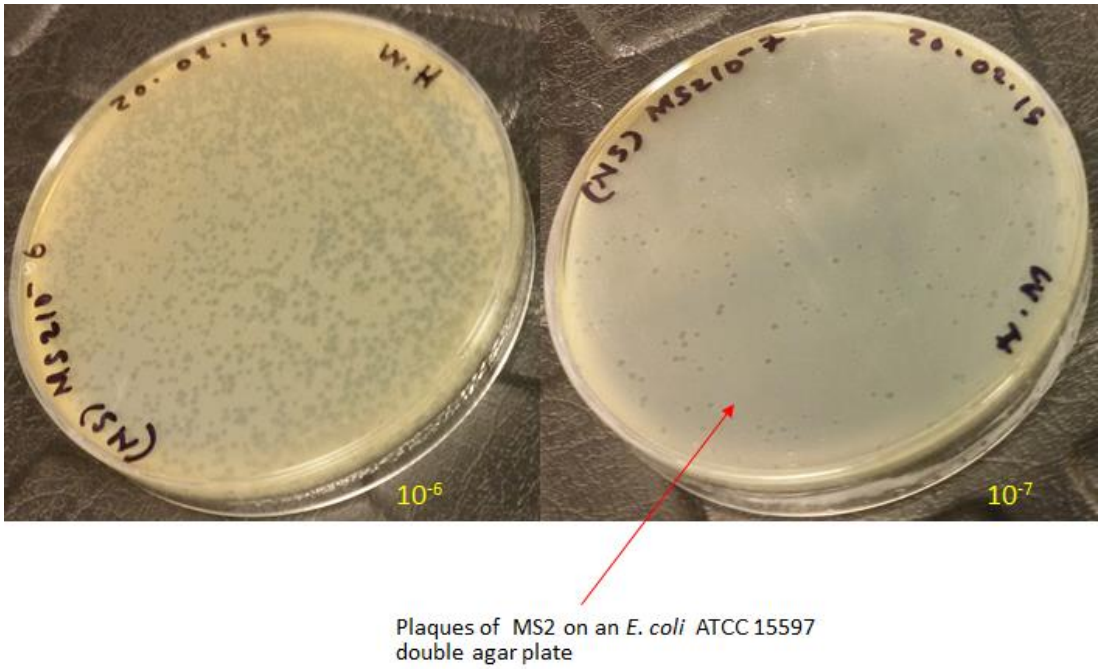

Figure 3. 2: Double layer plaque assay plates showing the infectivity of bacteriophage MS2 (ATCC #15597-B1) grown on *E. coli* (ATCC 15597).

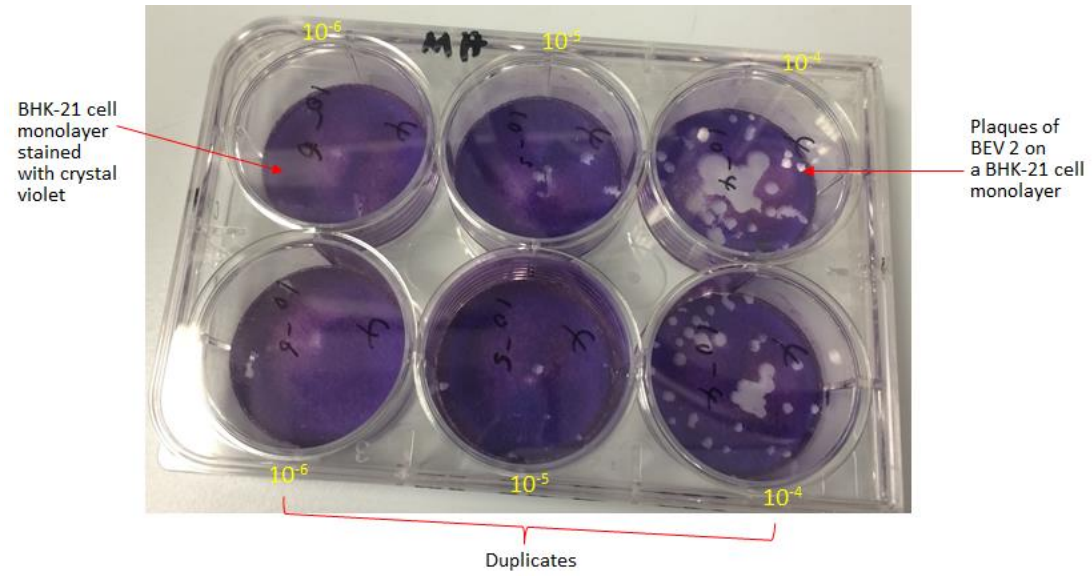

Figure 3. 3: A plaque assay 6-wells plate showing the infectivity of bovine enterovirus 2 grown on BHK-21 cells monolayer.

The $TCID_{50}$ assay (Section 2.2.4.2) was used to determine the infectivity and titre of MNV after purification and before and after PDI. Usually, 96 well plates (Figure 3.4) and the number of wells with cell deaths were counted and the titre determined using Reed-Muench$TCID_{50}$ formula. The plates (96 well plates) (Figure 3.4) were usually stained with crystal violet to make the dead cells visible. Ideally, wells with cell death and or no cell death are counted after 72 h of incubation. The titre observed for the concentrated MNV was 10^7 PFU/ml.

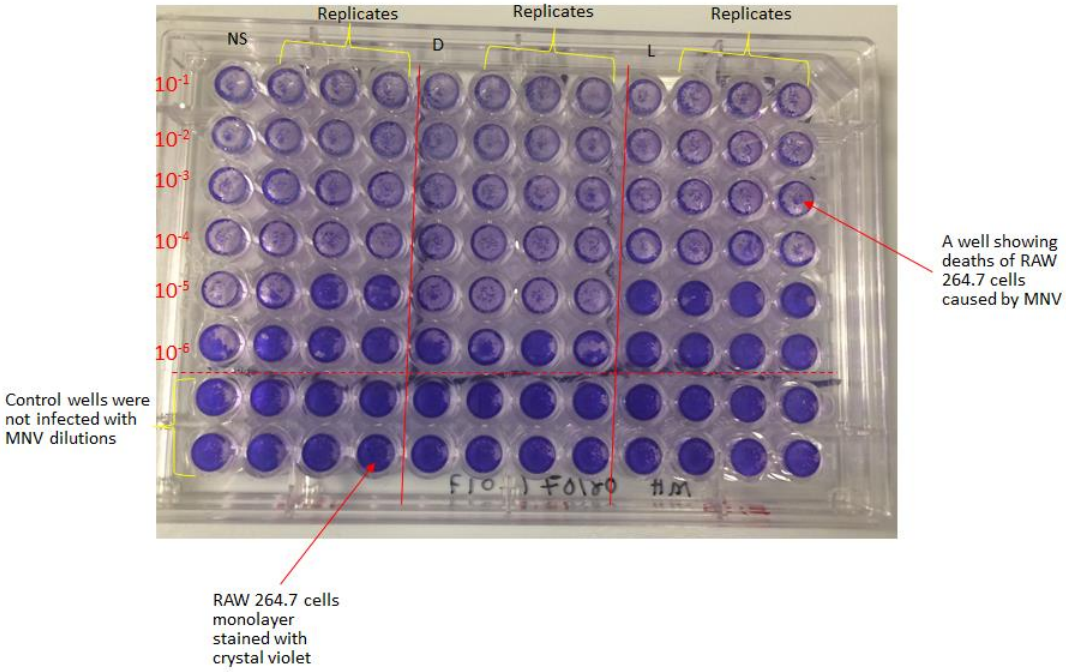

Figure 3. 4: A $TCID_{50}$ assay 96 wells plate showing the infectivity of murine norovirus grown on RAW 264.7 cells monolayer.

3.4 SDS-PAGE, western blot and TEM images of purified viral model organisms

3.4.1 MS2

MS2 was purified through a 15% - 45% (w/v) sucrose gradient by ultracentrifugation as described in Section 2.2.2.1 and gradient fractions collected from top to bottom were analysed by SDS-PAGE to identify MS2 peak fraction. The MS2 capsid consists of two structural proteins; 178 copies of coat protein and 1 copy of A-protein. The MS2 coat protein is ≈ 13.7 KDa while its A-protein is ≈ 44 KDa (Dai et al., 2017, Koning et al., 2016). Owing to the relative abundance of the coat protein over A-protein (i.e 178 copies of coat protein to 1 copy of A-protein per virion) we were not able to detect A-protein on SDS-PAGE (Figure 3.5 A1). Only the coat 13.7 KDa protein was observed. This was the case for western blot even for antibodies that were raised against MS2 capsid were used (Figure 3.5 A2); However, presumably since the large excess of coat protein dominated in the immune response, we were able to observe A-protein in western blot by using sequence specific antibodies raised against peptides corresponding to antigenic sites of the A-protein (Figure 3.5 A3). The SDS-PAGE showing a clear band of the coat protein of MS2 and also THE TEM image showed individual icosahedral MS2 particles (Figure 3.5 B) with no background confirming that the purification of MS2 was successful and the sample was of high purity. The sample was split into 50 µl aliquots and stored at -20 ^{o}C or -80 ^{o}C.

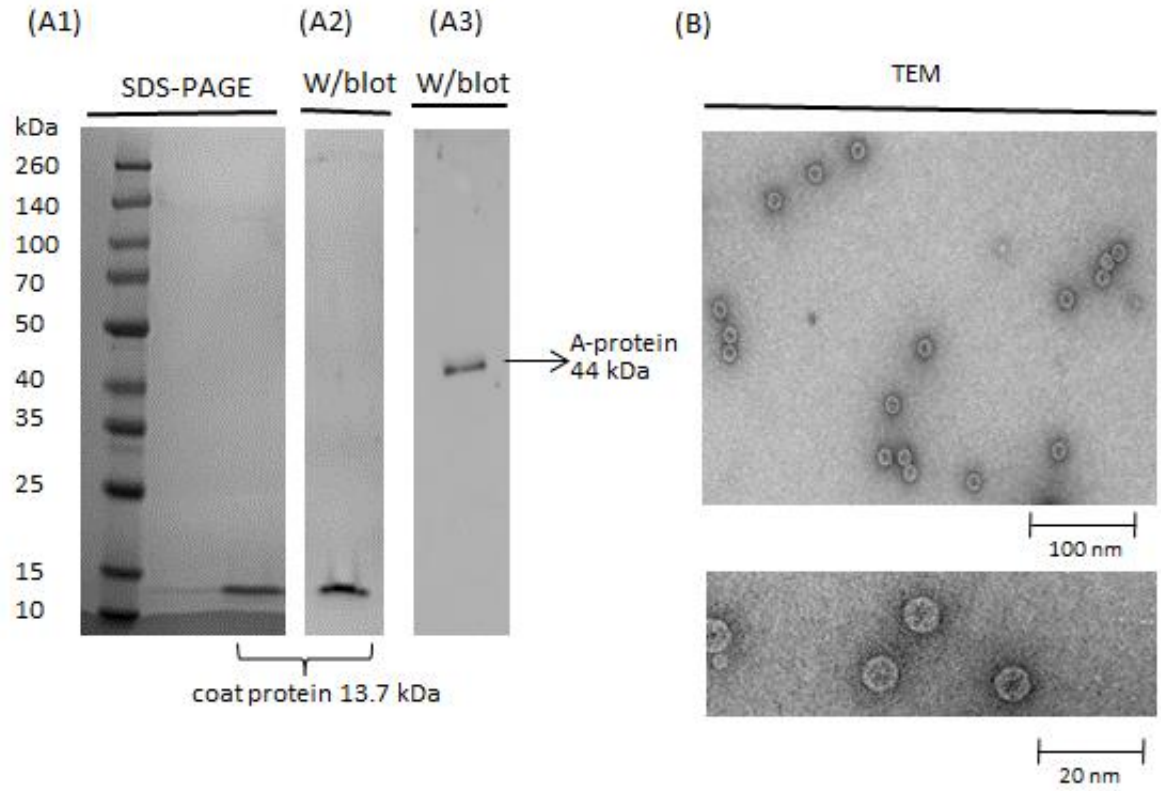

Figure 3. 5: Purified MS2 sample. (A1), SDS-PAGE showing a clear band that corresponds to the coat protein (13.7 KDa) of MS2. Electrophoresis was performed on Bio-Rad Mini Protean Tris-Glycine precast gels 4-15% (w/v) bisacrylamide - acrylamide, 12 well comb, 20 µl and Tris/glycine/SDS buffer as running buffer; (A2), western blot showing a clear band that corresponds to coat protein (13.7 KDa) of MS2 using anti-MS2 capsid polyclonal antibodies; (A3), western blot showing a band that corresponds to the A-protein (44 KDa) of MS2. Sequence specific antibodies were synthesised against peptides that corresponds to antigenic sites of A-protein of MS2; (B), TEM images of 4% (w/v) uranyl acetate negative stained MS2 showing individual icosahedral particles.

3.4.2 Phage Qβ

Phage Qβ was purified through a 15% - 45% (w/v) sucrose gradient by ultracentrifugation as described in Section 2.2.2.1 and gradient fractions collected from top to bottom were analysed by SDS-PAGE to identify phage peak fraction. Phage Qβ is very similar to MS2 and like MS2, its capsid consists of two structural proteins, the capsid comprises 178 copies coat protein and 1 copy of A2-protein. The

coat protein is ≈ 13.7 KDa while its A2-protein is similar to the MS2 A-protein and is about 44 KDa (Figure 3.6) (Gorzelnik et al., 2016). However, the coat protein subunits of phage Qβ are linked together by disulphide bonds in covalent pentamers and hexamers (Golmohammadi et al., 1996). We assumed that the reducing agent and heating step of the SDS-PAGE protocol would have broken down the pentamers and hexamers into smaller units such as dimers and trimers (Figure 3.6). The additional bands seen in SDS-PAGE were cross linked dimers and trimers of the coat protein, and not impurities, was further confirmed by the TEM image showing individual icosahedral phage particles (Figure 3.6) with no background. This also confirmed that the purification of phage Qβ was successful and the sample was of high purity. The sample was split into 50 µl aliquots and stored at -20 ^{o}C or -80 ^{o}C.

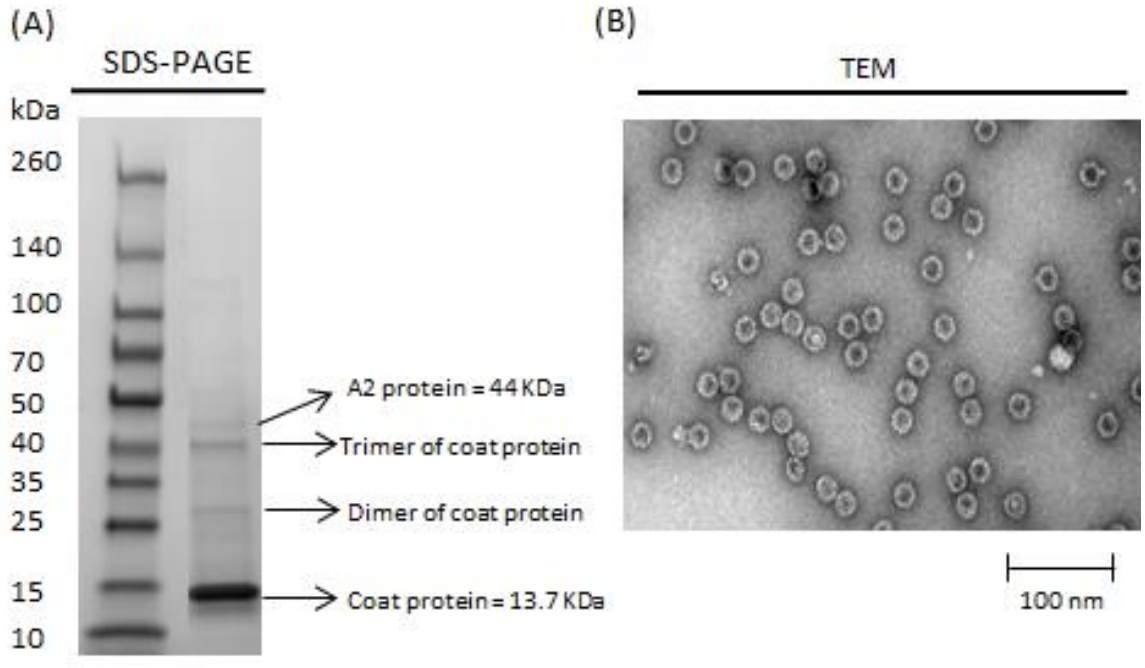

Figure 3. 6: Purified phage Qβ sample. (A), SDS-PAGE showing bands that corresponds to the trimer, dimer and monomer of coat protein (13.7 KDa) and A2 protein (44 KDa) of phage Qβ. Electrophoresis was performed on Bio-Rad Mini Protean Tris-Glycine precast gels 4-15% (w/v) bisacrylamide - acrylamide, 12 well comb, 20 µl and Tris/glycine/SDS buffer as running buffer; (B), TEM image of 4% (w/v) uranyl acetate negative stained phage Qβ showing individual icosahedral particles.

3.4.3 BEV

BEV was purified through a 15% - 45% (w/v) sucrose gradient by ultracentrifugation as described in Section 2.2.3.1 and gradient fractions collected from top to bottom were analysed by SDS-PAGE to identify the BEV peak fractions. The BEV capsid is composed 60 copies each of VP1 (34 KDa), VP2 (29 KDa), VP3 (27 KDa) and VP4 (7 KDa) (Kaminaka et al., 1999). SDS-PAGE showing the capsid proteins of BEV2 and the TEM image showed individual icosahedral BEV 2 particles (Figure 3.7) with no background confirmed that the purification of BEV 2 was successful and the sample was of high purity. The sample was split into 50 µl aliquots and stored at -20 ^{o}C or -80 ^{o}C.

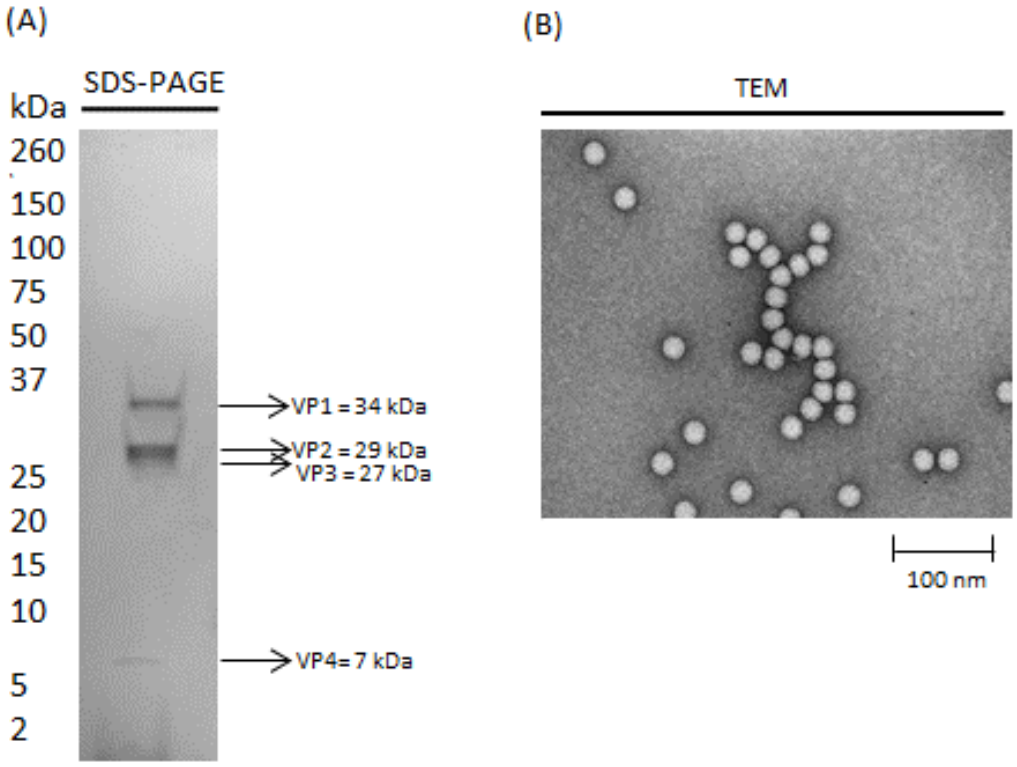

Figure 3. 7: Purified bovine enterovirus 2 (BEV 2) sample. (A), SDS-PAGE showing bands that corresponds to the capsid proteins of BEV 2; VP1 (34 KDa), VP2 (29 KDa), VP3 (27 KDa) and VP4 (7 KDa). Electrophoresis was performed on Bio-Rad Mini Protean Tris-Tricine precast gels 10-20% (w/v) bisacrylamide - acrylamide, 12 well comb, 20 µl and Tris/tricine/SDS buffer as running buffer; (B), TEM image of 4% (w/v) uranyl acetate negative stained BEV 2 showing individual icosahedral particles.

3.4.4 MNV

MNV was propagated, clarified and then concentrated by ultracentrifugation as described in Section 2.2.4.1. The concentrated MNV was used for PDI investigation with no further purification. This was because of the low titre usually associated with MNV and it was thought that purification through sucrose gradient by ultracentrifugation would further reduce the titre. Norovirus capsids are formed from 180 copies of VP1 (58 KDa) organised in a 3-quasi equivalent icosahedral symmetry. The western blot showed a clear band that corresponds to VP1 of MNV (Figure 3.8). However, because the concentrated MNV was not ultra-purified, SDS-PAGE showed several bands (Figure 3.8) indicating that other proteins were present in addition to MNV. TEM was not carried out as we knew the sample was not ultra-pure.

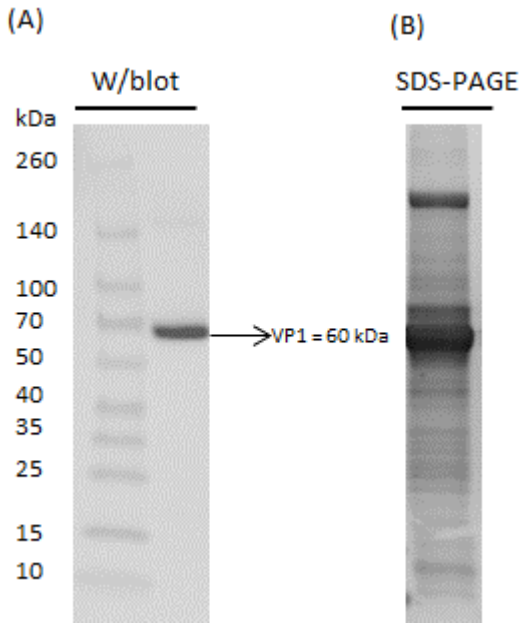

Figure 3. 8: Concentrated murine norovirus (MNV) sample. (A), western blot showing a clear band that corresponds to a major capsid protein (VP1) (58 KDa) of MNV; (B), SDS-PAGE showing several bands that is an indication of some impurities as the sample was not ultra-pure. Electrophoresis was performed on Bio-Rad Mini Protean Tris-Glycine precast gels 4-15% (w/v) bisacrylamide - acrylamide, 12 well comb, 20 µl and Tris/glycine/SDS buffer as running buffer.

3.5 Assay of dead *E. coli* cells to determine MS2 viability

We examined assayed dead *E. coli* cells by measuring the fluorescence of PI at λ_{ex} of 470 nm. The method is based on the ability of PI to go selectively into a cell with a compromised membrane, intercalate with DNA and fluoresce. In our case, membrane impairment was caused by bacteriophage infection. Fluorescence of PI in different samples of *E. coli* host cell infected with different dilutions of MS2 was measured (Figure 3.9).

We thought of using assay of dead *E. coli* by PI to indirectly test the viability of MS2. This was because, although the culturing (double layer agar plaque) method is still the gold standard method to determine viability of MS2 after inactivation by singlet oxygen, it has limitations such as being slow and laborious. Thus, there is a need to search for new methods to determine infectivity and titre. We exploited the fact that MS2 is lytic and its infection can cause membrane damage of its bacterial host. We expected that the control (no MS2 infection) and bacteria samples infected with dilutions higher than 10^6 (≤200 PFU/ml) of MS2 should have little MS2 that would damage the membrane and little PI would enter the cell and thus no fluorescence. However, our data showed otherwise (Figure 3.9). There was no clear difference in fluorescence of the bacteria samples with the MS2 infection and those with ≤200 PFU/ml or no MS2 infection and thus making it impossible for us to determine viability of MS2 by this method.

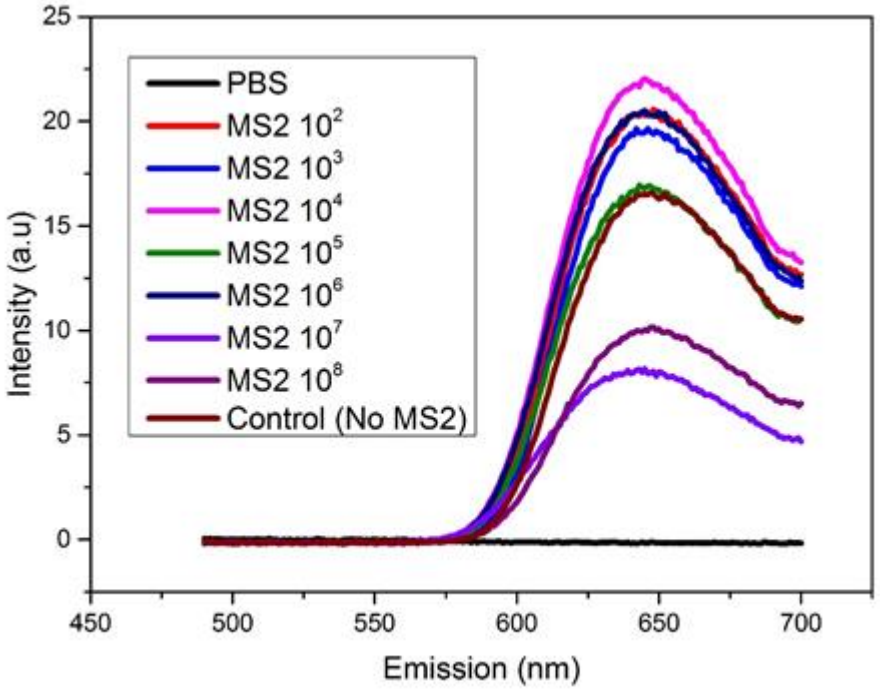

Figure 3. 9: Fluorescence scan of PI in different samples of *E. coli* host cell infected with MS2. Stock MS2 were diluted 10 fold from 10^2 - 10^8 as shown. Peak emission wavelength for all samples was 646 nm.

3.6 Enzyme activity assay in *E. coli* to determine MS2 viability

Since the assay of dead *E. coli* cells was not successful, we decided to assess the member of live *E. coli* cells using assay of host cell esterase activity to indirectly test the viability of MS2. This method is based on the hydrolytic cleavage of fluorescein diacetate (FDA) which is colourless into fluorescein which fluoresces yellow-green by esterases inside the cell. FDA is an acetylated derivative of the green fluorescent dye fluorescein (Boyd et al., 2008). The attachment of acetyl groups on the xanthene group renders the dye non-fluorescent, but it confers the ability to passively diffuse through a phospholipid bilayer (Boyd et al., 2008). Once FDA is in the cytoplasm, non-specific esterases de-acetylate the molecule to convert it to fluorescein and the by-products acetic acid/acetaldehyde (Boyd et al., 2008). FDA is neutral and penetrates the bacteria cells. However, fluorescein has a negative charge of 2 and cannot escape

from intact live cells. The cells that have impaired membrane by phage infection will have little or no fluorescence.

In order to determine the best type of sample for this method, three sets of samples were used; whole samples (WS) which were each 5 ml two hours log phase broth culture of *E. coli* incubated with 8 µl of 12 mM FDA for 15 min, supernatant samples (SS) were each 5 ml supernatant of two hours log phase broth culture of *E. coli* incubated with 8 µl of 12 mM FDA for 15 min and pellet samples (PS) were each 5 ml resuspended pellet of 5 ml two hours log phase broth culture of *E. coli* incubated with 8 µl of 12 mM FDA for 15 min. Fluorescence of each sample was scanned at λex of 470 nm. Our data showed that WS was probably the best sample for this method because the data shows the trend that was expected (Figure 3.10). It was expected that the control (no MS2) and bacterial samples infected with dilutions higher than 10^6 (≤ 200 PFU/ml) should have very little MS2 that would compromise the membrane or cause the death of the bacteria host cells. As such, they should have more fluorescence. The control with no MS2 had the highest fluorescence peak and WS infected the lowest dilution of MS2 (10^2) had the lowest fluorescence peak as expected (Figure 3.10 A). There was a linear relationship between MS2 dilutions (expressed in $\log_{10}$ PFU/ml) and their respective peak emission intensities (Figure 3.10 B). However, this method was not robust as it required more standardisation, so the plaque assay was retained. The other two samples; SS (Figures 3.11) and PS (Figures 3.12) were inconsistent.

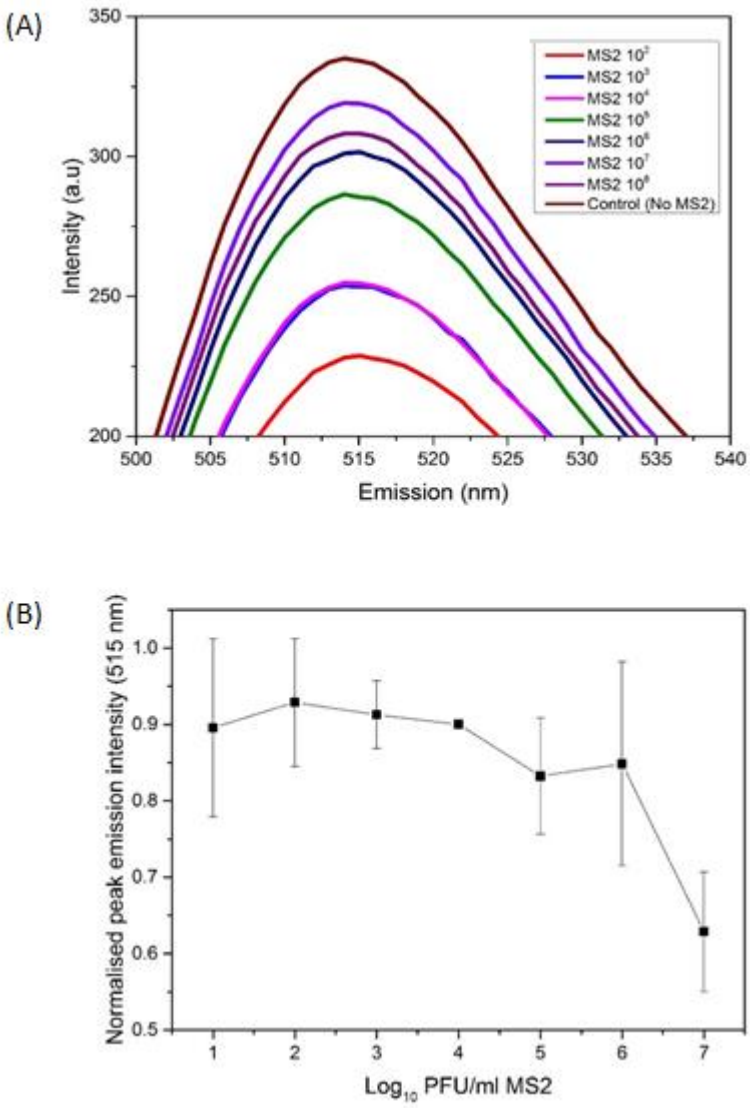

Figure 3. 10: Enzyme activity assay in *E. coli* to determine MS2 viability. (A), fluorescence scan of FDA in different samples of *E. coli* (whole sample) infected with MS2. Stock MS2 were diluted 10 fold from 10^2 - 10^8 as shown; (B), Intensity of peak emission at 515 nm against MS2 dilutions. 7 - 1 $\log_{10}$ PFU/ml correspond to dilutions 10^2 - 10^8 respectively. Data are mean ± standard deviation (n = 3).

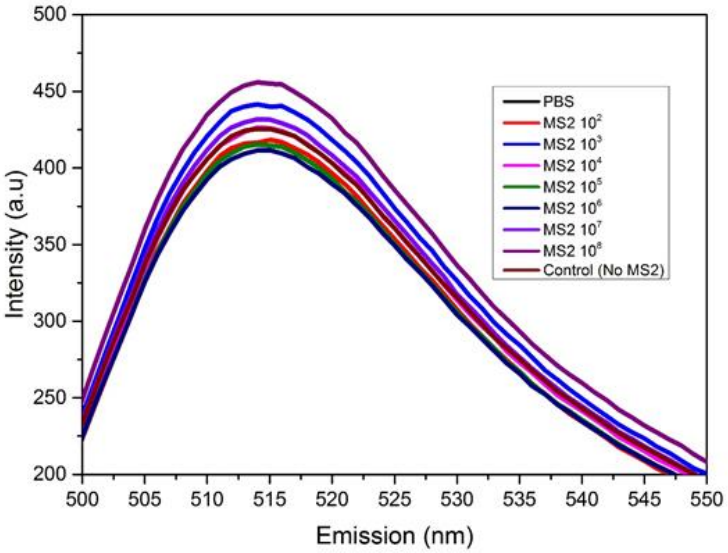

Figure 3. 11: Fluorescence scan of FDA in different samples of *E. coli* (supernatant sample without cells) infected MS2. Stock MS2 were diluted 10 fold from 10^2 - 10^8 as shown. Peak emission wavelength for all samples was 515 nm.

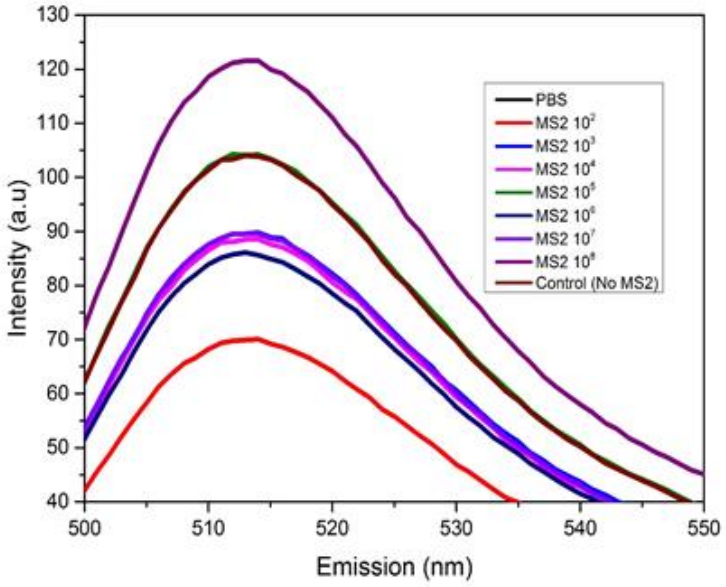

Figure 3. 12: Fluorescence scan of FDA in different samples of *E. coli* (pellet sample) infected MS2. Stock MS2 were diluted 10 fold from 10^2 - 10^8 as shown. Peak emission wavelength for all samples was 515 nm.

3.7 Spectral properties of PDI light source and absorbance spectra of photosensitisers

Spectral properties of the PDI light source (Schott KL 2500 LCD, Schott Ltd., UK) and the absorbance spectra of photosensitisers-TMPyP, Rose Bengal and methylene blue were determined. The PDI light source spectra (400 nm – 786 nm) (Figure 3.13 A) showed that it mainly emitted visible light including some near infrared. However, the emission was within the visible light regions. The PDI light spectra and its peak did not seem to be affected drastically by the different light intensities and colour temperatures/ filters available (Figure 3.13). The spectra absorption peaks for 32 $mW.cm^{-2}$ (2650 K, A), 200 $mW.cm^{-2}$ (2950 K, A), 450 mW cm^{-2} (3000 K, B) and 950 mW cm^{-2} (3000 K, C) were at 661 nm, 642 nm, 643 nm and 645 nm respectively (Figure 3.13 A). The absorption spectra of the photosensitisers in PBS showed that their absorption peaks were within visible light regions (Figure 3.13 B). The absorption peaks for TMPyP, Rose Bengal and methylene blue were at 422 nm, 550 nm and 666 nm respectively (Figure 3.13 B).

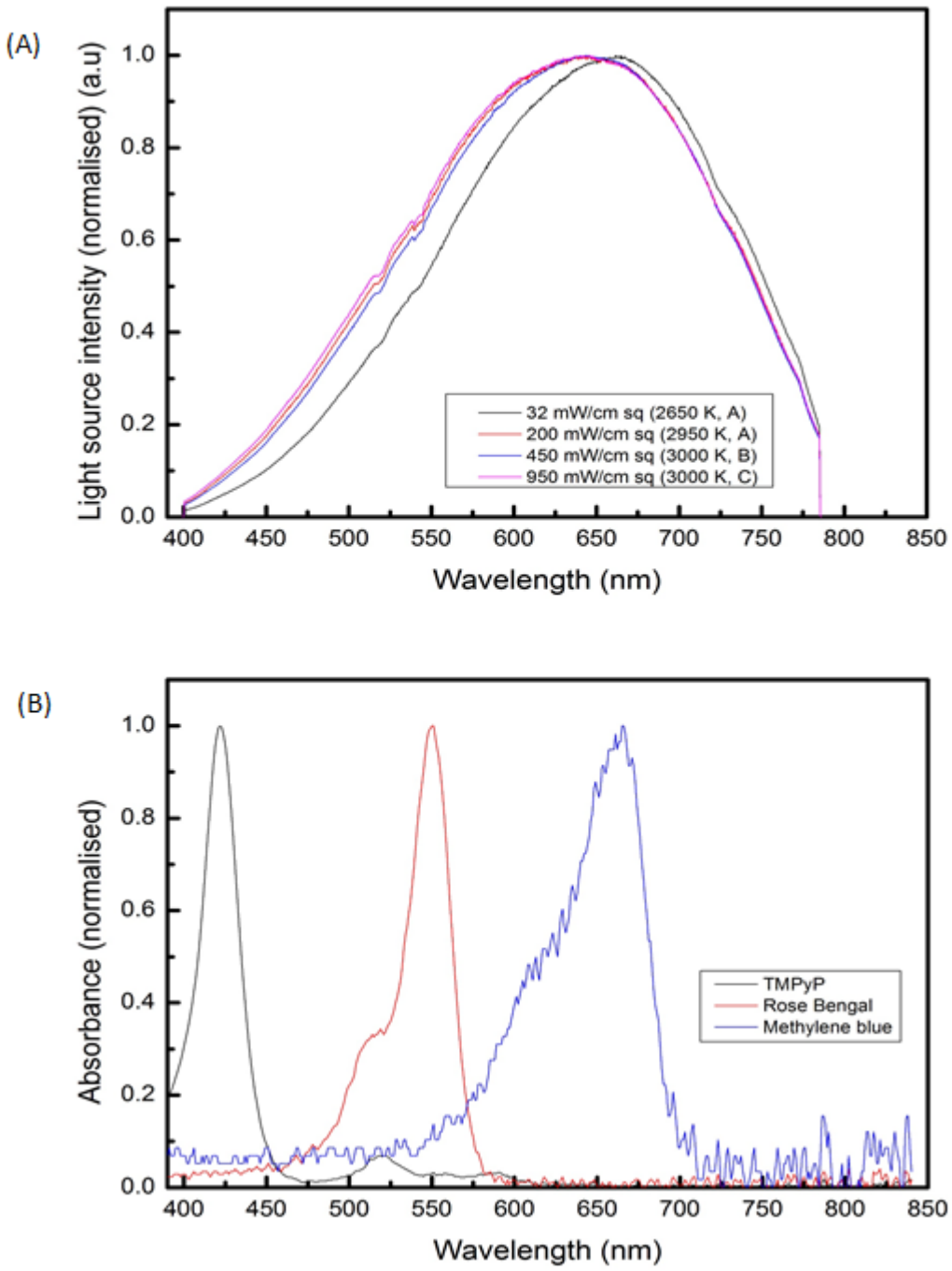

Figure 3. 13: Spectral properties of PDI light source and absorption spectra of photosensitisers. (A), light spectra of our PDI light source (Schott KL 2500 LCD, Schott Ltd., UK). The PDI light source spectra (400 nm – 786 nm) showed that it is mainly emitted visible light including some near infrared. The spectra peak is between 641 nm - 661 nm; (B), absorption spectra of the photosensitisers used in PDI investigations. The absorption peaks for TMPyP, Rose Bengal and methylene blue were at 422 nm, 550 nm and 666 nm respectively.

3.8 Detection of singlet oxygen generated by photosensitisers

Spectrophotometric measurement of the decrease in A_{318} of 2-amino-3-hydroxypyridine (AHP) when reacted with singlet oxygen was used to detect the singlet oxygen generated by TMPyP, Rose Bengal and methylene blue. An assay solution of 2-amino-3-hydroxypyridine (200 µM) and a photosensitiser (1 µM) dissolved in PBS was put in a conventional quartz cell with a light path length of 1 cm, and photo-irradiated with light of fluence rate of 466.45 $mW.cm^{-2}$ for 1 to 5 minutes. Changes in A_{318} before and after photo-irradiation were measured (Figure 3.14).

There are several methods of detecting singlet oxygen generated by photosensitisers in solution (Komagoe et al., 2011, Kohn and Nelson, 2007, Kraljic and Mohsni, 1978). We measured singlet oxygen produced by the photosensitisers (Komagoe et al., 2011). However, it is an indirect and semi-quantitative method. (Komagoe et al., 2011). Our data showed that singlet oxygen was generated by photosensitisers in solution as shown by the decrease in A_{318} (Figure 3.14). The decrease in A_{318} was proportionally related to illumination time (Figure 3.14), and the implication of this is that photodynamic inactivation of waterborne pathogens using these photosensitisers (TMPyP, Rose Bengal and methylene blue) will also be dependent on the illumination time amongst other factors.

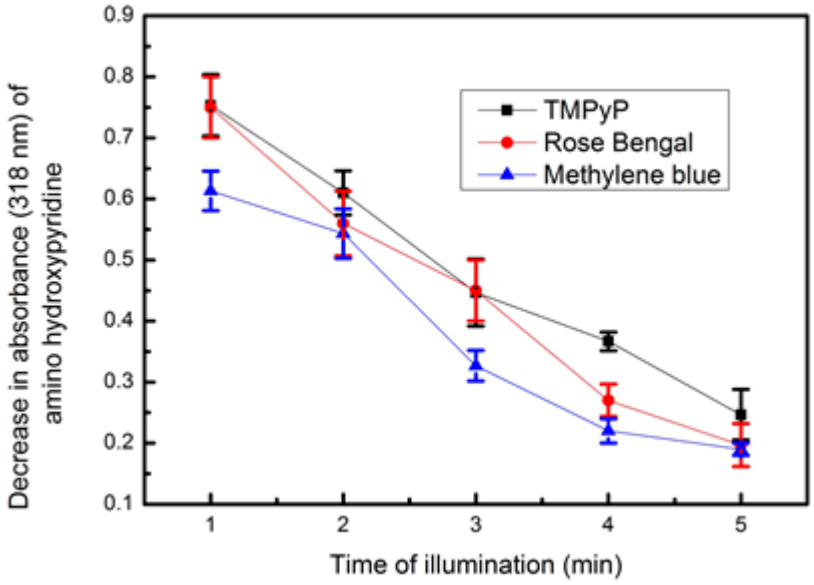

Figure 3. 14: Decrease in absorbance (318 nm) of 2-amino-3-hydroxypyridine due to singlet oxygen generated by the photosensitisers in solution after illumination at different time. Data are mean ± standard deviation (n = 3).

3.9 Conclusion

The data presented in this chapter showed that model viral organisms (bacteriophages MS2 and Qβ, bovine enterovirus and murine norovirus) were successfully propagated in their respective host cells and purified. The purified samples of the model viruses were of high purity except for MNV. The MNV samples were usually diluted 10 fold in PBS before PDI experiments to reduce (protein impurities) to the barest minimum. High purity was necessary to avoid interference that might be caused by impurities such as media proteins to PDI of these viruses. There are 2 possible ways the impurities could affect the PDI of these viruses, this is either by competing with the viruses in quenching the singlet oxygen and other ROS or by shielding the viruses thereby preventing direct damage induced by the singlet

oxygen. Either way, the rate and extent of PDI of these viruses would most likely be affected.

The use of 50% (v/v) saturate ammonium sulphate to precipitate viruses and other host cell protein present in the clarified lysate after the propagation and then subsequent purification through 15 - 45% (w/v) sucrose gradient proved to be an efficient method of achieving ultra-pure virus stock. This method is reproducible, easy and cheap as it involves the use of few chemicals.

Bacteriophages MS2 and Qβ were easier and cheaper to propagate and purify as compared to BEV 2 and MNV. Our effort to assess and standardise dead and or live host *E. coli* cells in order to determine the infectivity and titre of MS2 was not successful. It was assumed that these assays when standardised could make determination of infectivity and titre of MS2 much easier and quicker. We could not observe any significant difference in the fluorescence of PI of the test and control samples in assay of dead *E. coli* cells. Also, we could not observe any significant difference in the fluorescence of FDA of the test and control samples (SS and PS) in esterase activity assay of live *E. coli* host cells to indirectly test the viability of MS2 phage. And because of these reasons the double layer agar plaque assay was retained as a way of determining the viability of the phages before and after the PDI.

Our light source emits visible light and the photosensitisers (TMPyP, Rose Bengal and methylene blue) that were used for PDI investigations in this work have their absorption maxima within the visible region of the spectrum. This is important as this study was aimed at developing a sunlight driven water disinfection system that could be used to clean water in the regions of the world that lack energy infrastructures for

conventional centralised water treatment process. Also, because our light source does not include other regions of light spectrum that can inactivate microorganisms such as UV light, we are sure that the inactivations of model viruses and bacteria observed were solely as result of photodynamic effect during PDI experiments.

Chapter Four: Results II

Chapter 4: Results II

Photodynamic inactivation of bacteriophages MS2 and Qβ, murine norovirus and bovine enterovirus in solution

4.1 Overview

Although the ultimate aim of this work was to get photosensitisers such as TMPyP attached onto chitosan nanofiber and polymeric membrane before PDI of microbial pathogens in water, testing the photoinactivation capacity and efficiency of TMPyP and other photosensitisers in solution was the first step. To do this, we used bacteriophages MS2 and Qβ, murine norovirus and bovine enterovirus as model viruses. However, the majority of the PDI investigations were done using MS2. PDI of model viruses were investigated with different concentrations of TMPyP in solution, different light intensities and at different times of light illumination. The concentrations of TMPyP used were 0.1 µM to 50 µM, light intensities were 5 $mW.cm^{-2}$ to 466 $mW.cm^{-2}$ and illumination times were 10 sec to 120 min. Photosensitisers- Rose Bengal and Methylene blue were also used to investigate PDI of MS2 in solution. SDS-PAGE, western botting, native agarose electrophoresis, TEM, and DLS were used in trying to understand mechanisms of PDI in viruses. Effort was made to select a PDI resistant mutant MS2 in order to confirm the universality and irreversibility of the PDI damages in viruses. Also, RNA was extracted from MNV PDI samples and transfected in order to show the effects of PDI on its RNA genome.

In this chapter, data from PDI of the model viruses in solution are presented. The rate and extent of PDI were shown as reductions in log_{10} PFU/ml of the viruses. These data highlighted effects of several factors/conditions on the PDI of model viruses. Also, data are presented in this chapter that possibly reveal the mechanism and targets of PDI in the viruses used in this study.

4.2 Effects of concentration of TMPyP and illumination time on PDI of MS2

The dependency of the extent of PDI on TMPyP concentration/dose and illumination time were investigated in solution. PDI of MS2 was investigated at constant visible light intensity of 32 $W.cm^{-2}$ with different concentrations of TMPyP in solution and at different times of illumination. This light intensity (32 $W.cm^{-2}$) is low and is about 10% mid-day sunshine during summer in the UK but allows a graded response to be shown. Double layer agar plaque assay was used to carry out viability test and to determine the extent of PDI in MS2.

Our data showed that TMPyP with concentration of at least 0.2 µM in solution could achieve complete inactivation of MS2 within 60 sec when illuminated at 32 $W.cm^{-2}$ (Figure 4.1 A). At 10 seconds of illumination there were 1.5 log reductions in PFU/ml (Figure 4.1 B) and at 30 seconds of illumination there were 4 log reductions in PFU/ml of MS2 (Figure 4.1 B). There was no significant difference between the rate and extent of PDI in MS2 caused by 0.2 µM TMPyP (Figure 4.1 A) as compared to that caused by higher concentrations such as 50 µM TMPyP (Figure 4.1 C). In fact, complete MS2 inactivation was observed at 50 sec of PDI when 0.5 µM TMPyP was used (Figure 4.1 B) while it was 60 sec when 50 µM TMPyP was used (Figure 4.1 C). However, only the reductions of 4 log PFU/ml of MS2 was observed when 0.1 µM TMPyP was used for 60 sec PDI (Figure 4.1 A). TMPyP alone in the dark or light alone without sensitiser do not cause any detectable reduction in log PFU/ml of MS2 (Figure 4.1). Previous work has shown that tetra-porphyrins like TMPyP can efficiently inactivate bacteriophages such as phage T4-like in solution (Costa et al., 2008, Costa et al., 2010). It was reported that complete inactivation phage T4-like from sewage was achieved only at the highest TMPyP concentration used, 5 µM, and

illuminated at 40 $W.m^{-2}$ for 270 minutes. Complete inactivation within 1 minute was also reported but at higher concentrations of 1 mM and 10 µM of TMPyP illuminated at 2.2 $mW.cm^{-2}$ with a UV lamp (Casteel et al., 2004). In this work, we avoided using a UV lamp as source of light and used cold visible light source instead, as UVC can inactivate microorganisms directly.

Figure 4. 1: MS2 PDI in solution. Phage were illuminated at 32 $mW.cm^{-2}$. (A), PDI using different concentrations (0.1 µM to 0.4 µM) of TMPyP; (B), PDI using 0.5 µM TMPyP in solution from 10 to 60 sec; (C), PDI using 50 µM TMPyP in solution from 10 to 60 sec. The dark controls were treated with the concentration of photosensitiser shown but not illuminated whilst no photosensitiser controls (NS) were illuminated without photosensitiser present. Data are mean ± standard deviation (n = 3).
⬚, complete inactivation.

4.3 Effects of light intensity and co-pollutants on PDI of MS2

The ultimate aim of this project was to develop a sunlight driven water disinfection system that could be used in both developed and developing countries to produce safe drinking. However, in reality, sunlight intensity varies from place to place, position of the sun in the sky, different altitude/latitude and sky conditions (Figure 4.2).

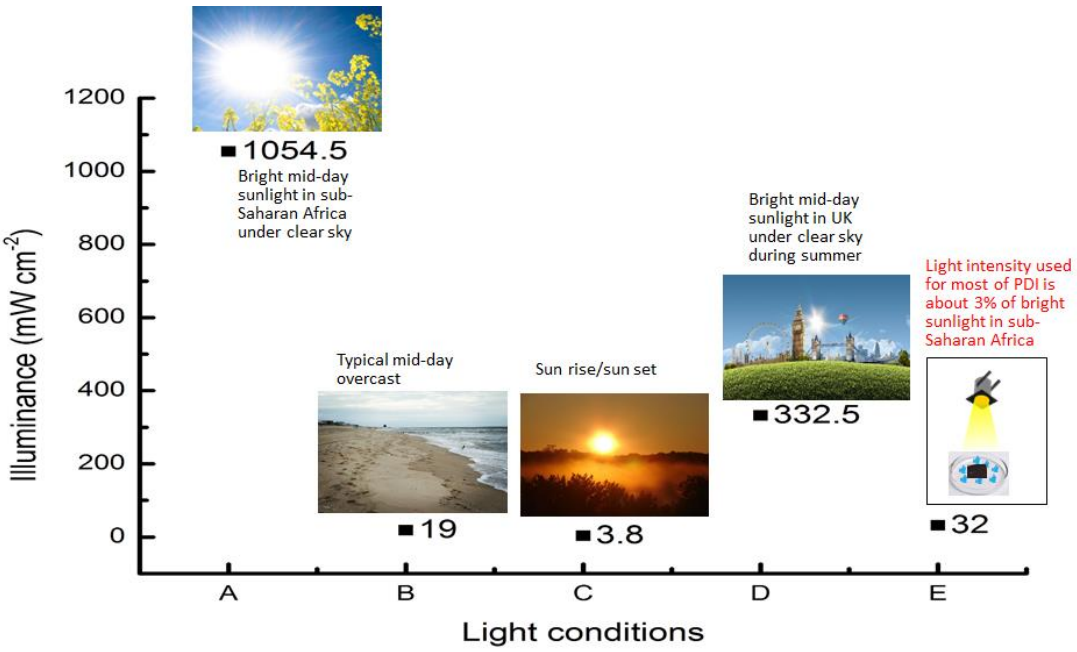

Figure 4. 2: Sunlight intensities differ according to place, position of the sun in the sky, different altitude/latitude and sky conditions. The light intensity used for most of our PDI investigations is about 3% of bright mid-day sunlight under clear sky conditions in the Sub-Saharan Africa and about 10% of mid-day sunlight during summer in Northern Europe.

Even though our data has shown that the illumination time has a proportional relationship with the rate and extent of PDI of MS2 (Figure 4.1), the effect of light intensity on PDI of MS2 was also investigated. This could inform the timing and climatic conditions for sunlight driven water disinfection. PDI of MS2 was investigated at a constant concentration of 0.5 µM of TMPyP in solution and 60 sec illumination but at different light fluences. The different light intensities used were from 5 $mW.cm^{-2}$ to 40 $mW.cm^{-2}$.

Also, we carried out experiments to determine the effect of co-pollutants on the rate and extent of PDI in MS2. This was to determine whether in a real-life situation, a pre-treatment such as removal of soluble organic pollutants by coagulation/precipitation or filtration would be required before PDI can be

effectively used for water disinfection during waste water treatment. We used PDI conditions (0.5 µM photosensitiser, 32 $mW.cm^{-2}$ and 30 sec and 60 sec of illumination) which caused a reductions of 4 log_{10} PFU/ml and complete inactivation of MS2 for 30 sec and 60 sec of illumination respectively. However, to test the effect of organic pollutants on PDI of MS2, in addition to these conditions the PDI was carried out in PBS that contained 0.1% (w/v) of humic acid.

In each PDI light experiment i.e. with photosensitiser present was carried out with two controls. These were a dark control, with photosensitiser but not illuminated and no sensitiser but still illuminated. Double layer agar plaque assay was used to carry out viability test and to determine the extent of PDI in MS2.

Our data showed that 20 $mW.cm^{-2}$, about 1.8 % of mid-day sunlight in sub-Saharan Africa, could achieve complete inactivation i.e. reductions of 9.5 log PFU/ml of MS2 PDI for 1 min using 0.5 µM TMPyP (Figure 4.3). We observed 3, 4 and 6 log reductions of PFU/ml of MS2 for the light intensities of 5, 10 and 15 $mW.cm^{-2}$ respectively for 1 min MS2 PDI, also using 0.5 µM TMPyP (Figure 4.3). This indicates that there is proportional relationship between the light intensity and extent of PDI of MS2. It has been reported that using tetra and tri cationic porphyrins as photosensitisers, the extent of PDI of phage T4-like depends on the type of sensitiser and its concentration, light source, energy dose and fluence rate (Costa et al., 2010). They observed that when the same light source and a fixed light dose was applied at different fluence rates, phage inactivation was significantly higher when low fluence rates were used (Costa et al., 2010). This contradicts our findings at least for the light intensities from 5 $mW.cm^{-2}$ to 20 $mW.cm^{-2}$ where we observed proportional inactivation of MS2 (Figure 4.3).

Our data also showed that 0.1% (w/v) of humic acid in solution gave 100% protection to MS2 during PDI (Figure 4.4). This was at least true for the PDI conditions used (0.5 μM photosensitiser, 32 $mW.cm^{-2}$ and 30 sec and 60 sec of illumination). No MS2 inactivation was observed. (Figure 4.4). This concentration [0.1% (w/v) equivalent to 1 mg/ml] of humic acid gave dark chocolate colour to PDI solution leading to reduction of light transmittance and therefore molecules of photosensitiser- TMPyP were not excited or few were excited and ultimately no or very few singlet oxygen and other ROS were generated. It is also possible that the humic acid quenched the singlet oxygen and other ROS generated or shield the virus from direct effect of singlet oxygen mediated oxidation. However, some studies have shown that constituents (dissolved and particulate) from stabilisation ponds as well as synthetic humic acid and natural humic acid extracted from a river can act as photosensitisers when exposed to full spectrum sunlight thereby inactivating MS2, adenovirus type 2 and bacteriophage PRD1 (Kohn and Nelson, 2007, Silverman et al., 2013). It was reported that the efficiency of these photosensitisers at inactivating MS2 was in order; synthetic humic acid > natural humic acid extracted from a river > constituents of a stabilisation pond (Kohn and Nelson, 2007).

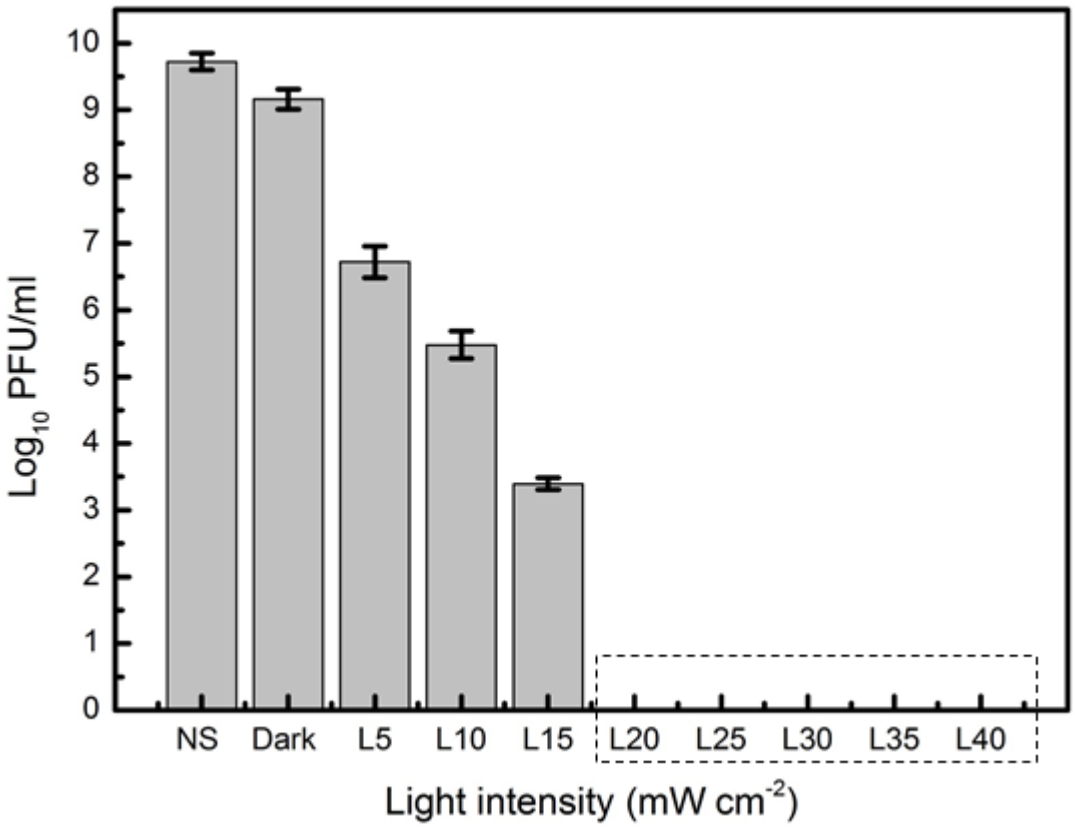

Figure 4. 3: PDI of MS2 using 0.5 µM TMPyP in solution. Phage were illuminated for 60 sec at different light intensities. L5 to L40 indicates fluence rates of 5 mW.cm^{-2} to 40 mW.cm^{-2}. The dark controls were treated with the concentration of photosensitiser shown but not illuminated whilst no photosensitiser controls (NS) were illuminated without photosensitiser present. Data are mean ± standard deviation (n = 3). ⬚, complete inactivation.

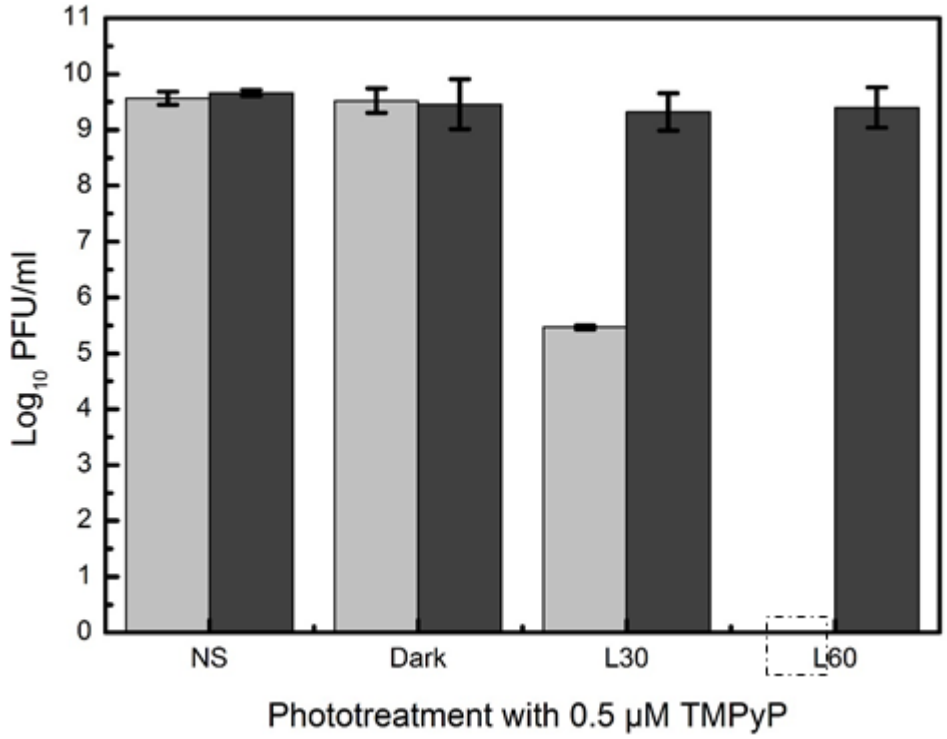

Figure 4. 4: PDI of MS2 in the presence and absence of humic acid. Phage were illuminated at 32 Mw.cm^{-2}. L30 and L60 indicates 30 sec and 60 sec illumination times respectively. The dark controls were treated with the concentration of photosensitiser shown but not illuminated whilst no photosensitiser controls (NS) were illuminated without photosensitiser present. Data are mean ± standard deviation (n = 3).

( ), No humic acid; ( ), 0.1% (w/v) humic acid; ( ), Complete inactivation

4.4 Selection and evolution of MS2 resistant to PDI

Our data showed that under PDI conditions of 0.5 µM TMPyP, 32 mW.cm^{-2} and 30 sec illumination, reductions of 4 log PFU/ml of MS2 (Figure 4.1) were found with about 5 log PFU/ml of the MS2 population still viable. In order to test whether MS2 could evolve into PDI resistant MS2, this viable population can be selected and then subjected to repeated cycles of PDI. Evolution experiments were carried out by subjecting MS2 to repeated cycles of PDI condition each time causing reduction of about 4 log PFU/ml of MS2. After each PDI cycle, the remaining viable MS2 were recovered by propagation in *E. coli* host cells and the titre was determined before

exposure to the next cycle of PDI. All experiments were in triplicate and a double layer agar plaque assay was used to test viability and to determine the extent of PDI.

Our data showed that even at the 10^{th} cycle of PDI, we could not observe any resistance of MS2 to PDI (Figure 4.5). Throughout the PDI cycles, we consistently observed reductions of 4 log PFU/ml of MS2 (Figure 4.5) and this indicates, that at least over the 10 cycles no resistance to PDI had emerged in the MS2 population. The lack of evolution of resistance of MS2 to PDI we observed confirms many reports and hypothesis that PDI modification/damage is universal and irreversible (Bourre et al., 2010, Jori et al., 2006). The universality and irreversibility of the PDI process as well as lack of resistance of microorganisms, especially viruses, to PDI is a positive news as there are reports of resistance to virtually every antimicrobial agent including water disinfectants. Chemical oxidants such as free chlorine and chlorine dioxide (CLO_2) are used for disinfection during wastewater treatment. Viruses are generally more resistant to disinfectants than traditional bacterial indicators such as *E. coli* and *Enterococci* (Mamane et al., 2007, Aronino et al., 2009). This is because compared to other organisms, RNA viruses, which are the largest group of human viral pathogens, have high mutation rates which increases diversity within their population and thereby helps then evolve to adapt to environmental stress (Zhong et al., 2016, Domingo et al., 1996, Duffy et al., 2008). There are many reports about emergence of resistant viruses upon continuous administration of antiviral drugs and exposure to common water disinfectants (Zhong et al., 2016, Lauring et al., 2013, Sanjuan et al., 2010). It has been shown that after repeated exposure of MS2 to ClO_2, resistant MS2 population to the disinfectant emerged (Zhong et al., 2016). The resistant population had fixed mutations which substituted ClO_2 –labile amino acids

with ClO_2 –stable ones thereby resulting in a more stable host binding protein (A-protein) in MS2 during inactivation and thus greater ability to maintain infectivity (Zhong et al., 2016).

PDI of bacteria and other eukaryotic cells strongly prevents activating a repair processes or inducing expression of antioxidative factors or stress proteins (Bourre et al., 2010, Jori et al., 2006). The cell death is primarily a consequence of singlet oxygen (and other ROS) mediated damage through a typical multi-target process which minimises the risk of both the onset of mutagenic processes and the selection of photoresistant cells (Wainwright, 1998, Zeina et al., 2001, Zolfaghari et al., 2009, Bourre et al., 2010). Thus, unlike chlorine disinfection, there is almost no chance of resistance and both traditional and emerging pathogens will be taking care off with the same and absolute efficiency.

(Placeholder5p. This image has been removed by the author of this thesis for copyright reasons)

Figure 4. 5: Repeated PDI cycles of MS2 in solution. (A), titre of MS2 before and after PDI of PDI cycles. Each PDI cycle was subjected to 0.5 µM TMPyP and illuminated at 32 $mW.cm^{-2}$ for 30 sec; (B), reductions of log_{10} PFU/ml of MS2 for each PDI cycle. Data are mean ± standard deviation (n = 3).

4.5 Effect of Rose Bengal and methylene blue in PDI of MS2

The PDI condition which caused complete inactivation of MS2 with TMPyP in solution (0.5 µM photosensitiser, 32 $mW.cm^{-2}$ and 1 min of illumination, Figure 4.1) was used to investigate the PDI of MS2 with Rose Bengal (RB) and methylene blue (MB). This

was to compare the extent of PDI of MS2 by these photosensitisers in solution in comparison to TMPyP. Also, other PDI conditions (1 µM and 5 µM of RB and MB, 32 $mW.cm^{-2}$ and 466 $mW.cm^{-2}$ and 5 min of illumination) were used to investigate PDI of MS2 in solution. Each PDI light experiment was carried out with two controls, these were a dark experiment (D) where the sample had photosensitiser but was not exposed to light and a no sensitiser experiment (NS) where photosensitiser was absent but the MS2 were exposed to light.

Our data showed that RB and MB did not cause any detectable inactivation of MS2 under PDI condition which caused complete inactivation of MS2 with TMPyP in solution (0.5 µM photosensitiser, 32 $mW.cm^{-2}$ and 1 min of illumination) (Figure 4.6). Even at higher concentrations of 1 µM and 5 µM each of RB and MB, no inactivation of MS2 was observed for samples illuminated at 32 $mW.cm^{-2}$ for 5 min (Figure 4.6). However, when illuminated at 466 $mW.cm^{-2}$ for 5min, reductions of 3 log PFU/ml of MS2 and complete inactivation were observed for samples treated with 1 µM and 5 µM of methylene blue respectively (Figure 4.6). At this light intensity and 5 min illumination, only reduction of 1 log PFU/ml MS2 was observed for sample treated with 5 µM Rose Bengal and no inactivation was observed for sample treated with 1 µM Rose Bengal (Figure 4.6).

The photosensitisers TMPyP, RB and MB are all soluble in water and have their absorption peaks within visible light range (Figure 3.13). This means that our source of light for PDI which generates only visible light can excite these photosensitisers to generate singlet oxygen and other ROS in solution and ultimately inactivate MS2 and other microorganisms. We have confirmed that the photosensitisers do generate singlet oxygen (Figure 3.14). Many studies have been reported that TMPyP, RB and

MB can cause PDI of viruses in solution (Casteel et al., 2004, Wainwright, 2004, Cho et al., 2010). However, our data (Figure 4.6) indicated that TMPyP is the most efficient in the PDI of MS2. This may be due to differences in the net charges of the photosensitisers used. In solution, TMPyP will have net charge of +4, methylene blue +1 and Rose Bengal -2. Attraction between MS2 (negatively charged) and TMPyP will be greater and thus there will be better proximity of MS2 to singlet oxygen generated by TMPyP. This is in agreement with many reports that tetra and tri cationic photosensitisers causes rapid and high rates of inactivation of microorganisms during PDI (Costa et al., 2008, Alves et al., 2009).

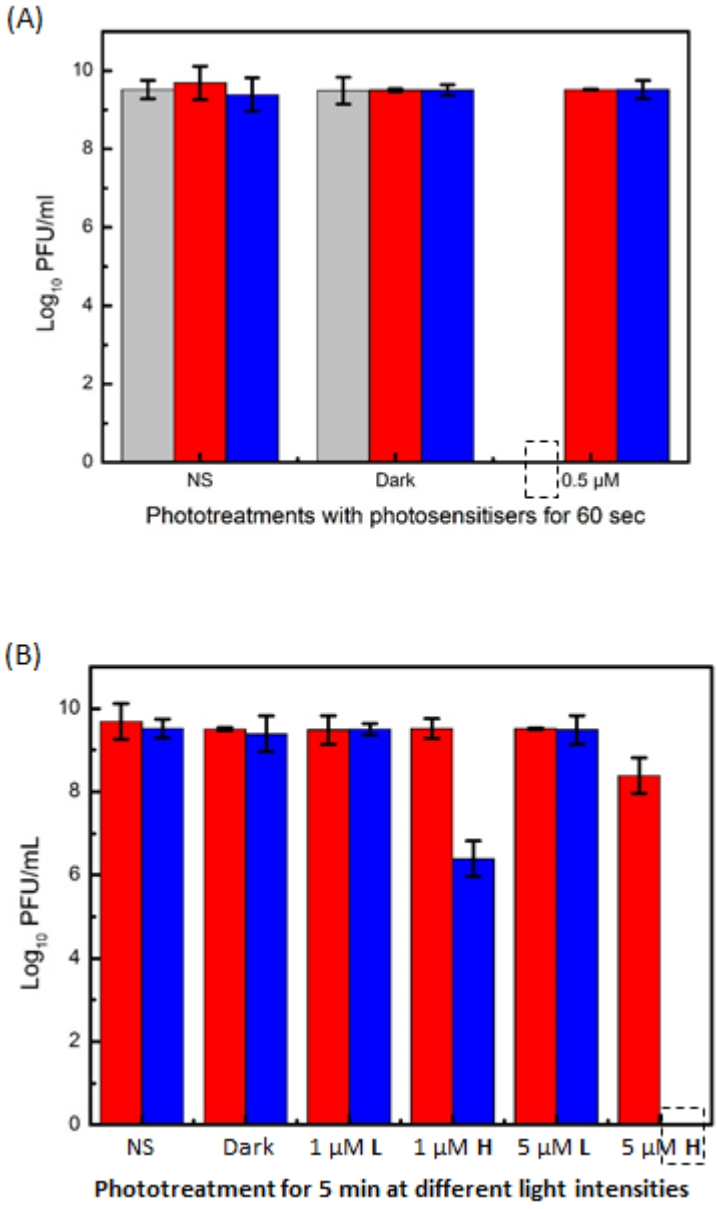

Figure 4. 6: MS2 phage PDI in solution using TMPyP, Rose Bengal and methylene blue. (A), PDI using 0.5 µM of photosensitisers each and illuminated at 32 mW cm^{-2}; (B), PDI using different light intensities. Samples with 1 µM and 5 µM photosensitisers were illuminated at 32 mW cm^{-2} which is a low (L) light intensity. Also, samples with same concentrations of the photosensitisers were illuminated at 466 mW cm^{-2} which is a high (H) light intensity. The dark controls were treated with the concentration of photosensitiser shown but not illuminated whilst no photosensitiser controls (NS) were illuminated without photosensitiser present. Data are mean ± standard deviation (n = 3).

( ), TMPyP; ( ), Rose Bengal; ( ), Methylene blue; ( ), Complete inactivation

4.6 Changes to MS2 capsid proteins induced by singlet oxygen during PDI

In order to investigate intra and inter changes induced by singlet oxygen to capsid proteins of MS2 during PDI, SDS-PAGE plus western blotting and native agarose gel electrophoresis of PDI-treated MS2 samples were carried out. Antibodies raised against the MS2 were able to detect all PDI-treated samples of MS2 and the dark experiment samples (Figure 4.7). Bands corresponding to 13.7 KDa of MS2 coat proteins were detected for all samples. However, some samples exposed to light (Figure 4.7 lanes 5-10) had additional bands. These bands were ≈ 27 KDa that are likely to correspond to dimers of MS2 coat protein.

(Placeholder6p. This image has been removed by the author of this thesis for copyright reasons)

Figure 4. 7: Western blot of MS2 after PDI. Phage were illuminated at 32 mW.cm^{-2} with 1 µM TMPyP in solution. NS = no sensitiser; D = dark experiment. After separation on SDS-PAGE and blotting to nitrocellulose paper, detection was performed using rabbit anti MS2 IgG at 1:500 dilution and secondary goat anti-rabbit HRP conjugate at 1:1000 dilution.

We also used native agarose gel electrophoresis of MS2 as it allowed visualisation of the PDI MS2 in its native form without reducing agents or heat-treatment. Stained material was observed in the well of light experiment samples treated with 50 µM of TMPyP, even at 1 min of PDI (Figure 4.8). This material is suggested to be MS2 particles aggregate that is retained within the wells. Complete retention of material within the well was observed for 60 min PDI -treated MS2 (Figure 4.8A).

(Placeholder7p. This image has been removed by the author of this thesis for copyright reasons)

Figure 4. 8: Native agarose gel electrophoresis of PDI treated MS2. Phage were illuminated at 32 mW cm^{-2}; (A), Native gel of MS2 PDI sample with 50 µM TMPyP in solution. The gels were stained with Instant Blue. NS = No sensitiser; D = dark experiment. (B), Gel of PDI treated MS2 with 1-50 µM TMPyP in solution for 60 min. NS= No sensitizer.

The formation of aggregates was proportional to the PDI time. Lower concentrations of TMPyP resulted in the formation of smaller aggregates of MS2 that could not be retained by the well but seemed to be restricted by the gel matrix (Figure 4.8B). The formation of aggregates was further confirmed by TEM and dynamic light scattering (Figure 4.9).

(Placeholder8p. This image has been removed by the author of this thesis for copyright reasons)

Figure 4. 9: TEM and DLS analysis of PDI treated MS2. (A) TEM images of PDI treated MS2, illuminated at 32 mW.cm^{-2} in 50 µM TMPyP solution. Untreated, PDI treated for 1 to 60 min and dark treated MS2 in 50 µM TMPyP solution are shown. The red arrows indicate large MS2 aggregates. (B) DLS analysis of PDI treated MS2 in 50 µM TMPyP solution, illuminated at at 32 mW cm^{-2}. (C) Average MS2 particle sizes of PDI treated MS2. Dark, treated with TMPyP but illuminated. Data are mean ± standard deviation (n = 3).

As shown in the figures 4.7 – 4.9 above, our data suggests that 1 min PDI-treatment of MS2 with 1 µM of TMPyP did not result to large changes to the viral particles. The observed cross-link/aggregation of PDI treated MS2 samples was seen with prolonged PDI treatment for 10 to 60 min (Figures 4.7 - 4.9). By using anti MS2 polyclonal antibodies for the western blots, monomers and dimers of MS2 coat protein were observed of 10 – 60 min PDI samples (Figure 4.7). Aggregation of the MS2 particles was seen and was proportional to the time of PDI and concentration

of TMPyP. This was shown by agarose native gel electrophoresis, TEM and DLS (Figures 4.8 and 4.9). Physical, chemical and biological consequences of singlet oxygen mediated oxidation of proteins could be effects such as enzyme inactivation, protein peroxide formation, side chain product formation and backbone fragmentation, formation of cross links and aggregates (Davies, 2003). In contrast to the very few reports of backbone fragmentation, there is considerable evidence for formation of high-molecular-weight aggregates (dimers and higher species) of proteins oxidised by singlet oxygen (Davies, 2003, Agon et al., 2006, Pattison et al., 2012). There are conflicting reports on the exact causes of cross-links and aggregates formed during singlet oxygen mediated oxidation of proteins. Some of the aggregates may be form by radical-radical termination reactions of tyrosine-derived phenoxyl radicals to give di- tyrosine (Davies, 2003, Pattison et al., 2012, Shen et al., 2000b, Shen et al., 2000a). However, other reports stated that di-tyrosine is not usually generated and is not implicated in the formation of cross links during singlet oxygen oxidation of proteins (Davies, 2003, Shen et al., 2000b). It has also been reported that aggregates and crosslinks may arise from secondary or dark reactions, independent of continuing formation of singlet oxygen (Davies, 2003). Histidine has been often implicated in the formation of crosslinks and aggregates of singlet oxygen oxidised protein. It has been proposed that products of histidine oxidation by singlet oxygen can react with lysine, cysteine or other histidine residues to give crosslinks. Some studies suggested histidine may be very important in aggregate formation as proteins that lack histidine residues do not generally form cross links (Davies, 2003, Shen et al., 2000a). This does not agree with our data as we observed formation of dimers of MS2 coat protein for PDI samples of 10 – 60 min (Figure 4.7) although MS2

coat protein does not contain histidine in its amino acid sequence. Therefore, dimerisation of coat protein is most probably as a result of di-tyrosine formation. Aggregation of MS2 particles of PDI samples (Figures 4.8 and 4.9) may also be due di-tyrosine formation and or secondary reactions. However, the presence of histidine residues in the A-protein (see Figures 1.14 and 2.1), which is part of capsid of MS2, may also contribute to formation of viral particle aggregates during PDI.

4.7 Detecting changes induced in A-protein of MS2 by singlet oxygen

After analysis of the coat protein as a target of PDI, we turned our attention to the A-protein (see Figure 1.14).

(Placeholder9p. This image has been removed by the author of this thesis for copyright reasons)

Figure 1.14: MS2 capsid showing the coat protein 13.7 KDa (178 copies) labelled blue and the A-protein 44 KDa (one copy) labelled red. The A- protein is shown slightly tilted from the surface of the coat protein and (as inset) projecting into the capsid lumen. The α-helix domain of the A-protein is attached to the RNA inside the capsid, while the β-sheet domain is surface-exposed and is believed to recognise and bind to the host bacteria pilus during infection. The model was created by docking the MS2 A-protein [PDB-5tc1] onto the MS2 capsid [PDB-2MS2] using PyMOL version 1.7rc1. This figure was repeated here for clarity.

Changes to the antigenic regions (Figure 4.10 A) caused by oxidation could result in loss of antigenicity and may correspond to the rate of PDI. In order to detect such antigenic changes, sequence-specific antibodies Ab1, Ab2, Ab3 and Ab4 were raised against 4 predicted epitopes of A-protein. Each of the sequence-specific antibodies was able to detect A-protein at ≈ 44 KDa in the untreated or dark treated MS2 (Figure 4.10).

(Placeholder10p. This image has been removed by the author of this thesis for copyright reasons)

(Placeholder11p. This image has been removed by the author of this thesis for copyright reasons)

Figure 4. 10: Western blot of PDI MS2 samples using sequence-specific antibodies to detect A-protein. (A), MS2 A-protein sequence; highlighted segments show epitopes 1 to 4 to which antibodies were raised. 1 µM of TMPyP and illumination at 32 mW cm^{-2} were used for PDI of MS2 and the following antibodies were used for immune detection after PDI: (B), Ab1; (C), Ab2; (D), Ab3; (E), Ab4. NS; no sensitiser; D, dark experiment and L1 to L60 denotes 1 min to 60 min of illumination. (F), shows blocking of the antigenic recognition by incubation of each antibody with its cognate peptide. Data are mean ± standard deviation (n = 3).

We propose that if oxidative damage to specific targets on the protein antigenicity is altered, then the ability for the antibodies to detect A-protein should be lost. Pre-treatment of these sequence-specific antibodies with their cognate peptides blocked antibody-binding thereby confirming the specificity of binding (Figure 4.10 E). The PDI of MS2 phage was performed with 1 µM TMPyP for all samples but at different times of illumination; 1 - 60 min (Figure 4.10). Ab1 and Ab3 did not detect A-protein for MS2 phage samples after 10 min of PDI (Figure 4.10 A and 4.10 C). However, both were able to detect A-protein for MS2 phage after 1 - 10 min of PDI (Figure 4.10 A and 4.10 C). Ab2 and Ab 4 failed to detect MS2 A-protein after even 1 min of PDI

(Figure 4.10 B and 4.10 D). Photosensitiser alone in the dark (D) or light alone (NS) did not cause any loss of antigenicity as all the 4 sequence-specific antibodies were able to A-protein in these samples (Figure 4.10).

We showed that, at a minimum concentration of 0.2 µM TMPyP in solution, MS2 was inactivated within 1 min of illumination at 32 $mW.cm^{-2}$. The primary steps of viral infections involve recognition and attachment of the virion to the host cell receptor. Changes to host receptor recognition sites on the virus capsid could inhibit attachment to host receptor thereby resulting in MS2 inability to infect the host cell. The MS2 capsid comprises 178 copies of a 13 KDa coat protein and 1 copy of a 44 KDa host recognition and attachment protein known as the A-protein (Dai et al., 2017, Koning et al., 2016). We hypothesised these two proteins to be potential targets for singlet oxygen generated by TMPyP in solution because of the short life and high reactivity of singlet oxygen. However, PDI of MS2 phage is very fast and as suggested by other reports (Costa et al., 2014, Hotze et al., 2009), this points to the fact that inactivation of its host recognition protein (A-protein) and not effects on its coat protein is likely responsible for its inactivation.

The A-protein of MS2 has two domains; an α-helical domain (amino acids 140-225, 269-313, and 375-393) with a bundle of six α-helices and a β-sheet domain (amino acids 1-139, 226-268 and 314-374) with six anti-parallel β-strands sandwiched between an N-terminal loop and helix-loop-helix motif (Dai et al., 2017). It is believed that interactions that occurred between helix-loop-helix motifs of one side of the β-sheet domain may be responsible for the attachment of MS2 through its A-protein to the bacterial F-pilus (Dai et al., 2017). Sequence-specific antibodies made against four selected antigenic regions of the A-protein were used. The antibodies were

specific as pre-treatment with their respective peptides blocked their binding to A protein. The antigenic sites of any given protein antigen are usually hydrophylic and surface and solvent accessible regions. Therefore, we assumed that the four selected antigenic determinant sites would be accessible to singlet oxygen during PDI of MS2. Oxidation could cause damage to these sites leading to loss of their antigenicity. However, we believe that the rate of damage caused and loss of antigenicity may vary according to their amino acid composition. Our data show that the sequence-specific antibodies against antigenic sites 1 and 3 failed to detect the A-protein after 10 min PDI (Figure 10, A, C) whilst sequence-specific antibodies against antigenic sites 2 and 4 did not detect A-protein even after 1 min PDI (Figure 10, B, D). This rate of loss of antigenicity of site 2 and site 4 corresponds to the rate of PDI we observed in previous work. It is possible that antigenic site 2 (which is within α-helix domain of A-protein) and antigenic site 4 (which is within β-sheet domain of A-protein) are specific regions of the A-protein responsible for MS2 attachment to the bacterial pilus and especially for the delivery of its genome inside the host. Antigenic site 1 has one tyrosine as the last amino acid of its sequence whilst site 2 has one histidine. Site 4 has a tryptophan and two tyrosine. The amino acids tyrosine, histidine and tryptophan in addition to methionine and cysteine are the most sensitive to oxidation by singlet oxygen. At physiological pH, (the pH condition of our experiments), bimolecular rate constants of these amino acids with singlet oxygen are around 10^7 k (M^{-1} S^{-1}) (Davies, 2003, Wilkinson et al., 1995). The positions of histidine and tryptophan, almost at the middle of antigenic sites 2 and 4 respectively are likely to contribute to their fast rate of antigenicity loss, unlike tyrosine which is the last amino acid of the sequence residue in site 1. The two tyrosines in site 4 might

also be a contributory factor to its fast rate of loss of antigenicity. The impact of change to the chemical structure of sites 2 and 4 caused by histidine and tryptophan oxidation are likely more than that of tyrosine of antigenic determinant site 1. This might be especially so as singlet oxygen oxidation of histidine and tryptophan leads to ring opening while it lead to ring closure in tyrosine (Davies, 2003).

4.8 PDI of model viruses: MS2 vs phage Qβ, MNV and BEV

In many studies aimed at PDI of human viruses, bacteriophage MS2 is often used as a model because of its similarity to a number of human viruses, e.g. enteroviruses. However, some experts believed that use of phage as model organisms in photoinactivation experiments does not accurately model inactivation of human viruses under all experimental conditions. So, in order to fully understand PDI of human viruses, there is need to study them directly (Silverman et al., 2013). Whilst the ideal situation would be to study the human pathogen directly, using animal viruses that are closely related to human viruses to study these viruses is more attractive because of health and safety reasons. Also, some human viruses e.g. human norovirus presently is difficult to be replicated in the laboratory whilst the closely related murine norovirus can be grown. There are many studies that have investigated PDI of viruses but in most cases no comparison was made between the extents of PDI among other viruses. After exhaustive investigation of MS2 PDI, we decided to use PDI conditions used on MS2 to investigate PDI of other model phage and mammalian viruses (bacteriophage Qβ, bovine enterovirus and murine norovirus).

Our data showed that when PDI condition (0.5 µM TMPyP, 32 mW cm^{-2} and 1 min of illumination) which caused complete inactivation (reductions of 9.6 log PFU/ml) of

MS2 with TMPyP in solution (Figure 4.1) was used for PDI of bacteriophage Qβ (very similar to MS2), a reduction of only 2 log PFU/ml of phage Qβ was observed (Figure 4.11). Complete inactivation (reductions of 10.4 log PFU/ml) of phage Qβ was observed after 8 min of PDI (Figure 4.11). Both native gel agarose electrophoresis (Figure 4.12 A) and TEM (Figure 4.12 B) confirmed that the PDI does not cause aggregation of phage Qβ particles even after 60 min of PDI. This is unlike MS2 where complete aggregation was observed after 60 min of PDI.

Figure 4. 11: Bacteriophage Qβ PDI in solution. Phage were illuminated at 32 mW cm^{-2}. The dark controls were treated with the concentration of photosensitiser shown but not illuminated whilst no photosensitiser controls (NS) were illuminated without photosensitiser present. Data are mean ± standard deviation (n = 3).

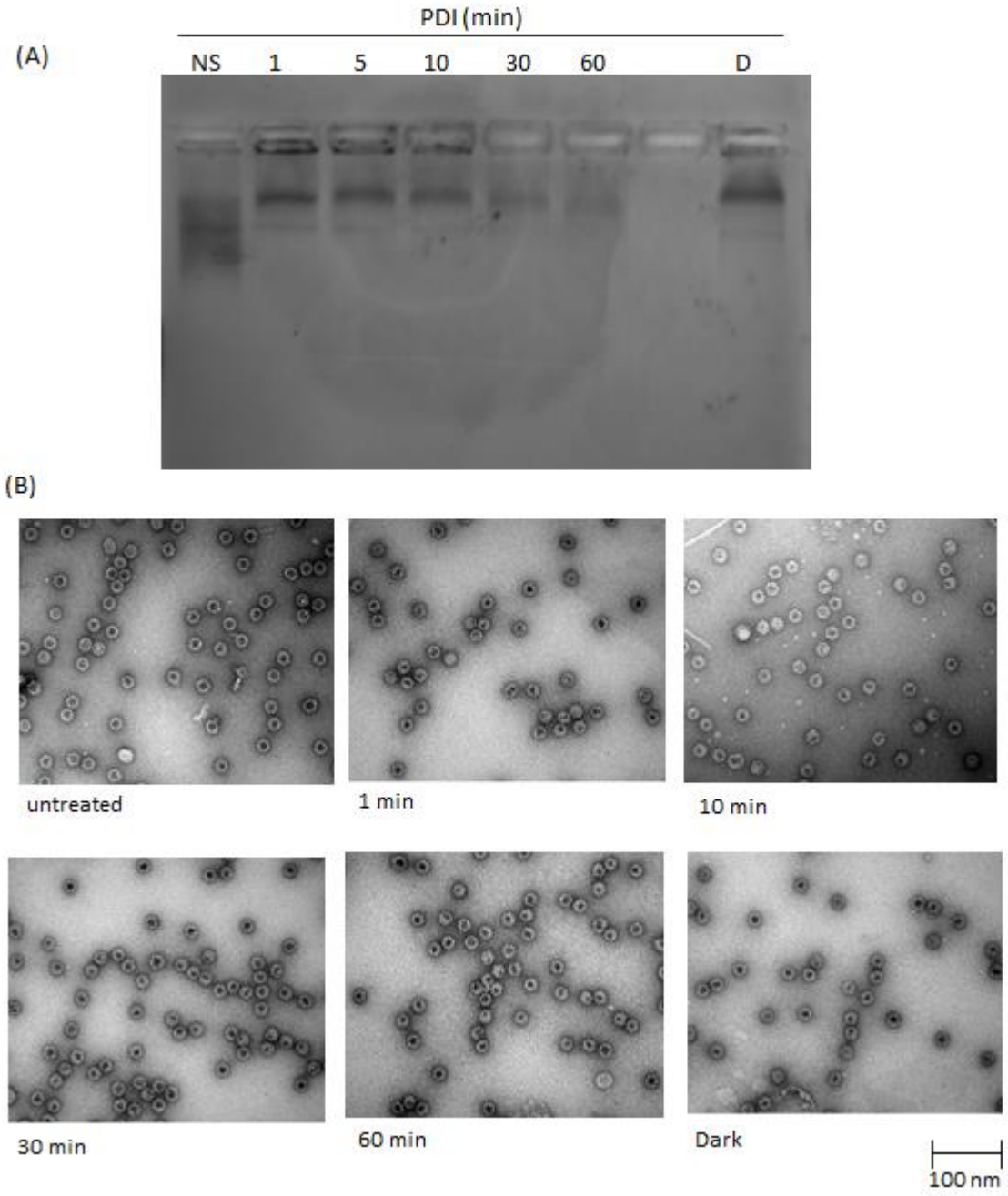

Figure 4. 12: Native agarose gel electrophoresis and TEM of PDI treated phage Qβ. Phage were illuminated at 32 mW cm^{-2}. (A), Native gel of phage Qβ PDI sample with 50 µM TMPyP in solution. The gel was stained with Instant Blue. NS = No sensitiser; D = dark experiment; (B), TEM images of PDI treated phage Qβ with 50 µM TMPyP solution. Untreated, PDI treated for 1, 10, 30 and 60 min and dark sample are shown.

For PDI of BEV 2 with TMPyP in solution, we observed (data not shown) that the PDI condition which caused complete inactivation (reductions of 9.6 log PFU/ml) of MS2 (Figure 4.1) and reductions of 2 log PFU/ml of phage Qβ (Figure 4.11) did not cause any inactivation of BEV. In fact, even 1 µM TMPyP in solution and 30 min of illumination did not cause any significant inactivation of the BEV 2 (Figure 4.13 A). For PDI at higher concentration of TMPyP 5, 10 and 50 µM, reductions of 0.7, 1.5 and 2.6 log PFU/ml of BEV 2 were observed respectively after 30 min illumination (Figure 4.13 A). After 120 min of PDI, 5 and 2 log reductions of PFU/ml of BEV were observed for 10 µM and 5 µM of TMPyP respectively (Figure 4.13 B). Both native gel agarose electrophoresis (Figure 4.14 A) and TEM (Figure 4.14 B) confirmed that the PDI did not cause aggregation of BEV particles even after 60 min of PDI

Figure 4. 13: BEV 2 PDI in solution. The BEV 2 samples were illuminated at 32 mW cm^{-2}. (A), PDI using different concentrations (1 µM to 50 µM) of TMPyP; (B), PDI using 5 and 10 µM TMPyP in solution from 30 to 120 min. The dark controls were treated with the concentration of photosensitiser shown but not illuminated whilst no photosensitiser controls (NS) were illuminated without photosensitiser present. Data are mean ± standard deviation (n = 3).

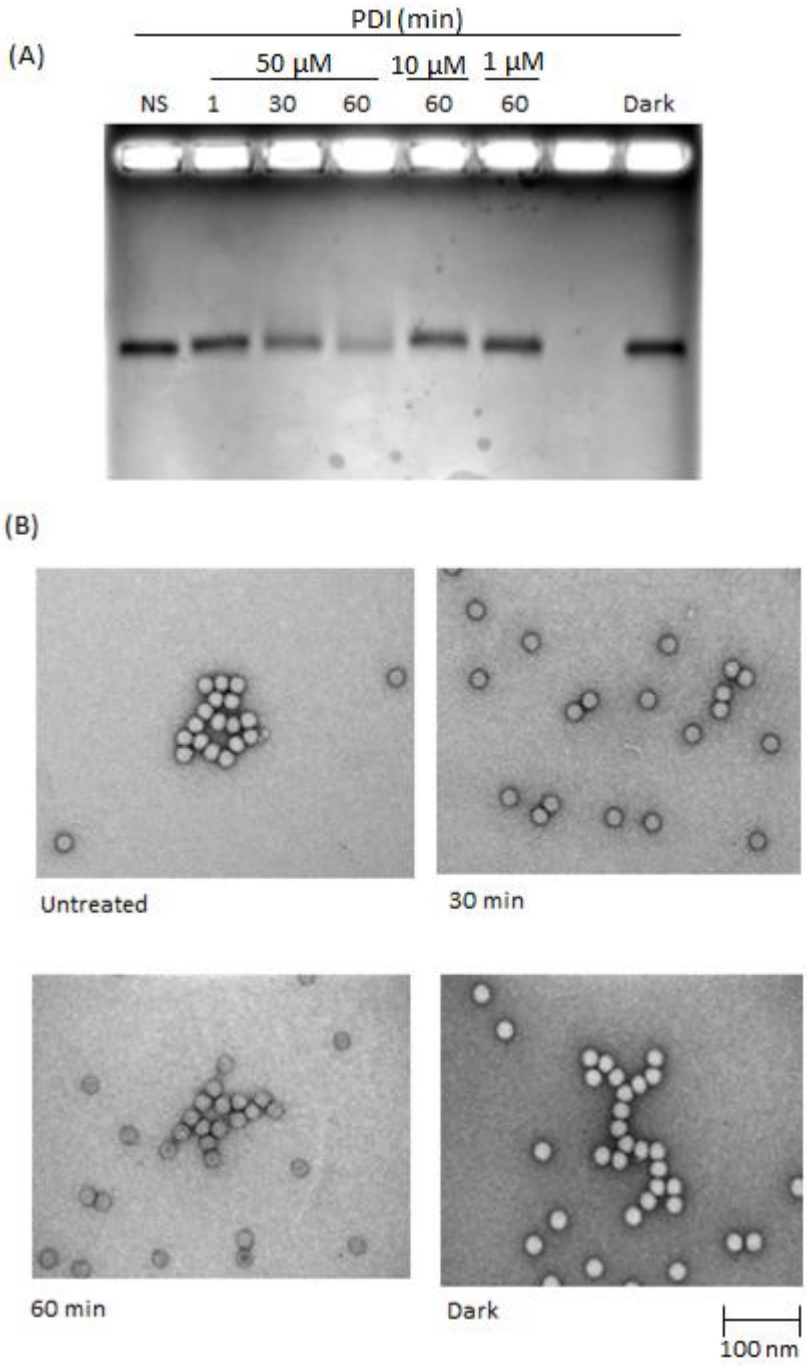

Figure 4. 14: Native agarose gel electrophoresis and TEM of PDI treated BEV 2. The BEV 2 samples were illuminated at 32 mW cm^{-2}. (A), Native gel of BEV PDI sample with TMPyP in solution. The gel was stained with Instant blue. NS = No sensitiser; D = dark experiment; (B), TEM images of PDI treated BEV with 50 µM TMPyP solution. Untreated, PDI treated for 30 and 60 min and dark sample are shown.

For PDI of MNV with TMPyP, we observed (data not shown) that the PDI condition which caused complete inactivation (Figure 4.1) and reductions of 2 log PFU/ml of phage Qβ (Figure 4.11) did not cause any inactivation of MNV. For PDI using 5, and 10 µM of TMPyP, reductions of 2 and 3 log $TCID_{50}$/ml of MNV were observed respectively after 20 min of illumination (Figure 4.15). Antibodies raised against VP1 (major capsid protein) of MNV were able to detect all PDI-treated samples of MNV including the dark experiment samples (Figure 4.15). Bands corresponding to 60 KDa of MNV VP1 were detected for all samples PDI. However, like MS2, samples exposed to light produced additional bands on SDS-PAGE (Figure 4.16). These bands at ≈ 180 KDa are likely to correspond to trimers of MNV VPI. We did not perform native gel agarose electrophoresis and TEM for PDI MNV samples because the samples were not ultra-pure.

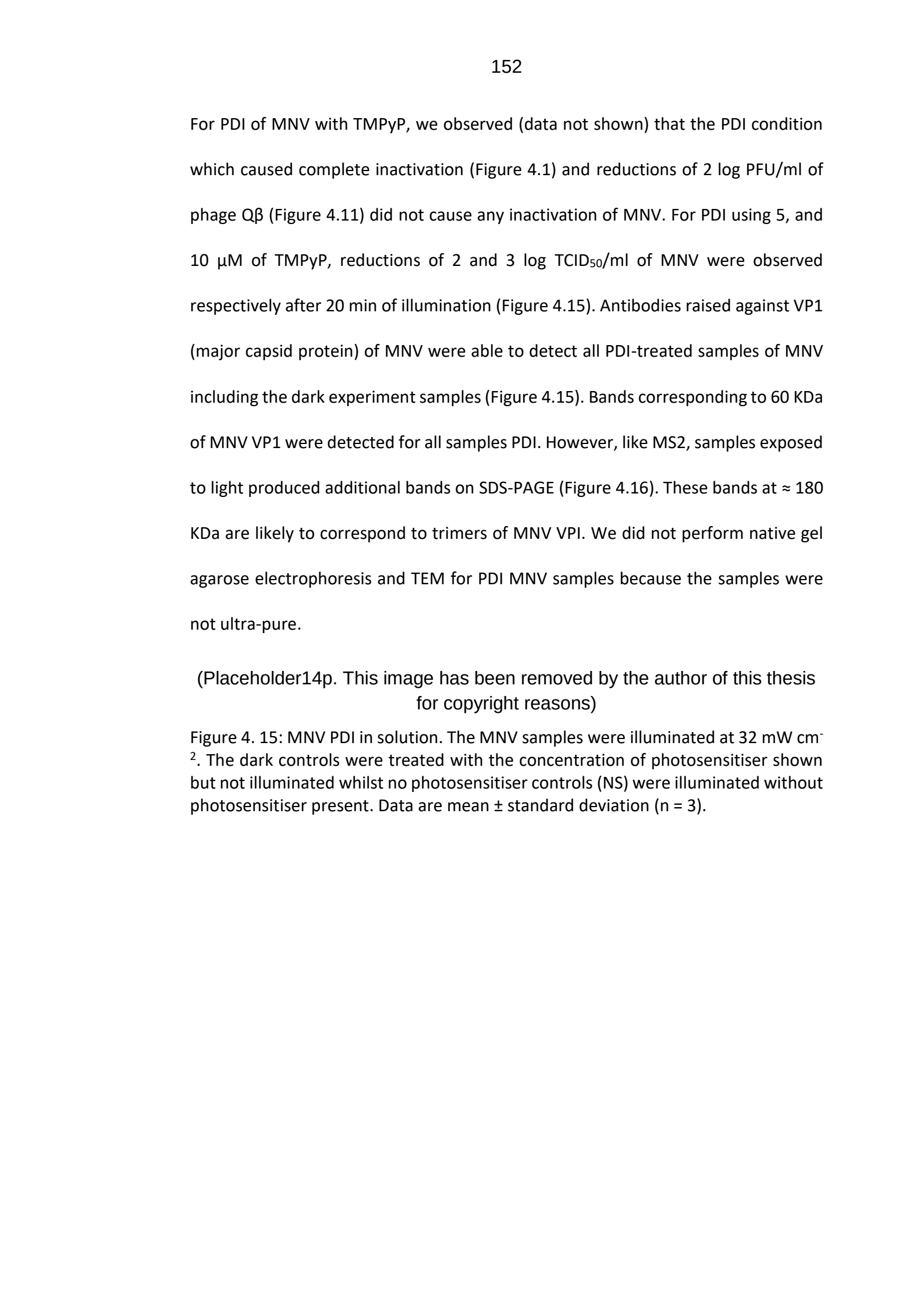

Figure 4. 15: MNV PDI in solution. The MNV samples were illuminated at 32 mW cm^{-2}. The dark controls were treated with the concentration of photosensitiser shown but not illuminated whilst no photosensitiser controls (NS) were illuminated without photosensitiser present. Data are mean ± standard deviation (n = 3).

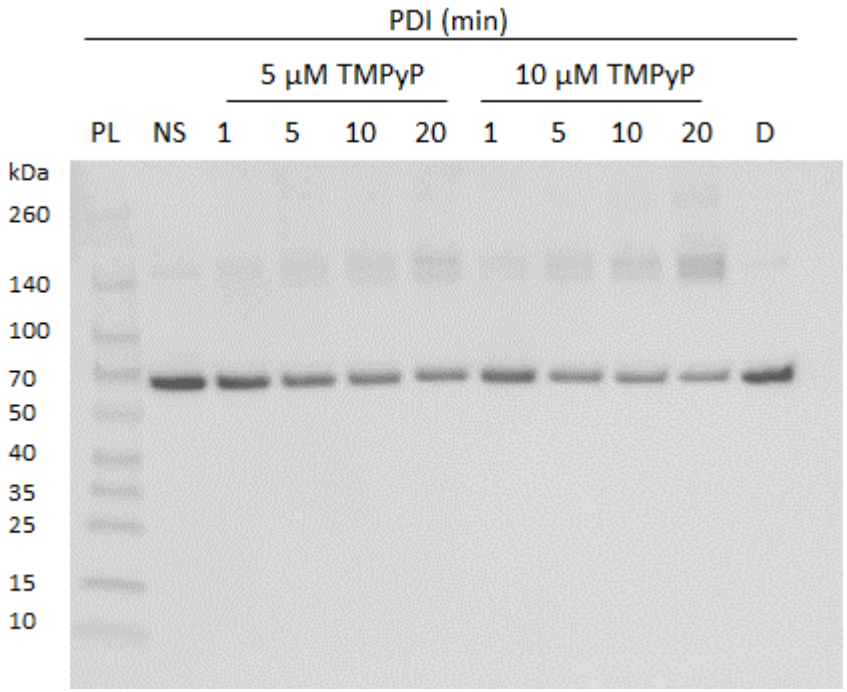

Figure 4. 16: Western blot of MNV after PDI with TMPyP. The MNV samples were illuminated at 32 mW cm^{-2}. NS = no sensitiser; D = dark experiment. After separation on SDS-PAGE and blotting to nitrocellulose paper, detection was performed using rabbit anti MNV VP1 IgG at 1:100 dilution and secondary goat anti-rabbit HRP conjugate at 1:1000 dilution.

The model viruses used in this work have similarities to each other which include being lytic, non-enveloped, icosahedral capsids, 27-30 nm in diameter with positive sense and single stranded RNAs as their genome. Bacteriophages MS2 and Qβ are also similar to the extent of using the same host bacteria to replicate. However, despite these similarities, the PDI data presented here has shown that the rate and extent of inactivation varies among these viruses. The rate and extent of PDI among these viruses was in the order MS2 > phage Qβ > MNV > BEV. In section 4.7, we have demonstrated that A-protein (host attachment protein) of MS2 is the target of PDI. We observed that PDI mediated change to the A-protein varies according to the amino acid sequence from one epitope of the protein to another. Those epitopes of the A-protein that had amino acid histidine, tryptophan and tyrosine in their

sequence lost antigenicity more quickly as compared to those regions that lacked these amino acids. The rate of antigenicity loss correlates to the rate of PDI of MS2 we observed. This data confirms many reports that amongst the amino acids, tryptophan, histidine, methionine, cysteine and tyrosine are the most susceptible to singlet oxygen under physiological pH conditions (Davies, 2003, Gracanin et al., 2007, Wilkinson et al., 1995). However, all of these studies were performed by examining proteins, peptides and or amino acids directly. There are no reports of how amino acid composition of capsid proteins, including host attachment proteins, of viruses affect the extent of PDI. The host attachment protein in MS2 phage is A-protein which is just one copy. Similarly, only one copy of A2-protein is present in phage Qβ. In BEV 2, it is the host attachment sites, 60 in all which are analogous to canyons in poliovirus across the 3 surface capsid proteins (VP1, VP2 and VP3) that mediate attachement. In MNV, it is the P2 subdomain of the VP1 that is responsible. There are potentially 90 host attachment sites formed from the P2 subdomains of the 180 copies of the VP1 that form the capsid of MNV. We observed from the compositions of these host attachment proteins/sites (Table 1.6) that presence of the most sensitive amino acid residues correlated to the extent of PDI of these viruses. The A-protein of MS2 has 44 sensitive amino acids (His, Trp, Tyr, Met, Cys) (Table 1.6) whilst the A2-protein of phage Qβ, P2 domain of MNV and host attachment sites of BEV have 28, 9 and 1 of these amino acids respectively (Table 1.6). However, in addition to their amino acid composition, surface accessibility and hydrophilicity of the host attachment proteins could also affect the sensitivity of PDI. This is because singlet oxygen and other ROS generated in solution can only attack those parts of proteins that are solvent accessible.

The lack of aggregation of viral particles observed after PDI of phage Qβ and BEV might be due to surface properties such as the net surface charge which is a function of the amino acid compositions of the capsid proteins of viruses. However, amino acid residues such as histidine and tyrosine are known to crosslink proteins when oxidised by singlet oxygen. Also in some instances, secondary dark reactions have been implicated in the formation of protein crosslink (Davies, 2003, Shen et al., 2000b, Shen et al., 2000a).

Table 4. 1: Most susceptible amino acid to single oxygen of the host attachment proteins/sites of model viruses.

Amino acids most susceptible to $^1O_2$*	***k*** **(M^{-1} S^{-1})**	**MS2 A-protein (x1)**	**Phage Qβ A2-protein (x1)**	**MNV P2 domain (x180) (x90)**	**BEV host attachment sites (x60)**
H (Histidine)	3.2×10^7	5	1	0	0
Y (Tyrosine)	0.8×10^7	16	14	6	1
W (Tryptophan)	3×10^7	12	5	1	0
M (Methionine)	1.6×10^7	8	2	1	0
C (Cysteine)	8.9×10^6	3	6	1	0
Total		**44**	**28**	**9**	**1**

4.9 RNA infectivity of PDI treated MNV

In order to assess the effect of PDI on the viral genome, the RNA of MNV PDI samples were extracted and purified using Direct-Zol Miniprep Plus kits. Purified RNA was then transfected into BHK-21 cells using Lipofectin reagent according to the recommended protocol. After transfection, the titre of each sample was determined

and compared to the titre of the original MNV samples from which RNA was extracted.

Our data showed that the process of extraction and purification of RNA and transfection efficiency caused loss of about 3 log $TCID_{50}$/ml of MNV (Figure 4.17). The titres before RNA extraction/purification of MNV PDI samples for dark and no sensitiser controls were 7.3 and 7.33 log $TCID_{50}$/ml respectively (Figure 4.15), whilst the titres of recovered MNV RNA transfection were 4.5 and 5.25 log $TCID_{50}$/ml respectively (Figure 4.17). We observed a significant decrease in RNA infectivity after 20 min of PDI for samples treated with 5 and 10 µM of TMPyP (Figure 4.17). About 1 and 3 log $TCID_{50}$/ml decrease in RNA infectivity were observed for samples treated with 5 and 10 µM of TMPyP respectively after 20 min of illumination (Figure 4.17). This correlates to MNV PDI we observed. For PDI using 5 and 10 µM of TMPyP, reductions of 2 and 3 log $TCID_{50}$/ml of MNV were observed respectively after 20 min of illumination (Figure 4.15).

Figure 4. 17: RNA infectivity of MNV subjected to PDI with TMPyP. The MNV samples were illuminated at 32 mW cm^{-2}. The dark controls were treated with the concentration of photosensitiser shown but not illuminated whilst no photosensitiser controls (NS) were illuminated without photosensitiser present. Data are mean ± standard deviation (n = 3).

It has been established that singlet oxygen is the most likely ROS to be implicated in viral PDI (Costa et al., 2013, Silverman et al., 2013). All ROS have a short-life and high reactivity, thereby causing damage only to molecules close to the point of generation (Costa et al., 2013). So capsid proteins, including host recognition proteins, are the immediate targets of singlet oxygen oxidation in non-enveloped viruses such as our model viruses. However, although virus capsids serve to protect the genome, they may contain pores that are permeable to small molecules like singlet oxygen thereby oxidising the genome simultaneously alongside the capsid proteins. The assembled MS2 capsid has 32 pores, of 2 nm in diameter which may be permeable to small molecules (Dedeo et al., 2010). Furthermore, under physiological conditions, the capsids of non-enveloped viruses can undergo a constant movement that suggests a dynamic state, referred to as “capsid breathing”. These include picornaviruses, nodaviruses, tombusviruses, sobemoviruses and others (Pulli et al., 1998). Although the permeability of viral capsids to singlet oxygen molecules has not been directly shown, it has been suggested that access to the viral genome could result in oxidation-induced damage to it.

RNA transfection of the viral PDI samples could be the most plausible method to assess how PDI affects the infectivity of RNA. We are not able to transfect RNA of the PDI samples of bacteriophages MS2 and Qβ. However, there is a report that used qRT-PCR and suggested that inactivation of MS2 by singlet oxygen is mostly attributed to degradation RNA genome thereby making it nonreplicable (Wigginton et al., 2012). This does not agree with our findings in section 4.6 and 4.7 as well as other studies that suggested that inactivation of MS2 by singlet oxygen is mostly

attributed to damage to A-protein (host attachment) of MS2(Costa et al., 2014, Hotze et al., 2009)

4.10 Conclusion

The data presented in this chapter show that the concentration of TMPyP (and Rose Bengal and methylene blue), time of illumination and light intensity all affect the rate and extent of PDI of MS2. The photosensitiser TMPyP is the most efficient in facilitating PDI of MS2 compared to the other photosensitisers tested, Rose Bengal and methylene blue. The order of rate and extent of PDI of MS2 by these photosensitisers in solution was TMPyP >>> methylene blue > Rose Bengal. This is likely to be related to the net charge on these photosensitisers as it has been established that cationic photosensitisers are generally more efficient in the PDI of microorganisms including viruses. The net charge for TMPyP is +4, +1 for methylene blue and -2 for Rose Bengal. It has also been shown here that PDI of MS2 with TMPyP in solution does not drive the evolution of a PDI resistant MS2 population indicating that resistance to PDI is unlikely to emerge. High efficiency and complete photodynamic inactivation of TMPyP at 0.2 µM made it the photosensitiser of our choice to attach onto chitosan nanofiber/polymeric membrane for water disinfection; this discussed in Chapter 5. Only low concentration of TMPyP on solid supports should be needed for the device to efficiently disinfect water. In this chapter, visible cold light was used and the fluence rate (radiant exposure) used for most PDI experiments was 32 mW cm^{-2}. This light intensity is only about 3% of bright mid-day time sunlight under clear sky conditions in Sub-Saharan Africa and about 10% of mid-day time sunlight during summer in Northern Europe. However, it

allowed a graded PDI response to be observed and the fact that even 5 mW cm^{-2} has been shown to cause inactivation of MS2 with TMPyP in solution is an indication that ultimately, sunlight could be used as source of light for this disinfection system.

Even though PDI of MS2 with TMPyP in solution can cause aggregation of viral particles, the aggregation of the MS2 particles was not attributable to MS2 inactivation. Our data suggested that a minimum concentration of 0.2 µM of TMPyP inactivates MS2 under 1 min illumination at 32 mW cm^{-2}. However, complete MS2 particle aggregation was only observed after 60 min of PDI. Although, formation of dimers of MS2 coat protein was observed after 10 min PDI. The cause of aggregation of MS2 particles may be due to either and or cumulative effects of formation of di-tyrosine from tyrosine residues that are present in coat proteins and A-protein, histidine residues present in A-protein and secondary dark reaction. Either way, multimerization of MS2 particles should also compromise infectivity. Sequence-specific antibodies for antigenic sites 2 and 4 on the A-protein of MS2 did not detect the epitopes after 1 min of PDI. This loss of antigenicity corresponds to the rate of PDI of MS2 we observed. We believe that histidine and tryptophan being most sensitive amino acids to singlet oxygen and their position almost in the middle of the sequence of these antigenic sites on the A-protein is probably responsible for the fast rate of antigenicity loss. We propose that A-protein of MS2 is the main target of PDI and that site 4 may be one of specific regions of the A-protein responsible for MS2 attachment to the bacterial pilus and delivery of its genome into the host. So, inactivation of MS2 is mostly to due to loss of binding and attachment property of A-protein to the host bacteria pilus. However, because MS2 has 32 pores on its capsid and we have observed decrease in RNA infectivity of MNV PDI samples, it is

also possible that singlet oxygen mediated oxidation of MS2 genome contributes to its inactivation.

Capsid proteins especially host attachment proteins are immediate targets of singlet oxygen oxidation in non-enveloped viruses such our model viruses. This is because all ROS have a short-life and high reactivity, thereby causing damage only to molecules close to the point of generation. The amino acid compositions and surface and solvent accessibility of the host attachment proteins of viruses can affect the extent of PDI. Therefore, the extent of PDI of our model viruses with TMPyP in solution in the order MS2 > phage Qβ > MNV > BEV can be attributable to the availabilty of most sensitive amino acids to singlet oxygen at their host attachment sites as well as solvent accessibility of these amino acids.

Chapter Five: TMPyP functionalisation of chitosan nanofiber and chitosan membrane

Chapter 5: Functionalisation of chitosan nanofiber and chitosan membrane with TMPyP for water disinfection

5.1 Overview

The photosensitiser TMPyP was immobilised onto chitosan nanofiber and chitosan membrane since in our preliminary investigation (Chapter 4) it was shown to result in rapid photodynamic inactivation (PDI) of MS2 and other model viruses when used in solution. Attaching TMPyP onto chitosan nanofiber mats and chitosan gel membranes would make it suitable for use in water disinfection during wastewater treatment and without releasing TMPyP into the water during treatment. Also, TMPyP-functionalised chitosan nanofibers and membranes could be re-used, reducing the cost and providing an environmental-friendly technology for water disinfection. In this study, chitosan nanofiber and chitosan gel membrane were chosen as the solid support to attach TMPyP for water disinfection because of the physico-chemical properties including ease of fabrication, presence of reactive amine group, a rigid and hydrophilic D-glucosamine structure and biocompatibility. Chitosan is also biodegradable, cheap and readily available. However, direct coupling of TMPyP onto chitosan nanofiber and membrane is not easily possible because the functional groups are not chemically compatible, so the nanofibers and membranes were first modified with pyromelitic dianhydride (PMA) to introduce carboxyl groups and facilitate electrostatic adsorption of the highly basic TMPyP. In addition, PMA should be able to crosslink closely adjacent $–NH_2$ groups and stabilise the chitosan nanofibers and membranes. The chitosan nanofiber mat/membrane-TMPyP composite produced was then tested for photodynamic inactivation of MS2 and *E. coli* BL21. Both stationary and flowing water models were employed during PDI

experiments in order to mimic what would be the set-up in waste water treatment plants.

In this chapter, data are presented on successful modification and functionalisation of chitosan nanofiber mats and chitosan gel membranes with TMPyP. Also, data on PDI of MS2 phage and *E. coli* BL21 using TMPyP functionalised chitosan nanofibers and membranes (CM-T) are shown.

5.2 Production, modification and TMPyP functionalisation of chitosan polymeric membrane

5.2.1 Production of chitosan membrane

Chitosan membranes were produced as described by Krajewska (1990, 1991). A solution of 1% (w/v) chitosan in 1% (v/v) acetic acid was made and then homogenised by shaking at 300 rpm and 60 ^{o}C for 30 min. The homogenised viscous chitosan solution was then cast into 4.5 cm diameter petri dishes, filling to depth of 3 mm. The petri dishes were placed in a hot air incubator set at 60 ^{o}C for 24 h to dry into a translucent chitosan membrane. The thickness of membranes after drying was 50-100 µm. The chitosan membranes were then neutralised by treatment with 0.5% (w/w) of sodium triphosphate in 2M NaOH for 30 min. After neutralisation, the membranes were washed in distilled H_2O (dH_2O) until the solution was not alkaline and then air dried to give a translucent brittle polymeric chitosan membrane (Figure 5.1).

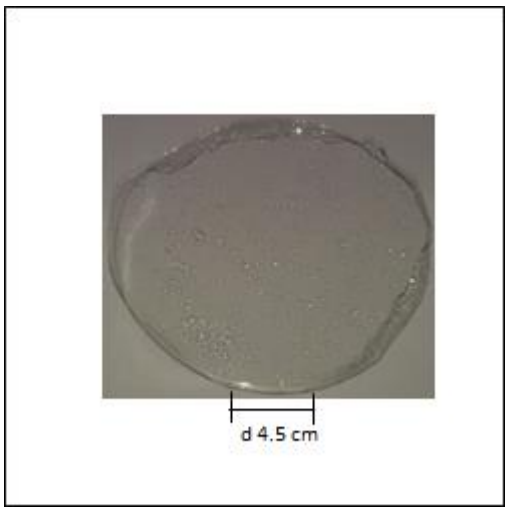

Figure 5. 1: Image of chitosan gel membrane. The diameter (d) of the membrane is 4.5 cm.

5.2.2 Modification of chitosan membrane using anhydrides

Direct adsorption of TMPyP onto chitosan membrane was not possible because the net charge of chitosan membrane is positive whilst TMPyP is a tetra cationic porphyrin. Therefore, the chitosan membranes were first modified by pyromellitic dianhydride (PMA) in order to introduce carboxyl groups and allow adsorption of the highly basic TMPyP.

Each membrane was immersed in 1% (w/v) pyromellitic dianhydride (PMA) in 20% (v/v) DMSO contained in a closed bottle and then placed on a 3D rocking platform set at 30 rpm for 24 h at room temperature. Two controls were used i.e. one with PMA replaced with succinic anhydride and the other was treated in DMSO only. The membranes were then washed in dH_2O several times and blow dried. The reaction scheme of PMA with chitosan amines is shown in Figure 5.2. The PMA modifies primary amine groups on the chitosan membranes and generates three free carboxyl groups (Figure 5.2 A). The fourth carboxyl group becomes linked in a peptide bond to the amine (Figure 5.2 A).

It is also likely that one or more of the three free carboxyl groups could form peptide bonds with two or more units of chitosan polymer, thereby crosslinking the chitosan units together (Figure 5.2 B).

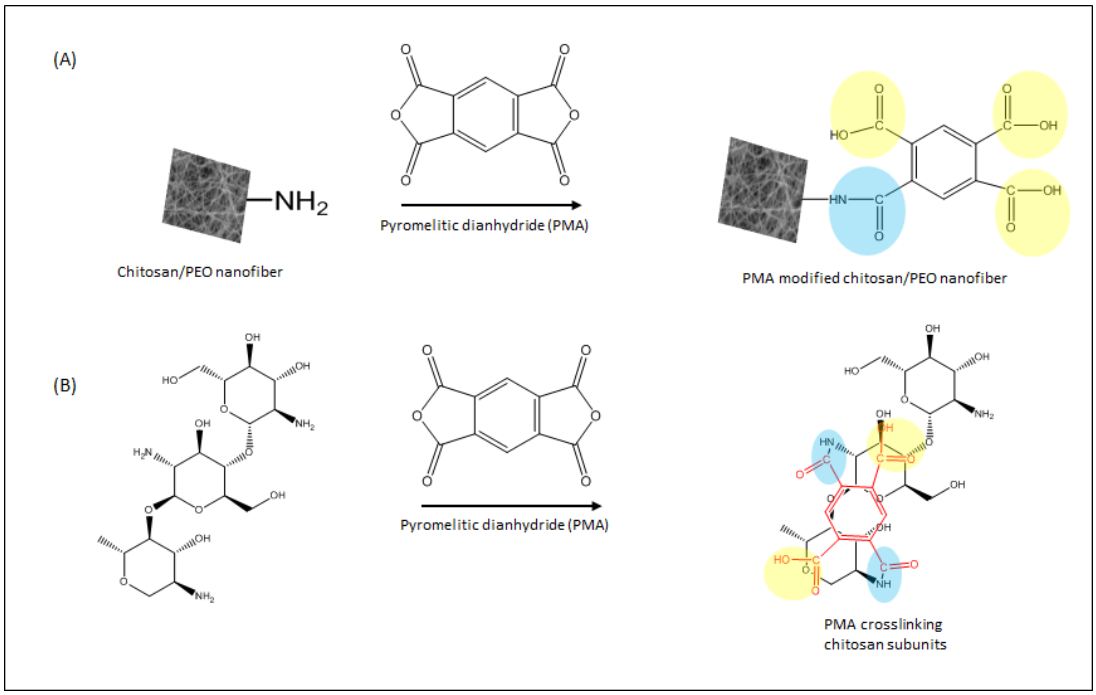

Figure 5. 2: Reaction scheme for modification of chitosan nanofiber mats and chitosan membranes. (A), Primary amine group of chitosan subunit formed a peptide bond (highlighted in blue) with pyromelitic dianhydride (PMA) to generate three free carboxyl groups (highlighted that will facilitate adsorption of the highly basic photosensitiser-TMPyP; (B), PMA crosslinking 2 subunits of chitosan. The schemes were prepared by ChemDraw Pro 13.0.

5.2.3 Midland blotting and scanning electron microscopy of PMA modified chitosan membrane

Midland blotting and SEM were used to characterise the membranes. The Midland blotting (Rushworth et al., 2014) was used to detect free amine groups in order to check complete modification of amine to carboxyl groups. To detect free amine groups, PMA modified membranes and non-modified controls were incubated in the presence of NHS-biotin (4 mg/ml in PBS containing 20% (v/v) DMSO) for 30 min in order to attach biotin to the free amine groups. After three washes in water followed

by drying in argon, the membranes were then incubated with HRP-streptavidin conjugate (1 μg/ml in PBS) for 30 minutes. Then, the membranes were incubated in the presence of an appropriate HRP-conjugated secondary antibody (1:1000 in PBS) for 1 hour to detect bound HRP-streptavidin. After the addition of the HRP-conjugated reagent, membranes were washed three times for 5 minutes each in PBS, once in PBS containing 0.1% (v/v) Tween-20 to aid removal of non-specifically bound HRP-conjugated secondary antibody, with a final wash in PBS. The membranes were dried in argon in between incubations and after washing steps. Finally, ECL reagent was pipetted carefully onto the membranes and chemiluminescence detected after 1 minute using a G-BOX Gel Imaging System. The SEM was undertaken to analyse the physical properties of PMA modified chitosan membranes as compared to unmodified chitosan membranes.

5.2.4 TMPyP functionalisation of chitosan membrane

PMA modified membrane and the 2 control samples (DMSO treated but unmodified membrane and unmodified membrane) were treated with TMPyP. Each membrane was immersed in 10 ml of 200 μM TMPyP contained in a closed Nunclon petri dish (d. 4.5 cm) and then placed on a 3D rocking platform set at 30 rpm for 30 min at room temperature. After the staining, each membrane was washed thoroughly in dH_2O under mechanical agitation until no TMPyP was detected in washing solution using A_{422}, the membranes were then allowed to dry and stored in the dark at room temperature.

5. 2.5 PDI of MS2 using TMPyP functionalised chitosan membrane

TMPyP functionalised chitosan membranes (CM-T) were used to investigate inactivation of MS2 by PDI. In addition to the stationary PDI model (Figure 5.3), we

also used a flowing water model to investigate PDI of MS2 using CM-T (Figure 5.4). A peristaltic pump was used to pump 10 ml MS2 sample (10^8 PFU/ml) at 0.33 ml/min into a PDI chamber containing CM-T while being illuminated with our source of light at 32 mW cm^{-2} (Figure 5.4). For the MS2 PDI stationary model, CM-T was immersed in 10 ml MS2 sample (10^9 PFU/ml) in a Nunclon petri dish (d. 4.5 cm) and was shaken intermittently while being exposed to light of 32 mW cm^{-2} (Figure 5.3). The different time of illuminations used were 30 min to 90 min. Each PDI light experiment (CM-T: Light) was carried out with two controls. These were a dark experiment (CM-T: Dark) and a membrane with no TMPyP present but exposed to light (CM only: Light). All experiments were triplicated using same set of TMPyP functionalised chitosan membranes (CM-T) and chitosan membranes without TMPyP (CM). Double layer agar plaque assay was used to carry out viability test and to determine the extent of PDI in MS2.

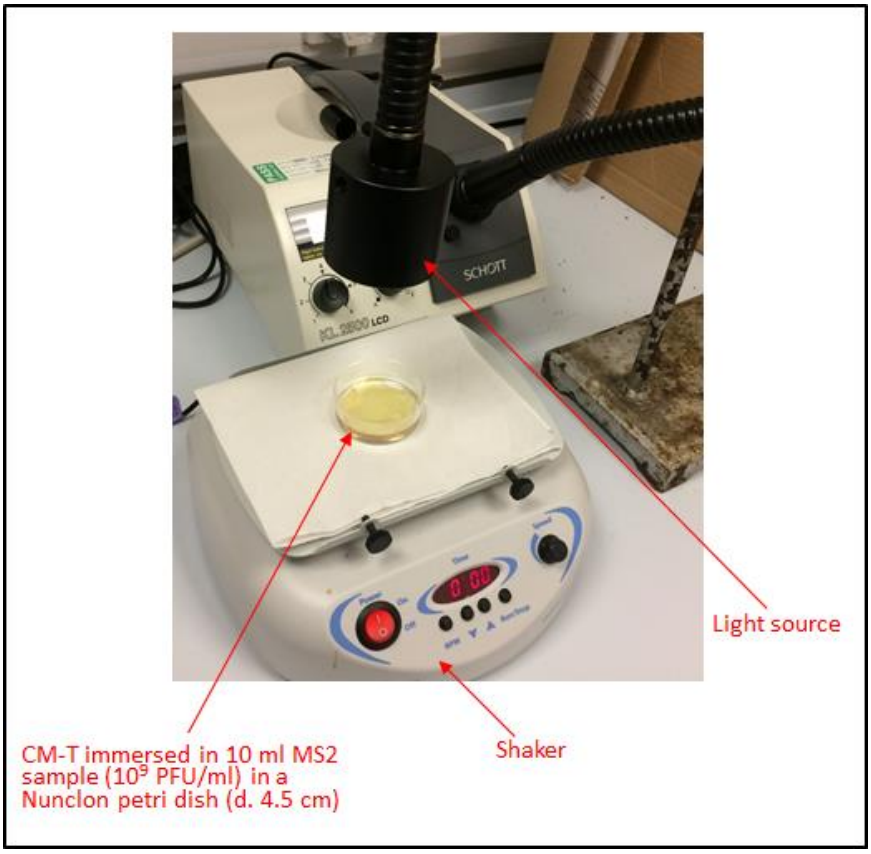

Figure 5. 3: Stationary water PDI setup with TMPyP functionalised chitosan membranes (CM-T). CM-T was immersed in 10 ml MS2 sample (10^9 PFU/ml) in a Nunclon petri dish (diameter 4.5 cm) and was shaken intermittently while being exposed to light of 32 mW cm^{-2}.

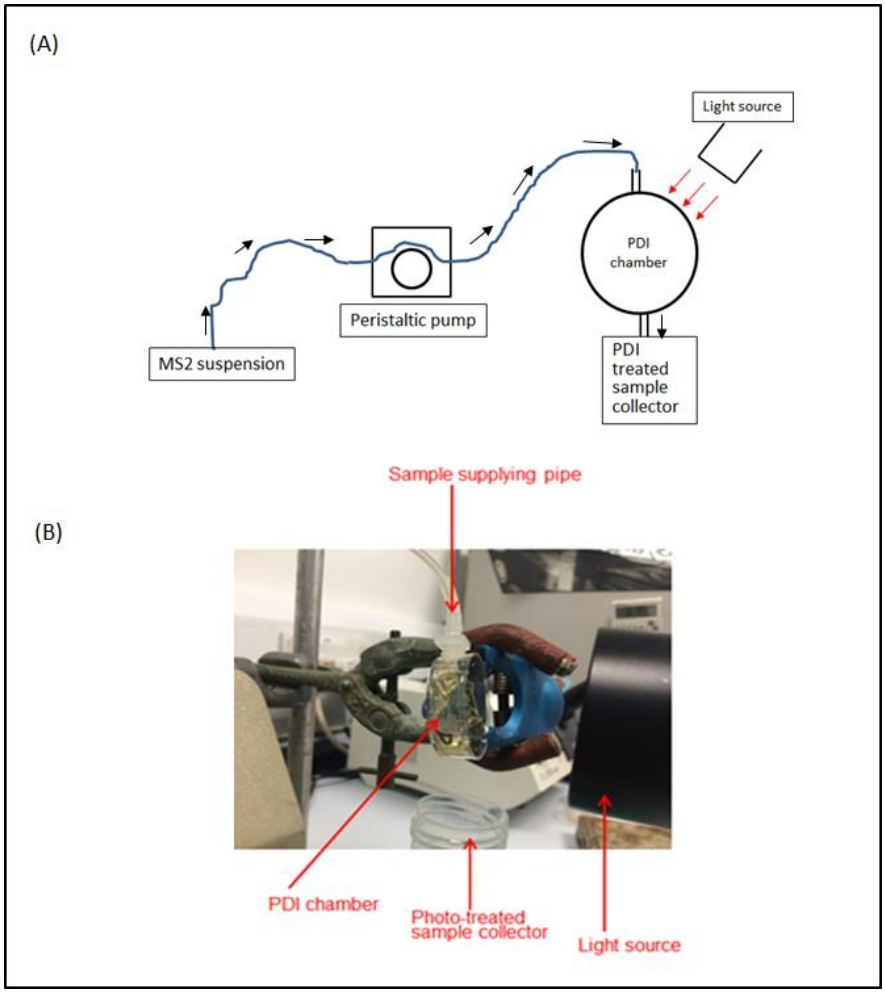

Figure 5. 4: A schematic (A) and image (B) of flowing water PDI setup with TMPyP functionalised chitosan membranes (CM-T). Peristaltic pump was used to pump MS2 sample (10^9 PFU/ml) into PDI chamber while being illuminated with light sources.

5. 2.5 PDI of *E. coli* BL21 using TMPyP functionalised chitosan membrane

TMPyP functionalised chitosan membranes (CM-T) were used to investigate inactivation of *E.coli* BL21 by PDI. The MS2 PDI stationary model conditions were used. The 3 h log phase bacteria culture was washed 3 times with 1 X PBS. The 50 ml 3 h log phase bacteria culture grown Tryptic Soy Broth (TSB) was first centrifuged at 1500 x g rpm for 10 min. After the centrifugation the supernatant was discarded and the bacteria cell pellet was resuspended in 50 ml PBS. It was then centrifuged at 1500 x g rpm for 10 min. The supernatant was discarded and resuspended in 50 ml

PBS. This washing step was done 3 times. After the washing, 10 ml each of bacteria cells was used for the PDI. CM-T was immersed in 10 ml of washed *E.coli* BL21 (10^7 CFU/ml) in a Nunclon Petri dish (4.5 cm diameter) and was shaken with a shaker intermittently while being exposed to light of 32 mW cm^{-2} for 90 min. PDI light experiment (CM-T: Light) i.e. TMPyP functionalised chitosan membrane and exposed to light were carried out with two controls; dark experiment (CM-T: Dark) i.e. TMPyP functionalised chitosan membrane and not exposed to light and no sensitiser experiment (CM: only) i.e. chitosan membrane without TMPyP but exposed to light. All experiments were triplicated using same set of TMPyP functionalised chitosan membranes (CM-T) and chitosan membranes without TMPyP (CM). Serial dilution and spread plate method were used to determine CFU/ml and the extent of PDI in *E.coli* BL21.

5.3 Results

5.3.1 SEM and characteristics of modified chitosan membrane

It has been reported that the photosensitiser-5,10,15,20-tetrakis (p-hydroxyphenyl) porphyrin (p-TAPP) could be immobilised onto chitosan membrane for water disinfection applications (Bonnett et al., 2006). In that study, p-TAPP was attached onto chitosan membrane by adsorption without prior modification of the membrane. The p-TAPP-chitosan composite was shown to have photomicrobicidal activity against *E.coli* (Bonnett et al., 2006). However, in our case, direct adsorption of TMPyP onto chitosan membrane was not possible because the net charge of chitosan membrane is positive whilst TMPyP is a tetra cationic porphyrin. Therefore, the chitosan membranes were first modified by PMA in order to introduce carboxyl groups and allow adsorption of the highly basic TMPyP.

The scanning electron microscopy images of dried modified chitosan membrane showed uniform contraction, compactness and folding of the membrane (Figure 5.5). The membranes modified with succinic anhydride became soluble in water while being washed in dH_2O (result not shown). Control experiments using succinic anhydride to modify the membrane amine group drastically affected its solubility and the whole membrane dissolved in water during the washing steps in H_2O. In contrast, membranes modified with PMA remained intact while in water and became denser and more compact compared to unmodified membranes under both wet and dried condition as shown using SEM (Figure 5.5).

Figure 5. 5: Images of PMA modified and unmodified chitosan membranes: (A1), unmodified chitosan membrane; (A2), (A3), SEM images of unmodified chitosan membrane; (B1), PMA modified chitosan membrane; (B2), (B3), SEM images of PMA modified chitosan membrane (Majiya *et al*., 2017).

It was expected that chitosan modification with acid anhydride derivatives might increase their solubility in water as observed with succinic anhydride to modify the chitosan membrane. This was in agreement with a previous study (Tangpasuthadol et al., 2003) which reported that such modification with succinic anhydride could increase the hydrophilicity and hygroscopic property of the chitosan in film or powdered forms. However, unlike succinic anhydride PMA is a bis-anhydride with anhydride groups either side of an aromatic ring. Typically, a PMA anhydride group will react with one amine group, with the other anhydride then being subjected to water attack. It is also likely that carboxyl-anhydride PMA molecules were able to

form peptide bonds with two or more units of chitosan polymer, thereby crosslinking the chitosan units together. This could account for the compactness and insolubility in water of chitosan membranes modified with PMA (Figure 5.5). By comparison, chitosan membranes prepared as described by Krajeswka (1990, 1991) are brittle in nature (Bonnett et al., 2006). Previous studies have reported reinforcing the chitosan membranes with nylon to overcome the brittleness before functionalisation with photosensitisers (Bonnett et al., 2006). However, modification with PMA improved the mechanical strength of the membranes and therefore, there was no need for membrane reinforcement.

5.3.2 Midland blot of modified chitosan membrane

The Midland blotting was performed to analyse the chemical properties of PMA modified chitosan membranes as compared to unmodified chitosan membranes. Unmodified chitosan membranes have free amino groups at position 6 of the chitosan monomer while modified membranes have free carboxyl groups. Chemiluminescence was detected for unmodified membranes as they possess amino groups (and therefore became tagged by NHS-biotin, allowing subsequent labelling with streptavidin-peroxidase) while it was not detected for modified membrane as they have free carboxyl groups (Figure 5.6). The two controls; unmodified chitosan membrane but treated in DMSO and unmodified chitosan membrane showed chemiluminescence after Midland blotting thereby confirming the presence of free amino groups whilst PMA modified chitosan membrane did not show chemiluminescence after Midland blotting (Figure 5.6). The absence of chemiluminescence for the modified membranes shows that PMA modification was successful.

(Placeholder17p. This image has been removed by the author of this thesis for copyright reasons)

Figure 5. 6: Images of chitosan membranes to confirm amine modification: (A1), PMA modified chitosan membrane; (A2), unmodified chitosan membrane but treated in DMSO; (A3), unmodified chitosan membrane; (B1), chemiluminescence not detected for PMA modified chitosan membrane; (B2), (B3), chemiluminescence detected for unmodified chitosan membranes (Majiya *et al*., 2017).

5.3.3 Adsorption of TMPyP onto modified chitosan membrane

PMA modified membrane and the 2 control samples (DMSO treated but unmodified membrane and unmodified membrane) were treated TMPyP. We observed that only PMA modified membrane retained the TMPyP after vigorous washing in dH_2O (Figure 5.7). It is clear that most of the amino groups, which gave net positive charge to the chitosan membranes, had been modified to introduce carboxyl groups thereby allowing efficient adsorption of the cationic TMPyP.

(Placeholder18p. This image has been removed by the author of this thesis for copyright reasons)

Figure 5. 7: Chitosan membranes functionalised with TMPyP. (A1), PMA modified membrane; (A2), 20% (v/v) DMSO treated but unmodified membrane; (A3), unmodified membrane. The corresponding samples after staining with TMPyP and washing in H_2O are shown in B1-B3 respectively (Majiya *et al*., 2017).

It is important to note that TMPyP attachment onto the PMA treated chitosan membranes is electrostatic and the dye could be released into medium of high ionic strength. We carried out all our PDI investigations in 1 X PBS comprising 10 mM Na_2HPO_4, 1.8 mM KH_2PO_4, 137 mM NaCl, and 2.7 mM KCl and there was no release of TMPyP into the solution as monitored by spectrophotometry. In practice, most potential drinking water from the environment, freshwater streams or lakes will

have low ionic strength. Within our study, monitoring the release of TMPyP from the chitosan membrane and washing to zero absorbance after staining of the membranes with TMPyP was important as even 0.2 µM of TMPyP could achieve complete inactivation of MS2 phage in solution within few minutes. This is shown from preliminary PDI investigations using TMPyP in solution in Chapter 4. The absorbance measurements at 422 nm the peak absorbance of TMPyP, of the solution before and after treatment of the membrane with TMPyP and wash solutions were determined. The concentration of TMPyP bound to the membrane could be calculated through absorbance measurement and it is the difference between the absorbance of TMPyP before staining of the membrane and absorbance of TMPyP contained in staining solution and wash solutions after staining of the membrane. However, there was no significant difference in the absorbance of staining solution before and after staining of the membranes and so, we were not able to determine the amount of TMPyP bound to each membrane. This is because only small amount of TMPyP was adsorbed onto the chitosan membrane due its low surface area to volume ratio and non-fibrous nature. Another way to quantify the concentration of TMPyP bound to the membrane is to unbind TMPyP from the membrane in high salt solution and then measure it.

5.3.4 PDI of MS2 phage using TMPyP functionalised chitosan membranes

TMPyP functionalised chitosan membranes (CM-T) were used to investigate inactivation of MS2 by PDI. Our data showed that for the stationary model of PDI of MS2 using CM-T, reductions of 3 and 7 log PFU/ml of MS2 were observed for 30 and 60 min of illumination respectively (Figure 5.8 A). Complete inactivation (reduction

of 9.6 log PFU/ml) of MS2 was observed with CM-T after 90 min illumination with the light at 32 mW cm^{-2} (Figure 5.8 A). For the flowing water model, complete inactivation of MS2 (reduction of 8.8 log PFU/ml) was observed for sample passed twice over the surface of CM-T at 0.33 ml/min while being illuminated with light of 32 mW cm^{-2} (Figure 5.8 B). Reduction of approximately 3 log PFU/ml were observed for sample passed once under the same conditions (Figure 5.8 B).

(Placeholder19p. This image has been removed by the author of this thesis for copyright reasons)

Figure 5. 8: PDI of MS2 using TMPyP functionalised chitosan membrane. CM, chitosan membrane; CM-T, TMPyP functionalised CM. MS2 were exposed to PDI in a static model (data part A) or a flowing model (data part B) where MS2 suspension at 10^8 PFU/ml were passed over CM or CM-T at 0.33 ml/min under light 32 mW cm^{-2} dark conditions. CM-T (Light, A), was passed over the surface of CM-T once while CM-T (Light, B) was passed over twice during the PDI. Data are mean ± standard deviation (n = 3) (Majiya *et al*., 2017). (┬), complete inactivation.

The same light intensity at 32 mW cm^{-2} was chosen and used as in our PDI studies in solution. This was to allow comparison between rate and extent of PDI with TMPyP in solution and while attached onto chitosan membrane. This light intensity is low and it is just about 3% of bright midday sunlight under clear sky conditions in sub-Saharan Africa. Subsequent PDI investigation will be employ much higher light intensities. However, use of real world light intensities would just give complete inactivation and reveal little detail of the inactivation rates. It is also clear that the PDI capacity of CM-T at low light intensity mean it could also be used in the UK and other northern European countries. In these nations the key advantage would be reduction in energy use for water treatment. The rate of PDI with TMPyP attached onto chitosan membrane was slower as compared to TMPyP in solution (as shown

in Chapter 4). This is expected as proximity of unattached TMPyP in solution to the microorganism will be greater as compared with attached TMPyP. However, the ultimate aim was achieved as CM-T can cause PDI of MS2 under flow conditions and re-use (Figure 5.9) with no apparent detectable decline in its PDI capacity and efficiency.

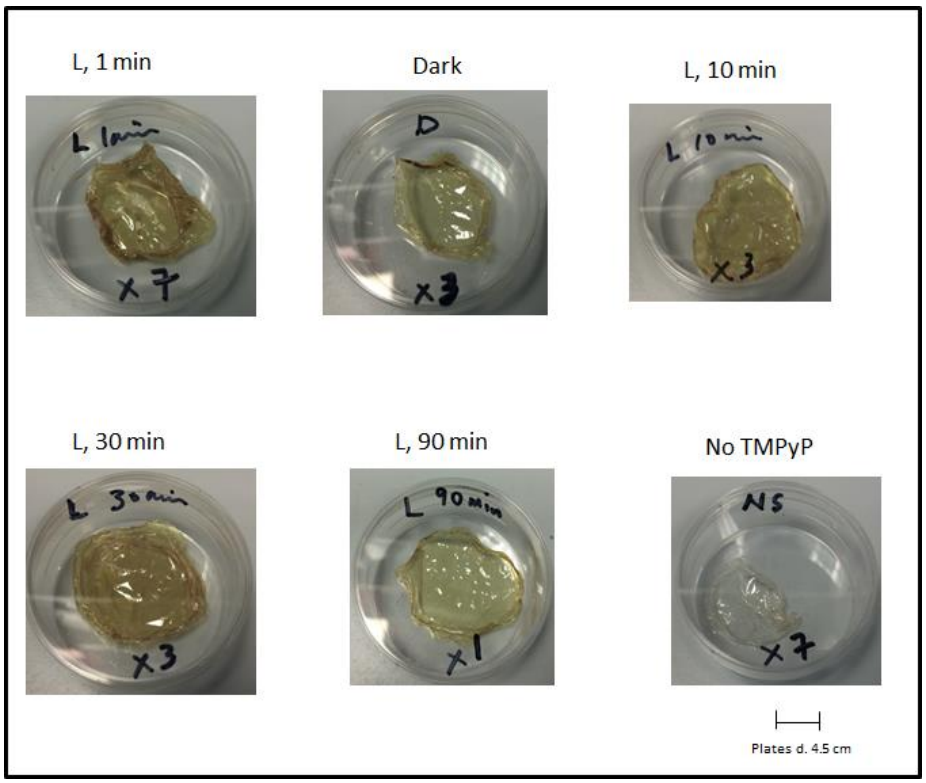

Figure 5. 9: Dried re-used TMPyP functionalised chitosan membranes (CM-T) for the PDI of MS2. The duration of PDI and number of re-uses (X) of the membranes are shown. The membranes became flattened and expanded to about 4.5 cm diameter while in PDI solution.

5.3.5 PDI of *E. coli* BL21 using TMPyP functionalised chitosan membranes

TMPyP functionalised chitosan membranes (CM-T) were used to investigate inactivation of *E.coli* BL21 by PDI. For the photodynamic inactivation of *E.coli* using CM-T under the same stationary model used for MS2, reductions of only 3 log CFU/ml of the bacteria was observed after 90 min of illumination (Figure 5.10). The

data also show that washing of the cells lead to reduction of about 1 log CFU/ml of the bacteria and the actual photodynamic inactivation was about 2 log reductions under these conditions (Figure 5.10).

(Placeholder20p. This image has been removed by the author of this thesis for copyright reasons)

Figure 5. 10: PDI of *E. coli* BL21 using TMPyP functionalised chitosan membrane. CM, chitosan membrane; CM-T, TMPyP functionalised CM. PDI light experiments were illuminated at 32 mW cm^{-2} for 90 min. CM-T (Dark), was not exposed to light; CM only (Light), was exposed to light; DP (direct plating), was washed but not treated either with CM-T or light; NW (cells not washed), was not treated either with CM-T or light. Data are mean ± standard deviation (n = 3) (Majiya *et al*., 2017).

The cells were washed to prevent interference of bacteria media (TSB) on the PDI of the bacteria. The organic component of the TSB could in principle compete with the bacterial components in quenching the singlet oxygen and other ROS generated during PDI. This would reduce singlet oxygen mediated damage and reduce the effectiveness of PDI. It is also important to realise that greater illumination time and intensity could increase bacterial killing. However, the use of MS2 photodynamic inactivation (stationary model) conditions for the *E.coli* experiment allowed direct comparison of the two types of organism. TMPyP in solution can bind to bacterial cell membranes in addition to ROS generated in solution. However the only possibility for PDI with TMPyP immobilised on chitosan membranes is direct cell damage by ROSs generated close to the support surface. The reduction in colony count of the bacteria after the PDI can be observed clearly when bacteria agar plates were compared (Figure 5.11).

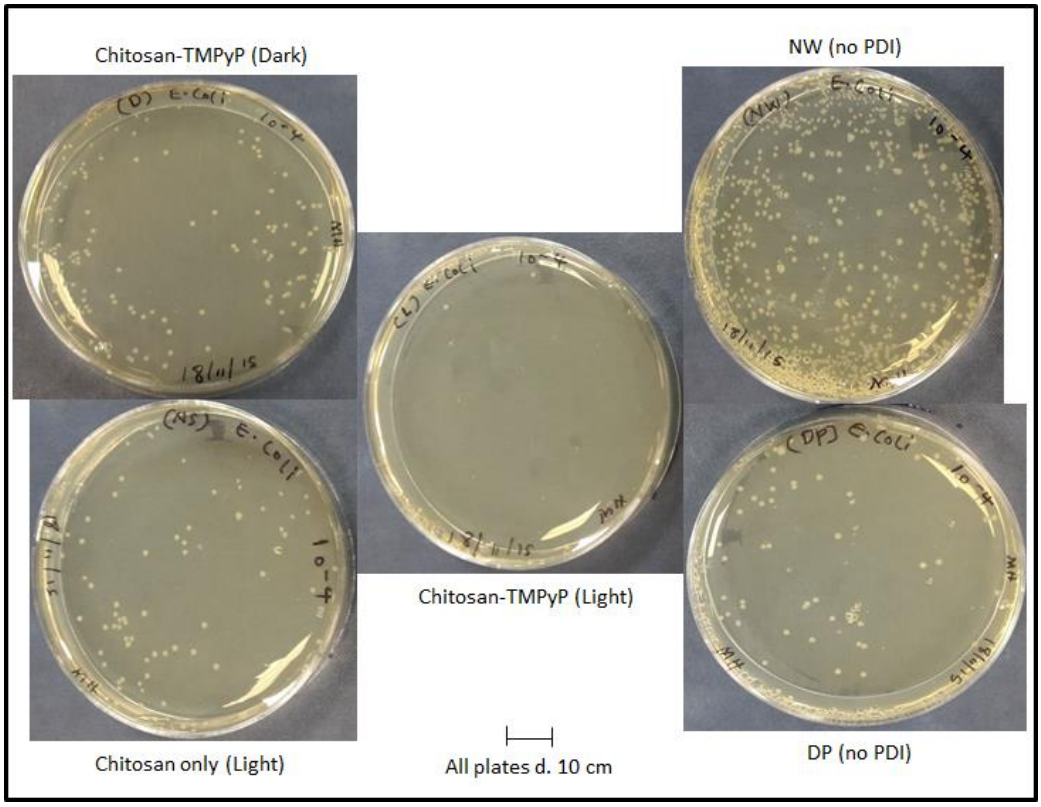

Figure 5. 11: PDI of *E. coli* BL21 using TMPyP functionalised chitosan membrane. PDI light experiments were illuminated at 32 mW cm^{-2} for 90 min. Chitosan-TMPyP (Dark), was not exposed to light; DP, direct plating, was washed but not treated either with CM-T or light; NW, cells not washed and not treated either with CM-T or light.

5.8 PMA Modified and TMPyP functionalised chitosan nanofiber

We were able to successfully functionalised chitosan polymeric membranes with TMPyP which is our photosensitiser of choice. Also, TMPyP functionalised chitosan membrane (CM-T) have been shown to inactivates MS2 and BL21 *E. coli*. However, chitosan polymeric membranes are non-fibrous and have a low surface area to volume ratio. This means, hypothetically that only small amount of TMPyP could be adsorbed onto the membranes. If a solid support such as a nanofiber mesh was utilised, this would provide a much higher surface area to volume ratio and more TMPyP could be immobilised. This, in turn would lead to more singlet oxygen generation during PDI and improve the PDI. Since we have established a protocol for

the modification and TMPyP functionalisation of polymeric chitosan membranes, chitosan electrospun nanofibers (Figure 5.12) were also tested as a solid support for attaching TMPyP for water disinfection. The chitosan/polyethylene oxide (PEO) (60:40 weight ratio) electrospun nanofiber was a gift from Dr A. M. Afifi, University of Malay, Kuala Lumpur. Electrospun nanofibers are usually fragile and lack the mechanical strength to withstand rigorous physical processes such as wastewater treatment and disinfection applications. However, chitosan/PEO (60:40 weight ratio) electrospun nanofiber is robust, fibrous and have a high surface area to volume ratio (5.12).

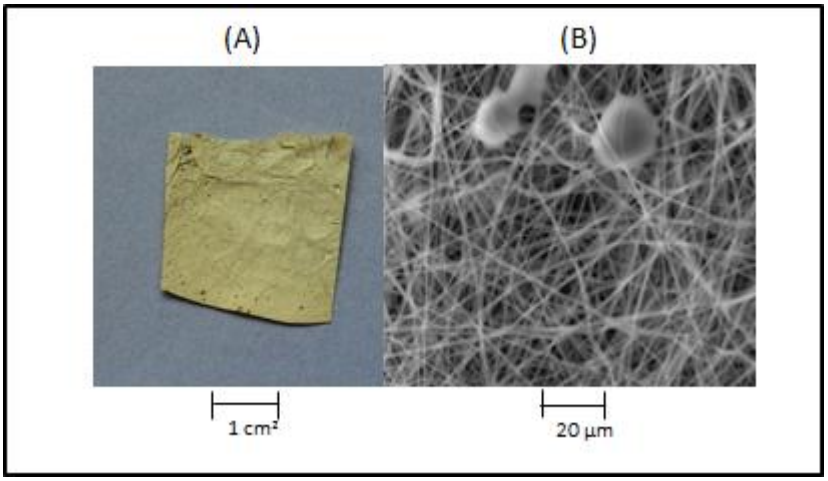

Figure 5. 12: Macro (A) and SEM (B) images of chitosan/polyethylene oxide (60:40 weight ratio) electrospun nanofiber mat. The material was a generous gift from Dr A. M. Afifi, University of Malay, Kuala Lumpur.

The blend of chitosan and PEO in the nanofiber was necessary as pure chitosan cannot form fibres. Chitosan in the nanofiber provided the mechanical strength while the PEO and surfactants allow electrospinning or yielding fibres with diameters ranging from 40 nm to 240 nm (Kriegel et al., 2009). Several blend of chitosan and PEO could be electrospun and higher chitosan content led to the thinner nanofibers.

It has been shown that increasing the chitosan/PEO ratio from 50:50 to 90:10 led to a decrease in fibre diameter from 123 to 63 nm (Pakravan et al., 2011). The electrospinability of pure chitosan is limited mainly because of its polycationic nature in solution, rigid chemical structure and specific inter and intra molecular interactions (Pakravan et al., 2011).

As with the polymeric chitosan membrane used earlier, direct adsorption of TMPyP onto chitosan/PEO nanofibers was not possible because the net charge of the nanofiber is positive and will not bind TMPyP, which is tetra cationic. The chitosan/PEO nanofibers were first modified by pyromellitic dianhydride (PMA) in order to introduce carboxyl groups and allow adsorption of the highly basic TMPyP. Therefore, the chitosan/PEO composite nanofibers were treated with PMA as previously described (Section 5.2.2)

Fourier-transform infrared spectroscopy (FTIR) was used to assess the success of the PMA modification of chitosan/PEO nanofiber. The FTIR transmission spectra were measured at room temperature on the unmodified chitosan/PEO nanofiber mat and modified chitosan/PEO nanofiber mat using a Perkin Elmer 65 FTIR-ATR instrument. A total of 128 scans were accumulated for signal averaging of each IR spectra measurement to ensure a high signal to noise ratio with a 4 cm^{-1} resolution. The spectra of the samples were recorded over a wavenumber range of 500-4000 cm^{-1}. Unmodified chitosan/PEO nanofibers have free amino groups at position 6 of the chitosan monomer while PMA modified chitosan/PEO nanofiber should have free carboxyl groups. Our FTIR data of unmodified chitosan/PEO nanofiber (CPN) and PMA modified chitosan/PEO nanofiber (PMA-CPN) showed that the modification was successful. Primary amine peak was observed in unmodified chitosan/PEO

nanofiber (Figure 5.13). While we could not observe any primary amine peak in PMA modified chitosan/PEO nanofiber (Figure 5.13). However, carboxylic acid peak was observed in PMA modified chitosan/PEO but was not observed in unmodified chitosan/PEO nanofiber. It was reported by Pakravan *et al*., (2011) that the FTIR spectra obtained at room temperature for chitosan/PEO nanofibers at various chitosan/PEO contents have an amine (NH2) stretch with strong peak observed at 1555 cm^{-1}. This confirmed the amine stretch that we observed in the unmodified chitosan/PEO nanofiber and lack of it in the PMA chitosan/PEO nanofiber (Figure 5.13).

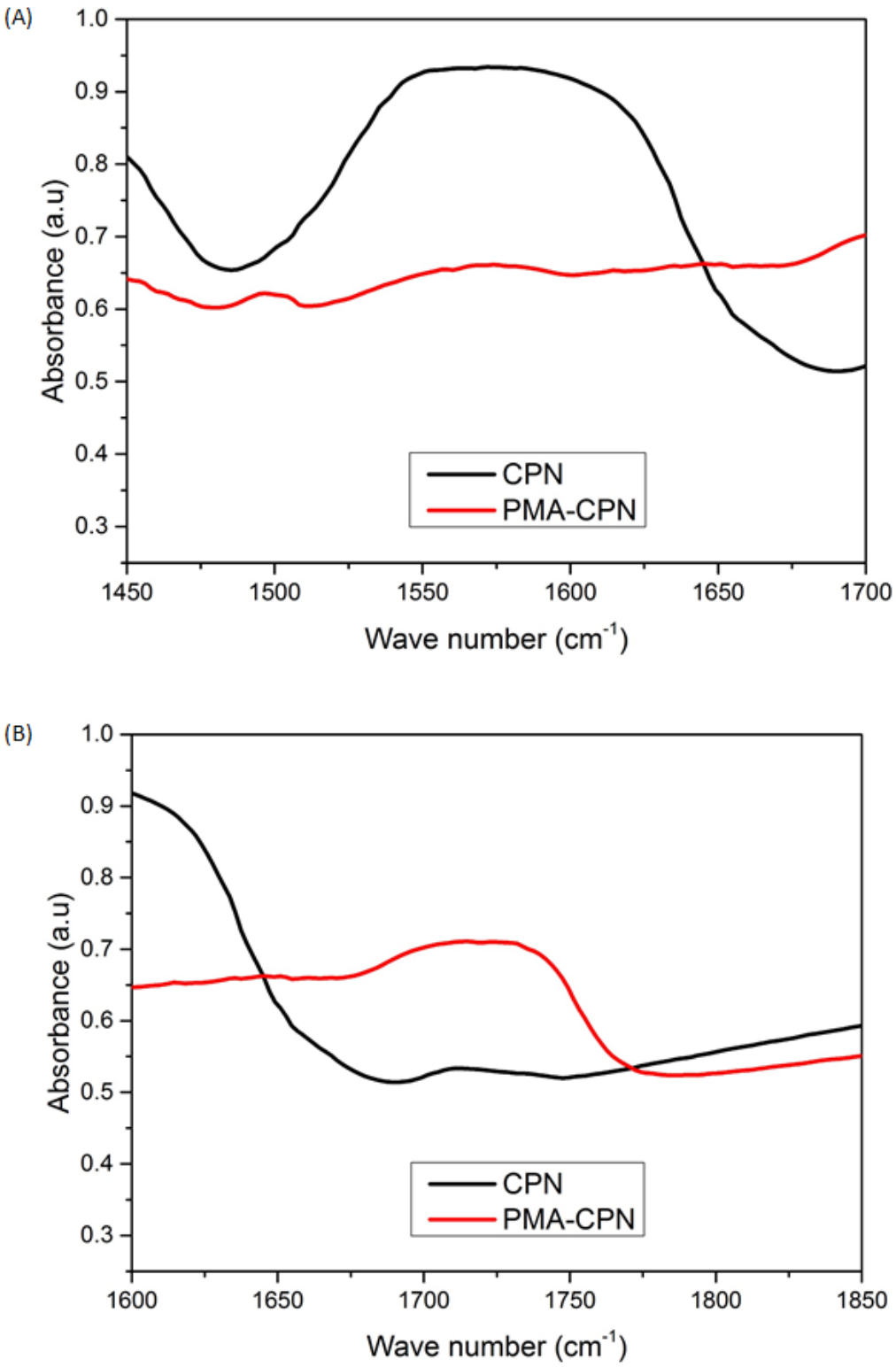

Figure 5. 13: FTIR data of unmodified chitosan/PEO electrospun nanofiber (CPN) and PMA modified chitosan/PEO electrospun nanofiber (PMA-CPN). (A), primary amine peak; (B) Carboxylic acid peak.

PMA modified chitosan/PEO nanofiber (PMA-CPN) and unmodified chitosan/PEO nanofiber (CPN) were incubated in TMPyP. Each nanofiber mat (1 cm square 100 µM thick) was immersed in 2 ml 0.25 mM TMPyP contained in a closed bottle (Figure 5.14) and from here, subsequent steps for TMPyP functionalisation of the nanofibers were as previously described in Section 5.2.4.

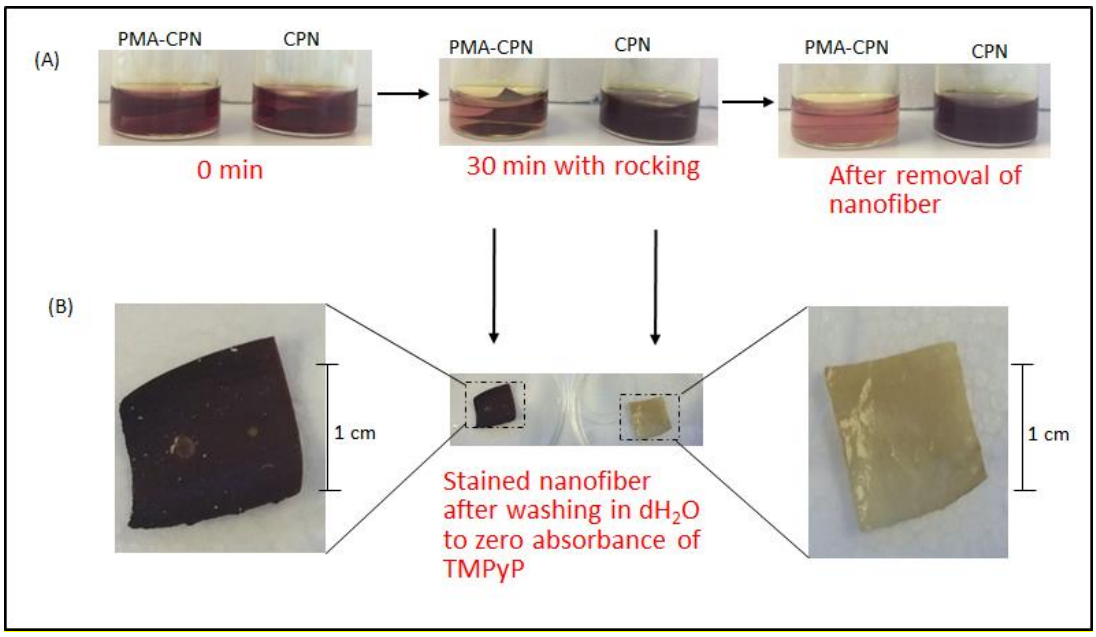

Figure 5. 14: Chitosan/PEO nanofiber functionalisation with TMPyP. (A), PMA modified chitosan/PEO nanofiber (PMA-CPN) and unmodified chitosan/PEO nanofiber (CPN) 30 min incubation in TMPyP; (B), PMA-CPN and CPN after washing in water.

We observed that only the PMA modified chitosan/PEO nanofiber retained the TMPyP after vigorous washing in dH_2O (Figure 5.14). It is evident that most of the amino groups which gave net positive charge to the chitosan had been modified allowing efficient adsorption of the cationic TMPyP. We monitored the release of TMPyP from the nanofiber and washed in dH2O to zero absorbance after staining of the membranes with TMPyP. This is very important as even 0.2 µM of TMPyP can achieve complete inactivation of MS2 phage in solution within few minutes. As expected, we observed that much more TMPyP could be bound by PMA modified

chitosan/PEO nanofiber (PMA-CPN) as compared to chitosan membrane. Absorbance at 422 nm (the peak absorbance of TMPyP) of reaction solution before and after staining of the nanofiber with TMPyP and wash solutions was determined. The concentration, expressed as percentage of TMPyP bound onto the nanofiber was calculated as difference between the absorbance of TMPyP before staining and absorbance of TMPyP within reaction solution and wash solutions after staining. Our data showed that 1 cm^2 of the nanofiber with thickness of 100 µm could take up around 83% of TMPyP from a 2 ml solution of 0.25 mM TMPyP (Figure 5.14).

5.9 PDI of MS2 phage using TMPyP functionalised chitosan/PEO nanofiber

TMPyP functionalised chitosan/PEO nanofibers (CPN-T) were used to investigate inactivation of MS2 by PDI. Initially, the stationary model was used as previously described in Section 5.2.5. The CPN-T was pre-wet and immersed in 1 ml MS2 (10^9 PFU/ml) for the PDI.

Our data showed reductions of 2 and 5 log PFU/ml of MS2 were observed for 1 and 4 min illumination respectively (Figure 5.15). Complete inactivation (reduction of 9.6 log PFU/ml) of MS2 was observed with CPN-T after 6 min illumination with the light at 32 mW cm^{-2} (Figure 5.15). The same light intensity at 32 mW cm^{-2} was chosen and used as in our PDI studies in solution and with CM-T. This was to allow comparison between rate and extent of PDI with TMPyP in solution and while attached onto chitosan membrane and nanofiber mats. The rate of PDI of MS2 could be increased by using much higher light intensities, although it is clear that the efficient PDI shown by CPN-T at low light intensity means it could also be used in the UK and other

northern European countries. The rate of PDI with TMPyP attached onto chitosan nanofiber was slower as compared to TMPyP in solution (as shown in chapter 4). However, it was faster than PDI with CM-T. This was expected as the proximity of unattached TMPyP in solution to the microorganism will be greater as compared with attached TMPyP. The PDI with CPN-T was faster than with CM-T because the nanofiber has a much higher surface area to volume ratio. So, more TMPyP could be attached thereby generating more ROS to inactivate MS2. Each CPN-T was re-used at least 3 times for the PDI investigation of MS2 with no detectable decline in its PDI capacity and efficiency, and it is likely that many cycles of use could be realised.

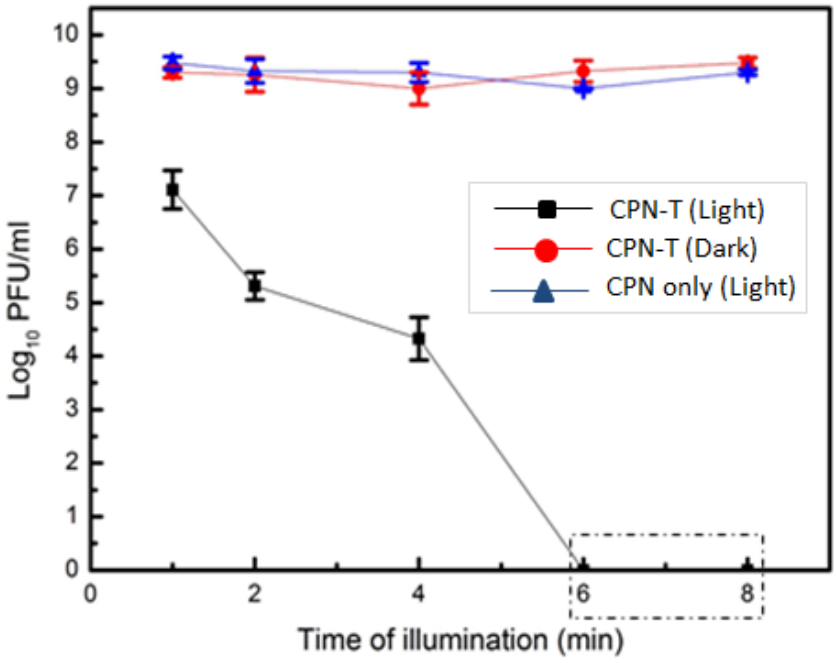

Figure 5. 15: PDI of MS2 using TMPyP functionalised chitosan/PEO nanofibers. CPN, chitosan/PEO nanofiber; CPN-T, TMPyP functionalised CPN. PDI light experiments were illuminated at 32 mW cm^{-2} while CPN-T (Dark) was not exposed to light. ⬚, complete inactivation.

5.10 conclusion

The data presented in this chapter has shown that TMPyP attached onto chitosan membrane (CM-T) and chitosan/PEO nanofibers (CPN-T) can inactivate MS2 and *E. coli* BL21. This means TMPyP functionalised chitosan nanofiber/membrane could be used as a simple, cheap, environmentally friendly device for water disinfection.

Both chitosan membrane (CM-T) and chitosan/PEO nanofiber (CPN-T) have a number of merits. Both use chitosan which is non-toxic, biodegradable, wettable, cheap and readily available. It also shows good mechanical strength to withstand the wear and tear of the water disinfection process. We described a method of modifying chitosan nanofiner/membrane without affecting its solubility in water using pyromelitic dianhydride (PMA). The PMA modified chitosan nanofibers and membranes could also be used to adsorb positively charged dyes and heavy metals from contaminated water thereby remediating the water totally although this feature has not been explored in this study. CM-T and CPN-T have been re-used several times for the same purpose with no detectable decline in their PDI capacity and efficiency and this would ultimately reduce cost. Furthermore, the flowing water model for PDI mimic something close to the process in water treatment plants, although much more development is needed to arrive at pilot scale testing. Overall, chitosan/PEO nanofiber is better than chitosan membrane as solid support for attaching TMPyP for water disinfection because the nanofiber had a much higher surface area to volume ratio.

The fact that CM-T and CPN-T were able to photodynamic inactivate MS2 and *E. coli* while using light intensity of 32 mW cm^{-2} which is low compared to daytime sun brightness, is an indication that this research can lead way to simple sunlight driven

water disinfection system that could be used as a zero man-made energy input system to produce clean and safe drinking water in both developed and developing countries.

Chapter Six: General discussion

Chapter 6 General discussion

6.1 Overview

It was first proposed in 1994 that the photodynamic effect using immobilised photosensitisers might be used for water disinfection. This would be especially effective in developing nations, where contaminated surface water is a major problem and bright solar irradiation is available for free (Bonnett et al., 1994). It is around 23 years now and no successful disinfection of water using the photodynamic effect of a photosensitiser during wastewater treatment has been reported in either developed or developing countries. This is in spite of ongoing worldwide research into the possibility of using this technology during wastewater treatment. Common issues which have held back this area have been finding the right solid supports, coupling chemistries and photosensitisers with appropriate properties suitable for sustainable usage in water disinfection. The motivation behind the research includes reduction of energy and chemical usage to the bare minimum. Sunlight can be used as the source of light for the photodynamic effect and photosensitisers could be attached on to solid supports so that after phototreatment of water the supported photosensitiser is not released into the water and disinfection systems could be re-used for water disinfection making it cheap and environmentally friendly.

The ultimate aim of this work was to develop a sunlight-driven water bioremediation system. In this study, we chose the photosensitiser - 5, 10, 15, 20-tetrakis (1-methyl-4-pyridinio) porphyrin tetra *p*-toluene sulfonate (TMPyP) since preliminary studies with TMPyP in solution showed it caused a rapid photodynamic inactivation (PDI) of our model viral organisms (bacteriophages MS2 and Qβ, murine norovirus and bovine enterovirus). Native gel electrophoresis, SDS-PAGE and western blotting,

TEM and DLS were used to analyse pre- and post-PDI samples of our viruses. This was to observe inter capsid and intra capsid proteins changes due to singlet oxygen mediated oxidation. In addition, in order to identify targets and unravel the actual mechanism of ROS mediated inactivation, sequence specific antibodies against predicted target sequence in the A-protein were made. The target sequences selected were all candidate sites for involvement of A-protein binding to the bacterial pilus. Also, Attempt were made to select mutants MS2 resistant to singlet oxygen mediated inactivation. Finally, the RNA of MNV PDI samples was extracted and transfected in order to know whether RNA infectivity itself was affected by the PDI.

Chitosan nanofiber and polymeric membranes were used as solid supports for attaching TMPyP. However, the chitosan nanofibers mats and membranes were first modified with pyromelitic dianhydride to introduce carboxyl groups and facilitate adsorption of the highly basic TMPyP. The TMPyP functionalised chitosan nanofiber/membrane produced were then used for PDI of bacteriophage MS2 and *E. coli* BL21. Both stationary and flowing water models were employed during the PDI experiments. The TMPyP functionalised chitosan nanofiber mats and membranes was shown to cause PDI of MS2 and *E. coli* BL21 in aqueous solution.

In this chapter key results are discussed highlighting the implications, impacts and future prospects of this work as well as challenges encountered along the way.

6.2 Specific findings within this report

In this work, we observed that PDI of MS2 with TMPyP in solution caused inter and intra capsid protein changes. We observed aggregation of MS2 particles through native agarose gel electrophoresis and confirmed this by TEM and DLS. No

aggregation of phage Qβ and BEV was observed. We also observed crosslinking of MS2 coat protein through western blotting after PDI. Also, crosslink of the major capsid protein VP1 (formation of trimers) within MNV was observed. Complete MS2 particle aggregation was observed after 60 min of PDI. Formation of dimers of MS2 coat protein was observed after 10 min PDI. However, because there was no correlations between MS2 particle aggregation or crosslinking of its coat protein and complete inactivation of MS2 within 1 min of PDI, we turned our focus to the host bacteria attachment protein, the A-protein which is also part of MS2 capsid. Using sequence specific antibodies, generated against peptides corresponding to regions of the MS2 A-protein, we were able to show that A-protein is the key target of PDI in MS2. Changes to epitopes caused by ROS mediated oxidation should result in a switch in antigenicity from a native, and detectable state to a non-native state and correlates with the rate of PDI. Sequence-specific antibodies for antigenic sites 2 and 4 on the A-protein of MS2 did not detect these after 1 min of PDI. This rate of loss of antigenicity corresponds to the rate of PDI of MS2 we observed previously. Histidine and tryptophan are the most sensitive amino acids to singlet oxygen and their position almost in the middle of the sequence of these antigenic sites on the A-protein is probably responsible for the fast rate of antigenicity loss. This approach provides a novel approach to evaluate the effect of ROS caused by PDI, on different regions of viral target proteins.

Several studies have been reported on PDI of viruses in solution. Many of the PDI studies have revealed that the rate and extent of PDI of viruses is dose dependent. In most of the PDI studies, much of the work was focused on inactivation kinetics

with little emphasis on the molecular targets of the PDI and its mechanism from a biological perspective.

Changes to viral proteins as result of PDI have been measured by SDS-PAGE and infrared (IR) spectroscopy (Costa et al., 2014). However, these methods are not specific to PDI-mediated effects. The use of SDS-PAGE is limited to overall effects on viral proteins but cannot give detail of the domains affected. In addition, the reaction of singlet oxygen with proteins results in multiple effects including oxidation of side chains, backbone fragmentation, dimerisation and/or aggregation, unfolding or conformational changes. These effects can result in enzymatic inactivation and alterations in cellular handling and turnover. Owing to the presence of reducing agents in SDS-PAGE as well as heat-treatment of proteins, there is significant reduction in assay sensitivity. Similarly, IR spectroscopy cannot detect changes induced by PDI on specific protein residues but only give an overall effect on proteins. Matrix assisted laser desorption ionization (MALDI) and electrospray ionisation (ESI) mass spectrometry have also been applied to the evaluation of site-specific protein damage due to singlet oxygen oxidation (Rule Wigginton et al., 2010).

In most viral PDI investigations, one or two model viruses were used and no comparisons were made with other viruses. After exhaustive PDI investigation of MS2, we also used PDI to investigate other model viruses-bacteriophage Qβ, bovine enterovirus and murine norovirus. Bacteriophage Qβ is very similar to MS2 and it was chosen to see how difference in amino acid composition of the virus attachment protein affected the rate of PDI. BEV and MNV are good models for eukaryotic viruses especially enteric viruses that are known to cause viral waterborne diseases

and importantly are viruses which infect eukaryotic, and specifically mammalian cells. The model viruses have some similarities which include being lytic, non-enveloped, icosahedral capsid, 27-30 nm in diameter, positive sense and single stranded RNA as their genome. Although these model viruses are similar to great extent, the PDI data showed that the inactivation varied among them. The rate and extent of PDI among these viruses was in the order MS2 > phage Qβ > MNV > BEV. This may be because of the amino acid compositions, surface accessibility and hydrophilicity of their host attachment proteins. This is because ROS) generated in solution can only attack those parts of proteins that are solvent accessible. This can possibly lead way in classifying viruses into; very sensitive, mildly sensitive and less sensitive to PDI based on amino acid compositions and solvent accessibility of their host attachment proteins/sites.

6.3 Photosensitisers as water disinfectants and supplements

We used 3 photosensitisers (TMPyP, Rose Bengal and methylene blue) for PDI of our model viruses in solution and we found out that TMPyP was the most efficient. TMPyP is a porphyrin, Rose Bengal is a xanthene dye and methylene blue is a phenothiazinium dye (DeRosa and Crutchley, 2002). These photosensitisers have the following required properties of a good photosensitiser;

High absorption coefficient in the visible spectra; the emission spectra of light source we used in this work was 400 nm – 786 nm and the absorption peaks for TMPyP, Rose Bengal and methylene blue were at 422 nm, 550 nm and 666 nm respectively. Also, sunlight could as well be used to excite these photosensitisers. A typical solar spectrum (solar AM1.5) is 300- 1400 nm (Loeb et al., 2016) with a peak at 500 – 600 nm (Jemli et al., 2002).

A triple state of appropriate energy ($E_T \geq 95$ kJ mol^{-1}); this allows for efficient energy transfer to ground state oxygen in the water which can then be converted to singlet oxygen. The E_T of methylene blue and Rose Bengal are 133.9 kJ mol^{-1} and 175 kJ mol^{-1} respectively (Loeb et al., 2016, DeRosa and Crutchley, 2002).

High quantum yield of the triple state ($\Phi_T > 0.4$) and long triplet state lifetimes ($T_T >$ 1 μs); the efficiency of the photosensitiser is dependent on the photophysical properties of its lowest excited triple state. The Φ_Δ *(*quantum yield*)* of methylene blue and Rose Bengal in aqueous solution are 0.52 and 0.76 respectively (DeRosa and Crutchley, 2002). The singlet oxygen Φ_Δ (which is directly proportional to triple state energy and quantum yield of the triple state of the photosensitiser) of TMPYP is 0.74 in PBS (Lei et al., 2010).

Many photosensitisers including these 3 photosensitisers are highly coloured organic compounds that are soluble in water. Even though photoactive antimicrobials are not generally toxic molecules, there are health and safety concerns for ingesting these photosensitisers in water (Wainwright et al., 2017). Therefore, a successful photodynamic water disinfection system will require attachment of the photosensitiser onto a solid support to prevent release into water during and after treatment. This is also a practical consideration anyway, since contamination with free photosensitiser would be unacceptable to the consumer. Also, the photosensitiser functionalised solid support can be reutilised thereby reducing the cost of the treatment. However, even though there are many photosensitisers that have been shown to be efficient in PDI of microorganisms in solution, only a few have been successfully attached onto solid supports that could ultimately be used for water disinfection. This may be due to difficulties in finding appropriate solid

supports and efficient photosensitisers with the right functional groups and coupling chemistries. At the moment, successfully photosensitiser functionalised solid supports are either too fragile for disinfection of large volumes of water or too costly and therefore not suitable for world's poorest regions. These include rural areas in the sub-Saharan and south east-Asia where conventional centralised wastewater treatment is usually lacking. In this work, we are not able to attach TMPyP onto chitosan nanofiber mats and membranes covalently because of the lack of appropriate functional groups. Although, parallel research within the Millner group is close to synthesising TMPyP analogous with pendant reactive groups such as alkynes, amines (Mrs K Chowdhury- personal communication). Covalent photosensitiser coupling would be preferable to electrostatic adsorption that we used to attach TMPyP onto chitosan nanofibers and membranes in this work, since covalent coupling would not be affected by ionic strength and pH of the water. However, in practice since most application will be for freshwater sterilisation this will not be a problem. The TMPyP functionalised chitosan nanofibers and membranes we fabricated showed photodynamic inactivation capacity against MS2 and *E. coli* BL21. However, we observed substantial differences in the rate of PDI of MS2 with TMPyP in solution and when immobilised. The rate of PDI with TMPyP attached onto chitosan nanofibers and membranes was slower compared to TMPyP in solution. This was in agreement with other reports of photosensitisers attached onto solid supports (Henke et al., 2013, Suchanek et al., 2014, Bonnett et al., 2006, Carvalho et al., 2010). This was expected as the proximity to the microorganism of TMPyP in solution will be far greater as compared with immobilised TMPyP and because the singlet oxygen generated has limited diffusion path length in water, 200

nm – 400 nm, corresponding to a lifetime of ~ 3 µs (Loeb et al., 2016). These are some of the problems delaying the first successful application of PDI for water disinfection. However, using photosensitisers that are nontoxic, readily available, cheap, medicinal and nutritious might not require attachment onto solid support for water disinfection application. The types of photosensitisers that will suit these descriptions will be of natural origin especially plants. The attractiveness of phytochemical compounds (plant extracts) that may be used relies on the fact that they are natural and economical alternatives to chemically synthesised antimicrobials and also because most of the compounds of plant origin are Generally Recognised As Safe (GRAS) (Randazzo et al., 2016). Recently, there are several reports about the potential use of natural photosensitisers such as chlorophyllin, alpha-terthienyl, hypericin and curcumin to control foodborne pathogens and spoilage microorganisms (Randazzo et al., 2016, Luksiene and Brovko, 2013, Astuti et al., 2016). Chlorophyll is the most abundant biological pigment that is commonly found in plants, bacteria, bryophytes and algae. Chlorophyll plays a vital role in photosynthesis in these organisms (Arof and Ping, 2017, Guo et al., 2017, Ballottari et al., 2013). Chlorophylls are natural pigments and therefore safe, environmental friendly, easily available and cheap. It has also been shown to be an excellent dietary supplement because it has nutritional and medicinal benefits. Chlorophyll can be easily extracted from the leaves of many plants (Arof and Ping, 2017). Curcumin is a phenolic compound extracted from turmeric rhizomes (*Curcuma longa*) and approved by the EU as a food additive (E100) (Randazzo et al., 2016). It has been consumed for medicinal purposes for many centuries (Gupta et al., 2012). It is also is inexpensive, well tolerated and as food supplement in several countries (Gupta et

al., 2012). It has been shown that curcumin has antioxidant, anti-inflammatory, anticancer, antiatherosclerosis, hepato and neuroprotective properties (Gupta et al., 2012, Penha et al., 2017). Finally, several papers have reported that curcumin has promising photoxicity against bacteria (including multiresistant), fungi and viruses that could be an advantage for food sterilisation and disinfection applications (Penha et al., 2017, Randazzo et al., 2016, Yang et al., 2016).

6.4 Available solar energy and water disinfection capacity of PDI

Our source of light for the PDI of model viruses in this work was visible cold light (400 nm – 786 nm) and the light intensity used for most of the PDI experiments was 32 mW cm^{-2}. This light intensity is only about 3% of bright mid-day time sunlight under clear sky conditions in the Sub-Saharan Africa and about 10% of mid-day time sunlight during summer in the Northern Europe. Such a relatively low intensity was intentionally used to provide a graded response, since high intensity would tend to yield totally dead organisms and reveal little detail of the PDI process. In this work, we have shown that 5 mW cm^{-2} can cause inactivation of MS2 with TMPyP in solution and light intensity affected the rate of inactivation of MS2 in flux dependent manner. This was true at least for light intensities from 5 mW cm^{-2} to 20 mW cm^{-2}. However, in reality, even though intensity of solar irradiation varies from place to place, position of the sun in the sky, different altitude/latitude and sky conditions, it present us with much wider spectrum (300 – 1200 nm) including UV, visible and near infra-red regions (Jemli et al., 2002, Gueymard et al., 2002, Loeb et al., 2016). This means that several photosensitisers could be excited, including photosensitisers that have multiple absorption peaks and or absorption peak in either of these regions. Furthermore, on a clear sky condition, about 8% of solar irradiation constitutes UV

radiation (< 400 nm) (Jemli et al., 2002). This has already been exploited in solar disinfection (SODIS) of water especially in remote and infrastructure deficient areas. SODIS involves exposing water to direct sunlight for at least 6 h. it is believed that microbial inactivation results from exposure to UV radiation (320 – 400 nm) with a minor contribution from heating (Loeb et al., 2016, Davies et al., 2009). Several studies have been reported for SODIS in polyethylene terephthalate (PET) bottles for inactivations of *E. coli* (Dejung et al., 2007, Dunlop et al., 2011, Fisher et al., 2012) and a few reported for inactivation of MS2 (Fisher et al., 2012, Carratalà et al., 2016) and *C. parvum* oocysts (Gómez-Couso et al., 2009). It is believed that the inactivation rate, especially for MS2, depends on organic matter and dissolved oxygen concentrations which promotes the generation of ROS under radiation. However, although SODIS is very cheap and simple and should be suitable for world's poorest regions for water disinfection, it has limitations such as unpredictable UV radiation intensity available, requirement for pre-filtration, and long exposure time to ensure safely sterilised water. The amount and proportion of UV radiation in the solar spectrum depends on latitude and cloud coverage (Hunter, 2009). Hypothetically, it could be suggested that when other PDI conditions remained the same as we did in this work but use sunlight instead as source of light, we should expect higher rate of inactivations of the model viruses and bacteria than what we observed in the laboratory. This means in real life situation, sunlight driven photodynamic disinfection of water is feasible with shorter duration illumination because of synergistic effects of UV radiation and photosensitisation.

6. 5 Model organisms for photodynamic disinfection of water

Waterborne pathogens can be broadly divided into bacteria, viruses, protozoa and helminths. The development of effective photodynamic disinfection systems that will be universal for the inactivation of waterborne pathogens will be required to be tested against the most resistant organisms from each of these groups. WHO guidelines for evaluating household water treatment options recommended *Cryptosporidium pervum* oocysts, *E. coli* and bacteriophage MS2 as model organisms for the diversity of organisms responsible for waterborne diseases (WHO, 2011a). There are several reports about effectiveness of PDI against bacteria and viruses but very few PDI investigations were reported on protozoa and helminths because they can be filter out relatively easily. (Loeb et al., 2016). *E. coli* is usually used as model for bacteria in many PDI investigations. *E. coli* is a coliform and gram-negative bacterium belonging to the family *Enterobacteriaceae* and is used as a marker for sewage contamination, as it is taken as surrogate for the presence of other pathogenic faecal organisms. Several other bacteria have been used as models in PDI studies. However, in most cases preferences were given to gram negative bacteria since gram positive bacteria, including those resistant to antibiotics, are easily inactivated by PDI as compared to gram negative bacteria. This is due to differences in the structure of their cell wall and membranes. Gram negative bacteria have an additional outer membrane apart from the cytoplasmic (inner) membrane, giving them extra protection against antimicrobial agents including ROS produced during photosensitisation. MS2 has been used as a viral model organism in several studies aimed at photoinactivation and chemical disinfection of human viruses because of its similarity in size and morphology to some human viruses (Kohn and Nelson, 2007,

Zhong et al., 2016). Also, it is non-pathogenic to humans and easy to propagate. However, some researchers have the opinion that to use phage as model organisms in photoinactivation experiments may not accurately reflect inactivation of human viruses (Silverman et al., 2013). Use of animal viruses that are closely related to human viruses to study PDI is attractive because of health and safety reasons. Also, some human viruses e.g. human norovirus is presently difficult to propagate in the laboratory whilst the closely related murine norovirus can be propagated easily (Taube et al., 2010, Orchard et al., 2016, Katpally et al., 2010). We used four model viruses in this work; these are bacteriophages MS2 and Qβ, bovine enterovirus 2 (BEV 2) and murine norovirus (MNV). These viruses are non-enveloped, have icosahedral capsids and positive single stranded RNA as their genome. Positive single stranded RNA viruses are the largest group of viral pathogens (Koonin et al., 2015, Heil et al., 2004, Dent et al., 2013, Harrison et al., 1978). We observed that MS2 is very sensitive to PDI especially when photosensitiser- TMPyP was used in solution. This agreed with several reports that showed that singlet oxygen is exceptionally effective against MS2 (Loeb et al., 2016). Although the model viruses used in this work are similar to a great extent, the rate and extent of PDI varies among these viruses even under the same PDI conditions. The rate and extent of PDI among these viruses was in the order; MS2 > phage Qβ > MNV > BEV. It is suggested that there is need to establish the PDI kinetics for a wider range of waterborne viruses. *Cryptosporidium pervum* oocysts and eggs of *Ascaris lumbricoides* could be used as PDI models for waterborne protozoa and helminths. To date, the rate and extent of PDI for *Cryptosporidium pervum* oocysts has not been explicitly published (Loeb et al., 2016).

6. 6 Water quality suitable for PDI of waterborne microorganisms

The source of water and its characteristics can determine the efficiency, performance and cost of conventional disinfection methods. Synergistic effect of 2 or more disinfection methods coupled with pre-treatment of water is the best way to efficiently inactivate resistant waterborne pathogens. This should apply to PDI too. Most reports concerning the prospects of using PDI for water disinfection report work under laboratory conditions where the effect of co-pollutants was not usually tested. In this work we observed that 0.1% (w/v) of humic acid gave 100 % protection to MS2 under the PDI conditions we used, although higher light intensity may reduce this. A plausible explanations for this include the humic acid quenching the ROS generated, or shielding the virus from direct effect of singlet oxygen mediated damage. It is very possible also that because at this concentration of humic acid gave dark brown colour to the PDI solution and light transmittance through the solution was drastically reduced, in turn reducing ROS production. At higher light intensity and longer duration of illumination, inactivation may be observed. This is because humic acid as well as greater excitation of the photosensitiser (TMPyP) and other soluble organic pollutants in waste waters could also act as photosensitisers when exposed to the full spectrum of sunlight (Kohn et al., 2007, Silverman et al., 2013). Natural organic matter (NOM) in water is the main causes of UV attenuation and ROS scavenging, especially hydroxyl radicals (Haag and Hoigne, 1986). However, singlet oxygen seem to be preferentially quenched by interaction with water and therefore concentration of NOM may in reality have negligible impact (Haag and Hoigne, 1986, Loeb et al., 2016). Comparative studies involving 4 solar driven disinfection technologies, including photocatalysis, photosensitiser (PDI), UV-C light-emitting

diodes (LED) and upconversion, showed that there were near identical percentage reductions in treatment capacity with decreasing water quality for all systems with the striking exception of singlet oxygen generating photosensitisers (Loeb et al., 2016). Typically, NOM concentrations of ~10^{-5} M are found in clear surface water and tap water (Leenheer and Croué, 2003). Ground water or borehole well water is very clear while some surface water may have high turbidity, colour and particulate matter. Ground water can have a dissolved organic carbon (DOC) concentration as low as 0.1 mg-C/L while surface waters tend to have higher DOC in the range of 2-10 mg-CL/L (Osterloh, 2008). However, it seems that it is turbidity, colour and particulate matter contents of water rather than its DOC which does not cause water colouration that most affects the treatment capacity of PDI.

6.7 Further work

Although there are several studies reporting the effectiveness of PDI of microorganisms in solution, it has not been successfully used for water disinfection during waste water treatment anywhere in the world. This may be due to difficulties in finding the right solid supports and coupling chemistry to attach the most effective photosensitisers. Also, there seems to be more interest in the synthesis and photochemistry of the photosensitisers and inactivation kinetics of some selected bacteria and few viruses. No inactivation kinetics have been reported for oocysts of *C. parvum* which is known to cause outbreak of the waterborne disease, Cryptosporidiosis, even in developed nations where chlorination of drinking water is standard practice and prescribed by law. Also, presently within this field there are no standards for PDI parameters and conditions and so there is a wide variation of

inactivation kinetics reported in different studies even for the same organisms and photosensitisers.

We have demonstrated in this our work that photosensitisers whether in solution or attached onto solid supports could cause inactivation of model viruses and *E. coli* BL21. However, due to time constraints, we are not able to validate our findings by using the immobilised photosensitisers on either membrane or nanofiber mats to treat wastewater under solar irradiation. Testing these materials under real life situations will be the next action in the course of developing a cheap and efficient sunlight driven water disinfection system. Even though positive sense RNA viruses are the largest group of human pathogens, there is a need to study other viruses, both in the same group and in other classes of viruses, such as the DNA and enveloped viruses. This is very important because of viral diversity. There is also a need to establish inactivation kinetics for other common pathogens.

Several studies revealed that the rate of PDI in microorganisms depends on the concentration of photosensitiser and duration of PDI in a dose dependent manner. However, there are few investigations of how other factors such as light source, intensity, co-pollutants and model organism itself could affect PDI. In most of the PDI studies, much of the work has been focused on the quantitative aspects of the inactivation with little emphasis on the molecular targets of the PDI in microorganisms. It is the complete elucidation and understanding of targets and mechanisms of PDI in microorganisms that will provide a basis to improve the design and operation of photodynamic water disinfection as well as engineering new systems. However, despite the difficulties faced in producing photodynamic

disinfection materials; it has many attractions for dealing with persistent, resistant and emerging water pathogens.

Chapter Seven: References

Chapter 7: References

ADEYEMI, O. O., NICOL, C., STONEHOUSE, N. J. & ROWLANDS, D. J. 2017. Increasing type 1 poliovirus capsid stability by thermal selection. *Journal of Virology,* 91**,** e01586-16.

AGON, V. V., BUBB, W. A., WRIGHT, A., HAWKINS, C. L. & DAVIES, M. J. 2006. Sensitizer-mediated photo-oxidation of histidine residues: Evidence for the formation of reactive side-chain peroxides (vol 40, pg 698, 2006). *Free Radical Biology and Medicine,* 40**,** 2242-2242.

AHMED, A., RUSHWORTH, J. V., HIRST, N. A. & MILLNER, P. A. 2014a. Biosensors for whole-cell bacterial detection. *Clinical microbiology reviews,* 27**,** 631-646.

AHMED, S. M., HALL, A. J., ROBINSON, A. E., VERHOEF, L., PREMKUMAR, P., PARASHAR, U. D., KOOPMANS, M. & LOPMAN, B. A. 2014b. Global prevalence of norovirus in cases of gastroenteritis: a systematic review and meta-analysis. *The Lancet Infectious Diseases,* 14**,** 725-730.

ALEGRíA, A. E., FERRER, A., SANTIAGO, G., SEPÚLVEDA, E. & FLORES, W. 1999. Photochemistry of water-soluble quinones. Production of the hydroxyl radical, singlet oxygen and the superoxide ion. *Journal of Photochemistry and Photobiology A: Chemistry,* 127**,** 57-65.

ALVES, E., COSTA, L., CARVALHO, C. M. B., TOME, J. P. C., FAUSTINO, M. A., NEVES, M. G. P. M. S., TOME, A. C., CAVALEIRO, J. A. S., CUNHA, A. & ALMEIDA, A. 2009. Charge effect on the photoinactivation of Gram-negative and Gram-positive bacteria by cationic meso-substituted porphyrins. *Bmc Microbiology,* 9.

ALVES, E., FAUSTINO, M. A., TOMÉ, J. P., NEVES, M. G., TOMÉ, A. C., CAVALEIRO, J. A., CUNHA, Â., GOMES, N. C. & ALMEIDA, A. 2011. Photodynamic antimicrobial chemotherapy in aquaculture: photoinactivation studies of Vibrio fischeri. *Plos One,* 6**,** e20970.

ALVES, E., SANTOS, N., MELO, T., MACIEL, E., DORIA, M. L., FAUSTINO, M. A. F., TOME, J. P. C., NEVES, M. G. P. M. S., CAVALEIRO, J. A. S., CUNHA, A., HELGUERO, L. A., DOMINGUES, P., ALMEIDA, A. & DOMINGUES, M. R. M. 2013. Photodynamic oxidation of Escherichia coli membrane phospholipids: new insights based on lipidomics. *Rapid Communications in Mass Spectrometry,* 27**,** 2717-2728.

AMIN, M. M., HASHEMI, H., BOVINI, A. M. & HUNG, Y. T. 2013. A review on wastewater disinfection. *International Journal of Environmental Health Engineering,* 2**,** 22.

AMORNCHAI, W., HOVEN, V. P. & TANGPASUTHADOL, V. 2004. Surface modification of chitosan films-grafting ethylene glycol oligomer and its effect on protein adsorption. *Macromolecular Symposia,* 216**,** 99-107.

AROF, A. K. & PING, T. L. 2017. Chlorophyll as Photosensitizer in Dye-Sensitized Solar Cells. *Chlorophyll.* InTech.

ARONINO, R., DLUGY, C., ARKHANGELSKY, E., SHANDALOV, S., ORON, G., BRENNER, A. & GITIS, V. 2009. Removal of viruses from surface water and secondary effluents by sand filtration. *Water Research,* 43**,** 87-96.

ARROJADO, C., PEREIRA, C., TOMÉ, J. P., FAUSTINO, M. A., NEVES, M. G., TOMÉ, A. C., CAVALEIRO, J. A., CUNHA, Â., CALADO, R. & GOMES, N. C. 2011. Applicability of photodynamic antimicrobial chemotherapy as an alternative to inactivate fish pathogenic bacteria in aquaculture systems. *Photochemical & Photobiological Sciences,* 10**,** 1691-1700.

ASTUTI, S. D., ZAIDAN, A., SETIAWATI, E. M. & SUHARININGSIH. Chlorophyll mediated photodynamic inactivation of blue laser on Streptococcus mutans. AIP Conference Proceedings, 2016. AIP Publishing, 120001.

AU, H. T., PHAM, L. N., VU, T. H. T. & PARK, J. S. 2012. Fabrication of an antibacterial non-woven mat of a poly (lactic acid)/chitosan blend by electrospinning. *Macromolecular research,* 20**,** 51-58.

BALLOTTARI, M., MOZZO, M., GIRARDON, J., HIENERWADEL, R. & BASSI, R. 2013. Chlorophyll triplet quenching and photoprotection in the higher plant monomeric antenna protein Lhcb5. *The Journal of Physical Chemistry B,* 117**,** 11337-11348.

BANFI, S., CARUSO, E., BUCCAFURNI, L., BATTINI, V., ZAZZARON, S., BARBIERI, P. & ORLANDI, V. 2006. Antibacterial activity of tetraaryl-porphyrin photosensitizers: an in vitro study on Gram negative and Gram positive bacteria. *Journal of Photochemistry and Photobiology B: Biology,* 85**,** 28-38.

BAUMLER, W. & MAISCH, T. 2012. Fast and Effective: Intense Pulse Light Photodynamic Inactivation of Bacteria. *Lasers in Surgery and Medicine,* 44**,** 43-43.

BONNETT, R. 1995. Photosensitizers of the porphyrin and phthalocyanine series for photodynamic therapy. *Chemical Society Reviews,* 24**,** 19-33.

BONNETT, R., BUCKLEY, D., GALIA, A., BURROW, T. & SAVILLE, B. 1994. PDT sensitisers: a new approach to clinical applications. *Biologic Effects of Light***,** 303-311.

BONNETT, R., KRYSTEVA, M. A., LALOV, I. G. & ARTARSKY, S. V. 2006. Water disinfection using photosensitizers immobilized on chitosan. *Water Research,* 40**,** 1269-1275.

BOTHNER, B., TAYLOR, D., JUN, B., LEE, K. K., SIUZDAK, G., SCHLUTZ, C. P. & JOHNSON, J. E. 2005. Maturation of a tetravirus capsid alters the dynamic properties and creates a metastable complex. *Virology,* 334**,** 17-27.

BOURRE, L., GIUNTINI, F., EGGLESTON, I. M., MOSSE, C. A., MACROBERT, A. J. & WILSON, M. 2010. Effective photoinactivation of Gram-positive and Gram-negative bacterial strains using an HIV-1

Tat peptide-porphyrin conjugate. *Photochemical & Photobiological Sciences,* 9**,** 1613-1620.

BOYD, V., CHOLEWA, O. M. & PAPAS, K. K. 2008. Limitations in the Use of Fluorescein Diacetate/Propidium Iodide (FDA/PI) and Cell Permeable Nucleic Acid Stains for Viability Measurements of Isolated Islets of Langerhans. *Curr Trends Biotechnol Pharm,* 2**,** 66-84.

CAMARGO, C. R., MARTINS, V. D. C. A., DE GUZZI PLEPIS, A. M. & RODRIGUES, J. 2014. Photoinactivation of Gram-Negative Bacteria in Circulating Water Using Chitosan Membranes Containing Porphyrin. *Issues,* 1.

CARRATALÀ, A., CALADO, A. D., MATTLE, M. J., MEIERHOFER, R., LUZI, S. & KOHN, T. 2016. Solar Disinfection of Viruses in Polyethylene Terephthalate Bottles. *Applied and Environmental Microbiology,* 82**,** 279-288.

CARVALHO, C. M., ALVES, E., COSTA, L., TOMÉ, J. P., FAUSTINO, M. A., NEVES, M. G., TOMÉ, A. C., CAVALEIRO, J. A., ALMEIDA, A. & CUNHA, A. N. 2010. Functional cationic nanomagnet− porphyrin hybrids for the photoinactivation of microorganisms. *ACS nano,* 4**,** 7133-7140.

CARVALHO, C. M. B., GOMES, A. T. P. C., FERNANDES, S. C. D., PRATA, A. C. B., ALMEIDA, M. A., CUNHA, M. A., TOME, J. P. C., FAUSTINO, M. A. F., NEVES, M. G. P. M. S., TOME, A. C., CAVALEIRO, J. A. S., LIN, Z., RAINHO, J. P. & ROCHA, J. 2007. Photoinactivation of bacteria in wastewater by porphyrins: Bacterial beta-galactosidase activity and leucine-uptake as methods to monitor the process. *Journal of Photochemistry and Photobiology B-Biology,* 88**,** 112-118.

CASTEEL, M. J., JAYARAJ, K., GOLD, A., BALL, L. M. & SOBSEY, M. D. 2004. Photoinactivation of hepatitis A virus by synthetic porphyrins. *Photochemistry and Photobiology,* 80**,** 294-300.

CEKLOVSKY, A., CZIMEROVA, A., PENTRAK, M. & BUJDAK, J. 2008. Spectral properties of TMPyP intercalated in thin films of layered silicates. *Journal of Colloid and Interface Science,* 324**,** 240-245.

CHEN, B. Y. & WESTERHOFF, P. 2010. Predicting disinfection by-product formation potential in water. *Water Research,* 44**,** 3755-3762.

CHO, M., LEE, J., MACKEYEV, Y., WILSON, L. J., ALVAREZ, P. J. J., HUGHES, J. B. & KIM, J. H. 2010. Visible Light Sensitized Inactivation of MS-2 Bacteriophage by a Cationic Amine-Functionalized C-60 Derivative. *Environmental Science & Technology,* 44**,** 6685-6691.

CHOI, S. S., LEE, H. K. & CHAE, H. S. 2010. In vitro photodynamic antimicrobial activity of methylene blue and endoscopic white light against Helicobacter pylori 26695. *Journal of Photochemistry and Photobiology B: Biology,* 101**,** 206-209.

CLARK, B. & MCKENDRICK, M. 2004. A review of viral gastroenteritis. *Current opinion in infectious diseases,* 17**,** 461-469.

COOPER, A., OLDINSKI, R., MA, H., BRYERS, J. D. & ZHANG, M. 2013. Chitosan-based nanofibrous membranes for antibacterial filter applications. *Carbohydrate Polymers,* 92**,** 254-259.

COSTA, D. C. S., GOMES, M. C., FAUSTINO, M. A. F., NEVES, M. G. P. M. S., CUNHA, A., CAVALEIRO, J. A. S., ALMEIDA, A. & TOME, J. P. C. 2012a. Comparative photodynamic inactivation of antibiotic resistant bacteria by first and second generation cationic photosensitizers. *Photochemical & Photobiological Sciences,* 11**,** 1905-1913.

COSTA, L., ALVES, E., CARVALHO, C. M. B., TOME, J. P. C., FAUSTINO, M. A. F., NEVES, M. G. P. M. S., TOME, A. C., CAVALEIRO, J. A. S., CUNHA, A. & ALMEIDA, A. 2008. Sewage bacteriophage photoinactivation by cationic porphyrins: a study of charge effect. *Photochemical & Photobiological Sciences,* 7**,** 415-422.

COSTA, L., CARVALHO, C. M. B., FAUSTINO, M. A. F., NEVES, M. G. P. M. S., TOME, J. P. C., TOME, A. C., CAVALEIRO, J. A. S., CUNHA, A. & ALMEIDA, A. 2010. Sewage bacteriophage inactivation by cationic porphyrins: influence of light parameters. *Photochemical & Photobiological Sciences,* 9**,** 1126-1133.

COSTA, L., CARVALHO, C. M. B., TOME, J. P. C., FAUSTINO, M. A. F., NEVES, M. G. P. M. S., TOME, A. C., CAVALEIRO, J. A. S., LIN, Z., RAINHO, J. P., ROCHA, J., CUNHA, A. & ALMEIDA, A. 2009. Sewage bacteriophage photoinactivation by porphyrins immobilized in solid matrixes. *Current Research Topics in Applied Microbiology and Microbial Biotechnology***,** 338-341.

COSTA, L., ESTEVES, A. C., CORREIA, A., MOREIRINHA, C., DELGADILLO, I., CUNHA, A., NEVES, M. G. P. S., FAUSTINO, M. A. F. & ALMEIDA, A. 2014. SDS-PAGE and IR spectroscopy to evaluate modifications in the viral protein profile induced by a cationic porphyrinic photosensitizer. *Journal of Virological Methods,* 209**,** 103-109.

COSTA, L., FAUSTINO, M. A., TOMÉ, J. P., NEVES, M. G., TOMÉ, A. C., CAVALEIRO, J. A., CUNHA, Â. & ALMEIDA, A. 2013. Involvement of type I and type II mechanisms on the photoinactivation of non-enveloped DNA and RNA bacteriophages. *Journal of Photochemistry and Photobiology B: Biology,* 120**,** 10-16.

COSTA, L., FAUSTINO, M. A. F., NEVES, M. G. P., CUNHA, Â. & ALMEIDA, A. 2012b. Photodynamic inactivation of mammalian viruses and bacteriophages. *Viruses,* 4**,** 1034-1074.

CRINI, G. & BADOT, P. M. 2008. Application of chitosan, a natural aminopolysaccharide, for dye removal from aqueous solutions by adsorption processes using batch studies: A review of recent literature. *Progress in Polymer Science,* 33**,** 399-447.

CRINI, G., MARTEL, B. & TORRI, G. 2008. Adsorption of CI Basic Blue 9 on chitosan-based materials. *International Journal of Environment and Pollution,* 34**,** 451-465.

DAI, X., LI, Z., LAI, M., SHU, S., DU, Y., ZHOU, Z. H. & SUN, R. 2017. In situ structures of the genome and genome-delivery apparatus in a single-stranded RNA virus. *Nature,* 541**,** 112-116.

DARWENT, J. R., DOUGLAS, P., HARRIMAN, A., PORTER, G. & RICHOUX, M.-C. 1982. Metal phthalocyanines and porphyrins as photosensitizers for reduction of water to hydrogen. *Coordination Chemistry Reviews,* 44**,** 83-126.

DAVIES, C., ROSER, D., FEITZ, A. & ASHBOLT, N. 2009. Solar radiation disinfection of drinking water at temperate latitudes: inactivation rates for an optimised reactor configuration. *Water Research,* 43**,** 643-652.

DAVIES, M. J. 2003. Singlet oxygen-mediated damage to proteins and its consequences. *Biochemical and Biophysical Research Communications,* 305**,** 761-770.

DEDEO, M. T., FINLEY, D. T. & FRANCIS, M. B. 2010. Viral capsids as self-assembling templates for new materials. *Progress in molecular biology and translational science,* 103**,** 353-392.

DEJUNG, S., FUENTES, I., ALMANZA, G., JARRO, R., NAVARRO, L., ARIAS, G., URQUIETA, E., TORRICO, A., FENANDEZ, W. & IRIARTE, M. 2007. Effect of solar water disinfection (SODIS) on model microorganisms under improved and field SODIS conditions. *Journal of Water Supply: Research and Technology-Aqua,* 56**,** 245-256.

DEL VALLE, L. J., CAMPS, R., DÍAZ, A., FRANCO, L., RODRÍGUEZ-GALÁN, A. & PUIGGALÍ, J. 2011. Electrospinning of polylactide and polycaprolactone mixtures for preparation of materials with tunable drug release properties. *Journal of polymer research,* 18**,** 1903-1917.

DENG, L., YOUNG, R. J., KINLOCH, I. A., ZHU, Y. & EICHHORN, S. J. 2013. Carbon nanofibres produced from electrospun cellulose nanofibres. *Carbon,* 58**,** 66-75.

DENT, K. C., THOMPSON, R., BARKER, A. M., HISCOX, J. A., BARR, J. N., STOCKLEY, P. G. & RANSON, N. A. 2013. The asymmetric structure of an icosahedral virus bound to its receptor suggests a mechanism for genome release. *Structure,* 21**,** 1225-1234.

DEROSA, M. C. & CRUTCHLEY, R. J. 2002. Photosensitized singlet oxygen and its applications. *Coordination Chemistry Reviews,* 233**,** 351-371.

DOLMANS, D. E. J. G. J., FUKUMURA, D. & JAIN, R. K. 2003. Photodynamic therapy for cancer. *Nature Reviews Cancer,* 3**,** 380-387.

DOMINGO, E., ESCARMIS, C., SEVILLA, N., MOYA, A., ELENA, S., QUER, J., NOVELLA, I. & HOLLAND, J. 1996. Basic concepts in RNA virus evolution. *The FASEB Journal,* 10**,** 859-864.

DUFFY, S., SHACKELTON, L. A. & HOLMES, E. C. 2008. Rates of evolutionary change in viruses: patterns and determinants. *Nature reviews. Genetics,* 9**,** 267.

DUNLOP, P., CIAVOLA, M., RIZZO, L. & BYRNE, J. 2011. Inactivation and injury assessment of Escherichia coli during solar and photocatalytic disinfection in LDPE bags. *Chemosphere,* 85**,** 1160-1166.

DWIVEDI, A. & PANDE, U. 2012. Photochemical Degradation of Halogenated Compounds: A Review. *Sci. Revs. Chem. Commn,* 2**,** 41-452.

EICHNER, A., GONZALES, F. P., FELGENTRÄGER, A., REGENSBURGER, J., HOLZMANN, T., SCHNEIDER-BRACHERT, W., BÄUMLER, W. & MAISCH, T. 2013. Dirty hands: photodynamic killing of human pathogens like EHEC, MRSA and Candida within seconds. *Photochemical & Photobiological Sciences,* 12**,** 135-147.

EICHNER, A., HOLZMANN, T., SCHNEIDER, W., BAUMLER, W. & MAISCH, T. 2012. Blue light and dye: Photodynamic inactivation of enterohaemorrhagic Escherichia coli (EHEC) for the first time using TMPyP. *International Journal of Medical Microbiology,* 302**,** 29-29.

FISHER, M. B., IRIARTE, M. & NELSON, K. L. 2012. Solar water disinfection (SODIS) of Escherichia coli, Enterococcus spp., and MS2 coliphage: effects of additives and alternative container materials. *Water Research,* 46**,** 1745-1754.

GERSTENHABER, J. A., BRODSKY, R., HUNEKE, R. B. & LELKES, P. I. 2014. Electrospun soy protein scaffolds as wound dressings: Enhanced reepithelialization in a porcine model of wound healing. *Wound Medicine,* 5**,** 9-15.

GLEICK, P. H. & HOWE, C. W. 1995. Water in Crisis: A Guide to the World's Fresh Water Resources. *Climatic Change,* 31**,** 119-122.

GOENS, S. D., BOTERO, S., ZEMLA, A., ZHOU, C. E. & PERDUE, M. 2004. Bovine enterovirus 2: complete genomic sequence and molecular modelling of a reference strain and a wild-type isolate from endemically infected US cattle. *Journal of General Virology,* 85**,** 3195-3203.

GOLMOHAMMADI, R., FRIDBORG, K., BUNDULE, M., VALEGÅRD, K. & LILJAS, L. 1996. The crystal structure of bacteriophage Qβ at 3.5 Å resolution. *Structure,* 4**,** 543-554.

GOMES, M. C., WORANOVICZ-BARREIRA, S. M., FAUSTINO, M. A., FERNANDES, R., NEVES, M. G., TOMÉ, A. C., GOMES, N. C., ALMEIDA, A., CAVALEIRO, J. A. & CUNHA, Â. 2011. Photodynamic inactivation of Penicillium chrysogenum conidia by cationic porphyrins. *Photochemical & Photobiological Sciences,* 10**,** 1735-1743.

GÓMEZ-COUSO, H., FONTÁN-SAINZ, M., MCGUIGAN, K. G. & ARES-MAZÁS, E. 2009. Effect of the radiation intensity, water turbidity and exposure time on the survival of Cryptosporidium during simulated solar disinfection of drinking water. *Acta tropica,* 112**,** 43-48.

GORZELNIK, K. V., CUI, Z., REED, C. A., JAKANA, J., YOUNG, R. & ZHANG, J. 2016. Asymmetric cryo-EM structure of the canonical Allolevivirus Qβ reveals a single maturation protein and the genomic

ssRNA in situ. *Proceedings of the National Academy of Sciences,* 113**,** 11519-11524.

GRACANIN, M., HAWKINS, C. L., PATTISON, D. I. & DAVIES, M. J. 2009. Singlet-oxygen-mediated amino acid and protein oxidation: Formation of tryptophan peroxides and decomposition products. *Free Radical Biology and Medicine,* 47**,** 92-102.

GRACANIN, M., PATTISON, D. I. & DAVIES, M. J. 2007. Singlet oxygen-mediated tryptophan oxidation: Characterization of potential markers of protein oxidation. *Free Radical Research,* 41**,** S31-S31.

GUEYMARD, C., MYERS, D. & EMERY, K. 2002. Proposed reference irradiance spectra for solar energy systems testing. *Solar energy,* 73**,** 443-467.

GUO, J.-T., YANG, D.-C., GUAN, Z. & HE, Y.-H. 2017. Chlorophyll-Catalyzed Visible-Light-Mediated Synthesis of Tetrahydroquinolines from N, N-Dimethylanilines and Maleimides. *The Journal of organic chemistry,* 82**,** 1888-1894.

GUPTA, S. C., PATCHVA, S., KOH, W. & AGGARWAL, B. B. 2012. Discovery of curcumin, a component of golden spice, and its miraculous biological activities. *Clinical and Experimental Pharmacology and Physiology,* 39**,** 283-299.

HAAG, W. R. & HOIGNE, J. 1986. Singlet oxygen in surface waters. 3. Photochemical formation and steady-state concentrations in various types of waters. *Environmental Science & Technology,* 20**,** 341-348.

HAIDER, A., HAIDER, S. & KANG, I.-K. 2015. A comprehensive review summarizing the effect of electrospinning parameters and potential applications of nanofibers in biomedical and biotechnology. *Arabian Journal of Chemistry*.

HANAKOVA, A., BOGDANOVA, K., TOMANKOVA, K., BINDER, S., BAJGAR, R., LANGOVA, K., KOLAR, M., MOSINGER, J. & KOLAROVA, H. 2014. Study of photodynamic effects on NIH 3T3 cell line and bacteria. *Biomedical papers,* 158**,** 201-207.

HANG, A. T., TAE, B. & PARK, J. S. 2010. Non-woven mats of poly (vinyl alcohol)/chitosan blends containing silver nanoparticles: fabrication and characterization. *Carbohydrate Polymers,* 82**,** 472-479.

HANG, Y., ZHANG, Y., JIN, Y., SHAO, H. & HU, X. 2012. Preparation of regenerated silk fibroin/silk sericin fibers by coaxial electrospinning. *International journal of biological macromolecules,* 51**,** 980-986.

HARRISON, S., OLSON, A., SCHUTT, C., WINKLER, F. & BRICOGNE, G. 1978. Tomato bushy stunt virus at 2.9 Å resolution. *Nature,* 276**,** 368-373.

HEIL, F., HEMMI, H., HOCHREIN, H., AMPENBERGER, F., KIRSCHNING, C., AKIRA, S., LIPFORD, G., WAGNER, H. & BAUER, S. 2004. Species-specific recognition of single-stranded RNA via toll-like receptor 7 and 8. *Science,* 303**,** 1526-1529.

HENKE, P., LANG, K., KUBAT, P., SYKORA, J., SLOUF, M. & MOSINGER, J. 2013. Polystyrene Nanofiber Materials Modified with an Externally Bound Porphyrin Photosensitizer. *Acs Applied Materials & Interfaces,* 5**,** 3776-3783.

HERMANSON, G. T. 2013. *Bioconjugate techniques*, Academic press.

HEUNIS, T., BSHENA, O., KLUMPERMAN, B. & DICKS, L. 2011. Release of bacteriocins from nanofibers prepared with combinations of poly (D, L-lactide)(PDLLA) and poly (ethylene oxide)(PEO). *International Journal of Molecular Sciences,* 12**,** 2158-2173.

HOLZWARTH, J. M. & MA, P. X. 2011. Biomimetic nanofibrous scaffolds for bone tissue engineering. *Biomaterials,* 32**,** 9622-9629.

HONG, Y., FUJIMOTO, K., HASHIZUME, R., GUAN, J., STANKUS, J. J., TOBITA, K. & WAGNER, W. R. 2008. Generating elastic, biodegradable polyurethane/poly (lactide-co-glycolide) fibrous sheets with controlled antibiotic release via two-stream electrospinning. *Biomacromolecules,* 9**,** 1200-1207.

HOTZE, E. M., BADIREDDY, A. R., CHELLAM, S. & WIESNER, M. R. 2009. Mechanisms of Bacteriophage Inactivation via Singlet Oxygen Generation in UV Illuminated Fullerol Suspensions. *Environmental Science & Technology,* 43**,** 6639-6645.

HOVEN, V. P., TANGPASUTHADOL, V., ANGKITPAIBOON, Y., VALLAPA, N. & KIATKAMJORNWONG, S. 2007. Surface-charged chitosan: Preparation and protein adsorption. *Carbohydrate Polymers,* 68**,** 44-53.

HUANG, L., MCMILLAN, R. A., APKARIAN, R. P., POURDEYHIMI, B., CONTICELLO, V. P. & CHAIKOF, E. L. 2000. Generation of synthetic elastin-mimetic small diameter fibers and fiber networks. *Macromolecules,* 33**,** 2989-2997.

HUANG, Z.-M., ZHANG, Y., RAMAKRISHNA, S. & LIM, C. 2004. Electrospinning and mechanical characterization of gelatin nanofibers. *Polymer,* 45**,** 5361-5368.

HUNTER, P. R. 2009. Household water treatment in developing countries: comparing different intervention types using meta-regression. *Environmental Science & Technology,* 43**,** 8991-8997.

JACKSON, P. J., ANDREWS K O , V K CHAMBERS, K J CONNOR, A EGERTON, T HALL, T E IRVING, AND, G. S. & FAWELL, J. K. 1999. ALTERNATIVES TO CHEMICAL DISINFECTION OF DRINKING WATER. *Final Report to the Department of the Environment, Transport and the Regions*.

JAEGLE, M., BRIAND, J.-P., BURCKARD, J. & VAN REGENMORTEL, M. Accessibility of three continuous epitopes in tomato bushy stunt virus. Annales de l'Institut Pasteur/Virologie, 1988. Elsevier, 39-50.

JANG, K., BAEK, L. W., BACK, S. Y. & AHN, H. 2011. Electrospinning of porphyrin/polyvinyl alcohol (PVA) nanofibers and their acid vapor sensing capability. *Journal of nanoscience and nanotechnology,* 11**,** 6102-6108.

JEMLI, M., ALOUINI, Z., SABBAHI, S. & GUEDDARI, M. 2002. Destruction of fecal bacteria in wastewater by three photosensitizers. *Journal of Environmental Monitoring,* 4**,** 511-516.

JI, Y., GHOSH, K., SHU, X. Z., LI, B., SOKOLOV, J. C., PRESTWICH, G. D., CLARK, R. A. & RAFAILOVICH, M. H. 2006. Electrospun three-dimensional hyaluronic acid nanofibrous scaffolds. *Biomaterials,* 27**,** 3782-3792.

JIMENEZ-CLAVERO, M., DOUGLAS, A., LAVERY, T., GARCIA-RANEA, J. & LEY, V. 2000. Immune recognition of swine vesicular disease virus structural proteins: novel antigenic regions that are not exposed in the capsid. *Virology,* 270**,** 76-83.

JIN, B., AHN, J. E., KO, J. H., WANG, W., HAN, S. W. & KIM, S. K. 2008. Effect of the position and number of positive charges on the intercalation and stacking of porphyrin to poly [d (GC) 2], poly [d (AT) 2], and native DNA. *The Journal of Physical Chemistry B,* 112**,** 15875-15882.

JORI, G., FABRIS, C., SONCIN, M., FERRO, S., COPPELLOTTI, O., DEI, D., FANTETTI, L., CHITI, G. & RONCUCCI, G. 2006. Photodynamic therapy in the treatment of microbial infections: basic principles and perspective applications. *Lasers in Surgery and Medicine,* 38**,** 468-481.

KAMINAKA, S., IMAMURA, Y., SHINGU, H., KITAGAWA, T. & TOYODA, T. 1999. Studies of bovine enterovirus structure by ultraviolet resonance Raman spectroscopy. *Journal of Virological Methods,* 77**,** 117-123.

KARST, S. M., WOBUS, C. E., LAY, M., DAVIDSON, J. & VIRGIN, H. W. 2003. STAT1-dependent innate immunity to a Norwalk-like virus. *Science,* 299**,** 1575-1578.

KATPALLY, U., VOSS, N. R., CAVAZZA, T., TAUBE, S., RUBIN, J. R., YOUNG, V. L., STUCKEY, J., WARD, V. K., VIRGIN, H. W. & WOBUS, C. E. 2010. High-resolution cryo-electron microscopy structures of murine norovirus 1 and rabbit hemorrhagic disease virus reveal marked flexibility in the receptor binding domains. *Journal of Virology,* 84**,** 5836-5841.

KATTI, D. S., ROBINSON, K. W., KO, F. K. & LAURENCIN, C. T. 2004. Bioresorbable nanofiber-based systems for wound healing and drug delivery: Optimization of fabrication parameters. *Journal of Biomedical Materials Research Part B: Applied Biomaterials,* 70**,** 286-296.

KOHN, T., GRANDBOIS, M., MCNEILL, K. & NELSON, K. L. 2007. Association with natural organic matter enhances the sunlight-mediated inactivation of MS2 coliphage by singlet oxygen. *Environmental Science & Technology,* 41**,** 4626-4632.

KOHN, T. & NELSON, K. L. 2007. Sunlight-mediated inactivation of MS2 coliphage via exogenous singlet oxygen produced by sensitizers in natural waters. *Environmental Science & Technology,* 41**,** 192-197.

KOMAGOE, K., KATO, H., INOUE, T. & KATSU, T. 2011. Continuous real-time monitoring of cationic porphyrin-induced photodynamic inactivation of bacterial membrane functions using electrochemical sensors. *Photochemical & Photobiological Sciences,* 10**,** 1181-1188.

KONING, R. I., GOMEZ-BLANCO, J., AKOPJANA, I., VARGAS, J., KAZAKS, A., TARS, K., CARAZO, J. M. & KOSTER, A. J. 2016. Asymmetric cryo-EM reconstruction of phage MS2 reveals genome structure in situ. *Nature communications,* 7.

KOONIN, E. V., DOLJA, V. V. & KRUPOVIC, M. 2015. Origins and evolution of viruses of eukaryotes: the ultimate modularity. *Virology,* 479**,** 2-25.

KRAJEWSKA, B., LESZKO, M. & ZABORSKA, W. 1990. Urease Immobilized on Chitosan Membrane - Preparation and Properties. *Journal of Chemical Technology and Biotechnology,* 48**,** 337-350.

KRALJIC, I. & MOHSNI, S. E. 1978. New Method for Detection of Singlet Oxygen in Aqueous-Solutions. *Photochemistry and Photobiology,* 28**,** 577-581.

KRIEGEL, C., KIT, K., MCCLEMENTS, D. J. & WEISS, J. 2009. Electrospinning of chitosan–poly (ethylene oxide) blend nanofibers in the presence of micellar surfactant solutions. *Polymer,* 50**,** 189-200.

KROPINSKI, A. M., MAZZOCCO, A., WADDELL, T. E., LINGOHR, E. & JOHNSON, R. P. 2009. Enumeration of bacteriophages by double agar overlay plaque assay. *Bacteriophages: Methods and Protocols, Volume 1: Isolation, Characterization, and Interactions***,** 69-76.

LAURING, A. S., FRYDMAN, J. & ANDINO, R. 2013. The role of mutational robustness in RNA virus evolution. *Nature reviews. Microbiology,* 11**,** 327.

LEE, K. & LEE, S. 2012. Multifunctionality of poly (vinyl alcohol) nanofiber webs containing titanium dioxide. *Journal of Applied Polymer Science,* 124**,** 4038-4046.

LEENHEER, J. A. & CROUÉ, J.-P. 2003. Peer reviewed: characterizing aquatic dissolved organic matter. ACS Publications.

LEI, W., JIANG, G., ZHOU, Q., ZHANG, B. & WANG, X. 2010. Greatly enhanced binding of a cationic porphyrin towards bovine serum albumin by cucurbit [8] uril. *Physical Chemistry Chemical Physics,* 12**,** 13255-13260.

LEWIS, J. K., BOTHNER, B., SMITH, T. J. & SIUZDAK, G. 1998. Antiviral agent blocks breathing of the common cold virus. *Proceedings of the National Academy of Sciences,* 95**,** 6774-6778.

LIMA, S., PEABODY, D. S., SILVA, J. L. & DE OLIVEIRA, A. C. 2004. Mutations in the hydrophobic core and in the protein–RNA interface affect the packing and stability of icosahedral viruses. *The FEBS Journal,* 271**,** 135-145.

LIU, X., LIN, T., GAO, Y., XU, Z., HUANG, C., YAO, G., JIANG, L., TANG, Y. & WANG, X. 2012. Antimicrobial electrospun nanofibers of cellulose acetate and polyester urethane composite for wound

dressing. *Journal of Biomedical Materials Research Part B: Applied Biomaterials,* 100**,** 1556-1565.

LOEB, S., HOFMANN, R. & KIM, J.-H. 2016. Beyond the Pipeline: Assessing the Efficiency Limits of Advanced Technologies for Solar Water Disinfection. *Environmental Science & Technology Letters,* 3**,** 73-80.

LUBITZ, I., BOROVOK, N. & KOTLYAR, A. 2007. Interaction of monomolecular G4-DNA nanowires with TMPyP: evidence for intercalation. *Biochemistry,* 46**,** 12925-12929.

LUCENA, S. R., SALAZAR, N., GRACIA-CAZANA, T., ZAMARRON, A., GONZALEZ, S., JUARRANZ, A. & GILABERTE, Y. 2015. Combined Treatments with Photodynamic Therapy for Non-Melanoma Skin Cancer. *International Journal of Molecular Sciences,* 16**,** 25912-25933.

LUKSIENE, Z. & BROVKO, L. 2013. Antibacterial photosensitization-based treatment for food safety. *Food Engineering Reviews,* 5**,** 185-199.

MAISCH, T., KOWALEWSKI, E., HOLZMANN, T., SCHNEIDER-BRACHERT, W. & BAUMLER, W. 2012a. Photodynamic killing of enterohaemorrhagic Escherichia coli (EHEC) for the first time using TMPyP. *Experimental Dermatology,* 21**,** e40-e40.

MAISCH, T., SPANNBERGER, F., REGENSBURGER, J., FELGENTRAGER, A. & BAUMLER, W. 2012b. Fast and effective: intense pulse light photodynamic inactivation of bacteria. *Journal of Industrial Microbiology & Biotechnology,* 39**,** 1013-1021.

MAMANE, H., SHEMER, H. & LINDEN, K. G. 2007. Inactivation of E. coli, B. subtilis spores, and MS2, T4, and T7 phage using UV/H 2 O 2 advanced oxidation. *Journal of Hazardous Materials,* 146**,** 479-486.

MARTEL, B., DEVASSINE, M., CRINI, G., WELTROWSKI, M., BOURDONNEAU, M. & MORCELLET, M. 2001. Preparation and sorption properties of a beta-cyclodextrin-linked chitosan derivative. *Journal of Polymer Science Part a-Polymer Chemistry,* 39**,** 169-176.

MEI, Y., YAO, C., FAN, K. & LI, X. 2012. Surface modification of polyacrylonitrile nanofibrous membranes with superior antibacterial and easy-cleaning properties through hydrophilic flexible spacers. *Journal of membrane science,* 417**,** 20-27.

MUMPHREY, S. M., CHANGOTRA, H., MOORE, T. N., HEIMANN-NICHOLS, E. R., WOBUS, C. E., REILLY, M. J., MOGHADAMFALAHI, M., SHUKLA, D. & KARST, S. M. 2007. Murine norovirus 1 infection is associated with histopathological changes in immunocompetent hosts, but clinical disease is prevented by STAT1-dependent interferon responses. *Journal of Virology,* 81**,** 3251-3263.

OLIVEIRA, A., ALMEIDA, A., CARVALHO, C., TOMÉ, J., FAUSTINO, M., NEVES, M., TOMÉ, A., CAVALEIRO, J. & CUNHA, Â. 2009. Porphyrin derivatives as photosensitizers for the inactivation of Bacillus cereus endospores. *Journal of Applied Microbiology,* 106**,** 1986-1995.

ORCHARD, R. C., WILEN, C. B., DOENCH, J. G., BALDRIDGE, M. T., MCCUNE, B. T., LEE, Y.-C. J., LEE, S., PRUETT-MILLER, S. M., NELSON, C. A. & FREMONT, D. H. 2016. Discovery of a proteinaceous cellular receptor for a norovirus. *Science,* 353**,** 933-936.

OSTERLOH, F. E. 2008. Inorganic materials as catalysts for photochemical splitting of water. *Chem. Mater,* 20**,** 35-54.

PAKRAVAN, M., HEUZEY, M.-C. & AJJI, A. 2011. A fundamental study of chitosan/PEO electrospinning. *Polymer,* 52**,** 4813-4824.

PARASHAR, U. D., HUMMELMAN, E. G., BRESEE, J. S., MILLER, M. A. & GLASS, R. I. 2003. Global illness and deaths caused by rotavirus disease in children. *Emerging Infectious Diseases,* 9**,** 565-572.

PATEL, M. M., WIDDOWSON, M.-A., GLASS, R. I., AKAZAWA, K., VINJÉ, J. & PARASHAR, U. D. 2008. Systematic literature review of role of noroviruses in sporadic gastroenteritis. *Emerging Infectious Diseases,* 14**,** 1224.

PATTISON, D. I., RAHMANTO, A. S. & DAVIES, M. J. 2012. Photo-oxidation of proteins. *Photochemical & Photobiological Sciences,* 11**,** 38-53.

PENHA, C. B., BONIN, E., DA SILVA, A. F., HIOKA, N., ZANQUETA, É. B., NAKAMURA, T. U., DE ABREU FILHO, B. A., CAMPANERUT-SÁ, P. A. Z. & MIKCHA, J. M. G. 2017. Photodynamic inactivation of foodborne and food spoilage bacteria by curcumin. *LWT-Food Science and Technology,* 76**,** 198-202.

PULLI, T., LANKINEN, H., ROIVAINEN, M. & HYYPIÄ, T. 1998. Antigenic sites of coxsackievirus A9. *Virology,* 240**,** 202-212.

RAMESH KUMAR, P., KHAN, N., VIVEKANANDHAN, S., SATYANARAYANA, N., MOHANTY, A. & MISRA, M. 2012. Nanofibers: effective generation by electrospinning and their applications. *Journal of nanoscience and nanotechnology,* 12**,** 1-25.

RANDAZZO, W., AZNAR, R. & SÁNCHEZ, G. 2016. Curcumin-mediated photodynamic inactivation of norovirus surrogates. *Food and environmental virology,* 8**,** 244-250.

REDMOND, R. W. & GAMLIN, J. N. 1999. A compilation of singlet oxygen yields from biologically relevant molecules. *Photochemistry and Photobiology,* 70**,** 391-475.

REED, L. J. & MUENCH, H. 1938. A SIMPLE METHOD OF ESTIMATING FIFTY PER CENT ENDPOINTS 1 2. *American journal of epidemiology,* 27**,** 493-497.

RHO, K. S., JEONG, L., LEE, G., SEO, B.-M., PARK, Y. J., HONG, S.-D., ROH, S., CHO, J. J., PARK, W. H. & MIN, B.-M. 2006. Electrospinning of collagen nanofibers: effects on the behavior of normal human keratinocytes and early-stage wound healing. *Biomaterials,* 27**,** 1452-1461.

RULE WIGGINTON, K., MENIN, L., MONTOYA, J. P. & KOHN, T. 2010. Oxidation of virus proteins during UV254 and singlet oxygen mediated inactivation. *Environmental Science & Technology,* 44**,** 5437-5443.

SANJUAN, R., NEBOT, M. R., CHIRICO, N., MANSKY, L. M. & BELSHAW, R. 2010. Viral mutation rates. *Journal of Virology,* 84**,** 9733-9748.

SCHIFFMAN, J. D. & SCHAUER, C. L. 2007. Cross-linking chitosan nanofibers. *Biomacromolecules,* 8**,** 594-601.

SCHOENEN, D. 2002. Role of disinfection in suppressing the spread of pathogens with drinking water: possibilities and limitations. *Water Research,* 36**,** 3874-3888.

SHANNON, M. A., BOHN, P. W., ELIMELECH, M., GEORGIADIS, J. G., MARINAS, B. J. & MAYES, A. M. 2008. Science and technology for water purification in the coming decades. *Nature,* 452**,** 301-310.

SHEN, H. R., SPIKES, J. D., SMITH, C. J. & KOPECEK, J. 2000a. Photodynamic cross-linking of proteins - IV. Nature of the His-His bond(s) formed in the rose bengal-photosensitized cross-linking of N-benzoyl-L-histidine. *Journal of Photochemistry and Photobiology a-Chemistry,* 130**,** 1-6.

SHEN, H. R., SPIKES, J. D., SMITH, C. J. & KOPECEK, J. 2000b. Photodynamic cross-linking of proteins - V. Nature of the tyrosine-tyrosine bonds formed in the FMN-sensitized intermolecular cross-linking of N-acetyl-L-tyrosine. *Journal of Photochemistry and Photobiology a-Chemistry,* 133**,** 115-122.

SILVERMAN, A. I., PETERSON, B. M., BOEHM, A. B., MCNEILL, K. & NELSON, K. L. 2013. Sunlight Inactivation of Human Viruses and Bacteriophages in Coastal Waters Containing Natural Photosensitizers. *Environmental Science & Technology,* 47**,** 1870-1878.

SMYTH, M., FRY, E., STUART, D., LYONS, C., HOEY, E. & MARTIN, S. J. 1993. Preliminary Crystallographic Analysis of Bovine Enterovirus. *Journal of Molecular Biology,* 231**,** 930-932.

SMYTH, M., TATE, J., HOEY, E., LYONS, C., MARTIN, S. & STUART, D. 1995. Implications for viral uncoating from the structure of bovine enterovirus. *Nature Structural & Molecular Biology,* 2**,** 224-231.

SNOWDEN-SWAN, L., J PIATT & LESPERANCE, A. 1998. Disinfection Technologies for Portable Water and Wastewater Treatment: Alternatives to Chlorine Gas. *Report for U.S Army Forces Command Air Quality Division*.

SPANNBERGER, F., REGENSBURGER, J., FELGENTRAGER, A., BAUMLER, W. & MAISCH, T. 2012. Fast and effective: intense pulse light photodynamic inactivation of bacteria. *Experimental Dermatology,* 21**,** e40-e40.

SPASOVA, M., MANOLOVA, N., PANEVA, D. & RASHKOV, I. 2004. Preparation of chitosan-containing nanofibres by electrospinning of chitosan/poly (ethylene oxide) blend solutions. *e-Polymers,* 4**,** 624-635.

SPILLER, W., WÖHRLE, D., SCHULZ-EKLOFF, G., FORD, W. T., SCHNEIDER, G. & STARK, J. 1996. Photo-oxidation of sodium sulfide by sulfonated phthalocyanines in oxygen-saturated aqueous solutions containing detergents or latexes. *Journal of Photochemistry and Photobiology A: Chemistry,* 95**,** 161-173.

SUCHANEK, J., HENKE, P., MOSINGER, J., ZELINGER, Z. & KUBAT, P. 2014. Effect of Temperature on Photophysical Properties of Polymeric Nanofiber Materials with Porphyrin Photosensitizers. *Journal of Physical Chemistry B,* 118**,** 6167-6174.

SULLIVAN, S. T., TANG, C., KENNEDY, A., TALWAR, S. & KHAN, S. A. 2014. Electrospinning and heat treatment of whey protein nanofibers. *Food Hydrocolloids,* 35**,** 36-50.

TAKAMATSU, H. & ISO, K. 1982. Chemical evidence for the capsomeric structure of phage Qbeta. *Nature,* 298**,** 819-824.

TANGPASUTHADOL, V., PONGCHAISIRIKUL, N. & HOVEN, V. P. 2003. Surface modification of chitosan films. Effects of hydrophobicity on protein adsorption. *Carbohydrate Research,* 338**,** 937-942.

TAUBE, S., RUBIN, J. R., KATPALLY, U., SMITH, T. J., KENDALL, A., STUCKEY, J. A. & WOBUS, C. E. 2010. High-resolution x-ray structure and functional analysis of the murine norovirus 1 capsid protein protruding domain. *Journal of Virology,* 84**,** 5695-5705.

TAVARES, A., DIAS, S. R., CARVALHO, C. M., FAUSTINO, M. A., TOMÉ, J. P., NEVES, M. G., TOMÉ, A. C., CAVALEIRO, J. A., CUNHA, Â. & GOMES, N. C. 2011. Mechanisms of photodynamic inactivation of a Gram-negative recombinant bioluminescent bacterium by cationic porphyrins. *Photochemical & Photobiological Sciences,* 10**,** 1659-1669.

THAKUR, R., FLOREK, C., KOHN, J. & MICHNIAK, B. 2008. Electrospun nanofibrous polymeric scaffold with targeted drug release profiles for potential application as wound dressing. *International journal of pharmaceutics,* 364**,** 87-93.

TORRES-GINER, S., MARTINEZ-ABAD, A., GIMENO-ALCAÑIZ, J. V., OCIO, M. J. & LAGARON, J. M. 2012. Controlled Delivery of Gentamicin Antibiotic from Bioactive Electrospun Polylactide-Based Ultrathin Fibers. *Advanced Engineering Materials,* 14.

UNICEF 2012. Pneumonia and diarrhoea Tackling the deadliest diseases for the world's poorest children.

UNICEF 2016. One is too many: Ending Child Deaths from Pneumonia and Diarrhoea- Key Findings 2016.

UNICEF, W. A. 2014. Progress on Drinking Water and 2014 Sanitation UPDATE.

USEPA 1999a. Wastewater Technology Fact Sheet Cholorine Disinfection. *United States Environmental Protection Agency, Office of Water Washington, D.C.*

USEPA 1999b. Wastewater Technology Fact Sheet Ultraviolet Disinfection. *United States Environmental Protection Agency, Office of Water Washington, D.C.*

USUDA, J., KATO, H., OKUNAKA, T., FURUKAWA, K., TSUTSUI, H., YAMADA, K., SUGA, Y., HONDA, H., NAGATSUKA, Y., OHIRA, T., TSUBOI, M. & HIRANO, T. 2006. Photodynamic therapy (PDT) for lung cancers. *Journal of Thoracic Oncology,* 1**,** 489-493.

VALEGÅRD, K., LILJAS, L., FRIDBORG, K. & UNGE, T. 1990. The three-dimensional structure of the bacterial virus MS2. *Nature,* 345**,** 36-41.

WAINWRIGHT, M. 1998. Photodynamic antimicrobial chemotherapy (PACT). *The Journal of antimicrobial chemotherapy,* 42**,** 13-28.

WAINWRIGHT, M. 2004. Photoinactivation of viruses. *Photochemical & Photobiological Sciences,* 3**,** 406-411.

WAINWRIGHT, M., MAISCH, T., NONELL, S., PLAETZER, K., ALMEIDA, A., TEGOS, G. P. & HAMBLIN, M. R. 2017. Photoantimicrobials—are we afraid of the light? *The Lancet Infectious Diseases,* 17**,** e49-e55.

WALTER, T. S., REN, J., TUTHILL, T. J., ROWLANDS, D. J., STUART, D. I. & FRY, E. E. 2012. A plate-based high-throughput assay for virus stability and vaccine formulation. *Journal of Virological Methods,* 185**,** 166-170.

WANG, X., REN, J., GAO, Q., HU, Z., SUN, Y., LI, X., ROWLANDS, D. J., YIN, W., WANG, J. & STUART, D. I. 2015. Hepatitis A virus and the origins of picornaviruses. *Nature,* 517**,** 85.

WHO 2009. Risk Assessment of Cryptosporidium in Drinking Water.

WHO 2011a. Evaluating household water treatment options: Health-based targets and microbiological performance specifications.

WHO 2011b. Guidelines for drinking-water quality - 4th ed.

WHO 2012. Global costs and benefits of drinking-water supply and sanitation interventions to reach the MDG target and universal coverage.

WHO 2016. Quantitative Microbial Risk Assessment: Application for Water Safety Management.

WHO, U. A. 2015. Progress on Sanitation and DrinkingWater: 2015 Update and MDG Assessment.

WIGGINTON, K. R., PECSON, B. M., SIGSTAM, T., BOSSHARD, F. & KOHN, T. 2012. Virus Inactivation Mechanisms: Impact of Disinfectants on Virus Function and Structural Integrity. *Environmental Science & Technology,* 46**,** 12069-12078.

WILKINSON, F., HELMAN, W. P. & ROSS, A. B. 1995. Rate constants for the decay and reactions of the lowest electronically excited singlet state of molecular oxygen in solution. An expanded and revised compilation. *Journal of Physical and Chemical Reference Data,* 24**,** 663-677.

WITZ, J. & BROWN, F. 2001. Structural dynamics, an intrinsic property of viral capsids. *Archives of virology,* 146**,** 2263-2274.

WNEK, G. E., CARR, M. E., SIMPSON, D. G. & BOWLIN, G. L. 2003. Electrospinning of nanofiber fibrinogen structures. *Nano Letters,* 3**,** 213-216.

WOERDEMAN, D. L., YE, P., SHENOY, S., PARNAS, R. S., WNEK, G. E. & TROFIMOVA, O. 2005. Electrospun fibers from wheat protein: investigation of the interplay between molecular structure and the fluid dynamics of the electrospinning process. *Biomacromolecules,* 6**,** 707-712.

YANG, M., LEE, G., SI, J., LEE, S.-J., YOU, H. J. & KO, G. 2016. Curcumin Shows Antiviral Properties against Norovirus. *Molecules,* 21**,** 1401.

YE, T. X., YE, S. L., CHEN, D. M., CHEN, Q. A., QIU, B. & CHEN, X. 2012. Spectroscopic characterization of tetracationic porphyrins and their noncovalent functionalization with graphene. *Spectrochimica Acta Part a-Molecular and Biomolecular Spectroscopy,* 86**,** 467-471.

ZEINA, B., GREENMAN, J., PURCELL, W. & DAS, B. 2001. Killing of cutaneous microbial species by photodynamic therapy. *British Journal of Dermatology,* 144**,** 274-278.

ZHANG, Y., VENUGOPAL, J., HUANG, Z.-M., LIM, C. & RAMAKRISHNA, S. 2005. Characterization of the surface biocompatibility of the electrospun PCL-collagen nanofibers using fibroblasts. *Biomacromolecules,* 6**,** 2583-2589.

ZHAO, L., LI, M., LIU, M., ZHANG, Y., WU, C. & ZHANG, Y. 2016. Porphyrin-functionalized porous polysulfone membrane towards an optical sensor membrane for sorption and detection of cadmium (II). *Journal of Hazardous Materials,* 301**,** 233-241.

ZHONG, Q., CARRATALÀ, A., NAZAROV, S., GUERRERO-FERREIRA, R. C., PICCININI, L., BACHMANN, V., LEIMAN, P. G. & KOHN, T. 2016. Genetic, Structural, and Phenotypic Properties of MS2 Coliphage with Resistance to ClO2 Disinfection. *Environmental Science & Technology,* 50**,** 13520-13528.

ZOLFAGHARI, P. S., PACKER, S., SINGER, M., NAIR, S. P., BENNETT, J., STREET, C. & WILSON, M. 2009. In vivo killing of Staphylococcus aureus using a light-activated antimicrobial agent. *Bmc Microbiology,* 9**,** 27.

Chapter Eight: Appendices

Chapter 8: Appendices

8. 1: TEM of PDI MS2

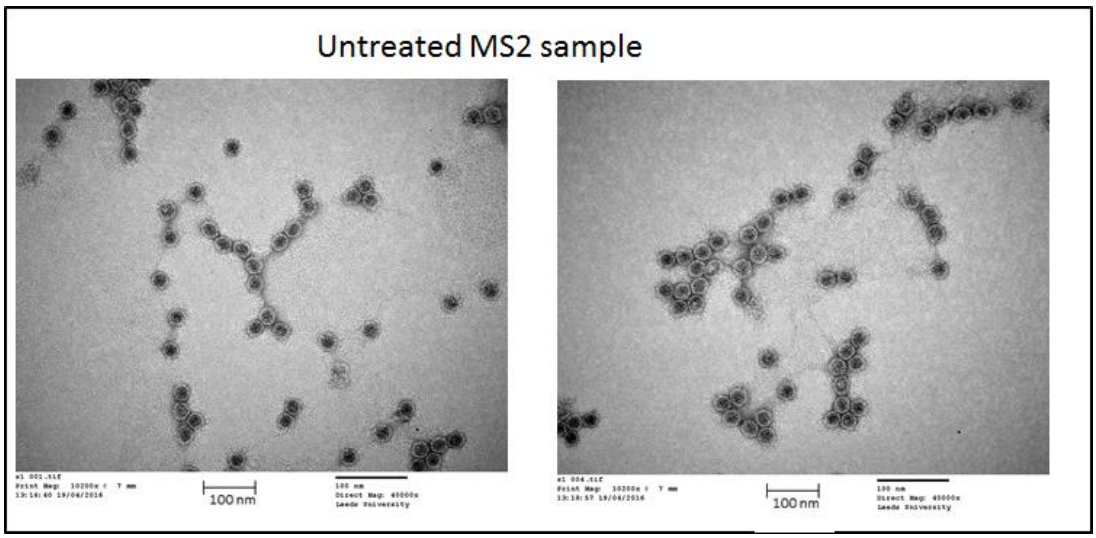

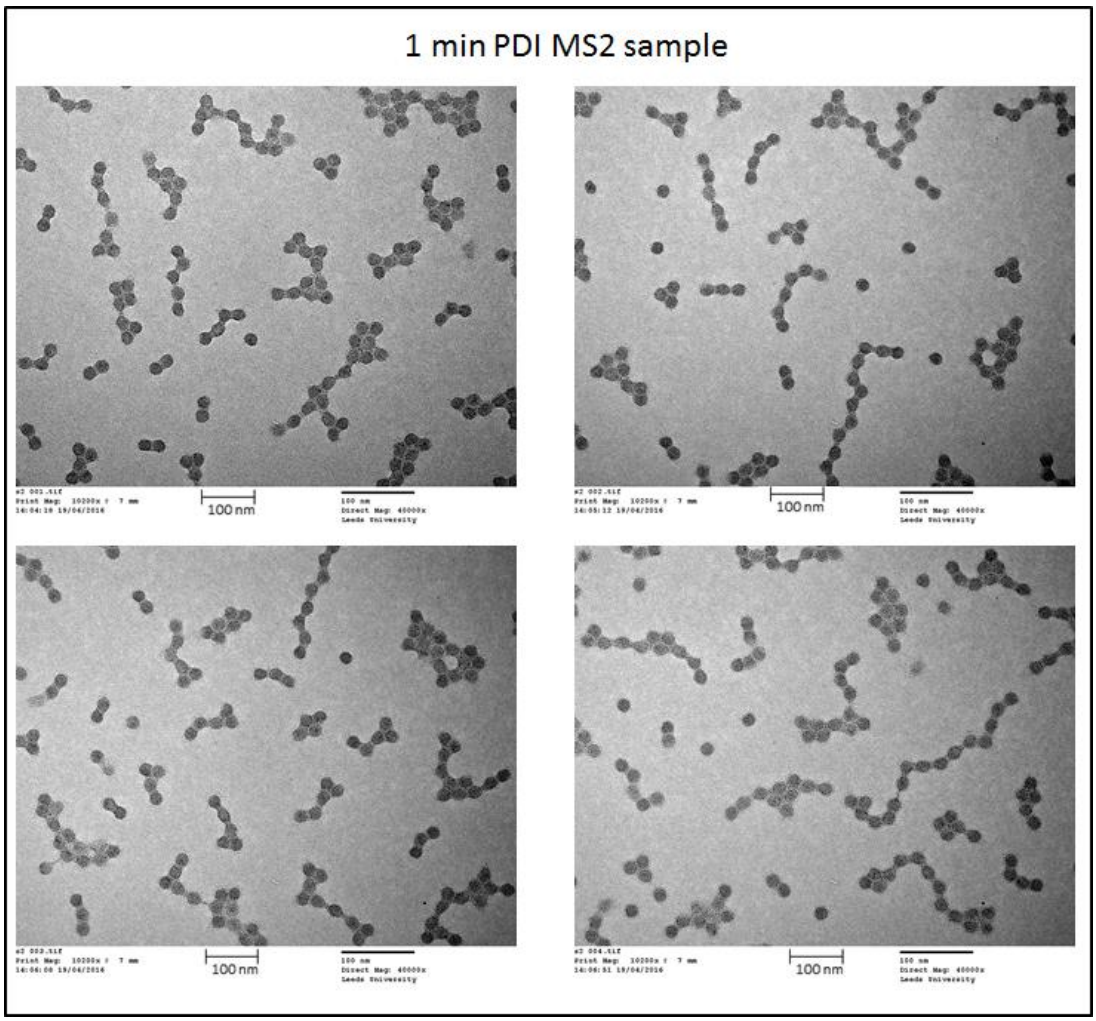

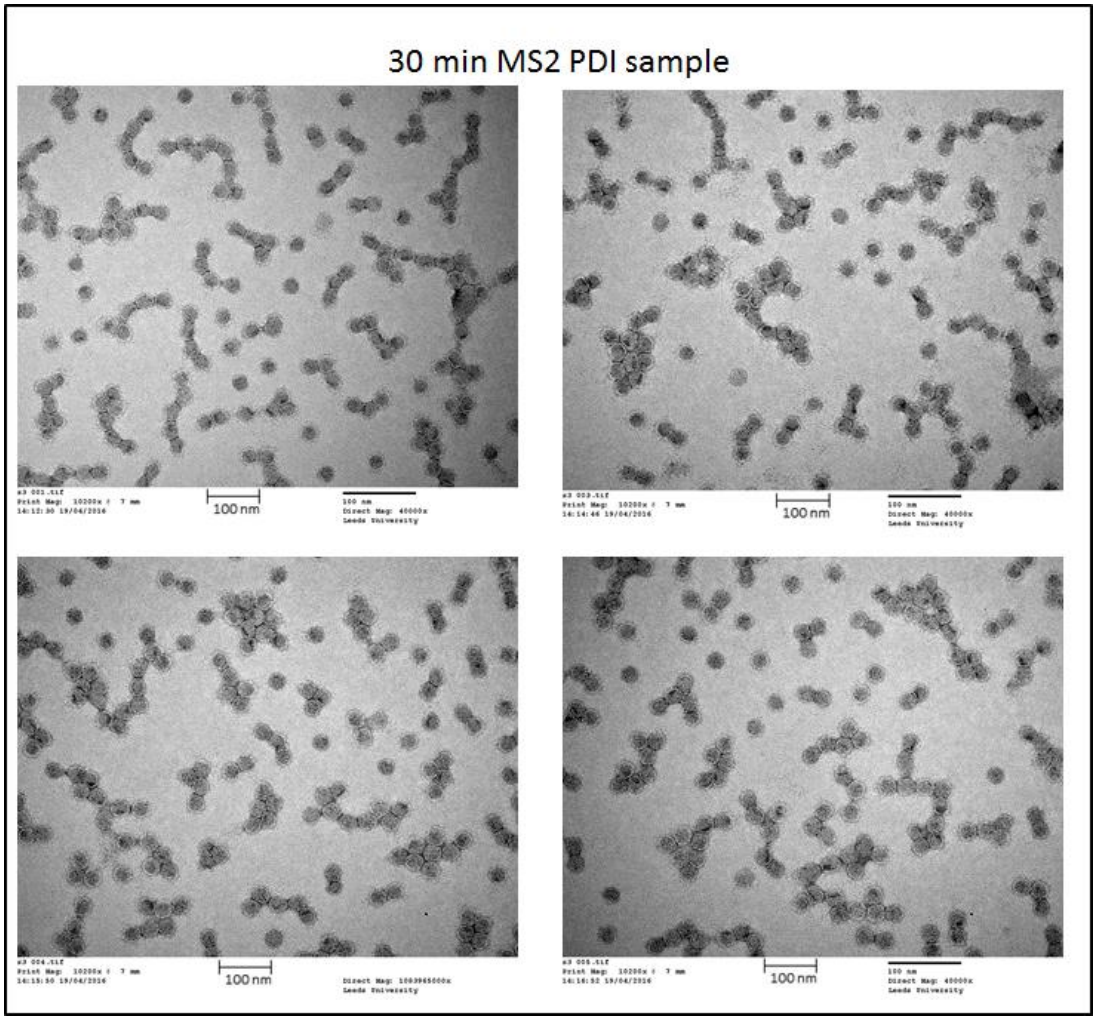
30 min MS2 PDI sample
100 nm
100 nm
100 nm
100 nm

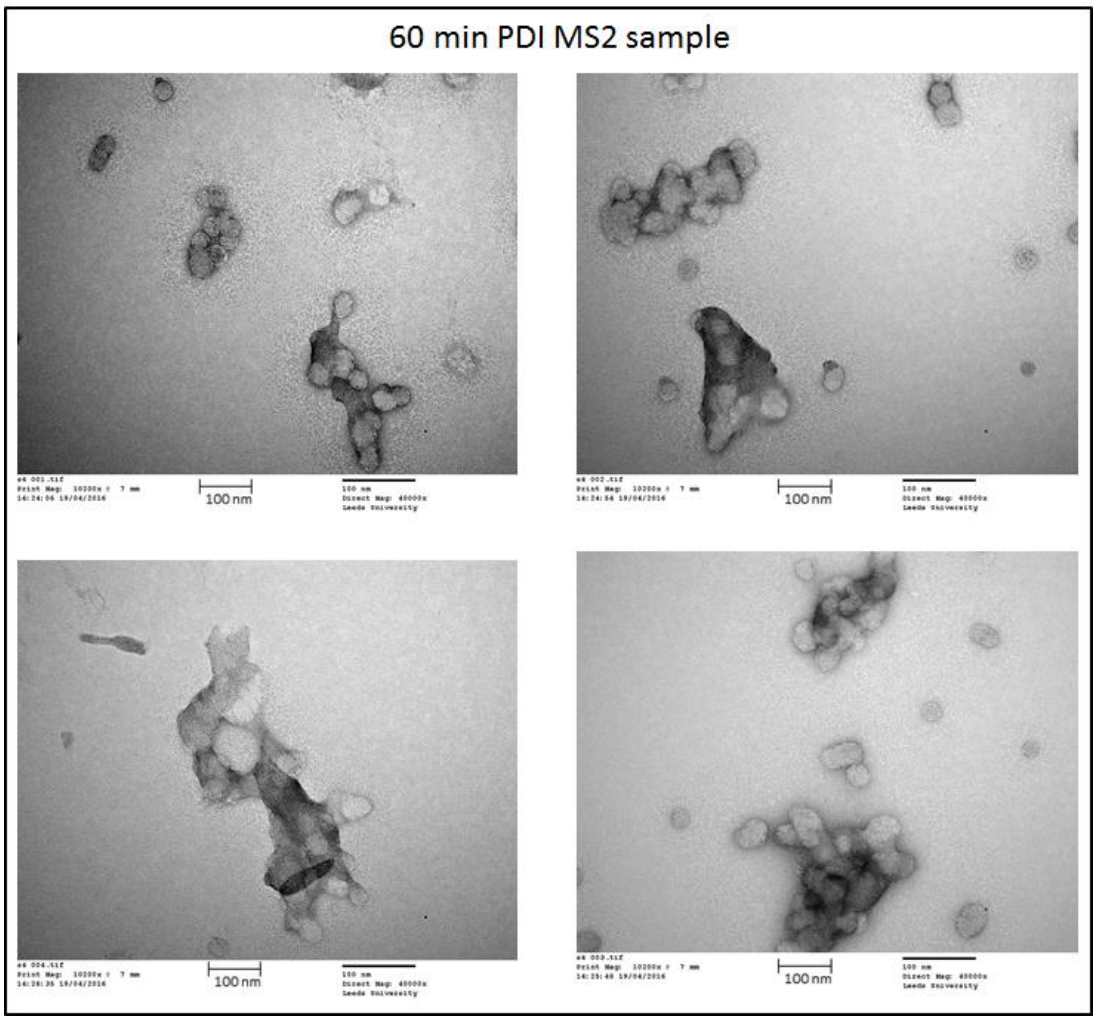
60 min PDI MS2 sample
100 nm
100 nm
100 nm
100 nm

8.2 Western blot of PDI MS2 samples using sequence-specific antibodies to detect A-protein

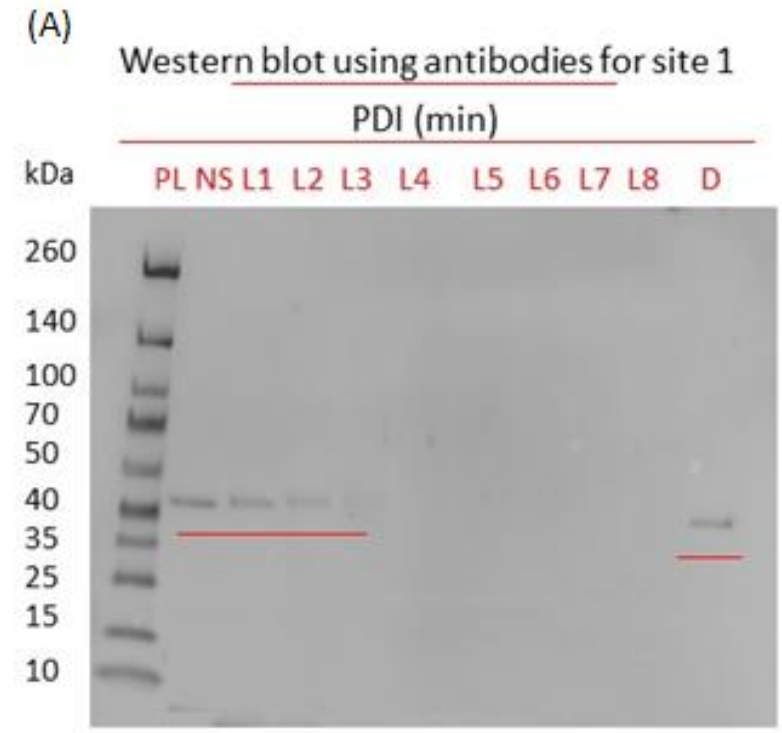

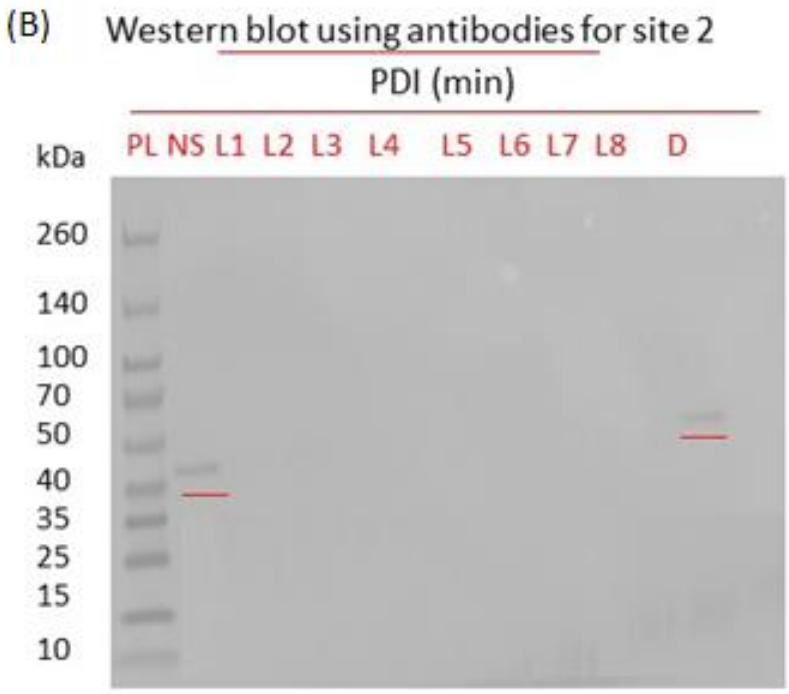

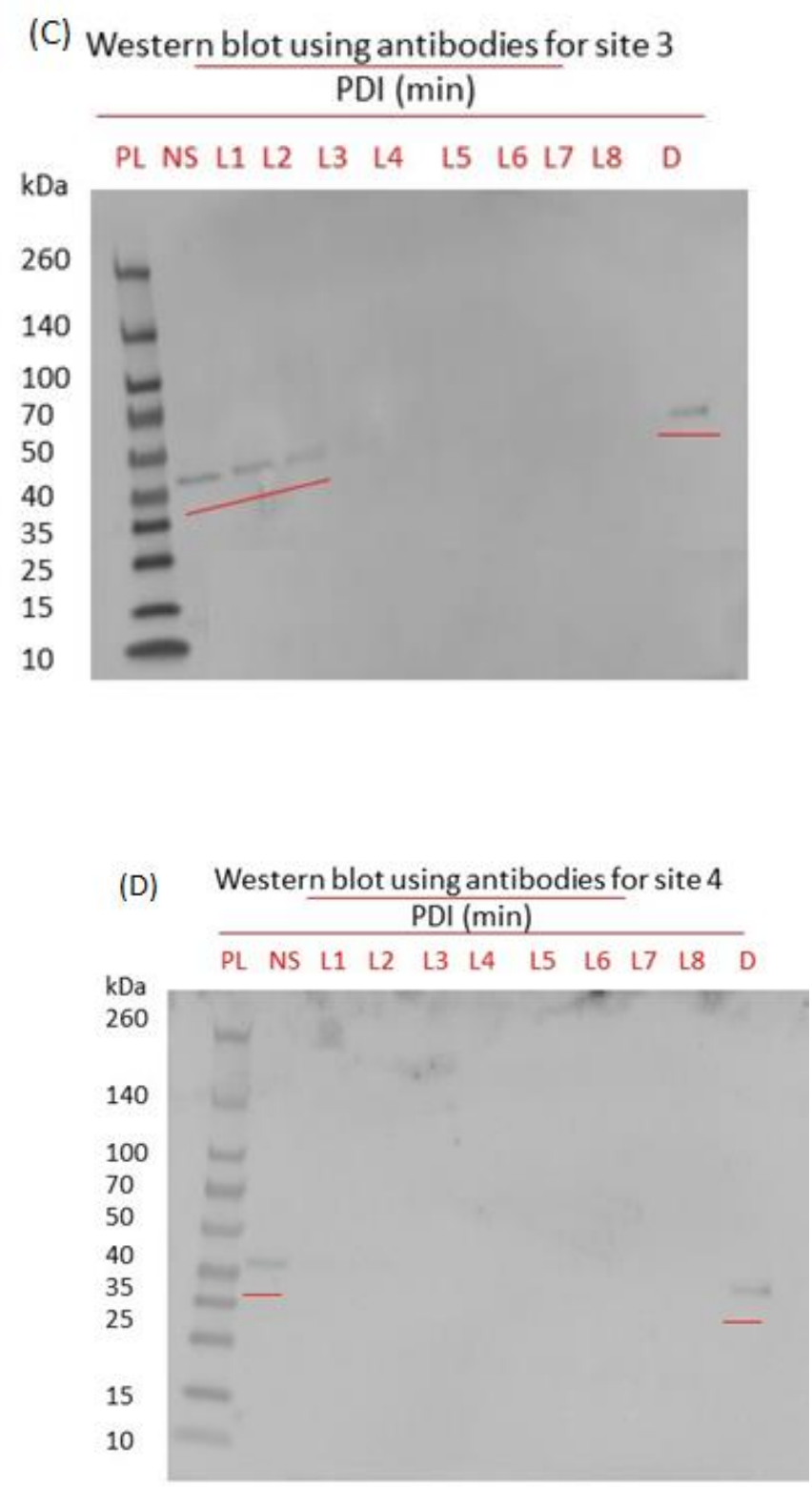

Western blot of PDI MS2 samples using sequence-specific antibodies to detect A-protein. 1 µM of TMPyP and illumination at 32 mW cm^{-2} were used for PDI of MS2 and the following antibodies were used for immune detection after PDI: (A), Ab1;

(B), Ab2; (C), Ab3; (D), Ab4. NS, no sensitiser; D, dark experiment and L1 to L60 denotes 1 min to 60 min of illumination.